SYMPOSIUM ON SURFACE SCIENCE 2010

St. Christoph am Arlberg, Austria
March 7 - 13, 2010

CONTRIBUTIONS

EDITORS
Friedrich Aumayr, Christoph Lemell and Peter Varga
TU Wien

Components for Surface Analysis

Systems & Components for Surface Analysis

- Electron Energy Spectrometers
- Ion, Electron, UV, and X-Ray Sources
- Scanning Probe Microscopes
- LEED Optics
- Deposition Equipment

... for XPS, UPS, AES, SEM/SAM, STM/AFM, LEEM, PEEM, SIMS/SNMS, LEED, HREELS, ISS

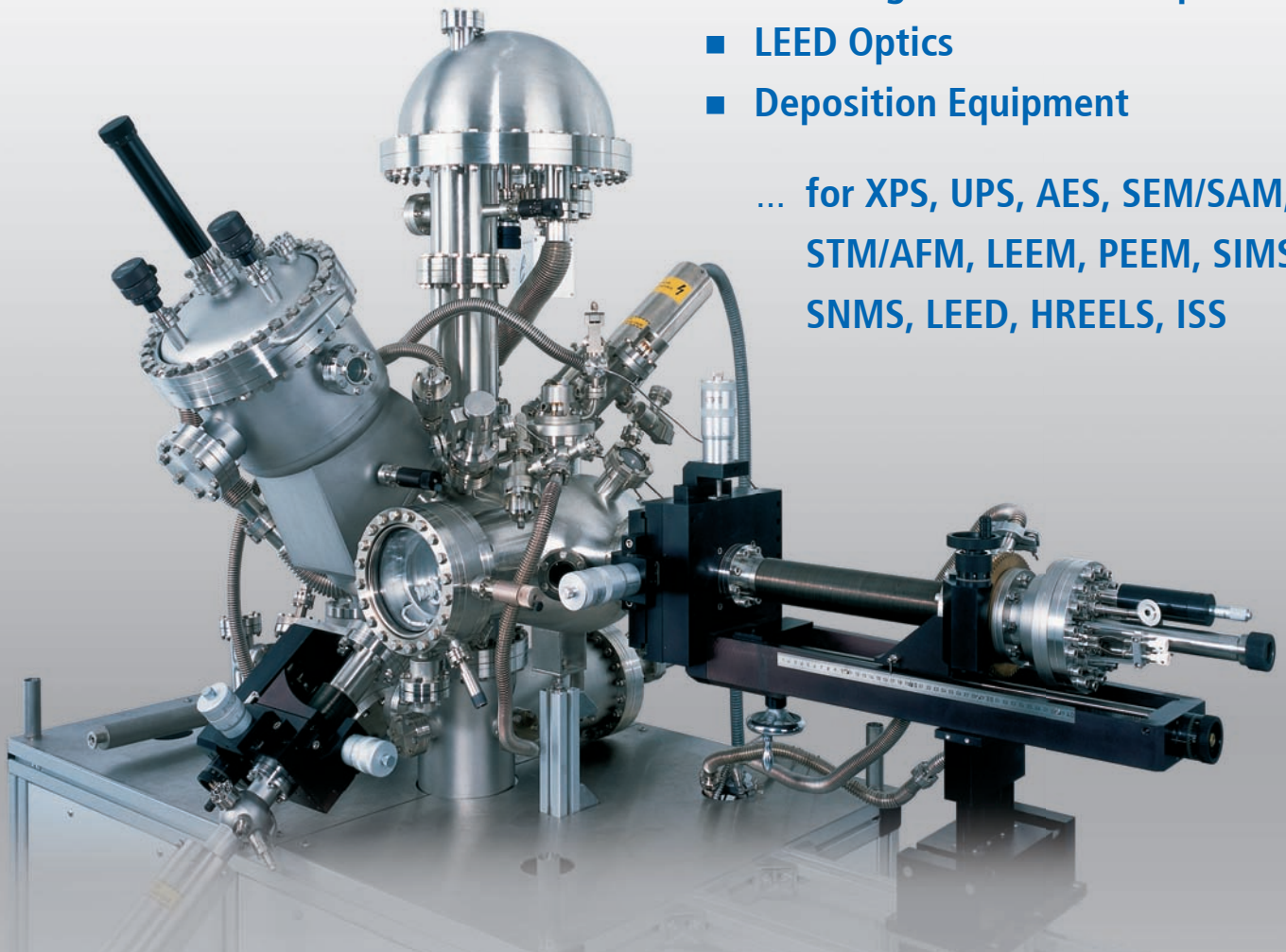

SPECS Surface Nano Analysis GmbH
Voltastrasse 5
13355 Berlin
Germany
Tel.: +49 30 46 78 24-0
Fax: +49 30 4 64 20 83
Email: support@specs.de
Web: www.specs.de

ISO 9001 Certificate

SYMPOSIUM ON SURFACE SCIENCE 2010

St. Christoph am Arlberg, Austria
March 7 - 13, 2010

CONTRIBUTIONS

EDITORS
Friedrich Aumayr, Christoph Lemell and Peter Varga
TU Wien

This symposium is organized by

Friedrich Aumayr and Peter Varga
Institute of Applied Physics (IAP)
Vienna University of Technology (TU Wien)
Wiedner Hauptstr. 8-10/E134
1040 Vienna, Austria

Medieninhaber: F. Aumayr and P. Varga, Institut für Angewandte Physik, Technische Universität Wien, Adresse: Wiedner Hauptstr. 8-10/E134, A-1040 Wien
Druck: R. & W. Smutny OEG, A-1110 Wien

PREFACE

We would like to welcome all participants and accompanying persons to the 23rd Symposium on Surface Science (3S). In 1983 - 3S was founded as a winter school by members of the Institut für Allgemeine Physik (renamed recently to Institute of Applied Physics) of the Vienna University of Technology (TU Wien). Its format has been chosen very similar to that of the Gordon Conferences, with ample time for the participants for discussions and joint outdoor activities. The attendance of the symposium was kept below 100 participants so that active communication between all members could be guaranteed. The conference seeks to promote the growth of scientific knowledge and its effective exchange among scientists in the field of surface physics and related areas, including applied topics.
At the beginning, 3S took place every second year exclusively in Austria, but from 1990 on every year switching between France and Austria. During the years 1998 - 2001 3S became a real global conference, with venues in the US and Canada, Bulgaria and Japan before going back to Austria and France again. Last year 3S was hold for the first time in Switzerland. This year we are happy to organize 3S for the 5th time in the Arlberg area of Austria.
We hope that all participants will experience a lively and successful meeting while enjoying the surrounding in this beautiful mountain region.

Fritz Aumayr Peter Varga

Dates and locations of 3S conferences:

1983	(31.01.-04.02.)	Obertraun	A	2000	(15.02.-18.02.)	Kananaskis Village	CAN
1985	(27.01.-02.02.)	Obertraun	A	2001	(07.01.-13.01.)	Furano	J
1988	(22.05.-28.05.)	Kaprun	A	2002	(03.03.-09.03.)	St.Christoph/Arlberg	A
1990	(11.03.-17.03.)	La Plagne	F	2003	(30.03.-05.04.)	La Plagne	F
1991	(10.02.-16.02.)	Obertraun	A	2004	(29.02.-06.03.)	St.Christoph/Arlberg	A
1992	(15.03.-21.03.)	La Plagne	F	2005	(13.03.-19.03.)	Les Arcs 1800	F
1993	(09.05.-15.05.)	Kaprun	A	2006	(05.03.-11.03.)	St. Christoph/Arlberg	A
1994	(06.03.-12.03.)	Les Arcs	F	2007	(11.03.-17.03.)	Les Arcs 2000	F
1995	(23.04.-29.04.)	Kaprun	A	2008	(02.03.-08.03.)	St. Christoph/Arlberg	A
1997	(26.01.-31.01.)	Aussois	F	2009	(08.03.-14.03.)	St. Moritz	CH
1998	(29.03.-04.04.)	Park City	US	2010	(07.03.-13.03.)	St. Christoph/Arlberg	A
1999	(21.02.-27.02)	Pamporova	BUL				

SYMPOSIUM ON SURFACE SCIENCE 2010

St. Christoph am Arlberg, Austria
March 7-13

Time Schedule

Sunday, 7 March 2010

16:00 – 18:30	**Registration**
20:00 – 20:20	**Opening**
	Chair: P. Varga
20:25 – 20:45	**F.J. Giessibl** *Reuniting Scanning-Tunneling-and Atomic-Force-Microscopy*
20:45 – 21:05	**W.-D. Schneider** *Size and material dependent electron transport across nano-tunneling contacts: From pseudo-gaps to Coulomb blockade*
21:05 – 21:25	**A. Garcia-Lekue** *Vibrational spectroscopy of single molecules using functionalized STM tips*

Monday, 8 March 2010

Chair: A.P. Seitsonen

08:00 – 08:20 **C. Wöll**
Sign reversal of adsorbate vibrational bands: Monitoring electronic structure changes on rutile TiO_2(110) using IR-spectroscopy

08:20 – 08:40 **G. Thornton**
Electron traps and their effect on the surface chemistry of TiO_2(110)

Chair: W.A. Hofer

16:30 – 16:50 **K. Reuter**
Structure and energetics of azobenzene at coinage metals using dispersioncorrected DFT approaches

16:50 – 17:10 **G. Pirug**
Surface chain structure of formic acid on Au(111) studied by Microchannelplate (MCP) LEED

17:10 – 17:30 **N. Lin**
Single-Molecule Characterization and Manipulation of Bis-terpyridine Molecules

17:30 – 17:50 **M. Buck**
Changing directions: from in-plane structures to a new type of self-assembled monolayer

17:50 – 18:10 **T. Greber**
Switching the surface texture by hydrogen intercalation

18:10 – 18:30 **D. Menzel**
Progress in surface photochemistry on nanoparticles: Internal energy distributions of NO from $(NO)_2$ on AgNPs of varied size.

Chair: K.H. Ernst

19:30 – 19:50 **J.V. Barth**
Random 2D string networks based on divergent coordination assembly

19:50 – 20:10 **H. Marbach**
Towards the engineering of molecular architectures: exploiting local moleculesubstrate interactions on composite surfaces to anchor or functionalize porphyrins

20:10 – 20:30 **J. Björk**
The porous surface network of TAPP: Identifying adatoms and bonding mechanism

20:30 – 20:50 **L. Vitali**
Portrait of the potential barrier at metal-organic nanocontacts

Tuesday, 9 March 2010

Chair: M. Wolf

08:00 – 08:20 **A. Gölzhäuser**
Fabrication of Graphene and Graphenoid 2D-Materials from Self-Assembled Monolayers

08:20 – 08:40 **R. Fasel**
On-surface cyclodehydrogenation: A route to chemically tailored nanographenes and graphene nanoribbon heterojunctions?

Chair: U. Heinzmann

16:30 – 16:50 **C. Ambrosch-Draxl**
Light-emitting Peapods for Photonic Devices

16:50 – 17:10 **P. Ruffieux**
Bottom-up fabrication of graphene nanostructures using molecular precursors

17:10 – 17:30 **G. Dong**
Understanding graphene formation on transition metals

17:30 – 17:50 **A.L. Vázquez de Parga**
Field Emission Resonances on periodically rippled graphene

17:50 – 18:10 **H. Dil**
Topological insulators: a new surface science playground

18:10 – 18:30 **F. Meier**
Interference of spin states in photoemission from Sb/Ag(111)

Chair: P. Müller

19:30 – 19:50 **T. Koshikawa**
Novel Spin-polarized LEEM

19:50 – 20:10 **F. Leroy**
Dewetting of silicon-on-insulator thin films measured by low-energy electron microscopy

20:10 – 20:30 **Y. Suchorski**
Laterally-resolved reaction kinetics: PEEM microscopy of catalytic CO oxidation on polycrystalline Pt

20:30 – 20:50 **D. Sánchez-Portal**
In overlayers on Si(111): is the hexagonal In-(√7 x √3)-Si(111) reconstruction formed by a single or double layer?

Wednesday, 10 March 2010

Chair: W. Eberhard

08:00 – 08:20 **M.S. Altman**
Adatom-Vacancy Mechanism of Step Motion on the Si(111) (1x1) Surface

08:20 – 08:40 **E. Lundgren**
Self-Propelled Motion of Mesoscopic Ga Droplets and nanomechanical properties of free-standing InAs nanowires from STM

Chair: F. Aumayr

16:30 – 16:50 **S. Facsko**
Surface nanostructures induced by slow highly charged ions

16:50 – 17:10 **C. Lemell**
Track formation in fast atom-insulator interactions

17:10 – 17:30 **R. Schuch**
Guiding of Slow Ne^{7+}-Ions through Insulating Nano-Capillaries of Various Cross Section

Chair: S. Müller

17:30 – 18:30 **Posterintroduction**

S. Blomberg
The oxidation and CO reduction of Pd nano particles: A high pressure x-ray photoelectron spectroscopy study

P. Cabrera-Sanfelix
Substrate Cooperative Effects on Water Adsorption: Hydrogen Bond Strengthening

L. Diekhöner
Kondo effect of substitutional Co atoms at Cu(100) and Cu(111) surfaces

K.-H. Ernst
Buckybowls at surfaces: tilting and tiling

T. Frederiksen
Transport properties of touching molecules

L. Hammer
Nanostructured cobalt oxide films on Ir(100)

W.A. Hofer
Cooperative molecular dynamics in surface reactions

R. Kalousek
Surface plasmon polaritons in the vicinity of a metal corner

G. Kowarik
Transmission of 4.5 keV Ar^{9+} ions through a single glass macrocapillary

M. Leisch
Influence of surface defects on hydrogen outgassing of stainless steel

P. Müller
Step bunching to step meandering transition induced by electromigration on Si (111) vicinal surface

V. Navarro
Fischer-Tropsch synthesis followed at high pressures with STM and XRD

P. Scheiber
Single Adatom Diffusion on Pt and Pt(x)Co(1-x)(111) Surfaces

A.P. Seitsonen
Theoretical investigation of BN-nanomesh on Rh (111)

U. Starke
Quasi-free Standing Epitaxial Graphene on SiC by Hydrogen Intercalation

F.C. Tabak
The development of an easy-to-use, versatile MEMS SPM scanner

E. Taglauer
He^+ Ion scattering from noble metal and alloy surfaces: Influence of Surface Structure and Composition on Neutralization

P. Wahl
Competition of Magnetism and Correlation in a Cobalt Dimer: from Kondo Screening to Local Moment Antiferromagnetism

W. Widdra
Atomic, electronic, and vibrational structure of epitaxial manganese oxide films: A combined STM, STS, and HREELS study

M. Wolf
Dynamics of electron solvation mediated by Na-D_2O complexes in amorphous ice

19:30 – 21:30 **Postersession**

Thursday, 11 March 2010

Chair: P.M. Echenique

08:00 – 08:20 **H. Brune**
STM spin-excitation spectra on individual atoms against XMCD ensemble measurements

08:20 – 08:40 **M. Scheffler**
Comments on Two Catalytic Processes: Oxidative Coupling for Methane Conversion to Ethylene and Oxidation of Ethylene to Ethylene Oxide

Chair: W. Widdra

16:30 – 16:50 **G. Rupprechter**
Formation, thermal stability and activity of PdZn nearsurface alloys: a combined PM-IRAS, XPS and TPD study

16:50 – 17:10 **A. Arnau**
Mapping electron resonances on nanosized alkali metal dots grown on Cu(100)

17:10 – 17:30 **A. Benali**
DFT Periodic study of Cu segregation within Al surfaces

17:30 – 17:50 **K. Morgenstern**
Confinement of the interface state between NaCl and Ag(111)

17:50 – 18:10 **S. Müller**
Modelling adsorbate-induced surface segregation in metal alloys

18:10 – 18:30 **M.E. Cañas-Ventura**
ReactorAFM; from vision to reality

Chair: L. Hammer

19:30 – 19:50 **S. Surnev**
Structure of zinc oxide nanolayers on a Pd(111) surface: STM and DFT study

19:50 – 20:10 **F. Mittendorfer**
Surface carbides in palladium catalysts?

20:10 – 20:30 **C.T. Herbschleb**
Live Catalysts under Industrial Conditions imaged with Atomic Resolution

20:30 – 20:50 **F.P. Netzer**
Strain effects in oxide nanostructures

Friday, 12 March 2010

Chair: U. Starke

08:00 – 08:20 **J. Gustafson**
Catalytic reaction between O_2, CO and NO over Rh(111)

08:20 – 08:40 **J. Libuda**
Activation of Small Molecules over Ceria Based Model Catalysts: Why do Nanostructured Materials Behave Differently?

Chair: M. Leisch

16:30 – 16:50 **H. Ibach**
Vibration Spectroscopy of Water on Stepped Gold Surfaces

16:50 – 17:10 **A. Kakizaki**
Spin-split electronic structures of non-magnetic surfaces observed by highefficiency spin-and angle-resolved photoelectron spectroscopy

17:10 – 17:30 **T. Sikola**
Localized surface plasmons and their application in plasmonics

17:30 – 17:50 **S.Yu. Krylov**
Vanishing friction: Super-slipperiness or thermolubricity?

17:50 – 18:10 **E.V. Chulkov**
Dynamics of excited electrons in thin films of lead

Chair: E. Taglauer

18:30 – 18:50 **Ch. Linsmeier**
Surface chemistry of fusion first wall materials – from fundamental data to modeling

18:50 – 19:10 **T. Juffmann**
Wave and particle in molecular quantum interference lithography

19:10 – 19:30 **H. Pfnür**
Charge density waves without Peierls transitions

19:30 – 19:45 **Giant Slalom Race Award Ceremony**

20:00 – **Conference Dinner**

The turbopump innovation.

Picking up the pace in vacuum technology.
Faster. Higher. Stronger.

- Complete series of pumps with pumping speeds of from 10–700 l/s
- Robust engineering and proven bearing system offer maximum reliability
- Compact design makes for minimum footprint
- Installation possible in any orientation

PFEIFFER VACUUM

Pfeiffer Vacuum Austria GmbH
Phone: +43 1 894 17 04 · Fax: +43 1 894 17 07 · office@pfeiffer-vacuum.at

www.pfeiffer-vacuum.net

Content

CONTRIBUTIONS

Sunday

Reuniting Scanning-Tunneling- and Atomic-Force-Microscopy

Franz J. Giessibl

Institute of Experimental and Applied Physics, University of Regensburg, D-93053 Regensburg, Germany, franz.giessibl@physik.uni-regensburg.de

Scanning tunneling microscopy (STM) and atomic force microscopy (AFM) both allow to characterize surfaces on the atomic level. However, STM and AFM measure different physical quantities and the experimental setup of an STM has been quite different from the setup of an AFM. Atomic resolution by AFM is mainly performed in the frequency modulation mode where in the initial experiments, a soft cantilever with a stiffness on the order of 20 N/m was oscillating with an amplitude of some tenth of a micrometer [1-3]. In addition to atomic imaging of surfaces, exciting breakthroughs like atom manipulation at room temperature [4] and atom identification [5] at room temperature have been achieved with the large-amplitude technique. However, an analysis of the noise and short-range sensitivity of dynamic atomic force microscopy shows that optimal results will occur when the oscillation amplitude A of the cantilever has a magnitude similar to the range λ of the forces at play [6,7] $A_{opt} \approx \lambda$. The range of chemical bonding forces is on the order of 0.1 nm. When the cantilever is to oscillate with amplitudes of 0.1 nm in a stable fashion under the influence of the forces between tip and sample, cantilevers with a stiffness of approximately 1 kN/m in stead of the commonly used 20 N/m are required. Soon after these findings, "subatomic" resolution, that is the imaging of features within single atoms, was demonstrated by force microscopy [8].

One of the advantages of the qPlus sensor as an implementation of the stiff-cantilever/small-amplitude technique is that simultaneous STM/AFM operation is easy and a gradual transformation of STM to AFM control is possible. The STM current is modulated when the tip oscillates at 50 pm or so, but the oscillation is so fast that the STM feedback is not perturbed by the oscillation and the average current is sufficient to control the microscope. In parallel, the frequency shift can be measured. A direct comparison of scanning tunneling microscopy and AFM data showed that when probing a tungsten tip with a graphite surface (a "light-atom probe"), subatomic orbital structures with a spatial resolution of less than one Angstrom can be obtained in the force map, while a map of the tunneling current only shows the known atomic resolution [9]. Optimized subatomic contrast is obtained when recording the higher harmonics of the cantilever motion as discussed in [10]. The idea of the light atom probe was carried further in a collaboration with the IBM Low Temperature STM group in Almaden, San Jose where the forces acting in atomic manipulation were measured. It requires quite a large force to move a CO molecule laterally [11]. A CO molecule that is adsorbed to a metallic probe tip is an excellent probe for the orbital structure of the front atom

of the metal tip [12]. Ideally, one wishes to create a probe with a perfectly perpendicularly oriented tip.

The greatest challenge of the qPlus sensor is the structure and stability of its probe tip. Due to the large size, metal tips that are cut or etched from metal wires or single crystal tips can be used, cleaved ex situ [13] or in situ [14]. The precision of the force measurement depends on the accuracy, at which the oscillation frequency of the cantilever can be measured. This accuracy depends crucially on the deflection noise density n_q, with typical values of 100 fm/√Hz. This noise can be minimized with novel preamplifier schemes [3].
Frequency stability over long times and during temperature variations is also important in AFM. While the frequency of silicon cantilevers changes by approx. -35 ppm/K×(T-T_{ref}), the frequency of quartz tuning forks only varies by approx -0.04 ppm/K^2×(T-T_{ref})^2 around room temperature. At helium temperatures, the frequency variation with temperature is also extremely low as shown in [15]. Combined STM and AFM is very simple when using the qPlus sensor. In the last years, a variety of STM experiments have been repeated with a combined STM/AFM using the qPlus sensor where crucial new information was gathered by the additional information on the forces that act. Ternes et al. have measured the tiny forces that act during atomic manipulation [11]. Gross et al. has measured the charge state of an individual Au atom and provided unprecedented spatial resolution of an organic molecule [16,17]. The enigmatic Si(001) surface has been revisited with combined STM/AFM [18], oxide surfaces are being studied with tuning fork based AFM [19] and commercial manufacturers of AFMs implement the qPlus technique [20,21]. It is expected, that the challenges described above will be met in the near future, opening new possibilities in atomic surface science.

[1] F.J. Giessibl, *Science* **267**, 68 (1995).
[2] S. Morita, R. Wiesendanger, E. Meyer (eds.) Noncontact Atomic Force Microscopy, Springer, Berlin (2002).
[3] S. Morita, F.J. Giessibl, R. Wiesendanger (eds.) NCAFM II, Springer, Berlin (2009).
[4] Y. Sugimoto, M. Abe, S. Hirayama, N. Oyabu, O. Custance, S. Morita, *Nature Materials **4,*** 156 (2005).
[5] Y. Sugimoto, P. Pou, M. Abe, P. Jelinek, R. Perez, S. Morita, O. Custance, *Nature* **446**, 64 (2007).
[6] F.J. Giessibl, H. Bielefeldt, S. Hembacher and J. Mannhart, *Appl. Surf. Sci.* **140**, 352 (1999).
[7] F.J. Giessibl, *Rev. Mod. Phys*. **75**, 949 (2003).
[8] F.J. Giessibl, H. Bielefeldt, S. Hembacher, J. Mannhart, *Science* **289**, 422 (2000).
[9] S. Hembacher, F. J. Giessibl, J. Mannhart, *Science* **305**, 380 (2004).
[10] F.J. Giessibl, *Surf. Interface Anal.* **38,** 1696 (2006).
[11] M. Ternes, C.P. Lutz, C.F. Hirjibehedin, F.J. Giessibl, A..J. Heinrich, *Science* **319**, 1066 (2008).
[12] F.J. Giessibl, C.F. Quate, *Physics Today* **59**, 44 (2006).
[13] F.J. Giessibl, S. Hembacher, H. Bielefeldt, J. Mannhart, *Appl. Phys. A* **72**, S15 (2001).
[14] T. Wutscher, diploma thesis, University of Regensburg 2008.
[15] S. Hembacher, F.J. Giessibl, J. Mannhart, *Appl. Surf. Sci.* **188**, 445 (2002).
[16] L. Gross, F. Mohn, P. Liljeroth, J. Repp, F. J. Giessibl, G. Meyer, *Science* **324**, 1428 (2009).
[17] L. Gross, F. Mohn, N. Moll, P. Liljeroth, G. Meyer, *Science* **325**, 1110 (2009).
[18] A. Sweetman, S. Gangopadhyay, R. Danza, N. Berdunov, P. Moriarty, *Appl. Phys. Lett*. **95**, 063112 (2009).
[19] G. H. Simon, T. König, H.-P. Rust, M. Heyde, H.-J. Freund, New Journal of Physics **11**, 093009 (2009).
[20] Createc GmbH, Erligheim, Germany.
[21] A. Bettac, J. Koeble, K. Winkler, B. Uder, M. Maier, A. Feltz, *Nanotechnology* **20,** 264009 (2009).

Size and material dependent electron transport across nano-tunneling contacts: From pseudo-gaps to Coulomb blockade

C. Brun, I.-P. Hong, F. Patthey, and W.-D. Schneider

Institut de Physique de la Matière Condensée, Ecole Polytechnique Fédérale de Lausanne (EPFL), CH-1015 Lausanne, Switzerland
(corresponding author: W.-D. Schneider, e-mail: wolf-dieter.schneider@epfl.ch)

The precise control and the detailed knowledge of the behaviour of electrical contacts when their effective contact area is reduced down to the nanoscale is crucial for a flawless functioning of nanodevices in a future development of nano-electronics. Here, using low-temperature scanning tunneling microscopy (STM) and spectroscopy (STS), we show that the electrical conductance between metallic nanocontacts and various types of materials (metal, semi-metal (highly oriented pyrolitic graphite (HOPG)), semiconductor, ultrathin dielectric films on metals) varies astonishingly upon reduction of the contact area.

As model systems for nanocontacts we have chosen to grow Pb islands of various lateral sizes and thicknesses down to a few nanometers on Si(111)-7x7, HOPG, BN/Ni(111), NaCl/Ag(111) and on Cu(111). Lead was thermally evaporated in an ultrahigh vacuum (UHV) chamber onto these different substrates. In each case the substrate temperature, the Pb flux and the Pb evaporation time were controlled and adapted to achieve favourable island growth conditions. The samples were transferred *in situ* into a custom-built STM operated in UHV at a base temperature of 4.6 K [1].

Lead has been selected because quantum size effects drive the growth of ultrathin Pb films and islands, which allowed us to obtain microscopically characterized ultrathin islands as models for nanocontacts. On Si(111) and on Cu(111) single crystal flat top Pb islands grow along the (111) direction on top of a one monolayer (ML) thick wetting layer (WL) [2,3]. On HOPG, BN/Ni(111), and on NaCl/Ag(111) flat top Pb islands grow on top of the substrate without the formation of a WL. The local imaging capabilities of the STM are used to precisely determine the nano-contact size and thickness on the atomic scale.

Using STS we determined the electrical conductance of these individual model-types of nano-contacts. We found that upon decreasing the contact area, i. e., the metallic Pb island area, charging effects across the junction formed by the nano-contact and the substrate reduce the conductance and lead to pseudo-gaps (on Si) or to Coulomb blockade (on HOPG, BN/Ni, and on NaCl) in the scanning tunneling spectra around zero bias voltage, where for Pb on NaCl a clear Coulomb staircase was observed. On the other hand, as expected for a metallic substrate

for Pb on Cu(111) the charging effects remain negligible. A theoretical analysis of the obtained experimental results provides a detailed understanding of how contacts of nanometer size will affect the electron transport in todays micro- and nano-electronics.

Support by the Swisss National Science Foundation is gratefully acknowledged.

[1] R. Gaisch, J.K. Gimzewski, B. Reihl, R.R. Schlittler, M. Tschudy, and W.-D. Schneider, Ultramicroscopy 42-44, 1621 (1992).

[2] I.-P. Hong, C. Brun, F. Patthey, I. Yu. Sklyadneva, X. Zubizarreta, R. Heid, V. M. Silkin, P. M. Echenique, K. P. Bohnen, E. V. Chulkov, and W.-D. Schneider, Phys. Rev. B 80, 081409(R) (2009), and references therein.

[3] C. Brun, I.-P. Hong, F. Patthey, I. Yu. Sklyadneva, R. Heid, P. M. Echenique, K. P. Bohnen, E. V. Chulkov, and W.-D. Schneider, Phys. Rev. Lett. 102, 207002 (2009), and references therein.

Vibrational spectroscopy of single molecules using functionalized STM tips

A. Garcia-Lekue* and T. Frederiksen
Donostia International Physics Center, DIPC, Donostia, Spain

D. Sanchez-Portal
Centro de Física de Materiales, CSIC-UPV/EHU, Donostia, Spain

A. Arnau
Dpto. Física de Materiales, UPV/EHU, Donostia, Spain and
Centro de Física de Materiales, CSIC-UPV/EHU, Donostia, Spain

(Dated: December 18, 2009)

In recent years, inelastic electron tunneling spectroscopy (IETS) has become a powerful tool for the analysis of molecules absorded on surfaces, since it provides valuable information on the adsorption site, orientation and bonding of the molecule to the surface. This vibrational spectroscopy technique is based on the measurement of changes in conductance due to phonon emission by molecular vibrations.

IETS measurements of single molecules are commonly performed using the scanning tunneling microscope (STM). In this experimental approach, vibrational spectra and inelastic images are achieved by placing a tip several angstroms away from the molecules absorbed on the surface. Using this set-up and by application of an external bias, discontinuities in conductance can be recorded when the bias is large enough to excite vibrational modes of the molecule-tip system. Despite being an extremely powerful technique for the investigation of inelastic transport properties, a precise knowledge of the morphology and chemical composition of the tip is missing in the IETS-STM experiments. However, tip effects might severely affect the outcome and interpretation of experimental data and consequently, understanding and being able to elucidate the role of the STM tip in IETS measurements is of key importance.

In this work, we report first-principles based vibrational spectra of a single carbon monoxide (CO) molecule absorbed on Cu(111) obtained using chemically modified tips. We assume the model system configuration shown in the inset of Figure 1, and STM tips functionalized with CO, CO_2 and C_2H_4 molecules. The vibrational modes and inelastic transport have been modeled using density functional thery (DFT), combined with non-equilibrium Green's function (NEGF) approach.

*Electronic address: wmbgalea@lg.ehu.es

The IETS spectra calculated using a CO terminated tip are represented in Figure 1, where we observe that the inelastic signal of the frustrated rotation of CO at ~ 35 meV is enhanced by a factor of ~ 2 when the tip CO molecule is allowed to vibrate. Additionally, vibrational modes not excited with a bare metallic tip, such as the center of mass of CO at ~ 57 meV, can be observed using functionalized tips [1]. Our results confirm previous experimental results and emphasize the relevance of tip effects on STM based vibrational spectroscopy [2].

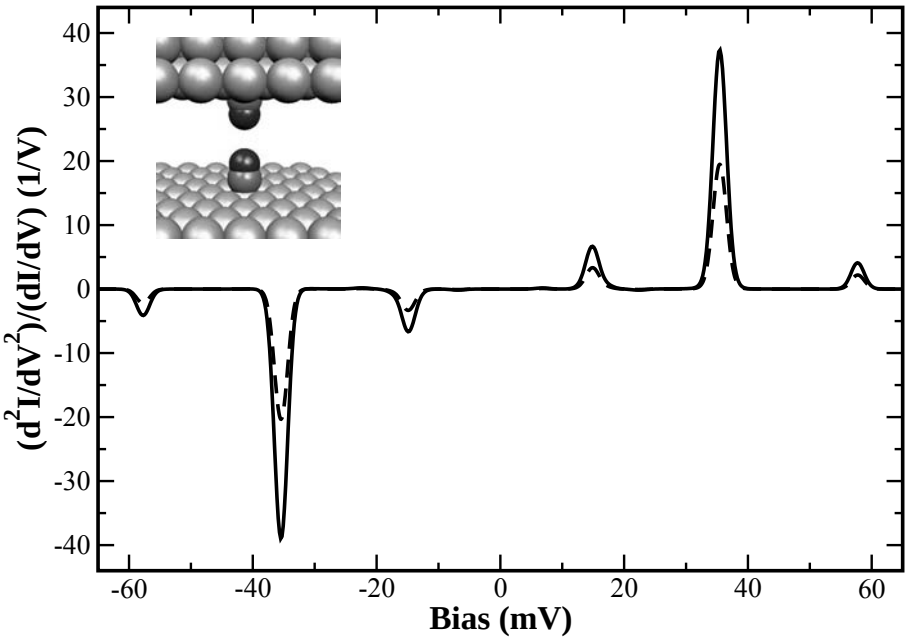

FIG. 1: Vibration spectra taken on top of a CO molecule adsorbed on Cu(111) surface using a frozen CO tip (dashed line) or a CO tip allowed to vibrate (solid line).

[1] L. Vitali, A. Garcia-Lekue, T. Frederiksen, D. Sanchez-Portal, R. Ohmann, K. Kern and A. Arnau, (accepted in Nanoletters).

[2] J.R. Hahn and W. Ho, Phys. Rev. Lett. **87**, 196102 (2001)

Monday

Sign reversal of adsorbate vibrational bands: Monitoring electronic structure changes on rutile TiO_2(110) using IR-spectroscopy

Mingchun Xu[a], YouKun Gao[a], Yuemin Wang[a,b] and Christof Wöll[c]

[a] Lehrstuhl für Physikalische Chemie I, Ruhr-Universität Bochum, 44780, Germany
[b] Laboratory of Technical Chemistry, Ruhr-Universität Bochum, 44780, Germany
[c] Institute of Functional Interfaces, Karlsruhe Institute of Technology, 76021 Karlsruhe, Germany, (email: Christof.Woell@KIT.edu)

The effect of doping on the surface (photo)chemistry of oxides and in particular of TiO_2 is presently attracting a significant amount of attention. This interest results from a number of questions in connection with a number of different applications, e.g. solar cells (Graetzel cell) and photochemistry. One prominent example is the removal of NO (photo)catalytically from the atmosphere, a process for which TiO_2 is one of the most effective photocatalysts [1]. In pristine TiO_2 the band gap is too large to absorb the majority of the solar spectrum; researchers have therefore investigated ways to reduce this gap by doping [1-3]. In the past few years, virtually all experimental information on the surface chemistry and local doping effects on TiO_2 surfaces have been obtained by scanning tunnelling microscopy (STM), a reliable identification of molecular reaction products and the effect of doping on photochemistry is lacking in many cases.

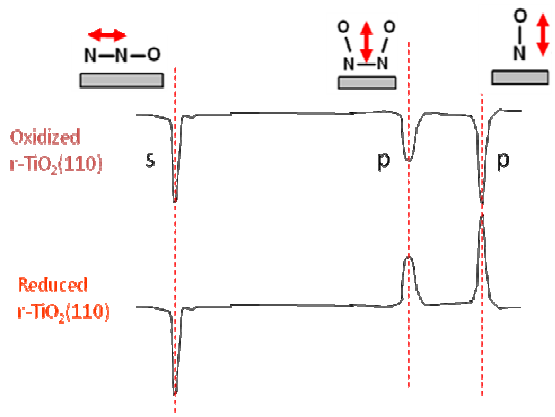

Fig. 1 IR-spectra recorded at grazing incidence for NO adsorbed on rutile TiO_2(110)

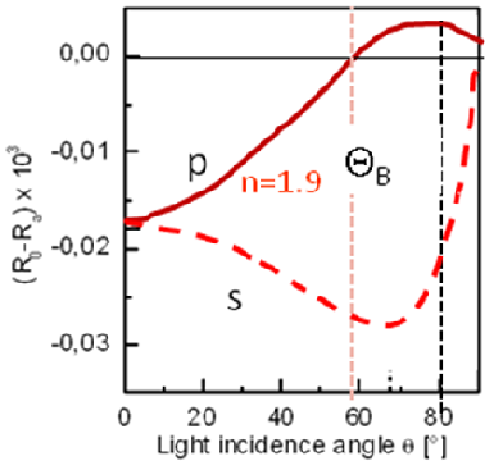

Fig. 2 Intensity of adsorbate vibrational bands predicted for s- and p-polarized IR-light incident on a dielectric substrate with an optical constant of n=1.9. Θ_B denotes the Brewster angle.

In this paper we demonstrate that electronic structure changes on single crystal oxide surfaces can also be investigated by a non-contact technique, reflection-absorption infrared spectroscopy (RAIRS) via changes in the sign of p-polarized vibrational bands. In contrast to STM, IR-spectroscopy allows for an unambiguous assignment of surface reaction products and intermediates.

Unfortunately, the application of this technique to oxide single crystal surfaces has in the past been hampered by sensitivity problems; in the case of TiO_2 we are aware of only one previous successful application of IR-spectroscopy to study adsorbate vibrations on a single

crystal [4]. These difficulties arise from the fact the signal intensity of adsorbate vibrational bands is reduced on by 2-3 orders of magnitude dielectric substrates relative to metals [5].

We demonstrate here that the intensity problems can be overcome with state-of-the-art RAIRS equipment [6,7]. We present the first RAIRS data for NO adsorbed on a single-crystal TiO_2 surface. While the s-polarized vibrational bands observed after adsorption of NO always lead to an increase in reflectivity ("negative" IR bands), the sign of the p-polarized bands is found to depend on the degree of surface reduction. For the fully oxidized surface the p-polarized NO-stretch vibrational bands are negative. Reduction of the sample (corresponding to a doping with O-vacancies) leaves the band positions unchanged but flips their sign from negative to positive. At the same time the band positions remain unchanged.

For understanding this unexpected observation one needs to consider the peculiarities which come into play when infrared-light impinges on a dielectric substrate at grazing incidence. A theoretical analysis reveals that the reflectivity can increase or decrease upon excitation of a vibrational band. This is in pronounced contrast to metals, where bands are always observed as absorption bands, i.e. the reflectivity increases. In addition, on oxides also the detection of vibrational bands with a transition dipole moment orientated parallel to the surface is possible, whereas on metals the screening of the s-polarized component of electric field by the substrate electrons makes the observation of such modes impossible ("surface selection rule"). A further important aspect is that at the Brewster angle for p-polarized light the reflectivity is zero, all light is refracted inside the dielectric.

IR-spectroscopy on oxide single crystal surfaces thus offers a fairly large number of new opportunities in surface chemistry, since in addition to spectroscopic information allowing for the identification of reaction intermediates and products also a determination of adsorbate orientation becomes possible if a polarizer is added to the IR-spectrometer.

In this presentation a number of examples for such new opportunities will be presented by showing very recent results for rutile and anatase TiO_2 substrates. As particularly important we consider the application of IR-spectroscopy to study light-induced chemical transformations of adsorbates, since this approach allows to study UV-induced processes on oxides substrate without the probe creating e-h pairs.

[1] T. L. Thompson, and J. T. Yates, Jr. , Chem. Rev. **106**, 4428 (2006).
[2] C. Di Valentin, U. Diebold, and A. Selloni, Chem. Phys. **339**, VII (2007).
[3] M. Batzill, E. H. Morales, and U. Diebold, Phys. Rev. Lett. **96**, 026103 (2006).
[4] B. Hayden, A. King, M.A. Newton, J. Phys. Chem. **B 103,** 203 (1999).
[5] J.Kattner and H. Hoffmann, in *Handbook of Vibrational Spectroscopy* J. M. Chalmers and P. R. Griffiths (Editors), John Wiley& Sons Ltd, Chichester, p. 1 (2002)
[6] Ch. Rohmann, Y. Wang, M. Muhler, J. B. Metson, H. Idriss, and Ch. Wöll, Chem. Phys. Lett. **460**, 10 (2008).
[7] Y. Wang, A. Glenz, M. Muhler, Ch. Wöll, Rev. Sci. Instrum., **80**, 113108 (2009).

Electron traps and their effect on the surface chemistry of TiO_2(110)*

Anthoula C. Papageorgiou, Oliver Yim, Nikolaos S. Beglitis[b], Chi L. Pang, Gilberto Teobaldi[1], Gregory Cabailh, Qiao Chen, Andrew J. Fisher, Werner A. Hofer[1], Geoff Thornton

London Centre for Nanotechnology, University College London, 17-19 Gordon Street, London WC1H 0AH, UK
(corresponding author: G. Thornton, e-mail: g.thornton@ucl.ac.uk)

[c]*Surface Science Research Centre, Department of Chemistry, University of Liverpool, Liverpool L69 3BX, UK*

This paper is concerned with the origin of the quasi-particle band gap state of TiO_2(110), ist charge state, and the effect on the surface chemistry. In the first part of the presentation we present Scanning tunneling microscopy and photoemission spectroscopy have been used to determine the origin of the Ti 3*d* derived band-gap state on rutile TiO_2(110). This state appears ~1 eV below the Fermi level in photoemission spectra, and has long been attributed to oxygen vacancies. However, recently an alternative origin has been suggested, namely sub-surface interstitial Ti species [1]. Here, we use electron bombardment to vary the oxygen vacancy density whilst monitoring the band-gap state with photoemission spectroscopy. Our results show that oxygen vacancies make the dominant contribution to the photoemission peak and that its magnitude is directly proportional to the oxygen vacancy density (see fig.1).

Oxygen vacancies on metal oxide surfaces have long been thought to play a key role in the surface chemistry. Such processes have been directly visualised in the case of the model photocatalyst surface TiO_2(110) in reactions with water and dioxygen [2]. These vacancies have been assumed to be neutral in calculations of the surface properties. However, by comparing experimental and simulated scanning tunnelling microscopy images and spectra (see fig. 2), we show that oxygen vacancies act as trapping centres and are negatively charged. We demonstrate that charging the defect significantly affects the reactivity by following the reaction of dioxygen with surface hydroxyl formed by water dissociation at the vacancies. Calculations with charged hydroxyl favour a condensation reaction forming water and surface oxygen adatoms, in line with experimental observations [3]. This contrasts with simulations using neutral hydroxyl where hydrogen peroxide is found to be the most stable product.

Support by the EPSRC (UK), Royal Society (London), and the European Union is gratefully acknowledged.

[1] S. Wendt et al, Science 320, 1755 (2008)
[2] O. Bikondoa, C. L. Pang, R. Ithnin, C. A. Muryn, H. Onishi, G. Thornton, Nat. Mat. **5**, 189 (2006)
[3] M. A. Henderson, Surf. Sci. 419, 174 (1999)
* Papageorgiou et al, Proc. Nat. Acad. Sci., in press; Yim et al, Phys. Rev. Lett., in press.

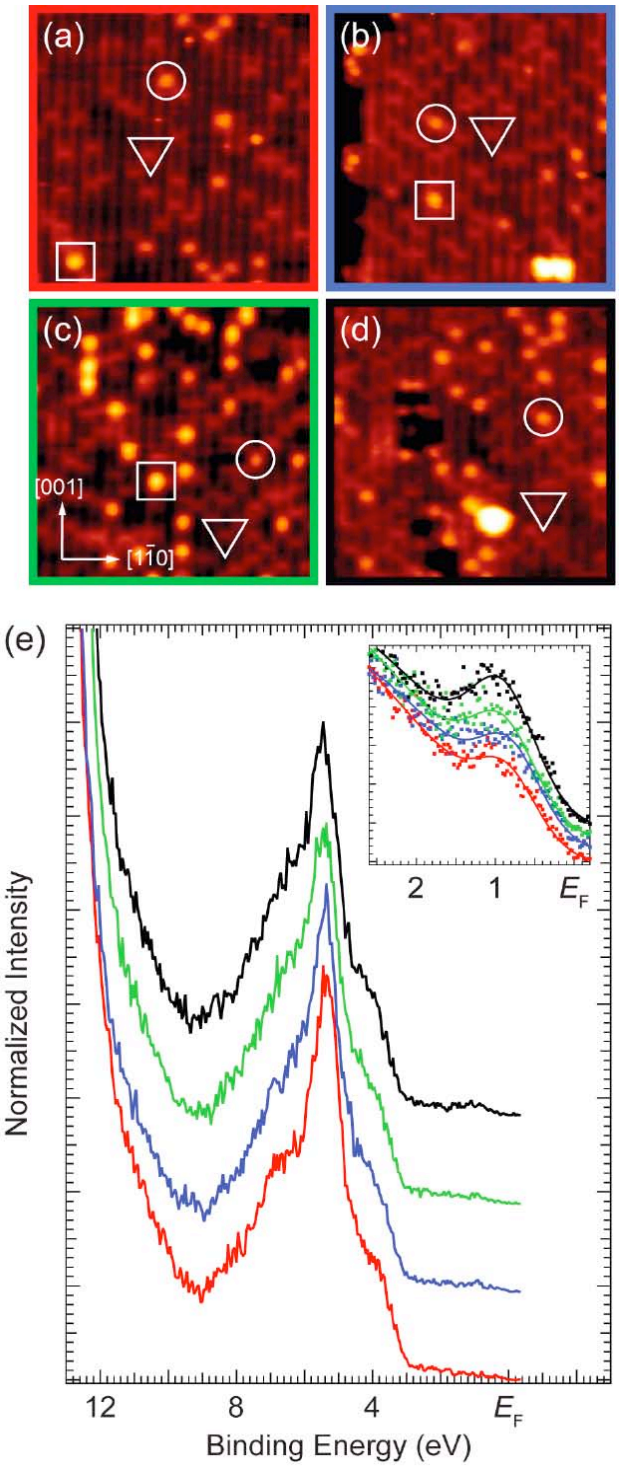

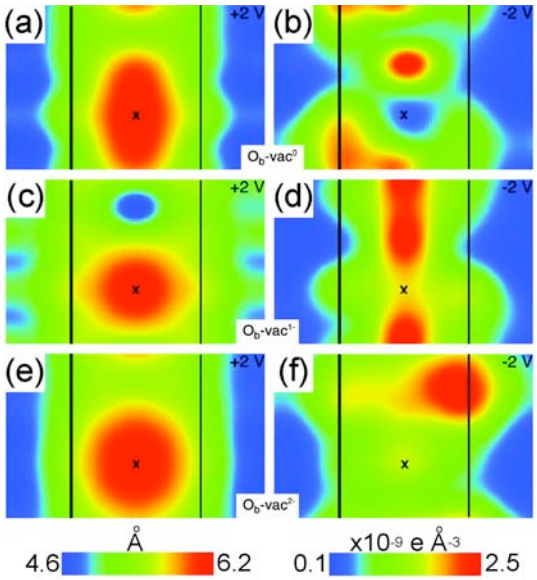

Fig. 2. Modeled STM and CITS appearance for O_b-vac. Simulated STM images (+2 V, 10^{-7} e Å^{-3}) and current maps (-2 V, same height above the surface as from the corresponding left-side topography) are shown for O_b-vac(0) in *A* and *B*, for O_b-vac(1-) in *C* and *D*, and for O_b-vac(2-) in *E* and *F*. Ti_{5c} rows are indicated by black lines and an 'X' marks the O_b-vac. STM simulations were performed with a tip-surface distance of ~5 Å.

FIG. 1. STM images (125 × 125 Å^2) of (a) the as-prepared TiO_2(110) surface (*r*-TiO_2) and its appearance following electron bombardment (kinetic energy ~75 eV, ~1 mA) for (b) 5 s, (c) 10 s, and (d) 20 s. Symbols indicate O-vacancies (triangles), bridging hydroxyls (circles) and hydroxyl pairs (squares). STM images were collected with a tunneling current ≤ 0.2 nA and a sample bias voltage of 1.3 V. (e) Corresponding UPS He I spectra of as-prepared *r*-TiO_2 (red) and after electron bombardment for 5 s (light blue), 10 s (green), and 20 s (black), all recorded under identical conditions. The inset in (e) shows the band-gap state region in more detail. The data points are shown as squares and the curves are the best fit to a Gaussian and polynomial background. The spectra are vertically offset for clarity. The spectra in (e) corresponding to each surface are color-coded with the color borders in (a)-(d). STM images and UPS spectra were collected at ~78 K and ~500 K, respectively.

Structure and energetics of azobenzene at coinage metals using dispersion-corrected DFT approaches

Erik R. McNellis[1], Jörg Meyer[1], and Karsten Reuter[1,2]

[1] *Fritz-Haber-Institut der Max-Planck-Gesellschaft, Faradayweg 4-6, D-14195 Berlin, Germany*
(corresponding author: K. Reuter, e-mail: karsten.reuter@ch.tum.de)

[2] *Lehrstuhl für Theoretische Chemie, Technische Universität München,*
Lichtenbergstr. 4, D-85747 Garching, Germany

The potential of a future molecular electronics has motivated many studies of functional organic molecules at metal surfaces. For first-principles theory it is particularly the possibly significant contribution of dispersive van der Waals (vdW) interactions in the molecule-substrate interaction that limits the common workhorse for large-scale calculations, density-functional theory (DFT) with semi-local exchange and correlation (xc) functionals. As higher-level theories including non-local vdW interactions by construction are presently barely tractable for corresponding system sizes, first insight could come from computationally inexpensive semi-empirical dispersion correction (DFT-D) schemes.

In these schemes an additional $C_6 R^{-6}$ pair potential term is added to the DFT Hamiltonian and heuristically reduced to zero for smaller interatomic distances by multiplication with a short-range damping function. While of proven accuracy for a range of molecular systems, the applicability of the DFT-D approach to organic molecules at metal surfaces is uncertain. This concerns notably the neglect of electronic screening. Partly covalently bonded molecules exhibit furthermore also shorter molecule-substrate bonds that therewith fall into the distance range where the uncertainties in the damping function mingle in an uncontrolled way with the deficiencies of the employed semi-local DFT xc functional. Aiming to elucidate by how much these shortcomings outweigh the improvement brought about by the account of long-range dispersive interactions we study the trends in energetics, geometric and electronic structure of the prototypical molecular switch azobenzene at the close-packed coinage metal surfaces using a range of differently constructed DFT-D schemes [1,2]. We obtain significantly changed adsorption geometries and a with up to ~2 eV sizable adsorption energy correction, which decisively affects the relative energetic ordering of the *trans* and *cis* metastable states of the switch. Comparison with

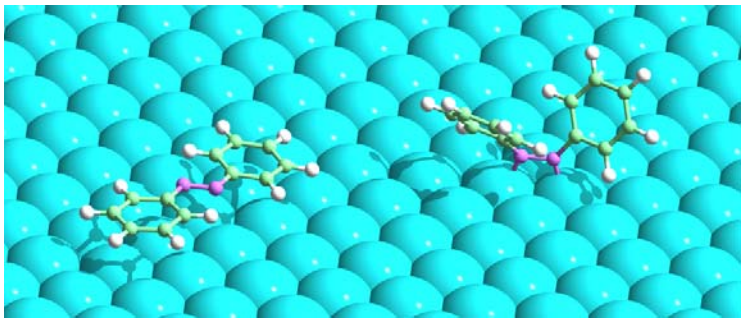

Fig. 1: Schematic adsorption geometry of trans (left) and cis (right) azobenzene.

detailed data from temperature programmed desorption and normal-incidence X-ray standing wave measurements for *trans* azobenzene at Ag(111) [3] shows that in particular the most recent DFT-D scheme due to Tkatchenko and Scheffler [4] provides excellent structural properties, albeit at a pronounced overbinding. Systematically analyzing the uncertainties in the semi-empirical approach we attribute this shortcoming primarily to the insufficient treatment of screening at the metal surface.

Funding by the DFG through SFB658 and computing time within the DEISA Extreme Computing Initiative are gratefully acknowledged.

[1] E. McNellis, J. Meyer, A. Dehghan Baghi, and K. Reuter, Phys. Rev. B 80, 035414 (2009)

[2] E.R. McNellis, J. Meyer, and K. Reuter, Phys. Rev. B 80, 205414 (2009)

[3] G. Mercurio, E.R. McNellis, I. Martin, S. Hagen, F. Leyssner, S. Soubatch, J. Meyer, M. Wolf, P. Tegeder, F.S. Tautz, and K. Reuter, Phys. Rev. Lett. (in press)

[4] A. Tkatchenko and M. Scheffler, Phys. Rev. Lett. 102, 073005 (2009)

Surface chain structure of formic acid on Au(111) studied by Microchannelplate (MCP) LEED

G. Pirug, M. Müller, and M. Kazempoor

Institut für Bio- und Nanosysteme (IBN3) and JARA-FIT,
Forschungszentrum Jülich GmbH, D 52425 Jülich, Germany
(corresponding author: G. Pirug, e-mail:g.pirug@fz-juelich.de)

Formic acid exists as a molecule in two different molecular structures, already. Two isomers can be distinguished according to the hydroxyl group being in a *cis* or *trans* configuration with respect to the carbonyl group. The corresponding energy difference amounts to 2 kcal/mole with the *cis* conformer as the more stable form.[1] H-bonding controls the formation of dimers and polymers in the vapor phase and the crystallization in the condensed phase. Based on the crystal structure as determined by X-ray diffraction techniques [2-4], the vibrational signature could be identified with respect to the coordination and conformation of the HCOOH molecules.[5-7]

The adsorption of formic acid on Au(111) surfaces is reversible molecular, as shown using high resolution energy electron spectroscopy (HREELS).[8] Apart from this weak adsorbate substrate interaction the ordering within the adsorbed layer is dominated by H-bonding. Based on the observed vibrational frequency of the out of plane δ(O-H) bending mode, which depends on the strength of the H-bonding [1], the formation of planar chains has been proposed excluding the presence of adsorbed monomers or dimers. The splitting of the C=O stretch mode into 2 vibrational losses at 1624 and at 1714 cm^{-1} suggests the formation of chains of *cis* molecules in the α-form rather than in the β-form, schematically shown in fig. 1.[7] Whereas the α-form has been constructed from H-bonded unperturbed formic acid monomers with reasonable H-bond lengths of 2.7 Å (fig. 1a), the β-form is drawn as identified in crystalline formic acid (fig 1b).[3]

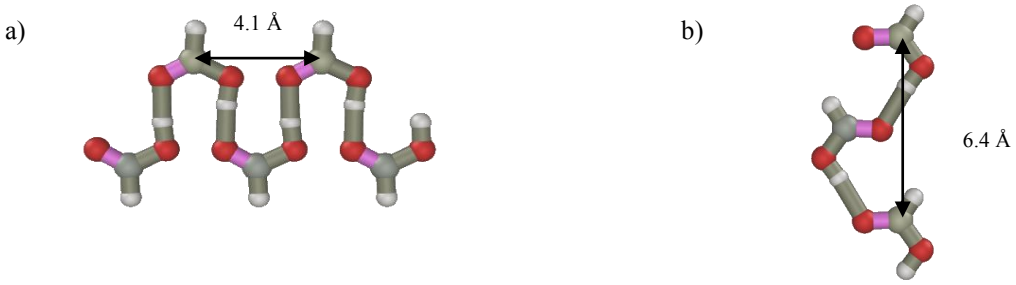

Fig 1: Planar chains of *cis* HCCOH a) α-form, b) β-form

The splitting of the C=O stretch mode has also been observed for adsorbed HCOOH layers on Pt(111).[9] Accordingly, Columbia at al. proposed a commensurate *rect.* (5 x $\sqrt{3}$) structure formed by planar chains of HCOOH in the α-form on Pt(111)

surface. But this structure model has not been proven so far. Our own attempt to find an ordered structure using a conventional LEED system failed due to the high electron beam sensitivity of the adsorbed layer, as well. The amplification of the diffracted electrons in a microchannelplate (MCP) LEED system allows a more gentle treatment due to a significant reduction of the primary electron current by $2x10^4$. The resulting LEED pattern together with a kinematic reconstruction is shown in Fig. 2.

a) b)

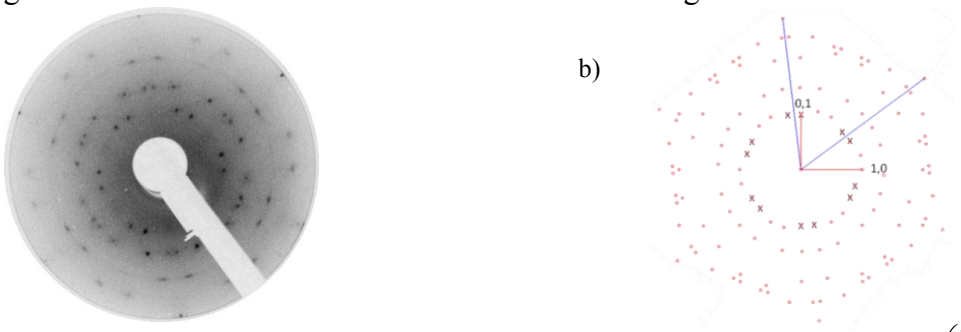

Fig 2: a) LEED pattern (65 eV) for HCOOH on Au(111), b) kinematic reconstruction of a p2mg structure $\begin{pmatrix} 1.9 & -.3 \\ 1.7 & 2.7 \end{pmatrix}$

First of all it should be noted, that the reconstruction of the Au(111) is not lifted consistent with the weak chemical adsorbate-substrate interaction. In addition a superstructure could be detected and identified as a rectangular incommensurate structure, as shown in Fig. 2b. Moreover missing (0 2n+1) spots point on a p2mg glide-mirror-plane symmetry.

Although both chain models exhibit glide-mirror-plane symmetry, the α-form can be excluded. These glide-mirror planes stand perpendicular to each other assuming that the unit vector of the α-form and β-form correspond to the short and long unit cell vector as determined by LEED, respectively. Consequently a two dimensional structure built by planar chains in the α- and β-form contains glide mirror planes perpendicular to the [0 1] or [1 0] direction. Hence only the β-form is consistent with missing (0 2n+1) spots. In addition, the unit vector of the β-form agrees with 6.4 Å reasonably well with 6.8 Å as determined by LEED. On the contrary, the unit vector of the α-form deviates with 4.1 Å significantly from the corresponding LEED value of 5.9 Å. With the latter value as the distance of adjacent chains a more or less uniform distribution of the C atoms in a rectangular unit cell is obtained.

Following the arguments given above the 2 vibrations at 1624 and 1714 cm^{-1} can no longer be related to a splitting of the C=O stretching mode due to the tautomerism in the α-form.

[1] T. Miyazawa, and K. S. Pitzer, J. Chem. Phys. 30, 1076 (1959)
[2] F. Holtzberg, B. Post, and I. Fankuchen, Acta Cryst. 6, 127 (1953)
[3] I. Nahringbauer, Acta Cryst. B34, 315 (1978)
[4] A. Albinati, K. D. Rouse, and M. W. Thomas, Acta Cryst. B34, 2188 (1978)
[5] R. C. Millikan, and K. S. Pitzer, J. Am. Chem. Soc. 80, 3515 (1958)
[6] Y. Mikawa, J. W. Brasch, and R. J. Jakobsen, J. Mol. Spectr. 24, 314 (1967)
[7] Y. Mikawa, R. J. Jakobsen, and J. W. Brasch, J. Chem. Phys. 45, 4750 (1966)
[8] M. Kazempoor, and G. Pirug, Appl. Phys. A87, 435 (2007)
[9] M. R. Columbia, A. M. Crabtree, and P. A. Thiel, J. Am. Chem. Soc. 114, 1231 (1992)

Single-Molecule Characterization and Manipulation of Bis-terpyridine Molecules

Nian Lin

Physics Department, The Hong Kong University of Science and Technology, Hong Kong, China

Bis-terpyridine (BTP) molecules are molecules in which two end terpyridine (TP) end groups are connected by an organic linker, as shown in Fig.1a. Due to the ability to bind to metal electrodes at the TP functions (Fig.1b) and to form long chains through TP-metal-TP coordination (Fig.1c), these molecules represent a prototype example as components for molecular electronics.

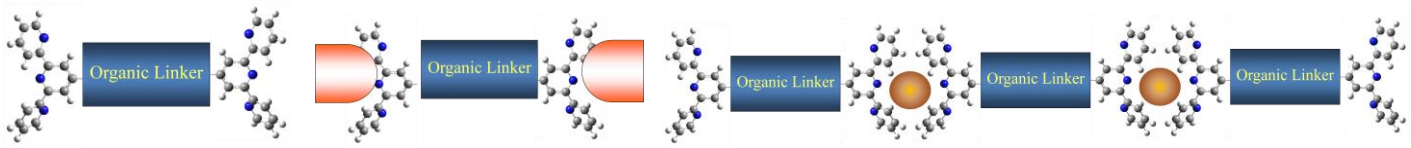

(a) (b) (c)

Fig. 1 Schematic structure of (a) BTP molecule (b) BTP attached to metal electrodes. (c) Coordination BTP chains.

In this presentation, I will discuss following three topics based on low-temperature STM studies on BTP molecules: (1) a BTP molecule showing single-molecule double heterojunction structure; (2) a series of BTP molecules exemplifying a novel mechanism to study single molecular conductance; (3) a BTP molecule behaving as a molecular rotor due to its intra-molecular torsional motion.

(1) A double heterojunction within a single molecule of a ~3nm length has been realized by covalently linking three molecular subunits with different energy gaps. As resolved by STM and confirmed by DFT calculations, the designed molecule as weakly adsorbed on a Cu(111) surface possesses highly localized molecular orbitals. It exhibits a narrow energy gap (~2.4eV) in the central subunit and a wider energy gap (>3.7eV) in the two end subunits, with energy levels aligned as a double heterojunction. Attachment of a single Cu atom to either end subunit lowers the energy levels of the local molecular orbitals without noticeably affecting other parts of the molecule. These studies prove the possibility of building molecular three-terminal devices and regulating their energy-level alignment (Fig. 2).

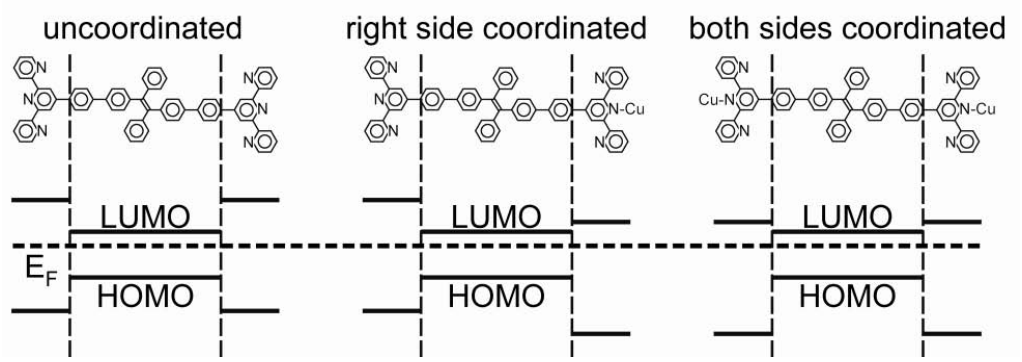

Fig. 2 Energy-level profiles of the double heterojunction BTP molecule and the manipulated staes by attachment of atoms.

(2) We have probed the superexchange coupling, a fundamental process occurred in charge transfer, at isolated molecules whose internal and external conditions are well-defined. The molecules under investigation possess an *s*-ϕ-*s* which consists of two identical molecular side groups linked symmetrically by a spacer. The coupling strength is obtained by measuring the energy splitting of the dimerized odd and even states of single molecules using scanning tunneling microscopy/spectroscopy, as illustrated in Fig. 3.. Our results confirm, at the single-molecule level, the theoretically predicated exponential decay behavior of the superexchange coupling, and derive a decay constant of 0.10 $Å^{-1}$ for poly-p-phenylene systems.

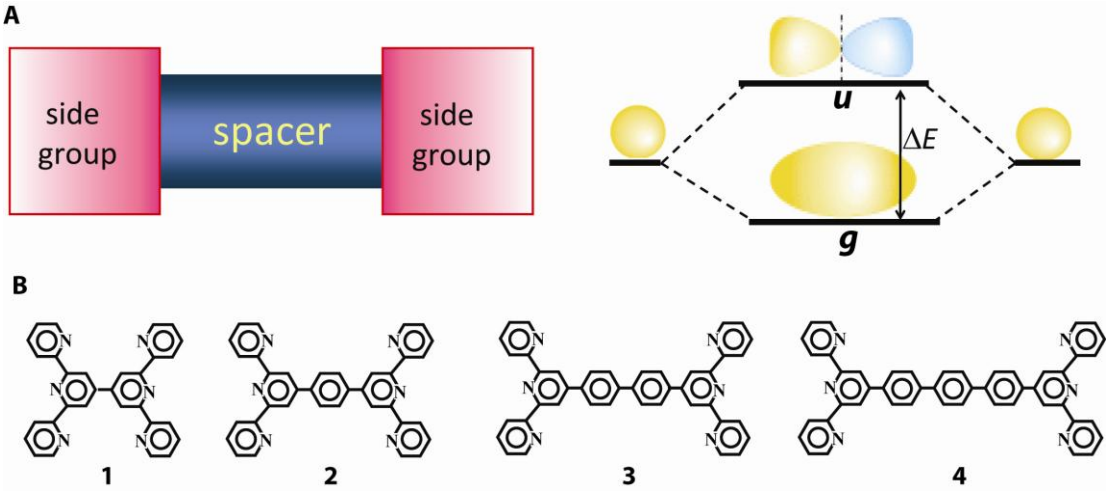

Fig.3 A. Left: Schematic drawing of a molecule of topology *s*-ϕ-*s*. Right: Orbital dimerization generates an even orbital (***g***) at a low energy and an odd orbital (***u***) at a high energy. B. Poly-p-phenylene bis-terpyridine compounds (**1**-**4**) used in our study.

(3) We study a BTP molecule with a "three-blade wheel" group as the linker ((Fig. 4a). As adsorbed on a surface, the two TP ends are fixed on the surface and the central wheel structure can vibrate/rotate around the longitudinal axis under the excitation of tunneling current. Three meta-stable configurations, which allow the intra-molecular torsion, are identified both experimentally and theoretically (Fig. 4b). A detail investigation of current-time spectra (Fig. 4c) acquired at different conditions shows that the excitation is a single-electron process with a threshold energy at 0.35eV.

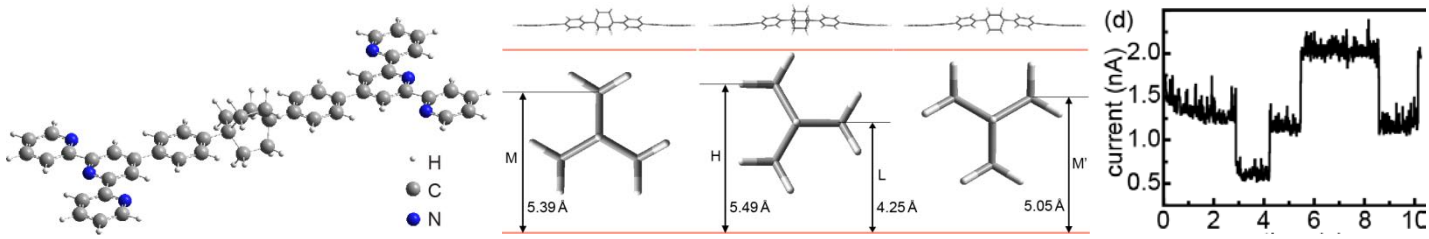

(a) (b) (c)

Fig. 4 (a) Molecular structure of the "three-blade wheel" BTP molecule. (b) DFT calculated three meta-stable configurations. (c) A typical current-time spectrum.

Changing directions: from in-plane structures to a new type of self-assembled monolayer

I. Cebula, C. Shen, C. Brown, M. Buck*

EaStCHEM School of Chemistry, University of St Andrews,
North Haugh, St Andrews KY16 9ST, United Kingdom
**mb45@st-and.ac.uk*

Supramolecular self-assembly involving hydrogen bonding, van der Waals interactions or metal coordination has become an established strategy to generate precisely defined surface structures [1-3]. To this end aromatic oligocarboxylic acids forming porous networks either through hydrogen bonding or metal coordination have been widely studied in UHV [4] and at the liquid-solid interface [5], including the electrified one [6]. While organisation into two dimensional structures parallel to the surface is usually observed for carboxylic acids, molecules can also adopt an upright orientation if carboxylates form as in the case of copper substrates [7,8].

Here we compare the solution based assembly of carboxylic acids such as isophtalic acid (IPA) and trimesic acid (TMA) (see Fig. 1) on two different substrate, namely clean Au(111) and Au(111) modified by a monolayer of Cu. Whereas, like in UHV, molecules adsorb in a flat lying geometry on the clean surface (Fig. 1, left) they adopt an upright orientation on the copper modified surface. Both IPA and TMA yield the same structure which is described by a rectangular $3x\sqrt{3}$ unit cell (9×5 Å^2). Furthermore, STM images of the mixed monolayer (Fig. 1, right) imply identical adsorption geometries. This is corroborated by XPS which reveals that in both cases two carboxylic acid moieties bind to the substrate as carboxylates. While

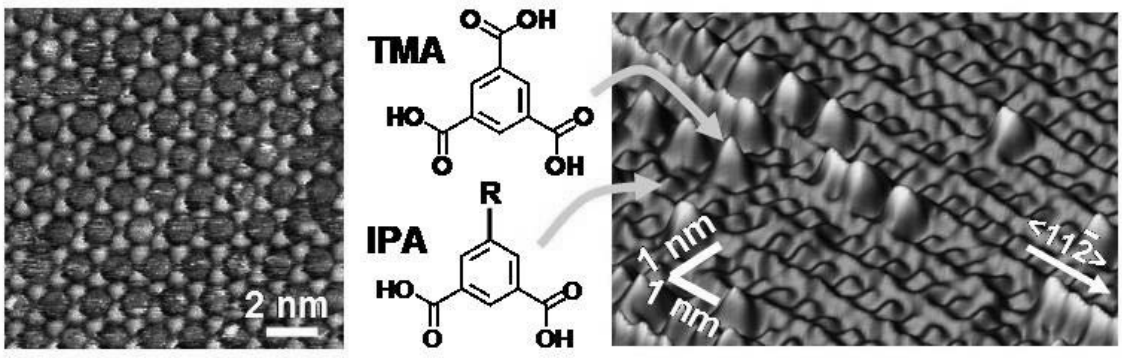

Fig. 1: (left) STM image of TMA lying flat on a clean Au(111) and forming a honeycomb structure. (right) STM image of a mixed monolayer of TMA and IPA (R=H) molecules standing upright on a Cu modified Au(111) surface. The additional COOH group of TMA pointing along the surface normal is reflected by the large protrusions.

IPA, thus, yields an inert surface, TMA produces a COOH functionalised surface which can be exploited further for surface chemistry. The results strongly suggest that the IPA moiety provides the basis for a new type of self-assembled monolayer (SAM). Key features are its versatility through variation of the residual moiety R, an excellent definition of the film structure and high rigidity due to the anchoring via two carboxylate moieties. It is, in particular, the latter which offers significant advantages over other types of SAMs with regard to the control of molecular orientation and tailoring of structures with molecular precision.

This work was supported by the European Union and EPSRC.

[1] J. V. Barth, Ann. Rev. Phys. Chem. 58, 375 (2007).

[2] T. Kudernac, S. B. Lei, J. Elemans, S. De Feyter, Chem. Soc. Rev. 38, 402 (2009).

[3] J.M. Gottfried, H. Marbach, Zeitschr. Physikal. Chem. 223, 53 (2009).

[4] A. Dmitriev, H. Spillmann, N. Lin, J. V. Barth, K. Kern, Angew. Chem. 42, 2670 (2003).

[5] L. Kampschulte, M. Lackinger, A. K. Maier, R. S. K. Kishore, S. Griessl, M. Schmittel, W. M. Heckl, J. Phys. Chem. B 110, 10829 (2006)

[6] Z. Li, B. Han, L. J. Wan, T. Wandlowski, Langmuir 21, 6915 (2005).

[7] C. C. Perry, S. Haq, B. G. Frederick, N. V. Richardson, Surf. Sci. 409, 512 (1998).

[8] A. Dmitriev, N. Lin, J. Weckesser, J. V. Barth, K. Kern, J. Phys. Chem. B 106, 6907 (2002).

Switching the surface texture by hydrogen intercalation

Thomas Brugger [1], Haifeng Ma [1], Marcella Iannuzzi [2], Simon Berner [1],
Adolf Winkler [3], Ari Seitsonen [2], Jürg Hutter [2], Jürg Osterwalder [1], and Thomas Greber [1]

[1] *Physik-Institut der Universität Zürich, Switzerland*
[2] *Physikalisch Chemisches Institut der Universität Zürich, Switzerland*
[3] *Institute of Solid State Physics, Graz University of Technology, Austria*

(corresponding author: T. Greber, e-mail: greber@physik.uzh.ch)

Intercalation - that is the reversible embedding of atomic or molecular species into a layered material - is a key concept for material's functionalization. Graphite is the prototype intercalation material in which the relatively weak bonding between sp^2 hybridized carbon sheets allows the packing of molecular species between subsequent layers. On transition metals, single sheets of carbon (graphene) and boron nitride (*h*-BN) may form corrugated, highly ordered nano-structures [1]. The lateral periodicity of these superstructures is determined by the lattice mismatch between the sp^2 layers and the substrate. For *4d* and *5d* transition metals the superlattice constant is about 10 times that of the free standing sp^2 layer. The deformation of the surfaces in the vertical direction - the *corrugation* - can reach values of 0.1 nm and is controlled by the bonding of B, C and N to the transition metals, where the lattice mismatch *and* the anisotropic bonding impose a dislocation network with out of plane strain in the sp^2 layer. The corrugation is the essential property that determines the texture and functionality of these superstructures and imposes a variety of new phenomena like single molecule trapping at room temperature [2, 3].
The surface texture of *h*-BN/Rh(111) *(nanomesh)* may be reversibly switched from corrugated to flat by intercalation of atomic hydrogen and back to corrugated by hydrogen desorption [4].

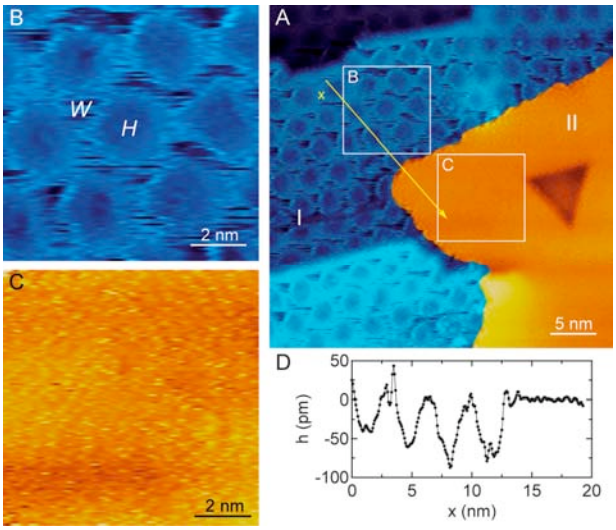

Fig. 1 Topographic scanning tunneling microscopy data of h-BN/Rh(111) after exposure to atomic hydrogen. a) Large scale image showing the coexistence of corrugated and flat h-BN (regions I and II respectively). b) Zoom into the pristine h-BN/Rh(111) area showing the wire (W) and the hole (H) regions. c) Zoom into the flat, hydrogen intercalated h-BN/H/Rh(111) area. d) Profile along the line in a) showing the transition from corrugated (I) to flat (II) h-BN.

The topographic STM data in Figure 1 show that after exposure to atomic hydrogen a new phase of single layer *h*-BN without strong long-range periodic corrugation (II) can coexist with the unaltered nanomesh (I). Phase II is basically flat whereas the pristine nanomesh (I) exhibits a corrugated hexagonal surface texture with a periodicity of 3.2 nm. The zoom-ins in Figure 1 display regions with and without corrugation. In the textured zoom-in eight nanomesh unit cells are seen, where the two topographic elements, the 'holes' and the 'wires' become visible [Fig. 1 b)]. The zoom into the untextured region is basically flat [Fig. 1 c)]. The height profile in Figure 1 d) shows the transition from the intact, corrugated region into the flat region. The surface in the flat region levels on the height of the wires, i.e. the loosely bound regions in the nanomesh. The He I photoemission spectra in Figure 2 confirm the flattening of the *h*-BN layer and indicate the hydrogen intercalation: The bands related to the holes of the nanomesh (π_β and σ_β) vanish after H exposure. Furthermore, annealing of the H exposed sample [*h*-BN/H/Rh(111)] to about 600 K recovers the original band splitting as a result of a switch-back to the pristine corrugation. Calculated N p_x densities of states (DOS) in the hole and wire sites are in line with [5] and have pronounced peaks at about 7 eV and 6 eV below E_F, respectively, which reproduce the experimentally observed σ band splitting of about 1 eV. The N p_x DOS with 1 monolayer of intercalated hydrogen feature the experimentally observed disappearance of the hole derived band in *h*-BN/Rh(111) under the exposure to atomic hydrogen (or deuterium).

In conclusion we have shown that exposure of a single layer of hexagonal boron nitride on Rh(111) to atomic hydrogen leads to a change of the surface texture where the corrugation vanishes. Mild annealing recovers the texture. Regarding similar sp^2-hybridized template systems the metallic analog of the nanomesh – graphene on Ru(0001) [3] – is an interesting candidate for further investigations and is expected to show similar switching behavior.

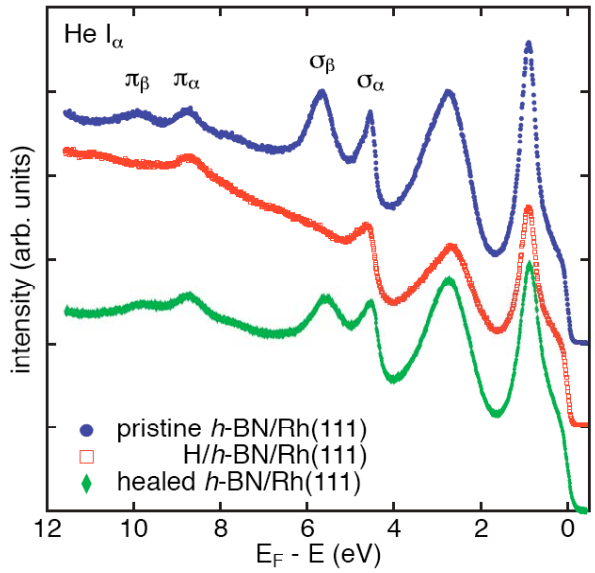

Fig. 2 h-BN/Rh(111) before (filled blue circles) and after (open red rectangles) hydrogenation; and after hydrogen desorption (filled green diamonds). He Iα normal emission UPS shows the vanishing of the σ_β and π_β peaks which are attributed to the holes (H) of h-BN/Rh(111) after exposure to atomic hydrogen, while the σ_α and π_α peaks corresponding to the wires (W) on h-BN/Rh(111), remain.

[1] T. Greber, arXiv 0904.1520.
[2] S. Berner et al. Angewandte Chemie Int. Ed. 46, 5115 (2007); H. Dil et al. Science 319, 1826 (2008).
[3] T. Brugger et al. Phys. Rev. B 79, 045407 (2009).
[4] T. Brugger et al. arXiv 0911.1317.
[5] R. Laskowski, P. Blaha, Th. Gallauner, and K.-H. Schwarz, Phys. Rev. Lett. 98, 106802 (2007).

Progress in surface photochemistry on nanoparticles: Internal energy distributions of NO from $(NO)_2$ on AgNPs of varied size.

D. Mulugeta[1], K. H. Kim[1], K. Watanabe[1,2], D. Menzel[1,3], and H.-J. Freund[1]

Fritz-Haber-Institut der Max-Planck-Gesellschaft, 14195 Berlin, Germany
(corresponding author: D. Menzel, e-mail: dietrich.menzel@e20.tum.de)

[1] *Fritz-Haber-Institut der MPG, Dept. CP, Faradayweg 4-6, 14195 Berlin, Germany*

[2] *New address: Oak Ridge National Laboratory, Center for Nanophase Materials Sciences, Oak Ridge, TN 37831-6487, USA*

[3] *Also at Physik-Department E20, Technische Universität München, 85748 Garching, Germany*

Nanoparticle-induced changes of adsorbate photochemistry[1,2] are of considerable interest; they are the subject of investigation of this group. At 3S'08 we reported about the photochemistry of NO dimers and Xe on Ag nanoparticles (AgNPs) supported on thin alumina films. We showed that for Xe on AgNPs plasmon excitation leads to a new mode of desorption which only exists on the NPs[3] and implies direct conversion of the plasmon-induced collective electron motion into atomic motion. For the quite complex photochemistry of the NO dimers[4], excitation of the Mie plasmon leads to strong enhancement of the photo-cross sections; off resonance a moderate enhancement suggests the influence of confinement of the excitations in the AgNPs. However, as judged from the translational energy of desorbing NO molecules the mechanism of the processes appears to be unchanged compared to Ag(111). It is assumed to proceed via the formation of transient negative ions (TNI) by hot electron tunneling into the adsorbate LUMO, as on Ag(111)[5] and rough Ag surfaces[6]. Size-dependent measurements show generally 1/R (~ surface/volume) dependence of the cross sections, while a strong additional enhancement for medium particle sizes (around 5 nm) occurrs for plasmon excitation which could be explained[7] by counteracting influences of the branching ratio of plasmon decay into hot electron production (increasing for decreasing particle size) and the total excitation cross section of the NPs (decreasing with the number of atoms per particle). Essentially unchanged translational energies of desorbing NO again suggest constant mechanism. Only for an excitation energy sufficient for forming holes in the d-band of Ag (here used 4.7 eV) these energies are strongly enhanced, which has been explained by a new mechanism via transient positive ions (TPI) formed by charge transfer from the d-holes at the surface[7].

In order to base these conclusions not only on the translational energy alone, and to improve our understanding of the mechanism, we have set up (1+1)-REMPI measurements of the desorbing NO and carried them out for the same range of particle sizes[8]. We find rotationally hot molecules which can be well characterized by Boltzmann plots, leading to a rotational temperature; the translational and rotational excitations are found to be positively correlated. The molecules are also hot vibrationally, but this excitation is decoupled from the rotational and translational excitations. These findings are in good agreement with the expectations of the TNI mechanism. There is no influence of excitation on or off the plasmon excitation, for excitation at 2.3 or 3.5 eV, corroborating the former conclusion that plasmon excitation only enhances the cross section via field enhancement without changing the mechanism. The exception is again found for 4.7 eV excitation and small particle sizes: all energies in the desorbing NO are dramatically enhanced, suggesting a new mechanism which we believe is indeed the TPI mechanism suggested before. The increase of internal and translational energies by this mechanism can be qualitatively understood in terms of a longer lifetime of the TPI as compared to the TNI because of the former's closer approach to the surface before it is quenched. The picture of the photo-processes induced in NO dimers on AgNPs by nanosecond laser pulses – for which the effects are linear in fluence and all excitations are well separated in time – is thus quite complete. Ongoing measurements with femtosecond pulses suggest dramatic changes in this regime which need more work to be fully understood.

We thank Walter Wachsmann for very able technical assistance.

Support by the Deutsche Forschungsgemeinschaft within priority program SPP1093 (Dynamik von Elektronentransferprozessen an Grenzflächen), the German-Israeli Foundation (Dynamics of Electronic Processes in a Confined Environment), the Fonds der Chemischen Industrie, and the NEDO International Joint Research Grant on Photon and Electron Controlled Surface Processes is gratefully acknowledged.

[1] V. P. Zhdanov and B. Kasemo, J. Phys.: Condens. Matter 16, 7131 (2004)

[2] K. Watanabe, D. Menzel, N. Nilius, and H.-J. Freund, *Chem. Rev.* 106, 4301 (2006)

[3] K. Watanabe, K. H. Kim, D. Menzel, and H.-J. Freund, *Phys. Rev. Lett.* 99, 225501 (2007)

[4] See e.g. C. I. Carlisle, and D. A. King, J. Phys. Chem. B 105, 3886 (2001)
T. Vondrak, D. J. Burke, and S. R. Meech, Chem. Phys. Lett. 327, 137 (2000)

[5] F. M. Zimmermann and W. Ho, Surf. Sci. Rep. 22, 127 (1995)

[6] R. T. Kidd, D. Lennon, and S. R. Meech, J. Phys. Chem. B 103, 7480 (1999)

[7] D. Mulugeta, K. H. Kim, K. Watanabe, D. Menzel, and H.-J. Freund, Phys. Rev. Lett. 101, 146103 (2008)

[8] Daniel Mulugeta, Ph.D. thesis FU Berlin 2010

Random 2D string networks based on divergent coordination assembly

Matthias Marschall[1,2], Joachim Reichert[1,2], Alexander Weber-Bargioni[2], Knud Seufert[1], Willi Auwärter[1], Svetlana Klyatskaya[3], Giorgio Zoppellaro,[3] Mario Ruben[3,4] and Johannes V. Barth[*]

*[1] Physik Department E20, TU München, James-Franck Str, D-85748 Garching, Germany; [2] Department of Physics & Astronomy, University of British Columbia, Vancouver, 2355 East Mall, V6T 1Z4, Vancouver, Canada; and [3] Institut für Nanotechnologie, Karlsruhe Institute of Technology, D-76021 Karlsruhe, Germany, [4]IPCMS-CNRS UMR 7504, Université de Strasbourg, 23 Rue du Loess, 67034 Strasbourg, France - *jvb@ph.tum.de*

The bulk properties of glasses and amorphous materials have been widely studied, but molecular-level elucidation of their structural details has been hindered by the lack of long-range order. Traditional experimental tools relying on ensemble averaging provided many important insights, however, the identification of local order characteristics requires imaging techniques addressing the individual constituents and topological defects. The direct, molecular-level investigation of random networks became notably possible with two-dimensional supramolecular systems assembled on well-defined surfaces that are amenable to *in situ* scanning tunnelling microscopy (STM) observations. For instance, a series of elementary structural motifs reflecting hydrogen bonding multiplicity was identified in kinetically trapped random networks obtained with nonsymmetrical cytosine molecules on a Au(111) surface under vacuum conditions at low temperatures. At solid-liquid interfaces, rod-like molecular building blocks with four peripheric isophthalic functional endgroups were shown to form porous networks with orientational symmetry that lack at the same time large-scale translational order. Here we explore 2D robust disordered coordination networks incorporating transition metal centers, realized with a surface-confined coordination assembly approach.

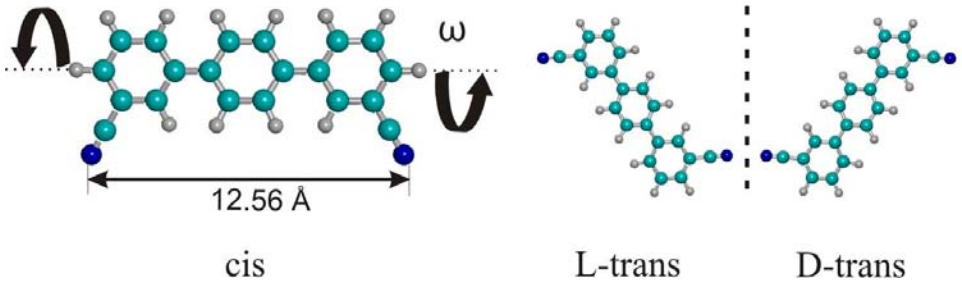

Fig. 1 – Deconvolution of the prochiral molecular linker [1, 1′;4′,1″]-terphenyl-3,3“-dicarbonitrile upon 2D confinement. The rotability around the phenyl backbone axis, indicated by the black arrows, accounts for the three different surface conformers: a, cis-conformation; b, L-*trans* and c, mirror-symmetric D-*trans* species.

We employed a ditopic linker that is non-linear, prochiral and deconvoluted in three stereoisomers upon two-dimensional confinement (cf. Fig. 1). Coordination assembly was induced by codeposited cobalt atoms engaging in lateral metal-ligand interactions with the linker carbonitrile endgroups. Our scanning tunneling microscopy data reveal irregular arrangements over the entire surface, in striking contrast to the highly regular honeycomb networks obtained with linear linker analogs. The present complex networks, realized both on Cu(111) and Ag(111), are based on a set of distinct three- and fourfold

Co-carbonitrile nodal coordination motifs of similar energy giving rise to bifurcation or string formation (cf. Fig. 2). The linker symmetry deconvolution and coordination multiplicity accounts for a library with many different coordination motifs entailing divergent assembly. We discuss how the interplay of - (i) local order induced by the metal-ligand interactions and (ii) multiple levels of isomerism and chirality - creates a topological conundrum to which the system's response is random reticulation.

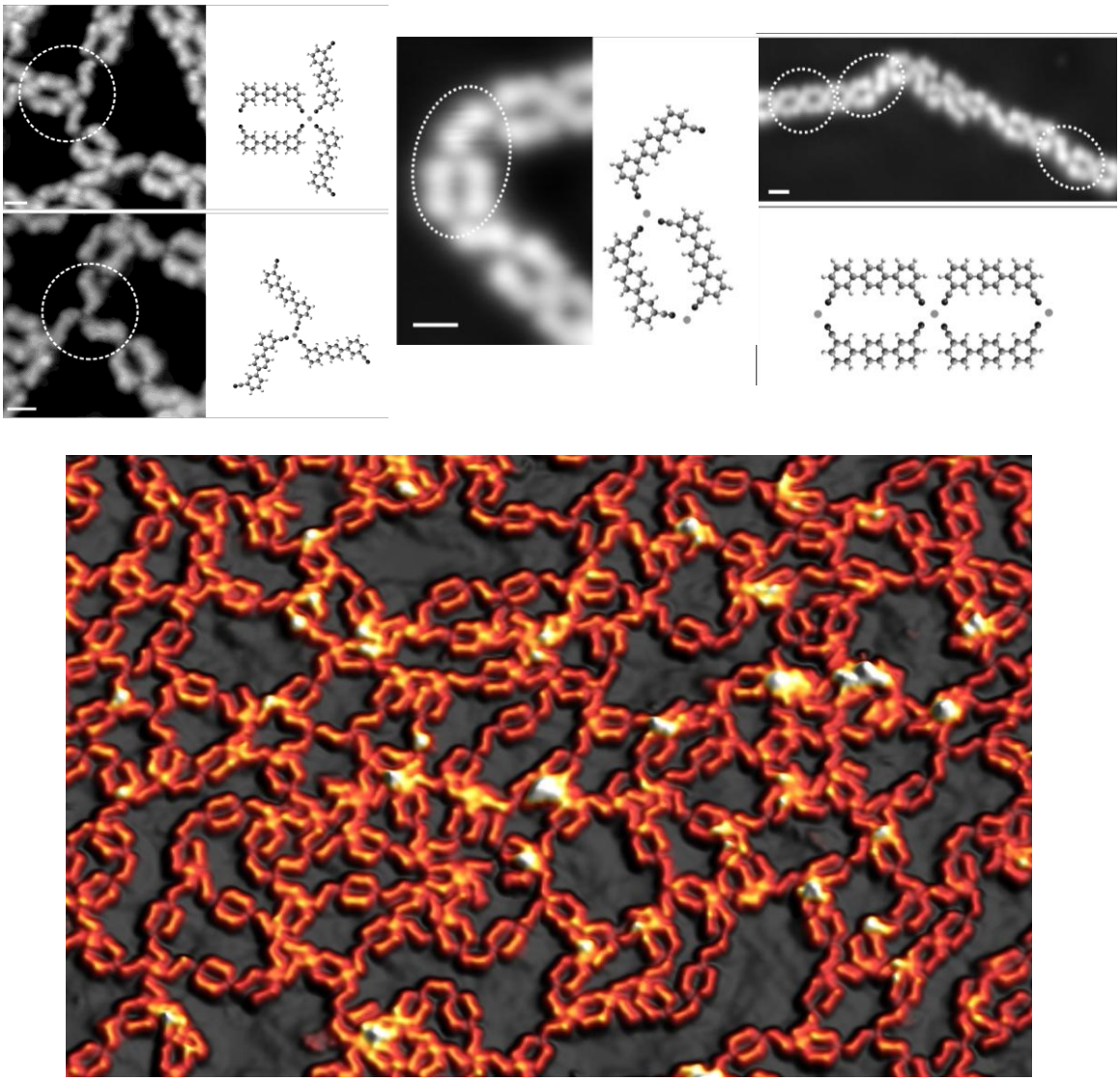

Fig. 2 – STM image of random coordination string network on Ag(111) with coexisting 3-fold and 4-fold coordination nodes. Important elementary bifurcation and chaining motifs underlying the disorderd layer formation are identified and modeled.

References: Otero, R. et al. *Science* **319**, 312 (2008); Blunt, M. O. et al. *Science* **322**, 1077 (2008); Zhou, H. et al. *J. Am. Chem. Soc.* **129**, 13774 (2007); Schlickum, U. et al., *Nano Lett.* **7**, 3813 (2007); Lin, N. et al., *Top. Curr. Chem.* **287**, 1 (2009); Kühne, D. et al. *J. Am. Chem. Soc.* **131**, 3881 (2009); Marschall, M. et al., *Nature Chem.*, in print (2010).

Towards the engineering of molecular architectures: exploiting local molecule-substrate interactions on composite surfaces to anchor or functionalize porphyrins

Florian Buchner, Elisabeth Zillner, Michael Röckert, Stephanie Gläßel, Hans-Peter Steinrück and Hubertus Marbach

Lehrstuhl für Physikalische Chemie II and Interdisciplinary Center for Molecular Materials (ICMM)
Universität Erlangen-Nürnberg, Egerlandstr. 3, 91058 Erlangen
(corresponding author: H. Marbach, e-mail: marbach@chemie.uni-erlangen.de)

The microscopic observation of organic molecules on well defined surfaces plays an important role in the understanding of fundamental chemical and physical processes as well as for the development of functional devices based on molecular architectures. Most approaches to generate such architectures are based on the self-assembly of a large number of molecules and correspondingly the "engineering part" mostly applies to a comparably large surface area. In this contribution we explore the possibility to pattern the surface by anchoring molecular building blocks at specific sites on a prestructured surface. Generally porphynoids appear to be ideal candidates to generate such functional molecular devices, since they combine an active site, usually a coordinated metal center, with a structure forming element [1]. In this contribution we investigate the dynamics and assembly of different tetraphenylporphyrins (TPP) and octaethyl porphyrins (OEP) on Ag(111), Cu(111), oxygen precovered Cu(111) (see Figure 1) and a composite Ni/Cu(111) surface (see Figure 2). The measurements are performed with scanning tunneling microscopy (STM) in ultra-high vacuum, mainly at room temperature. Based on STM images and movies the dynamics and assembly of the porphyrins are analyzed and the role of molecule-molecule and molecule-substrate interactions is discussed. The obtained findings demonstrate the possibility to locally anchor and/or functionalize (e.g. metalate [2-5]) the porphyrins on a prestructured surface. Corresponding experiments with porphyrins adsorbed on a Cu(11 1) surface prestructured with twodimensional Ni or oxygen islands of monoatomic height were successful and prove the principle of our approach as indicated in Figures 1 and 2. Based on these results a technique for the large scale patterning with porphyrins will be proposed.

This work has been funded by the DFG through Sonderforschungsbereich 583.

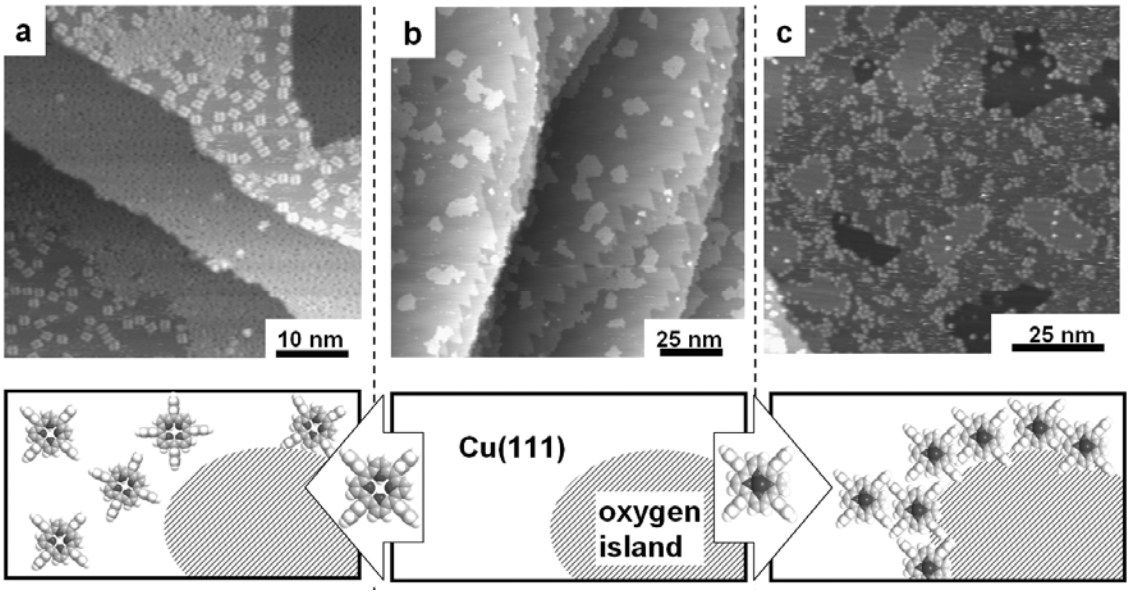

Figure 1. *RT STM images of a Cu(111) surface decorated with oxygen islan ds (b) with coadsorbed 2H TPP localized exclusivley on th e free Cu surface (a) and coadsorbed CoTPP(c) attached to the rim of the oygen islands..*

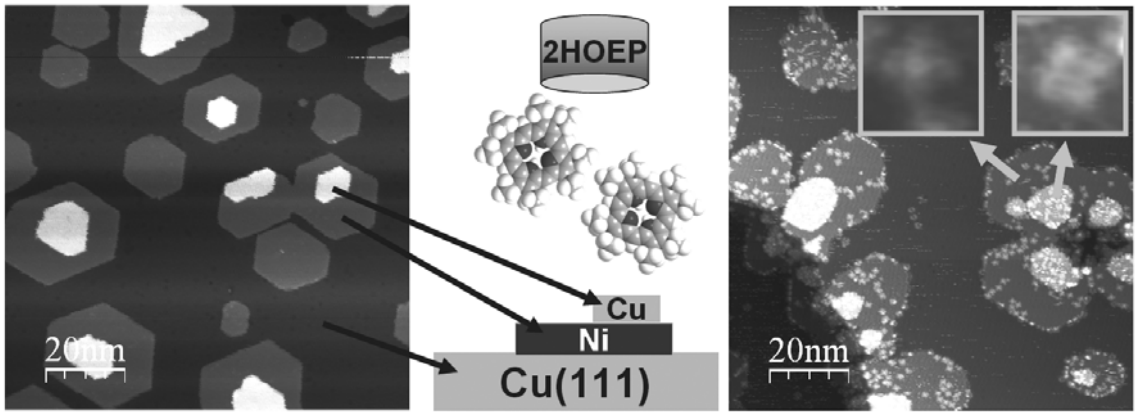

Figure 2. *RT STM images of a Cu(111) surface deco rated with Ni islands before (left) and after adsorption of 2HOEP (right). From the right micrograph it is aparent that the molecules are anchored on the Ni and "2nd floor" Cu islands. In the left insert the porphyrin exhibits a central protrusion indi cating the me talation of 2HO EP to NiOEP, whereas the porphyrin on the "2nd floor" Cu appears with a central protrusion indicative of 2HOEP.*

[1] J.M. Gottfried and H. Marbach, Z. f. Phys. Chem., 2009. **223**(1-2): p. 53-74

[2] F. Buchner et al., J. Phys. Chem. C, 2008. **112**(39): p. 15458-15465.

[3] F. Buchner et al., J. Phys. Chem. C, 2007. **111**(36): p. 13531-13538.

[4] F. Buchneret al., ChemPhysChem, 2007. **8**(2): p. 241-243.

[5] T.E. Shubina et al., JACS, 2007. **129**(30): p. 9476-9483.

The porous surface network of TAPP: Identifying adatoms and bonding mechanism

J. Björk, M. Matena[1], M. S. Dyer, M. Enache[1], T. A. Jung[1,2], M. Stöhr[1], and M. Persson

Surface Science Research Centre, Department of Chemistry, University of Liverpool, Liverpool L69 3BX, United Kingdom
(Corresponding author: J. Björk, e-mail: j.bjork@liverpool.ac.uk)

[1] *NCCR Nanoscale Science and Department of Physics, University of Basel, 4056 Basel, Switzerland*

[2] *Laboratory of Micro- and Nanotechnology, Paul-Scherrer-Institute, 5232 Villigen, Switzerland*

A novel approach of identifying adatoms in a metal—organic coordination network on Cu(111) is presented. The two-dimensional porous surface network of the 1,3,8,10-tetraazaperopyrene molecule (TAPP) is stabilised by Cu adatoms, which are coordinated to the nitrogen atoms of the molecule. The molecule—adatom interaction gives rise to an un-occupied resonance state, which provides a fingerprint for the presence of the adatoms. Furthermore, we illustrate that the chemisorption of the TAPP molecule in the network is mediated though the Cu adatoms, both characterised by a coordination bond lowering the nitrogen lone-pair orbitals, and an electron density from the adatoms into the LUMO of the TAPP molecule.[1]

The TAPP molecules on Cu(111) self-assemble into three main assembles at different annealing temperatures; a close-packed phase, a Cu-coordinated porous network, and a polymeric chain structure.[2] Low-energy electron diffraction experiments have shown that the porous network, which is formed at 150 °C, is commensurate with the Cu(111) substrate.[2,3] Total energy calculations using periodic density-functional theory (DFT) have shown that the porous network is stabilised by Cu adatoms. X-ray photoelectron spectroscopy experiments, together with simulated core-level shifts from periodic DFT have given further support to an adatom-coordinated porous network.[2]

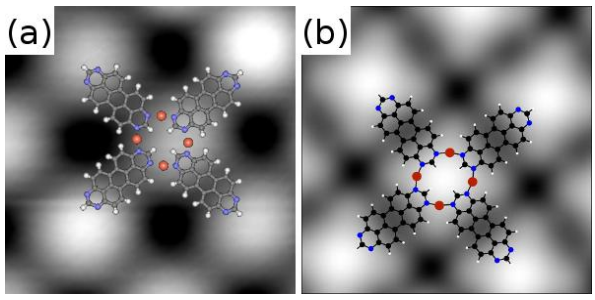

Figure 1: (a) Experimental constant current STM image, 3V/1pA, and (b) simulated constant current STM image with the LDOS integrated from the Fermi level to E_F+3.2 eV, of the porous network of TAPP on Cu(111), both images have the dimensions 4×4 nm^2.

Despite the strong indirect support for a Cu coordinated network, it is not possible to image the individual adatoms within the network using scanning tunnelling microscopy (STM) experiments. However, a characteristic bright protrusion has been observed in STM

experiments when tunnelling into the unoccupied states at high bias voltages, Fig. 1 (a). This bright protrusion appears in the centre of the common crossing of four neighbouring TAPP molecules and four adatoms, and it is well reproduced in the simulated constant current STM images, Fig. 1 (b). The bright protrusion is highly dependent on the Cu adatoms, as it disappears in the simulated STM images if the adatoms are removed. Finally, by analysing the electronic structure of an isolated overlayer of the Cu—TAPP network (i.e. with the Cu substrate removed) we are able to show that the bright protrusion originates from a single electronic state, observed as a resonance in the LDOS for the porous surface network.

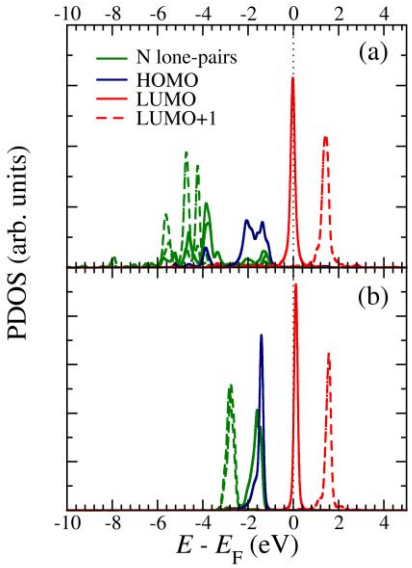

Figure 2: Projected density of states on the molecular orbitals of TAPP for (a) the porous network of TAPP, and (b) the porous network with the Cu adatoms removed while keeping TAPP and the Cu substrate in the porous network geometry.

We also illustrate, from periodic DFT, that the Cu adatoms are highly responsible for the formation of chemisorption bonds of the molecules in the porous network to the surface.[1] From calculations of the projected density of states (PDOS) onto the molecular orbitals of the isolated TAPP molecule, we show that the bonding is characterised by the lowering of the nitrogen lone-pair orbitals, and a partially filling of the LUMO of TAPP, Fig 2 (a). If the adatoms are removed from the network, while keeping TAPP and the Cu substrate in the network geometry, the nitrogen lone-pair orbitals of TAPP are hardly affected at all and the LUMO is shifted above the Fermi level, Fig 2 (b). This trend is also reflected in a Bader analysis of the different subsystems.[1] Thus the Cu adatoms both introduced a coordination bond, and donate electrons to the LUMO of TAPP.

This work was financially supported by the European Union through the Marie Curie Research Training Network PRAIRIES (MRTN-CT-2006-035810). Allocation of computer resources at the University of Liverpool is also gratefully acknowledged. The DFT calculations were performed using the VASP code.[4]

[1] J. Björk, M. Matena, M. S. Dyer, M. Enache, J. Lobo-Checa, L. H. Gade, M. Stöhr, T. A. Jung and M. Persson, in preparation.

[2] M. Matena, M. Stöhr, T. Riehm, J. Björk, S. Martens, M. S. Dyer, M. Enache, H. Wadepohl, J. Zegenhagen, T. A. Jung, and L. H. Gade, accepted by Chem. Eur. J.

[3] M. Matena, T. Riehm, M. Stöhr, T. A. Jung, L. H. Gade, Angew. Chem. Int. Ed. **47**, 2414 (2008).

[4] G. Kresse, and J. Furthmüller, Phys. Rev. B **54**, 11169 (1996).

Portrait of the potential barrier at metal-organic nanocontacts

Lucia Vitali[1,2,3], Giacomo Levita[1,4], Robin Ohmann[1], Alessio Comisso[5], Alessandro De Vita[5], and Klaus Kern[1,6]

[1] Max-Planck-Institut für Festkörperforschung, Heisenbergstr.1, D-70569 Stuttgart, (Germany)

[2] Centro de Fisica de Materiales, Centro Mixto CISC-UPV/EHU, San Sebastian (Spain)

[3] IKERBASQUE, Basque Foundation for Science, 48011, Bilbao, (Spain)

[4] INFM-DEMOCRITOS National Simulation Center and Center of Excellence for Nanostructured Materials (CENMAT) University of Trieste (Italy)

[5] Physics Department, King's College London Strand, London WC2R2LS (UK)

[6] Institut de Physique de la Matière Condensée, Ecole Polytechnique Fédérale de Lausanne (EPFL), CH-1015 Lausanne (Switzerland)

Electron transport through metal-molecule contacts greatly affects the operation and performance of electronic devices based on organic semiconductors and is at the heart of molecular electronics exploiting single molecule junctions. Much of our understanding of the charge injection and extraction processes in these systems relays on our knowledge of the potential barrier at the contact. Despite significant experimental and theoretical advances in our understanding of electron transport in molecular junctions, a clear rationale of the contact barrier at the single molecule level is missing. Here we exploit scanning tunneling microscopy to probe directly the nanocontact between a single molecule and a metal electrode. Contrary to the common assumption of a uniform barrier, we show here that this varies on the sub-molecular scale. Our experiments reveal that the local modulation, can amount to more than 1 eV across the 4-[trans-2-(pyrid-4-yl-vinyl)] benzoic acid molecule on the copper surface (see Figure 1). This spatial dependence reflects the interaction between specific molecular groups and the metal and allows clearly visualizing the processes leading to the formation of a built-in interface potential . Furthermore, this barrier can be opportunely be manipulated by the formation of specific metal-organic nano-contact.

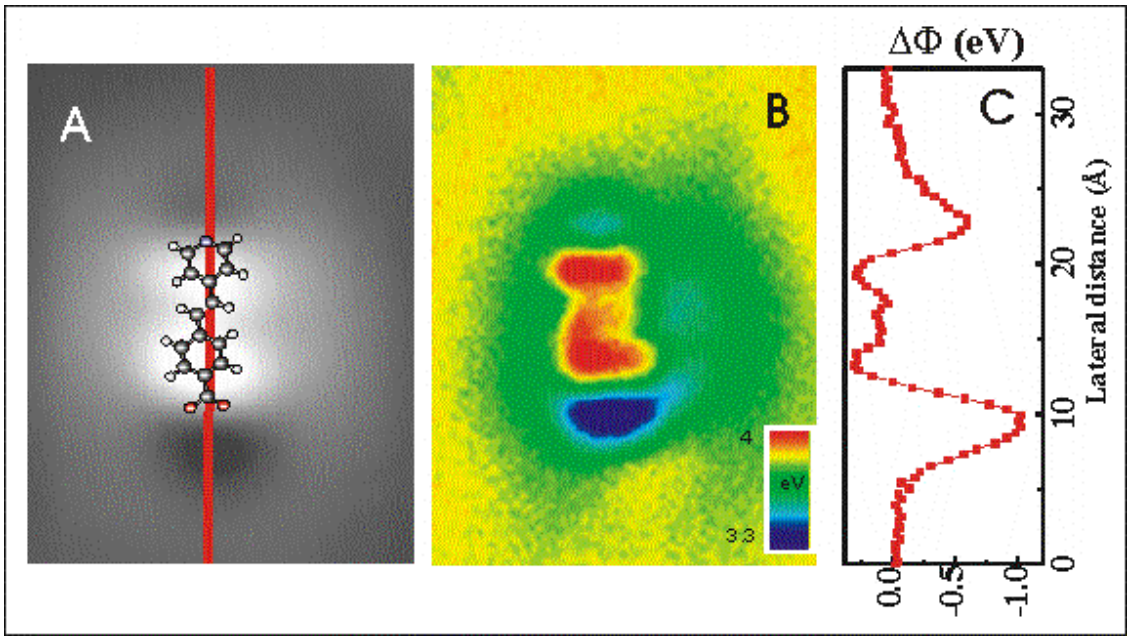

Figure 1: Potential barrier across the plane of a PVBA-Cu(111) nanocontact.
A. STM topographic image of the adsorbed molecule. B. Simultaneously acquired map of the potential barrier across the molecular plane averaged between tip and sample. C. work function variation along the molecular axis.

Tuesday

Fabrication of Graphene and Graphenoid 2D-Materials from Self-Assembled Monolayers

A. Turchanin, C.T. Nottbohm, M. Büenfeld, X. Zhang, A. Beyer, R. Stosch[1], D. Weber[1], T. Weimann[1], J. Mayer[2], Ch. Kisielowski[3], A. Gölzhäuser*

Fakultät für Physik, Universität Bielefeld, Bielefeld, Germany
[1]Physikalisch Technische Bundesanstalt, Braunschweig, Germany
[2]Gemeinschaftlabor für Elektronenmikroskopie, RWTH Aachen, Aachen Germany
[3]National Center for Electron Microscopy, Berkely, CA, USA

A route for the fabrication of graphene and graphenoid (similar to graphene) materials, whose electrical and mechanical behavior as well as surface functionalization can be tuned, is presented. Self-assembled monolayers (SAMs) of aromatic biphenyls are cross-linked by electron irradiation into mechanically stable carbon films and then detached from the surface. This results in mechanically stable carbon nanomembranes with a thickness of 1 nm and sizes up to several cm^2. Upon annealing the nanomembranes at ~1200K, the cross-linked SAMs transform into a graphitic phase that consists of patches of single layer graphene and graphenoids [1]. This transition is accompanied by a drop of the sheet resistivity from $\sim 10^8$ to $\sim 10^2$ kΩ/sq and a mechanical stiffening from ~10 to 50 GPa. Hence, this method produces two-dimensional materials with tunable conductivity and stiffness. When transferred onto SiO_2/Si substrates, they can be visualized by Raleigh interference contrast. By using SAMs of appropriate biphenyls, a chemical surface functionalization of can be achieved, which allows their tailoring for applications. Devices and applications are discussed.

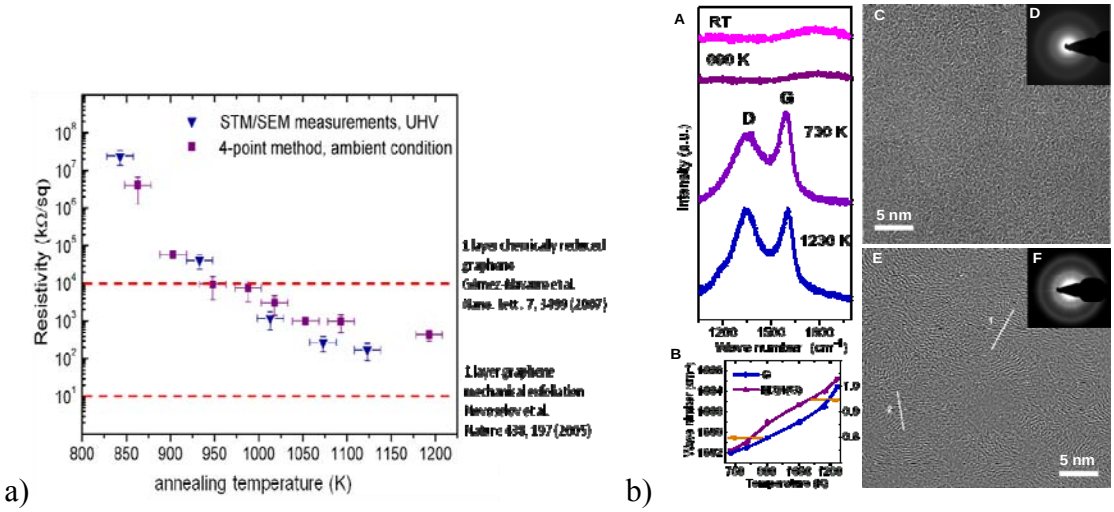

Sheet resistivity of nanomembranes as a function of temperature during pyrolysis a) with increasing annealing temperature, the sheet resistivity decreases. b) A) Raman spectra before and after pyrolysis at different temperatures. B) Temperature dependence of the frequency shift of the Raman bands C,E) HRTEM-images before and after pyrolysis (from [1]).

[1] A. Turchanin, A. Beyer, Ch. T. Nottbohm, X. Zhang, R. Stosch, A. Solugubenko, J. Mayer, P. Hinze, T. Weimann, A. Gölzhäuser, Adv. Mater. 21, 1233 (2009).

e-mail: ag@uni-bielefeld.de

On-surface cyclodehydrogenation: A route to chemically tailored nanographenes and graphene nanoribbon heterojunctions?

Kamel Aït-Mansour[1], Pascal Ruffieux, Jinming Cai, Marco Bieri, Rached Jaafar, Matthias Treier[2], Stephan Blankenburg, Carlo A. Pignedoli, Daniele Passerone, Teodoro Laino[3], Ralph Rieger[4], Xinliang Feng[4], Klaus Müllen[4], Oliver Gröning, and Roman Fasel

Empa, Swiss Federal Laboratories for Materials Testing and Research, nanotech@surfaces Laboratory, 3602 Thun and 8600 Dübendorf, Switzerland
(corresponding author: R. Fasel, e-mail: roman.fasel@empa.ch)

[1] *present address: Ecole Polytechnique Fédérale de Lausanne, IPMC, 1015 Lausanne, Switzerland*

[2] *present address: Université de Strasbourg, I.S.I.S., 67000 Strasbourg, France*

[3] *IBM Zurich Research Laboratory, 8803 Rueschlikon, Switzerland*

[4] *Max-Planck Institute for Polymer Research, 55128 Mainz, Germany*

Atomically thin sheets of sp^2-bonded carbon – so-called graphene and related structures – bear enormous potential for applications in future electronic devices. However, processability and tailoring of graphene-derived structures still represents a major hindrance on the way towards applications. We investigate on a surface chemical route that allows for the fabrication of tailored nanographenes and graphene nanoribbon heterojunctions.

In a first example, the cyclodehydrogenation of the prototypical polyphenylene cyclohexaphenylene to tribenzocoronene on Cu(111) as studied by scanning tunneling microscopy (STM) is discussed. We find that the thermally induced cyclodehydrogenation proceeds via two intermediate steps which can both be stabilized on the Cu(111) surface, yielding unprecedented insight into a dehydrogenative intramolecular aryl-aryl coupling reaction. The experimental observations are rationalized by hybrid *ab initio* / empirical simulations. Two additional reaction intermediates which are however not stable on Cu(111) are identified by the simulations.

In a second example, which deals with a hydrogen-bonded surface-supported binary molecular superlattice (Fig. 1), it is shown that cyclodehydrogenation can not only be induced thermally, but also in a highly selective way by means of the STM tip. Two sterically confined phenyl rings connected at 1,2-positions to a terminal benzene can efficiently be fused to a planar triphenylene unit by application of voltage pulses. Since this process is fully

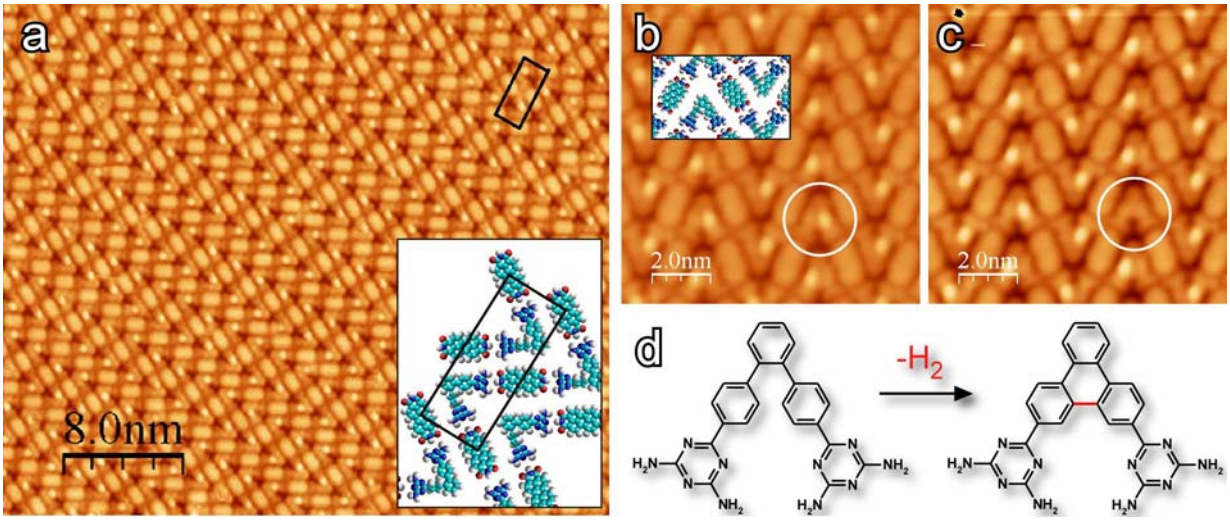

***Fig. 1**: Tip-induced cyclodehydrogenation in a binary supramolecular lattice. (a) Overview STM image of the molecular superlattice and molecular model.(b),(c) STM images before (b) and after (c) application of a -4V pulse at the location indicated by the white circle. (d) Cyclodehydrogenation reaction scheme.*

local, i.e. only the targeted molecule is reacted, it allows for the "writing" of nanopatterns of cyclodehydrogenated molecules in the binary supramolecular lattice.

Last but not least, the application of tip-induced cyclodehydrogenation for the fabrication of graphene nanoribbon (GNR) heterojunctions is discussed. Very recently, we have shown that graphene nanoribbons with atomically defined edge periphery, width and topology can be assembled by the surface-assisted polymerization of halogen-functionalized molecular building blocks followed by thermally induced cyclodehydrogenation [1,2]. Here, it will be shown that such GNRs may be trapped in intermediate situations where parts of the polymer have not yet or not fully cylodehydrogenated into planar GNRs. Tip-induced cyclodehydrogenation should allow to control the degree and lateral extent of cyclodehydrogenation and thus open a route to the fabrication of GNR heterojunctions with molecular precision.

Financial support form the Swiss National Science Foundation and generous allocation of computing time at the CSCS is gratefully acknowledged.

[1] please also see the presentation by Pascal Ruffieux

[2] J. Cai, P. Ruffieux, R. Jaafar, M. Bieri, T. Braun, S. Blankenburg, M. Muoth, A. P. Seitsonen, M. Saleh, X. Feng, K. Müllen, R. Fasel, *submitted*.

Light-emitting Peapods for Photonic Devices

Claudia Ambrosch-Draxl, Matus Milko, J. Gao[1], F. Cordella[1], P. Blondeau[2], E. Menna[2], B. Bártová[3], C. Hébert[3], and M. A. Loi[1]

Chair of Atomistic Modelling and Design of Materials, University of Leoben, Franz-Josef-Straße 18, A-8700 Leoben, Austria
(corresponding author: C. Ambrosch-Draxl, e-mail: cad@unileoben.ac.at)

[1] *Zernike Institute for Advanced Materials, University of Groningen, The Netherlands*

[2] *ITM-CNR and Dipartimento di Scienze Chimiche, Università di Padova, Padova, Italy*

[3] *EPFL SB-CIME & IPN-LSME, Bâtiment MXC, Lausanne, Switzerland*

Nano-hybrid materials consisting of single-wall carbon nanotubes (SWNT) with endohedrally bound organic molecules combine the unique mechanical and electronic properties of nanotubes with the optical characteristics of π-conjugated molecules. Hence they are considered as promising candidates for nano-devices in opto-electronic applications. Only recently it could be shown [1] that such peapods can be synthesized, and indeed emit light in the visible range of the spectrum.

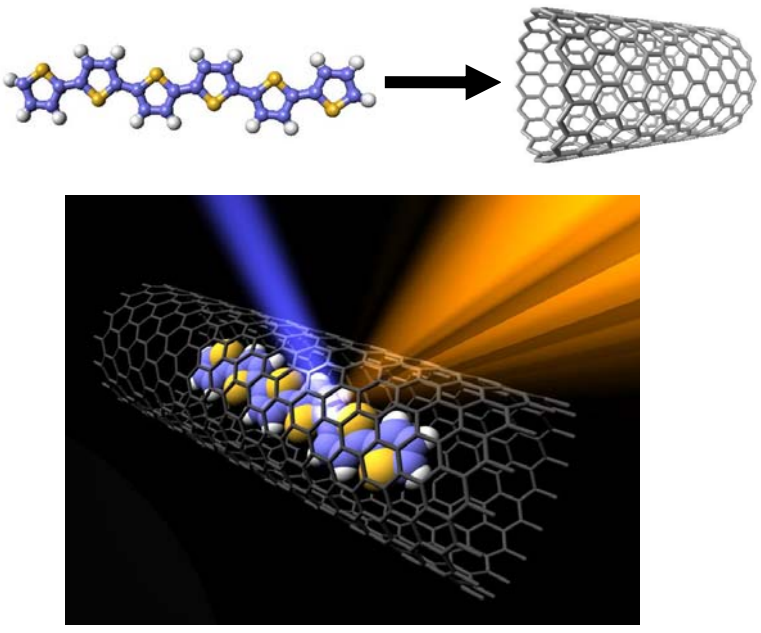

Figure 1: Top: schematic of the encapsulation of sexithiophene in SWNTs. Bottom: cartoon of the light emitting peapod. The yellow color indicates the sulfur, blue the carbon, and white the hydrogen atoms.

Raman spectroscopy and high resolution transmission electron microscopy have revealed the endohedral position of the guest molecules. Surprisingly, these are not located in a single array in the center of the tube but are instead arranged in two lines along the sidewalls. Density functional theory (DFT) including van der Waals interactions provides the maximal binding energy for the molecules in cofacial arrangement. The hybrids show photoluminescence in the visible range while a reduced lifetime of the excited state is symptomatic of molecule – SWNT electronic interactions.

Here we investigate in more detail structural, electronic and optical properties of the oligo-thiophenes series embedded in zig-zag nano-tubes with various diameters. From our first-principles calculations we find the systems to be exclusively bound through van der Waals forces. This observation is confirmed by the electronic structure as it appears as a mere superposition of the bands coming from the two components. Nevertheless, the electronic states are not purely aligned with respect to the vacuum level, but corrections arising from the tube curvature and corresponding charge rearrangements have to be taken into account. Our analysis allows for a prediction of the level alignment, which in turn could be used for the design of such materials yielding particular optical properties.

In this view, we analyze all possible optically allowed transitions between the molecule and its host that lead to new peaks in the spectra. We conclude that the excitonic effects which govern the low-energy emission in the isolated molecules are substantially altered by the interaction of the pea and the pod in the excited state.

Support by the Fonds zur Förderung der Wissenschaftlichen Forschung (project I107), is gratefully acknowledged.

[1] M. A. Loi, J. Gao, F. Cordella, P. Blondeau, E. Menna, B. Bártová, C. Hébert, S. Lazard, G. A. Bottone, M. Milko, and C. Ambrosch-Draxl, Adv. Mater. (2009), in print.

Bottom-up fabrication of graphene nanostructures using molecular precursors

J. Cai, P. Ruffieux, M. Bieri, R. Jaafar, T. Braun, S. Blankenburg, M. Muott[1], A. P. Seitsonen[2], M. Sahleh[3], X. Feng[3], K. Müllen[3], and R. Fasel

Empa, Swiss Federal Laboratories for Materials Testing and Research, nanotech@surfaces Laboratory, 3602 Thun and 8600 Dübendorf
(corresponding author: P. Ruffieux, e-mail: pascal.ruffieux@empa.ch)

[1]*Swiss Federal Institute of Technology Zurich, Department of Micro- and Nanosystems,* 8092 Zürich, Switzerland

[2]*IMPMC, CNRS and Université Pierre et Marie Curie,* 75252 Paris, France

[3]*Max-Planck Institute for Polymer Research,* 55128 Mainz, Germany

Due to its outstanding electronic and mechanical properties, graphene, a sheet of sp^2 bonded carbon atoms, has emerged as a promising material for the fabrication of nanoscale devices. Its exceptional electronic properties, such as the high charge carrier mobility, resistance to high current densities and ballistic transport over submicron scales are firmly related to the energy spectrum near the Fermi level, which is best described by massless Dirac fermions.

On the other hand, pristine graphene is a semimetal and thus not suitable for most electronic and optoelectronic applications, which generally require a semiconductor with a finite band gap. This limitation can potentially be overcome by structuring graphene on the nanometer scale, creating band gaps suitable for room temperature electronic applications [1].

Current efforts in this direction mainly concentrate on lithographic techniques or chemical treatments. However, both methods are limited with respect to their resolution and precision. In order to achieve graphene-based materials relevant for room temperature electronic applications a fabrication method allowing for atomic precision is required.

Here, we demonstrate the bottom-up fabrication of surface-supported 'porous graphene' based on a simple surface-chemical route (Fig. 1, [2]) where the precursor molecules are dehalogenated upon adsorption on the surface and covalently couple upon annealing. The resulting 2D polymer with atomically controlled pore structure is the first example of a sp^2-hybridized superhoneycomb network [3].

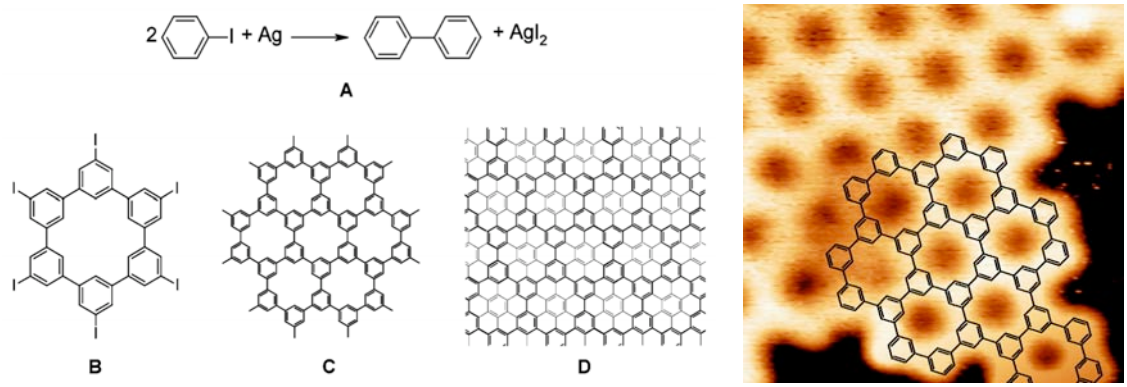

Fig. 1. (*left*) (A) Mechanism of the silver-promoted aryl-aryl coupling of iodobenzene to biphenyl. (B) Structure of cyclo-*m*-phenylene. (C) Structure of the polyphenylene superhoneycomb network. (D) Structural relationship of the plyphenylene superhoneycomb network. (*right*) Porous graphene. STM image of an edge of the sp^2-hybridized 2D polymer (with overlaid chemical structure) supported on a Ag(111) surface.

More recently, we have extended this surface-chemical approach to the fabrication of graphene nanoribbons (GNR). In addition to the surface-assisted coupling of the precursor molecules needed to form one-dimensional polymer chains temperature-induced cyclodehydrogenation is used for creating fully aromatic nanoribbons [4, 5]. This two-step process allows for the atomically precise fabrication of ultranarrow GNRs whose width, edge geometry and topology are exactly defined by the precursor monomer. The on-surface synthesis and characterization of two armchair GNRs with different widths and edge geometries will be discussed in detail in order to show the versatility of this approach.

Financial support form the Swiss National Science Foundation is gratefully acknowledged.

[1] V. Barone, O. Hod, and G. E. Scuseria, *Nano Letters* **6**, 2748 (2006).

[2] M. Bieri, M. Treier, J. Cai, K. Aït-Mansour, P. Ruffieux, O. Gröning, P. Gröning, M. Kastler, R. Rieger, X. Feng, K. Müllen, and R. Fasel *Chem. Commun*. 6919 (2009).

[3] N. Shima and H. Aoki, Phys. Rev. Lett., 1993, 71, 4389–4392.

[4] J. Cai, P. Ruffieux, R. Jaafar, M. Bieri, T. Braun, S. Blankenburg, M. Muoth, A. P. Seitsonen, M. Saleh, X. Feng, K. Müllen, R. Fasel, *submitted*.

[5] see also the presentation by Roman Fasel

Understanding graphene formation on transition metals

G. Dong, D.W. van Baarle, M.J. Rost and J.W.M. Frenken

Kamerlingh Onnes Laboratory, Leiden University, PO Box 9504, 2300 RA Leiden, The Netherlands
(corresponding author: J.W.M. Frenken, e-mail: Frenken@physics.leidenuniv.nl)

Graphene, single-layer graphite, is drawing much attention because of its special properties and potential use in future-generation electronics [1]. However, achieving high quality graphene reproducibly remains a challenge. Small quantities of high-quality graphene can be achieved for research purposes by use of the so-called "Scotch-tape" method. Most other methods, in particular those based on the direct growth of graphene, suffer from high defect densities caused by multilayer growth, chemical contamination, etc. These imperfections seriously influence the properties and the stability of the graphene.

Hydrocarbon chemical vapor deposition (CVD) on transition metals (TMs) provides a practical method to get precisely one monolayer of graphene[2], as TMs are catalysts for hydrocarbon decomposition, while newly arriving hydrocarbon molecules do not stick or decompose on graphene. In addition, because the solubility of carbon in TMs often highly depends on temperature, several groups have succeeded in also producing graphene from carbon that segregates from the near-surface region in the metal [2, 3]. The graphene formation process typically takes place at high temperatures, at which the interaction between carbon and TMs is very complex. An essential part of the process, such as the carbon segregation, may be taking place during cooling down of the sample. Often the properties of graphene are measured only at room temperature or below. From such observations it is very difficult to distinguish which source of carbon, segregated or directly deposited, has been responsible for the formation of the graphene layer and what the precise mechanism has been. This is why only a limited number of experiments has been devoted to the kinetic processes of this system [4, 5]. In addition, most of the experiment methods can be used *in-situ*, i.e. under growth conditions at high temperature, do not have atomic resolution. Obviously, atomic-scale measurement during graphene growth are really necessary, as they are essential for understanding the nucleation and growth mechanisms, which should form the basis for strategies to improve the quality of graphene.

Our scanning tunneling microscope (STM), which has been optimized for (fast) scanning at high sample temperatures and during substantial temperature variations [6, 7], has enabled us to follow the reaction and growth of graphene *in-situ*. We take on the exposure of clean Rh(111) to ethylene as a typical example of carbon deposition on TMs. Due to its lattice mismatch, graphene forms moiré patterns on Rh(111), which work as a 'magnifying glass' for atomic defects in the graphene. In this way, we get atomic-scale information about the graphene overlayer, even from STM images without direct atomic resolution. Our STM movies provide detailed observations of this growth system, from which we obtain for example the temperature ranges for graphene and carbide formation and for their stability, the

dependence of the form ing structures on tem perature and the role of the precise initial conditions. Armed with this inform ation, we can control t he qualit y of the graphene by choosing the proper starting situa tion and setting the conventional growth parameters, in this case the te mperature and the ethy lene pressure. Figure 1 shows an exa mple where we fir st seeded a Rh (111) surface with graphene is lands b y heating a pre-deposited sam ple fro m room temperature to 975K, after which we deposited further ethylene at that high temperature surface to obtain precisely one atom ic layer of graphene with a relatively high cry stalline quality. We a lso dem onstrate how to av oid carbide formation for this sy stem, by forcing the dissolved carbon t o form graphene when it segre gates. Together, these elements lead to an optimized growth recipe for low-stress, single- orientation, singl e-crystalline, single-lay er graphene.

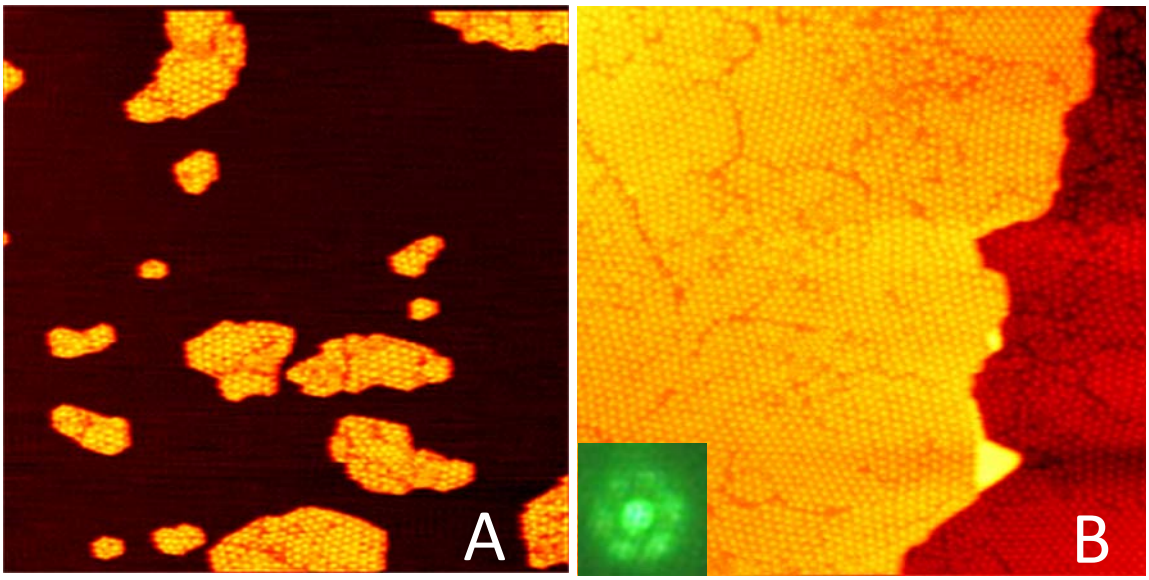

Fig. 1 *STM images of graphene formation on Rh(111), starting from a seeded surface. (A) The graphene seeded Rh surface, obtained by pre-exposing the initially clean surface to a low dose of ethylene at ro om temperature, fo llowed by annealing to 975K. (B) The complete graphene monolayer on Rh after 76 min of further ethylene exposure of the seeded surface at 975K .The image was acquired at the gr owth temperature. The insert shows the superstructure spots around a first-order Rh LEED spot. All images are 160 nm × 160 nm*

[1] R. M. Westervelt, Science 320, 324 (2008).
[2] J. Wintterlin, and M. L. Bocquet, Surf Sci 603, 1841 (2009).
[3] P. Sutter, Nature Materials 8, 171 (2009).
[4] E. Loginova et al., New Journal of Physics 11 (2009).
[5] K. F. McCarty et al., Carbon 47, 1806 (2009).
[6] M. S. Hoogeman et al., Rev Sci Instrum 69, 2072 (1998).
[7] M. J. Rost et al., Rev Sci Instrum 76, 053710 (2005).

Field Emission Resonances on periodically rippled graphene

B. Borca[1], S. Barja[1,2], M. Garnica[1,2], D. Sánchez-Portal[3,4],S. Silkin[3,4,5], E. Chulkov[3,4,6], F. Hermans[1], J.J. Hinarejos[1], A.L. Vázquez de Parga[1,2], A. Arnau[3,4,6], P.M. Echenique[3,4,6], R. Miranda[1,2]

[1]*Dep. de Física de la Materia Condensada, Universidad Autónoma de Madrid, Cantoblanco 28049, Madrid, Spain (corresponding author A.L. Vázquez de Parga: al.vazquezdeparga@uam.es)*

[2]*Instituto Madrileño de Estudios Avanzados en Nanociencia (IMDEA-Nanociencia), Cantoblanco 28049, Madrid, Spain*

[3]*Centro de Física de Materiales (CFM-MPC), Centro Misto CSIC-UPV/EHU, Campus Ibaeta, San Sebastian, Spain*

[4]*Donostia International Physics Centre (DIPC), Paseo de Manuel Lardizabal 4, 20018 San Sebastian, Spain*

[5]*IKERBASQUE, Basque Foundation for Science, Bilbao 48011, Spain*

[6]*Dep. de Física de Materiales (UPV/EHU), Facultad de Química de San Sebastian, Apartado 1072, 20080 San Sebastian, Spain*

Moiré patterns are generated by the superposition of two periodic structures with a lattice mismatch. They have been observed by means of Scanning Tunneling Microscopy (STM) on different systems and their interpretation, in some cases, is not straightforward. The influence, at the atomic scale, of these patterns in the local density of states of the overlayer is not clear and can be studied by STM.

The growth of graphene on metallic substrates allow us not only control the periodicity of the Moiré pattern but also tailor the interaction strength between the carbon atoms and the metallic substrates [1]. This modulation in the interaction gives rise to regions with larger (H-areas) and shorter (L areas) height of the graphene layer over the Ru(0001) surface (Figure 1a). Field Emission Resonances (FERs), which are detected by STM when applying voltages larger than the work function, can be used to explore with nanometer resolution, the inhomogeneities in the local surface potential landscape. Operating the STM in constant current mode implies a constant electric field between tip and sample and the expected energy position for the FERs is given by the expression founded by Gundlach some time ago [2].

The dZ/dV curves measured on gr/Ru(0001) are shown in Figure 1b, three unexpected features are observed: (i) the first graphene image state is localized on the H-areas, while it is more extended on the L-areas, (ii) it does not shift in energy following the 0.25 eV increase of local work function from L- to H-areas, and (iii) a new interfacial state at +3 eV appears in the L-areas. To further investigate and understand the origin of these features we performed first

principle calculations based on density functional theory (DFT). Our calculations explain the experimental data as consequence of the splitting and spatial localization of quasi-two dimensional bands due to the modulation of the strength of the interaction between the graphene layer and the metal surface. The evolution in energy of the different image states a surface resonances can be seen in Figure 1b versus the distance between graphene and the Ru(0001). Finally we will compare these results with the ones obtained on gr/Ir(111) where the interaction between graphene and Ir(111) is very weak [1]

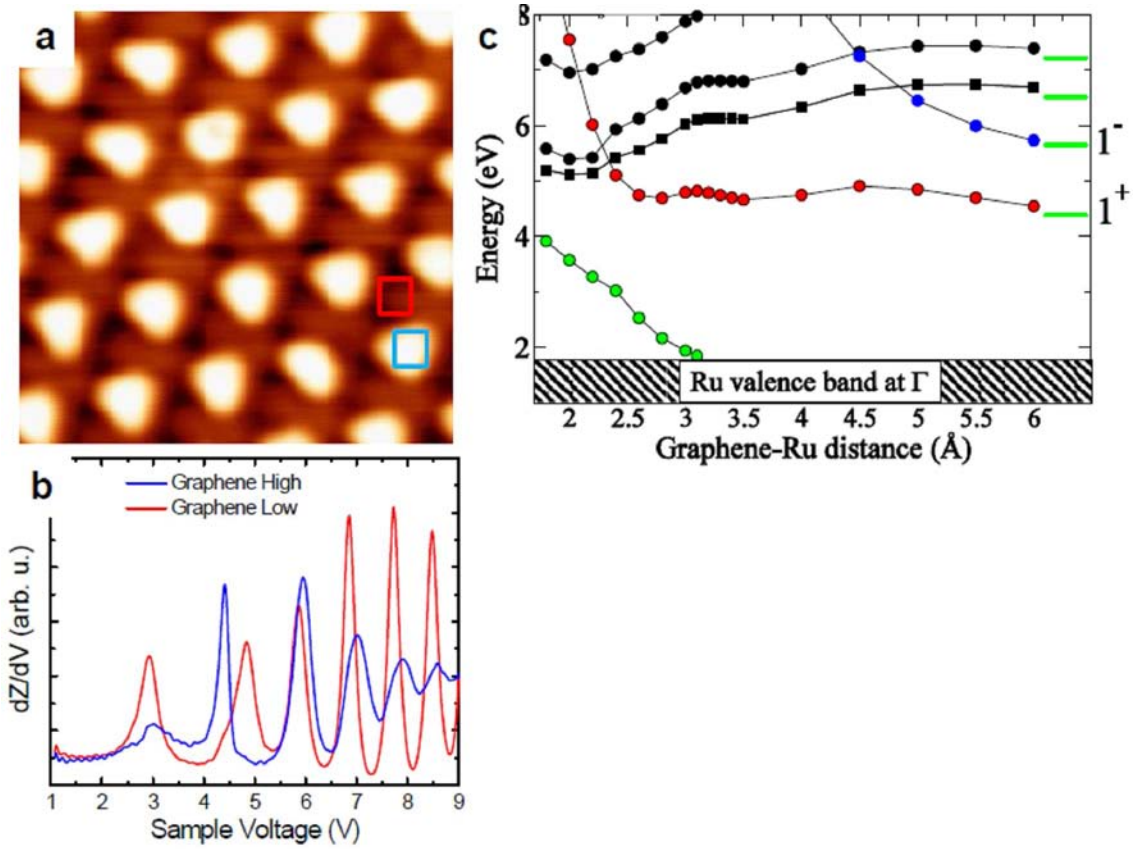

Figure 1: (a) (Upper panel) Scanning tunneling microscopy image measured at 4.6K, lower panel shows two curves measured on the moiré superstructure on the graphene surface. The blue curve is measured in the H-areas (blue box in uppr panel), it shows the presence of the first four FERs. The red curve shows the corresponding spectra measured in the L-areas of the moiré (red box in upper panel). There are two striking features in this curve, the appearance of a new peak at +3eV and the shift in energy of the first FER respect to the ono in the H area (blue). This energy shif tis in the opposite direction than tha change in the local value of the work function between H- and L-areas and twice its value. (b) Shows the calculated evolution of the energies (relative to the Fermi level) of the unoccupied states at Γ, whena strained graphene layer is approached to the surface. The green horizontal lines show the energy position of the different states for a free standing strained graphene layer. States labelled 1^+ and 1^- correspond to the first and second image state [3]. The green dots show the evolution in energy of a Ru(0001) surface resonance.

[1] A.B. Preobrajenski *et al.*, Phys. Rev. B **78,** 073401 (2008)
[2] K.H. Gundlach, Solid State Electron. **9**, 949 (1966)
[3] V.M. Silkin *at al.*, Phys. Rev. B **80**, 121408 (2009)

Topological insulators: a new surface science playground

Hugo Dil[1,2], Fabian Meier[1,2], Justin Wells[3], Philip Hofmann[3], David Hsieh[4], Zahid Hasan[4] and Juerg Osterwalder[1]

[1]*Physik-Institut, Universität Zürich, 8057 Zürich, Switzerland*
(corresponding author: Hugo Dil, jan-hugo.dil@psi.ch)
[2]*Swiss Light Source, Paul Scherrer Institute, 5232 Villigen, Switzerland*
[3]*Institute for Storage Ring Facilities (ISA) and iNANO, University of Aarhus, 8000 Denmark*
[4]*Department of Physics,Princeton University, Princeton, NJ 08544, USA.*

The quantum Hall effect (QHE) is a prime example of a physical effect that is not as much based on symmetry breaking, but rather on the topological order of the system. Where for the quantum Hall effect the time reversal symmetry still needs to be broken, this is no longer the case for the recently discovered quantum spin Hall effect (QSHE). In the QSHE the spin-orbit coupling takes the role of the magnetic field in the integer QHE.

Theory suggests that the QSHE can be observed for a novel class of materials termed topological insulators[1]. A topological insulator can be described as a band gap insulator, which at the surface supports one or more metallic spin-polarized surface states with a non-trivial topology. As illustrated in Figure 1 it is possible to distinguish two types of topologies for spin split surface states. The first in the trivial topology as for Au(111); the two spin-split bands both either connect to the bulk valence or conduction band. Here a small perturbation could shift both bands such that no states cross the Fermi level any more. In the non-trivial topology which we measured for Sb(111) each spin direction connects the valence and conduction bands[2]. Because time inversion symmetry still has to be obeyed the spin-split bands must cross at the zone centre. This means that the general band structure can not be destroyed with continuous deformations such as bending and stretching.

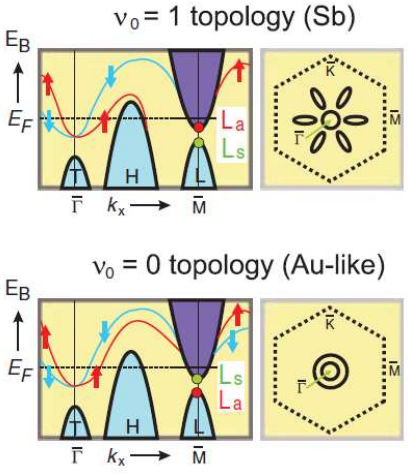

Figure 1

Verification of whether a system has a non-trivial topology is based on counting the number of Fermi level crossings between two time-reversal invariant momenta (mostly Γ-M). For a non-trivial system the number of spin-polarized crossings will always be odd. Therefore, the best technique to directly probe the topology is spin and angle-resolved photoemission spectroscopy (SARPES)[3]. In this presentation we will discuss some results we obtained for topological

insulators and their parent compounds.

The $Bi_{0.9}Sb_{0.1}$ bulk alloy was the first system which could be identified as a topological insulator[2]. The disadvantage of this system is however that the bulk band gap is only 50 meV and that there are as much as five spin polarized Fermi level crossings. The next generation of topological insulators is formed by Bi_2Te_3 and Ca doped Bi_2Se_3. These systems have only one spin-polarized Fermi level crossing and a bulk band gap of about 350 meV[4]. Furthermore, the charge neutrality point can be manipulated by surface doping with NO_2 and a so called Kramers' nodal helical ground state can be created, which can be viewed as a spin polarized version of graphene located at the zone centre.

A non-trivial surface state topology has also been identified for Bi(114)[5]. In Figure 2(a) a STM image of this strongly stepped surface is shown, which looks very one-dimensional. Also the electronic structure is strongly one-dimensional and the Fermi surface consists of two parallel spin-polarized surface states as schematically shown in Figure 2(b). Along these lines one could expect a one-dimensional variant of the QSHE for $Bi_{0.9}Sb_{0.1}$(114), a possibility which is thrilling not only for the surface science community.

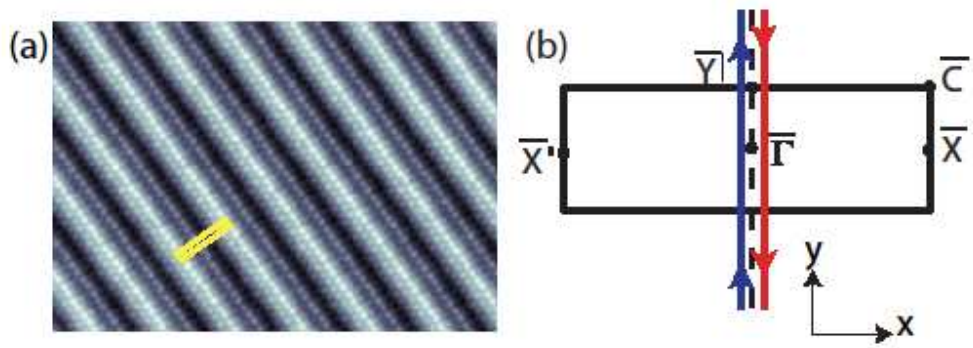

Figure 2

[1] C. L. Kane and E. J. Mele, Phys. Rev. Lett. **95**, 146802 (2005).

[2] D. Hsieh et al. Science **323**, 919 (2009).

[3] J. H. Dil, J. Phys.: Condens. Matter **21**, 403001 (2009).

[4] D. Hsieh et al. Nature **460**, 1101 (2009).

[5] J. W. Wells et al. Phys. Rev. Lett. **102**, 096802 (2009).

Interference of spin states in photoemission from Sb/Ag(111)

F. Meier[1,2], V. Petrov[3], H. Mirhosseini[4], L. Patthey[3], J. Henk[4]
J. Osterwalder[1], and J H. Dil[1,2]

[1] *Physik-Institut, Universität Zürich, Winterthurerstrasse 190, CH-8057 Zürich, Switzerland*
(corresponding author: F. Meier, e-mail: fabian.meier@psi.ch)

[2] *Swiss Light Source, Paul Scherrer Institut, CH-5232 Villigen, Switzerland*

[3] *St. Petersburg Polytechnical University, 29 Polytechnicheskaya St,, St Petersburg, Russia*

[4] *Max-Planck-Institut für Mikrostrukturphysik, D-06120 Halle (Saale), Germany*

Systems with naturally spin polarized electrons are a key element for spintronics, and ways to manipulate the spins are crucial. At surfaces and interfaces, the broken space inversion symmetry can lead to a spin splitting of electronic states in non-magnetic systems via the spin-orbit interaction. The effect leading to this spin splitting was formulated for a two-dimensional free electron gas and is known as the Rashba effect [1], which is commonly also used in a broader context. Experimentally, angle-reolved photoemission spectroscopy first showed the typical dispersion of a Rashba system for the Au(111) Shockley surface state [2]. Later spin-resolved experiments confirmed the high degree of spin polarization of the electrons photoemitted from these states [3], with helical spin structure tangential to the two spin-split Fermi surfaces. Recently, the search for even larger spin splittings has lead to the discovery of a new class of materials, among them the two surface alloys Bi on Ag(111) and Pb on Ag(111) [4,5]. In these systems, a combination of strong atomic spin-orbit interaction of heavy metals and structural effects enhance the local potential gradients at the surface.

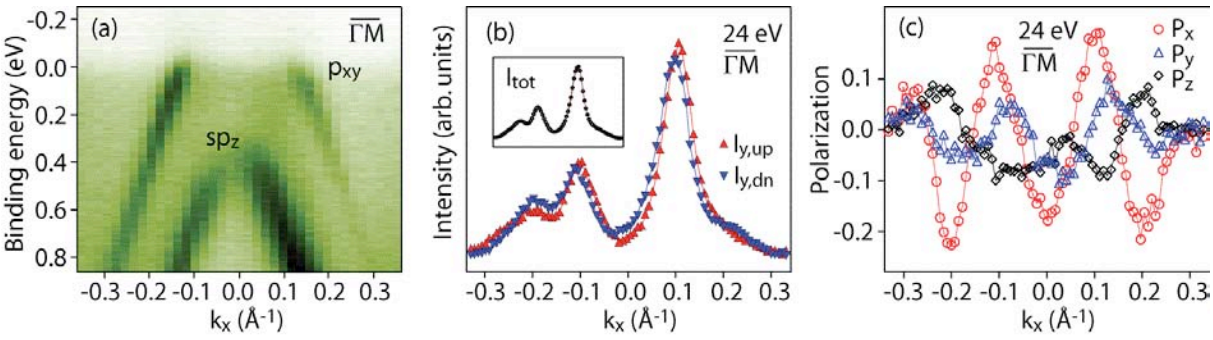

FIG. 1: (a) Spin integrated surface state band structure of the Sb/Ag(111) surface alloy. (b) Spin resolved and spin integrated (inset) momentum distribution curve intensity data at 0.6 eV binding energy. (c) Simultaneously obtained spin polarization curves.

Here we will discuss the structurally related system of Sb on Ag(111) which has only a small spin splitting [6]. The spin integrated band structure of Sb on Ag(111) around Γ is shown in Fig. 1 (a). The splitting is so small that we do not resolve it with spin integrated ARPES. Our spin-polarized ARPES data (Fig. 1 (b) and (c)) show nevertheless substantial spin polarization and permit to quantify the spin splitting. But more importantly, we will show that the measured spin polarization is at strong variance with that expected from the Rashba model. We will argue that the measured spin polarization can be interpreted along the lines of coherent superposition of spin states in the photocurrent. It is an intriguing property of quantum mechanics that spin states can interfere, hence the expectation value of the sum of two spinors can differ from the sum of the individual expectation values. In particular, the coherent addition of a spin-up and a spin-down spinor along some quantization axis does not yield zero polarization, but results in a spinor with ist expectation value placed within the plane orthogonal to the quantization axis. This is exactly what we observe.

Spin-state interference has previously been reported in resonant photoemission induced by circularly polarized light from magnetized Gd by Müller et al. [7]. In this system, orthogonal spin states can be prepared by the angular momentum transfer from the light and spin-orbit interaction on one hand, and by direct photoemission from magnetized states from the valence band on the other hand. By tuning the photon energy to the 4d resonance, the two spin states can be brought to interfere.

For the system at hand, the mechanism leading to interference effects are different. We will present a model which can explain our experimental findings and argue that it could also apply to similar systems, where the states are split by a small amount and spin polarized. Our model will be supported with several different spin-resolved ARPES measurements, which allows us to exclude other effects affecting the measured spin polarization [8-10]. Further, the experiment will be compared with fully relativistic spin-resolved one-step photoemission calculations.

Financial support by the Swiss National Foundation is gratefully acknowledged.

[1] Y. Bychkov and E. Rashba, JETP Lett. 39, 78 (1984)

[2] S. LaShell, B. A. McDougall and E. Jensen, Phys. Rev. Lett. 77, 3419 (1996)

[3] M. Hoesch, M. Muntwiler, V. N. Petrov, M. Hengsberger, L.Patthey, M. Shi, M. Falub, T. Greber and J. Osterwalder, Phys. Rev. B 69, 241401 (2004)

[4] C. R. Ast, J. Henk, A. Ernst, L. Moreschini, M. Falub, D. Pacilé, P. Bruno, K. Kern and M. Grioni, Phys. Rev. Lett. 98, 186807 (2007)

[5] D. Pacilé, C. R. Ast, M. Papagno, C. D. Silva, L. Moreschini, M. Falub, A. P. Seitsonen and M. Grioni, Phys. Rev. B 73, 245429 (2006)

[6] N. Müller, T. Khalil, M. Pohl et al., Phys. Rev. B 74, 161601 (2006)

[7] E. Tamura, W. Piepke and R. Feder, Phys. Rev. Lett. 59, 934 (1987)

[8] E. Tamura, W. Piepke and R. Feder, Phys. Rev. Lett. 59, 934 (1987)

[9] E. Tamura and R. Feder, EPL 16, 695 (1991)

[10] B. Schmiedeskamp, B. Vogt and U. Heinzmann, Phys. Rev. Lett. 60, 651 (1988)

Novel Spin-polarized LEEM

T.Koshikawa, M Suzuki, M Hashimoto, T Yasue, Y Nakagawa 1, A Mano [1], N Yamamoto [1], M Yamamoto [1], T Konomi [1], M Kuwahara [1], S Okumi [1], T Nakanishi [1], X Jin [2], T Ujihara [2], Y Takeda [2], T Kohashi [3], T Ohshima [3], T Saka [4], T Kato [5], and H Horinaka [6]

Fundamental Electronics Research Institute, Osaka Electro-Communication University, Neyagawa, Osaka 572-8530, Japan, 1 Graduate School of Science, Nagoya University, Nagoya 464-8602, Japan, 2 Graduate School of Engineering, Nagoya University, Nagoya 464-8603, Japan, 3 Central Research Laboratory, Hitachi Ltd., Kokubunji, Tokyo 185-8601, Japan, 4 Electrical and Electronics Engineering, Daido University, Nagoya 457-8530, Japan, 5 Daido Steel Co. Ltd., Nagoya 457-8545, Japan, 6 Graduate School of Engineering, Osaka Prefecture University, Sakai 599-8531, Japan

e-mail: kosikawa@isc.osakac.ac.jp

A novel spin-polarized LEEM (SPLEEM) has been developed, which has high spin polarization and very high brightness and an image of the magnetic domain can be accumulated in 20ms.

The conventional spin-polarized LEEM (SPLEEM) has the following problem,

1. Low spin polarization
2. Low brightness of electron gun
3. Low transmittance of electrons in the electron optics
4. Short life time of the NEA (negative electron affinity) cathode
5. Accumulation time of a magnetic image is not short (5-30 s) and it is impossible to obtain the dynamic SPLEEM images.

In order to overcome the above problem, we have developed the following points,

1. The strained superlattice has been used as the cathode, which has high spin polarization [1-3].
2. The back side illumination has been adopted, which gives us high brightness because the lens position of the laser can be located to the close of the cathode (about several mm) which is totally different from that of the conventional one (several tens cm) [1-3].
3. A new electron optics has been designed, which can transfer the100 % electron emitted from the cathode to the next optics.
4. Extreme high vacuum (EHV, 10^{-10} Pa order) at the electron gun can been kept

even during electron emission [1-3].

5. After the above development has been completed, an accumulation time of a SPLEEM image need less than 20ms/frame, which makes us the dynamic observation [4].

Fig. 1 shows the SPLEEM which is set up the high polarization and high brightness spin electron gun developed [4]. The images of Co/W(110) are shown in Fig. 2 [4]. An image of Co magnetic domain can be accumulated in 20ms, which is faster than the video rate (about 30ms/frame).

The project has been supported with the JST.

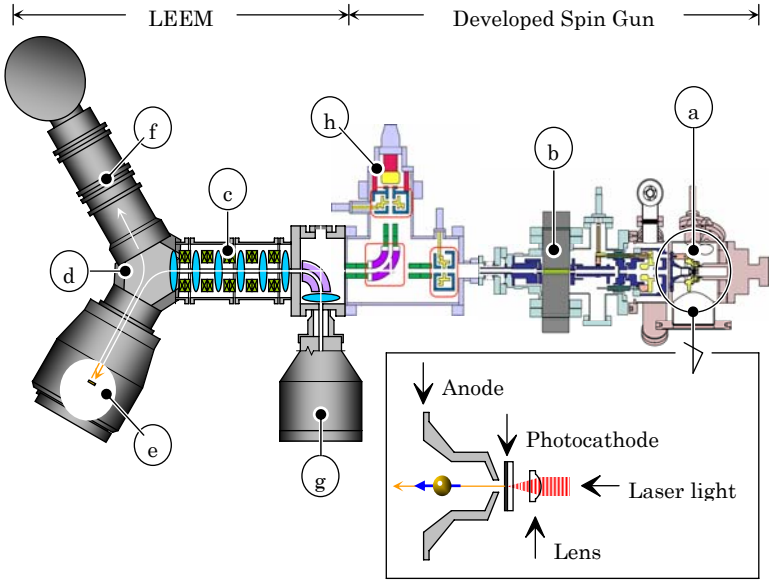

Fig. 1 Novel SPLEEM with high polarized and high brightness spin gun

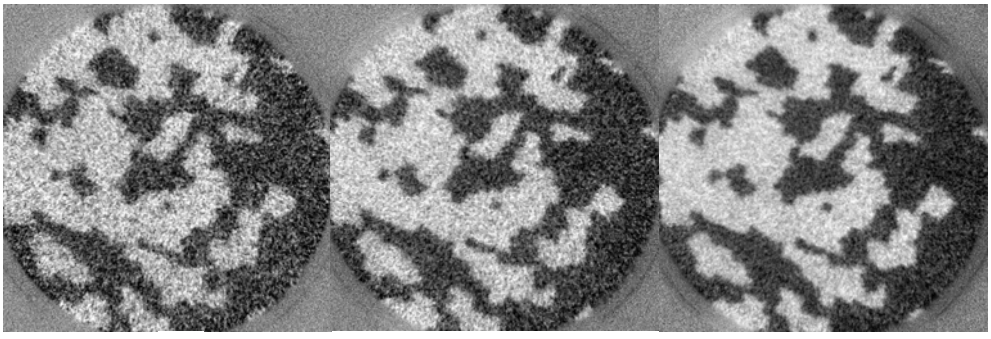

(a) (b)

Fig. 2 SPLEEM images of Co/W(110). (a) 20 ms, (b) 40ms, (c) 100ms/frame

1. X. G. Jin et. al.,: Appl. Phys. Express **1**, 045002 (2008).
2. N. Yamamoto et. al.,: J. Appl. Phys. **103**, 064905 (2008).
3. X. G. Jin et. al.,: J. Cryst. Growth **310**, 5039 (2008).
4. M.suzuki et. al.,, Appl. Phys. Express, (in press).

Dewetting of silicon-on-insulator thin films measured by low-energy electron microscopy

F. Leroy, E. Bussmann, F. Cheynis, P. Müller

CINaM-CNRS, UPR 3118,Campus de Luminy Case 913, 13288 Marseille cedex 9, France
(corresponding author: F.Leroy, e-mail:leroy@cinam.univ-mrs.fr)

Silicon-on-insulator (SOI) substrates are promising for next-generation microelectronic devices such as single-electron transistors [1,2] and field-effect transistors with high-speed operation and low power consumption. Active single-crystalline layers in the sub-10nm range will be required in the near future [3]. However, SOI is unstable when annealed at high temperature (900°C). The SOI film *dewets* resulting in agglomerated nanocrystals [4-7], or nanowires [8]. The solid dewetting of SOI thin films represents both a critical process limitation for the fabrication of advanced devices as well as an open question in basic physics.

Using low-energy electron microscopy (LEEM) and Grazing Incidence Small Angle X-ray Scattering (GISAXS), we have studied the evolution of the morphology and structure of dewetted thin-films from the nucleation of voids/holes until the growth of isolated Si nanocrystals. Depending on the surface preparation/ cleanness we find different dewetted morphologies [9]. For cleaned samples (see Fig. 1a) the dewetted areas are square-shaped holes with <110>-oriented sides. Inside the holes, fingers form aligned in well-defined crystallographic directions <103>, <105> and <100>. The fingers then break into Si aggregates. As shown by GISAXS (see Fig. 1b), and surface X-ray diffraction , the Si nanocrystals keep the initial crystallographic orientation of the film. It is noteworthy that the dewetting of the layer occurs on an amorphous material (SiO_2), showing that the crystallographic orientation of the top Si layer is a key parameter.

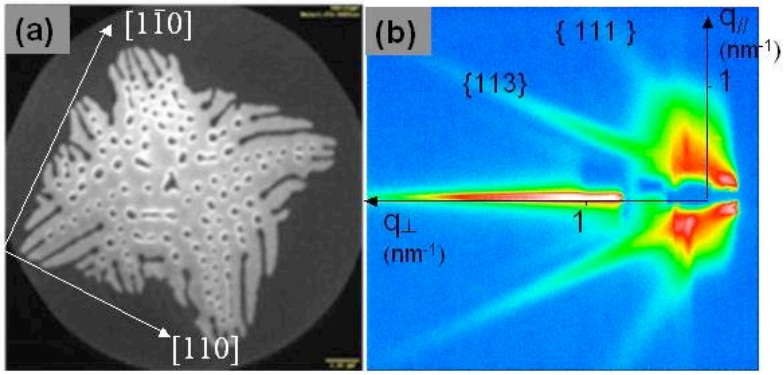

Fig. 1 : (a) LEEM image of a dewetted SOI(001) thin film (20 nm) annealed at 850°C (10 min). Field of view 25 µm. (b) GISAXS image with a X-ray beam aligned along <110> direction. Extended {113} and {111} facets are measured on the Si nanocrystals.

We have quantitatively characterized the shape evolution, size, and ordering of the Si nanocrystals at different stages of the dewetting process, and as function of film thickness and temperature. We find that the activation barrier of the dewetting is dependent on the thickness

of the SOI. We measure the dewetting kinetics using LEEM darkfield imaging. This technique reveals contrast between adjacent terraces by selecting a (2×1) reconstruction diffraction spot (Fig.2). We have measured during dewetting the mass transfer at the atomic level measuring the atomic step motion close to the edge of the hole, as well as the nucleation of new layers at the top of the (001) facet of the rim. These results are compared with theoretical models proposed in the literature [4,10,11].

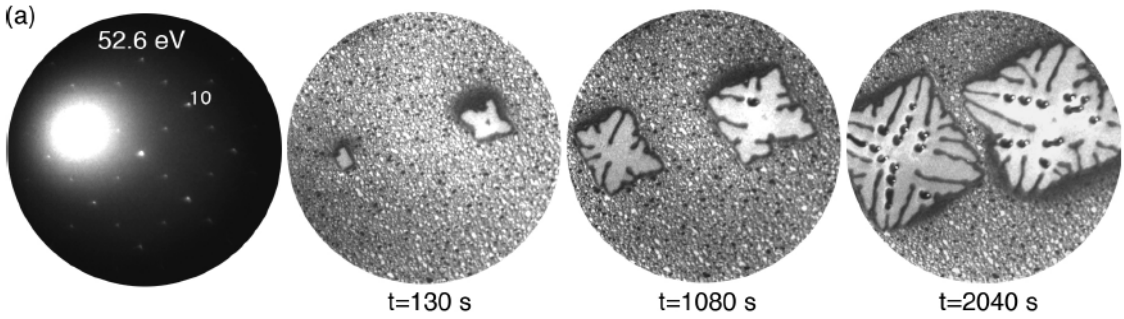

Fig. 2 LEED/LEEM of dewetting of 22 nm-thick SOI films prepared by (T = 910 °C, FOV 25 µm, E = 7.8 eV).

Support by ANR PNANO (ANR 08-Nano-036) is gratefully acknowledged.

[1] P. Zhang et al., Nature 439 (9) 703 (2006).
[2] Lundstrom, W. Schoenfeld, H. Lee, and P. M. Petroff, Science 286, 2312 (1999).
[3] M. Leong, B. Doris, J. Kedzierski, K. Rim, M. Yang, Science 306, 2057 (2004)
[4] D. T. Danielson et al. J. Appl. Phys. 100, 83507 (2006).
[5] R. Nuryadi, et al., J. Vac. Sci. Technol. B, 20(1), 167 (2002).
[6] B. Yang et al., Phys. Rev. B 72, 135413 (2005).
[7] E. Dornel et al. , Phys. Rev. B 73, 115427 (2006).
[8] Z.A. Burhanudin et al. Appl. Phys. Lett. 87, 121905 (2005).
[9] E. Bussmann, F. Cheynis, F. Leroy, P. Müller, submitted.
[10] E. Jiran and C. V. Thompson Thin Solid Films, 208 23-28 (1992).
[11] D.J. Srolovitz, S.A. Safran, J. Appl. Phys, 60, 255 (1986).

Laterally-resolved reaction kinetics: PEEM microscopy of catalytic CO oxidation on polycrystalline Pt

Y Suchorski[1], Ch. Spiel[1], D. Vogel[1,2], W. Drachsel[1], R. Schlögl[2], G. Rupprechter[1]

[1]*Institute of Materials Chemistry, Vienna University of Technology, A-1210 Vienna, Austria*
(corresponding author Y.Suchorski, e-mail: yuri.suchorski@imc.tuwien.ac.at)

[2]*Fritz-Haber-Institut der Max-Planck-Gesellschaft, D-14195 Berlin, Germany*

One of the goals of studies of reaction kinetics is to describe the catalyst behavior in a so-called kinetic phase diagram, in which the regions of monostability, bistability and temporal oscillations are displayed for various external parameters [1]. The use of the term "phase diagram" for the description of kinetic transitions from, e.g., active to inactive states is justified by the analogy to equilibrium thermodynamics [2]. The appearance of instabilities, bifurcations or kinetic oscillations, for example for CO oxidation on platinum metal surfaces, is thus related to the existence of different competitive reactive "phases".
For heterogeneous systems, such kinetic studies are mainly performed by mass-spectroscopy (MS) and suffer from the spatial averaging. As a result, the obtained kinetic phase diagram usually reflects a superposition of reactive properties of different surface regions which may differ significantly from each other, e.g. for metal-oxide systems [1].
However, kinetic transitions in a catalytic reaction can not only be pursued by MS techniques but also by *in situ* visualization of the reaction using modern surface microscopies, such as PEEM (photoemission electron microscopy, [3]), LEEM (low energy electron emission microscopy, [4]), MIEEM (metastable impact electron emission microscopy, [5]), FEM/FIM (field emission and field ion microscopies, [6]). For catalytic CO oxidation it was possible to obtain kinetic phase diagrams using visualizing methods, e.g. PEEM, which correspond well to the MS measurements [7]. However, until now, such diagrams were created solely by spatial averaging of PEEM data, similarly as for MS, and the main advantage of the imaging techniques, namely the possibility to obtain the laterally-resolved information, was not exploited for locally-resolved kinetic studies yet.
In present contribution we show for the first time how local kinetic phase diagrams can be obtained for individual differently oriented domains of a polycrystalline Pt foil, by processing the video-PEEM data obtained during monitoring catalytic CO oxidation (Fig.1). Considering the weighted contributions of particular [100]-, [110]- and [100]-oriented grains, present on the polycrystalline Pt foil, we were able to construct the global phase diagram from PEEM data, and compare it with the global kinetics obtained from simultaneous MS measurements .

The activity of the various facets, as wells as the influence of the heterogeneity of the sample surface on kinetic phase transitions is discussed in terms of grain- and facet-boundary effects, and is compared to metal-oxide interfaces [1].

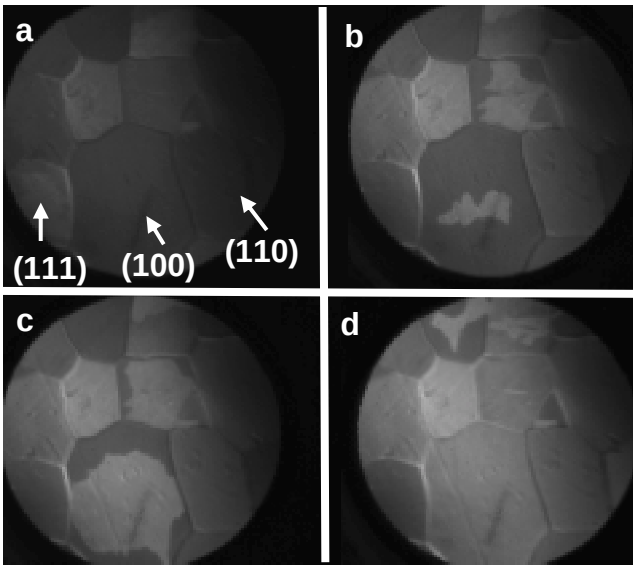

Fig. 1. PEEM video-frames illustrating the kinetic transition from the active (oxygen covered → dark) to inactive (CO covered → bright) steady state. Particularly, local changes on the (100)-oriented domain are clearly visible. T = 453 K, p_{O2} = 1.3x10^{-5} mbar, p_{CO} is varied in the 10^{-5} mbar range.

Acknowledgement: Technical support by. J. Frank (IMC, TU Vienna) is cordially acknowledged.

References

[1] Y. Suchorski, R. Wrobel, S. Becker, H. Weiss, J. Phys. Chem. C, 112 (2008) 50, and references therein.

[2] F. Schlögl, Ber. Bunsenges. Phys. Chem. 84 (1980) 351.

[3] G. Ertl, Ang. Chemie 120 (2008) 3579.

[4] B. Rausenberger, W. Swiech, C.S. Rastomjee, M. Mundschau, W. Engel, E. Zeitler, A.M. Bradshaw, Chem. Phys. Lett. 215 (1993) 109.

[5] G. Lilienkamp, Y. Suchorski, *Surf. Interface Anal.38 (* 2006) 378

[6] Y. Suchorski, W. Drachsel, *Top. Catal. 46 (*2007) 201, and references therein.

[7] M. Berdau, G.G. Yelenin, A. Karpowicz, M. Ehsasi, K. Christmann, J.H. Block, J. Chem. Phys. 110 (1999) 11551.

In overlayers on Si(111): is the hexagonal In-($\sqrt{7}\times\sqrt{3}$)-Si(111) reconstruction formed by a single or double layer?

[1]S. Rigamonti, [1,2]A. Arnau and [1,2]D. Sánchez-Portal

[1] *Donostia International Center (DIPC), Paseo Manuel de Lardizabal 4, 20018 San Sebastián, Spain*

[2] *Centro de Física de Materiales CFM-MPC, Centro Mixto CSIC-UPV/EHU and Departamento de Física de Materiales, Facultad de Química,UPV/EHU Apdo. 1072, 20080 San Sebastián, Spain*

Here we present a theoretical study of the In-($\sqrt{7}\times\sqrt{3}$)-Si(111) reconstruction. This surface has been the subject of many experimental studies [1-9]. Despite these studies there are still many unknowns. For example, the exact coverage and number layers comprising the structure is still under debate. Also two variants of the $\sqrt{7}\times\sqrt{3}$ structure have been observed, the so-called quasi-hexagonal and rectangular reconstructions. The quasi-hexagonal reconstruction, however, has also been interpreted as an incommensurated (1x1)R30^{o} structure [3].

A very recent angle-resolved photoemission spectroscopy (ARPES) measurement of the rectangular In-$\sqrt{7}\times\sqrt{3}$ overlayer shows a band structure that seems to correspond to a strictly confined two-dimensional (2D) electron gas [5]. However, in order to get a good agreement between the measured bands and those of a 2D electron gas it was necessary to assume an unrealistically large charge transfer from the Si substrate to the In overlayer [5].

We have performed first-principles density functional theory (DFT) calculations for realistic models of the In-($\sqrt{7}\times\sqrt{3}$)-Si(111) rectangular and hexagonal reconstructions. We have considered one, two and three layers of In on Si(111). We obtained the relaxed structures, the band structures and the 2D Fermi surface. The relaxed structure of the single-layer rectangular reconstruction, corresponding to 1.2 ML coverage, is similar to the model proposed from scanning tunnelling microscopy (STM) images by Kraft et al. [6]. It is pseudomorphic with a slightly distorted (001) layer of the bulk body-centred tetragonal (bct) structure of In. Surprisingly, this single-layer structure produces a band structure which is very different from the experimental one. However, the double-layer structure, however, gives a band structure and a Fermi surface in almost perfect agreement with experiment. As expected, and in contrast with the experimental interpretation, the charge transfer between Si and the In bilayer is negligible. We thus propose that the ARPES in Ref.[5] corresponds to a In bilayer and not to the single-layer structure of Ref.[6].

We have not been able to stabilize any $\sqrt{7}\times\sqrt{3}$ quasi-hexagonal reconstruction similar to that proposed in Ref.[6]. In all cases the relaxed structures were strongly distorted and, in the sole cases where they converged to ordered structures, they showed a (1x1) periodicity. Thus, we speculate that the apparently quasi-hexagonal $\sqrt{7}\times\sqrt{3}$ structure observed by STM could actually correspond to the modulation, induced by the Si(111) structure, of the electronic states nearby the Fermi level of a rectangular In single-layer. Indeed, our calculations show that the simulated STM images of such In layer are very much dependent on the registry with the Si(111) substrate. However, the STM images of the In bilayer are much less sensitive to the registry with the underlying Si surface.

[1] J. Kraft, M. G. Ramsey and F. P. Netzer, Phys. Rev. **55**, 5484 (1997)

[2] A. Pavlovska, E. Bauer and M. Giessen, J. Vac. Sci. Technol. B **20**, 2478 (2002)

[3] A. Pavlovska and E. Bauer, Surf. Interface Anal. **37**, 110 (2005)

[4] A. A. Saranin et al. Phys. Rev. B **74**, 035436 (2006)

[5] E. Rotenberg, H. Koh, K. Rossnagel, H. W. Yeom, J. Schäfer, B. Krenzer, M. Rocha and S. Kevan, Phys. Rev. Lett. **91**, 246404 (2003)

[6] J. Kraft, S. L. Surnev and F. P. Netzer, Surf. Sci. **340**, 36 (1995)

[7] S. L. Surnev, J. Kraft and F. P. Netzer, J. Vac. Sci. Technol. A **13**, 1389 (1995)

[8] J. Kraft and F. P. Netzer, Surf. Sci. **357-358**, 740 (1996)

[9] J. Kraft, M. G. Ramsey and F. P. Netzer, Surf. Sci. **372**, L271 (1997)

Wednesday

Adatom-Vacancy Mechanism of Step Motion on the Si(111) (1x1) Surface

K.L. Man, A.B. Pang and M.S. Altman

Department of Physics, Hong Kong University of Science and Technology, Clear Water Bay, Kowloon, Hong Kong
(corresponding author: M.S. Altman, e-mail: phaltman@ust.hk)

Atomic steps are common defects at surfaces that can play an important role in many physical phenomena. Step motion occurs when mass is transported to, from and between steps during growth, sublimation, and coarsening. The resulting step morphology will be affected, or can even be dictated, by the nature of the kinetic processes that contribute to mass transport. These processes include surface diffusion, step attachment/detachment and step permeability. The question also arises whether mass is transported mainly by atoms, by vacancies, or even by a combination of the two. A thorough understanding of step morphological evolution therefore requires full knowledge of the mass transport mechanisms, including identification of the transporting species, and how they collectively define step motion kinetics.

In the present work, we have investigated the mechanisms of mass transport that give rise to step motion on the Si(111) (1x1) surface. Interest in step motion kinetics on this surface is motivated by intriguing electromigration-induced step morphological evolution behavior that produces either regular step arrangements, step bunching or step meandering instabilities depending upon the sample temperature in the range 1150 – 1650 K and the direction of the DC heating current [1,2]. We studied step motion kinetics by examining two-dimensional island and vacancy island coarsening behavior using low energy electron microscopy (LEEM) [Fig. 1]. The experimentally measured island and vacancy island areas vs. time during decay can be described by a power law, $A(t) = A_0 \cdot (t_0 - t)^{\alpha}$, where $A(t)$ is the area of the island or vacancy island at time t, A_0 is the initial area, t_0 is the total decay time until disappearance, and α is the decay exponent [Fig. 2]. For the highly symmetric geometry investigated, (vacancy) island on (bottom) top of a concentric (vacancy) island, the temperature dependence of the decay time and decay exponent

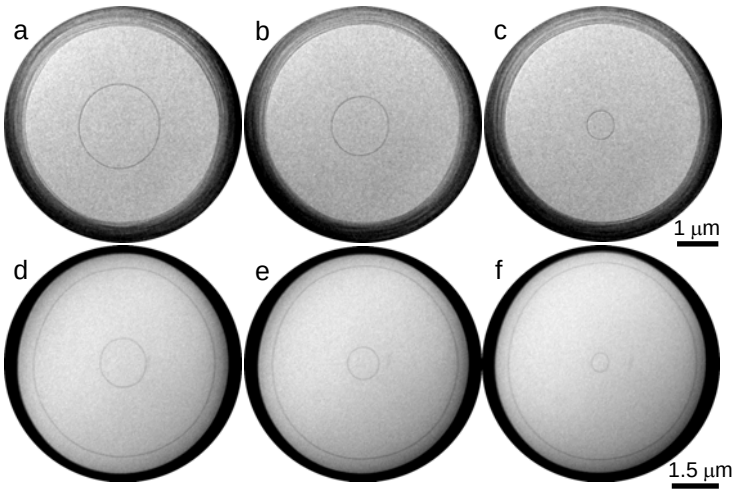

Fig. 1: LEEM images of (a)-(c) island decay and (d)-(f) vacancy island decay on the Si(111) (1×1) surface at 1163K.

can be evaluated using a continuum model of the decay process to obtain quantitative information on kinetic processes, including energetics that control mass transport and sublimation [3].

Our studies reveal a significant difference between island decay and vacancy island decay time, although nearly identical decay exponents, at 1163K [Fig. 2]. The disparity between island and vacancy island decay parameters is exacerbated at higher temperature. Usually, differences between the decay of these complementary objects are attributed to asymmetry between attachment/detachment of adatoms at the upper and lower sides of steps, i.e. asymmetric step attachment/detachment kinetics. However, results of modeling that include such asymmetry reveal that the observed behavior cannot be explained so simply. Alternatively, we find that the observed behavior can be caused by the combined action of adatom and vacancy motion. This model suggests the participation of a low density of fast moving vacancies, with occasional adatom-vacancy annihilation that mimics adatom desorption. The actual situation may, in fact, lie somewhere between the two considered scenarios. Regardless of the cause, these observations should have serious implications for the understanding of electromigration-induced step morphological evolution of vicinal Si(111) surfaces, and more generally for treatments of step motion during growth, sublimation and coarsening on various surfaces.

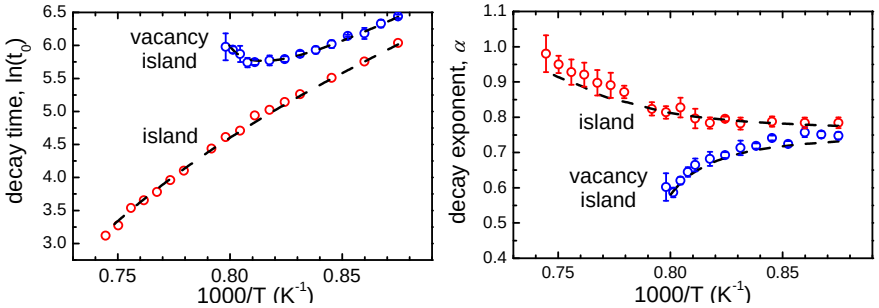

Fig. 2: The temperature dependence of island and vacancy island decay time and decay exponent on Si(111) (1x1). The dashed lines are best fits of continuum modeling that attribute net mass transport to the combined action of adatoms and vacancies.

This work was supported by the Hong Kong Research Grants Council under Grant No. HKUST600108.

References

[1] A.V. Latyshev, A.B. Krasilnikov, A.L. Aseev, L.V. Sokolov, and S.I. Stenin, Surf. Sci. **254**, 90 (1991).

[2] K.Yagi, H. Minoda, and M. Degawa, Surf. Sci. Rept. **43**, 45 (2001).

[3] A.B. Pang, K.L. Man, M.S. Altman, T. Stasevich, F. Szalma, and T.L. Einstein, Phys. Rev. B **77**, 115424 (2008).

Self-Propelled Motion of Mesoscopic Ga Droplets and nanomechanical properties of free-standing InAs nanowires from STM

E. Hilner[1], A. Fian[1], J. N. Andersen[1], E. Lundgren[1] and A. Mikkelsen[1] A.A. Zakharov[2], M. Lexholm[3], B. Mandl[3], L. Samuelson[3],

[1] *Division of synchrotron radiation research, Lund University, Sweden*

[2] *MAXLAB, Lund University, Sweden*

[3] *Division of solid state physics, Lund University, Sweden*

The first part of this contribution will address the self-propelled motion of Ga droplets on a GaP(111) surface with and without the pre-deposition of Au nanoparticles. Thermal decomposition of III-V surfaces is well known: Above the maximum temperature for congruent evaporation the group V component will preferentially desorb and the group III component condense into droplets. The droplets have in some cases been observed to move across the surface, something that is seen also in other material systems e.g. organic liquids or metal alloys. Self-propelled droplet motion is especially fascinating and have very recently been investigated for Ga droplets on GaAs(001) [1] and GaP(111)B [2]. Droplets in both cases move in straight lines leaving a trail behind them on the surface. We have found that by depositing a small amount of Au nano particles (diam. 50 nm, ~1 Au particle /μm²) on the GaP(111)B surface before annealing we can change the droplet dynamics so that instead of unidirectional movement they perform a random walk. We have used Spectroscopic PhotoEmission and Low Energy Electron Microscopy (SPELEEM) and Scanning Tunneling Microscopy (STM) to acquire dynamical, chemical and structural information about the system from the micron to the atomic scale. The random movement of Ga droplets when gold nano particles are added makes it possible to study droplet coalescence which happens very rarely when the droplets move parallel to each other on the clean GaP(111)B surface. Our results indicate that there is an upper limit for droplet size above which droplets can no longer coalesce. It is intriguing how the extremely low amount of Au in the nano particles with a volume ~10^9 times smaller than the micrometer sized Ga droplets can completely change the dynamics of droplet motion.

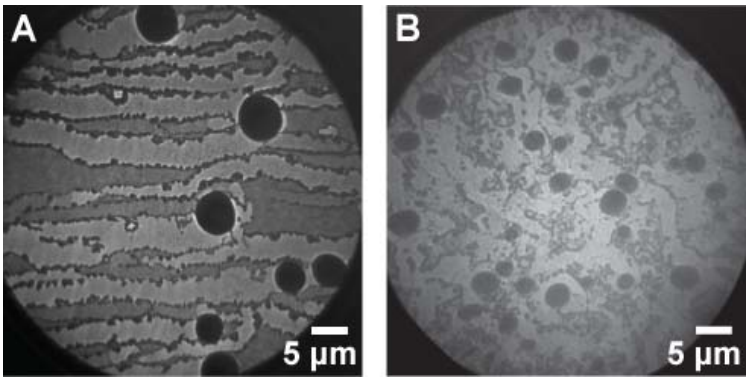

Figure 1: LEEM images A) Ga droplets with trails on the clean GaP(111)B surface. The droplets moves in straight lines. (SV=3.3V) [2]. B) Ga droplets on a GaP(111)B where gold nano particles were deposited. The Ga droplets moves randomly (SV=16V).

The second part of the contribution will demonstrate a new approach to extract information on mechanical properties of free standing nanowires by an STM. The mechanical properties and dynamics of nanostructures are currently receiving much attention due to both the promise of novel nanomechanical devices and interesting fundamental questions of the mechanical properties down to the quantum mechanical regime of low dimensional objects. However, obtaining information on the vibrations of nanoscale objects with extremely high precision below even the Angstrom level is far from trivial. The Scanning Tunnelling Microscope (STM) inherently measures distances to the sub-Angstrom level due to exponential dependence on the tunnelling current with distance. But the STM is usually confined to measurements on flat 2D surface and as a result no such measurements have previously been reported on nanoscale objects with large aspect ratios such as free standing semiconductor nanowires. We demonstrate a scheme that allows a standard STM to be used to measure mechanical resonances of free-standing InAs nanowires with high precision. We can measure resonance frequencies including angular and radial dependencies, the Q-factor of the wires, and measure stress-strain curves on the nanoscale. We can measure resonance features from many nanometers down to the sub-nanometer level and have presently measured very high resonance frequencies around 200MHz.

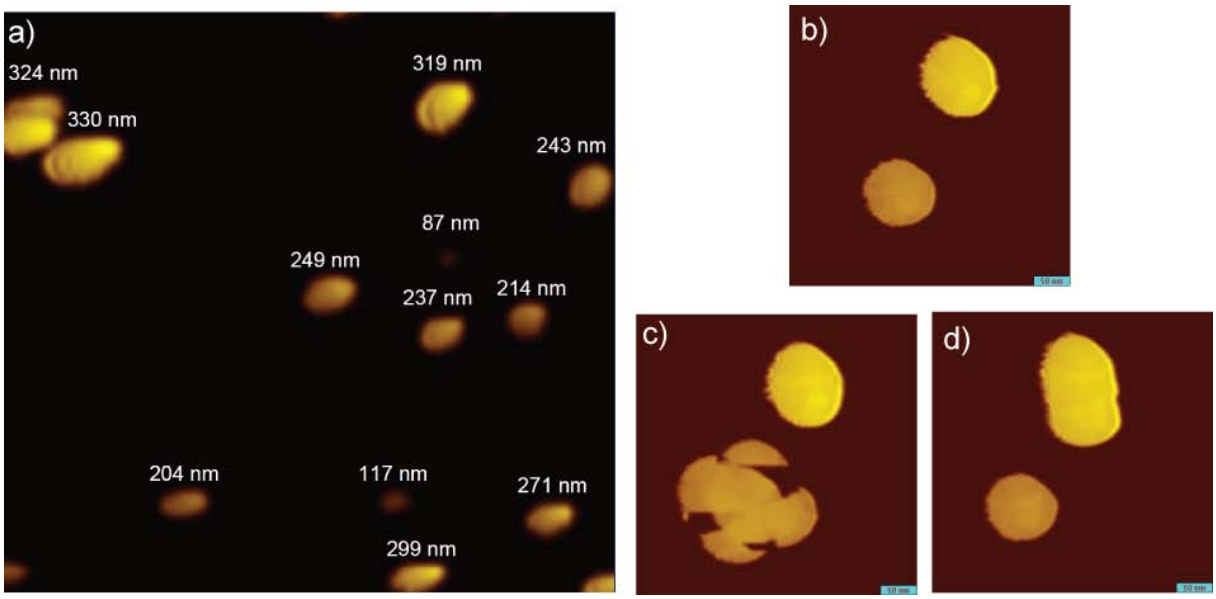

Figure 2: a) 1x1 μm^2 STM image of an array of wires. These wires are nominally 1800nm high. The values on the image are height differences with a respect to a zero value ~400nm below the top of the highest wire. b) 300x300nm^2 STM image of two wires with nominal length of 3000nm. c) Same wires as in b), but with a 300mV oscillating voltage with a frequency of 5.35MHz applied. At this specific frequency a resonance in darker wire is seen. d) Same wires as in b), but with a 300mV oscillating voltage at 6.10MHz. A resonance at the brighter of the two wires is observed at this frequency.

[1] J. Tersoff et al., Science **324**, 236 (2009).

[2] E. Hilner et al., Nano Lett. **9** 2710 (2009).

Surface nanostructures induced by slow highly charged ions

S. Facsko, R. Heller, R.A. Wilhelm, A.S. El-Said, W. Meissl[1], G. Kowarik[1], R. Ritter[1], and F. Aumayr[1]

Institut für Ionenstrahlphysik und Materialforschung, Forschungszentrum Dresden-Rossendor e.V., D-01328 Dresden, Germany

(corresponding author: S. Facsko, e-mail:s.facsko@fzd.de)

[1] *Institut für Allgemeine Physik, Technische Universität Wien, A-1040 Wien, Austria*

Surface modifications induced by the irradiation with ions have been investigated for long time. Depending on their energy the ions create a crater resulting from nuclear sputtering or can induce the formation of hillocks at high kinetic energies. For highly charged ions (HCI) the situation is more complex. In addition to their kinetic energy HCI posses also potential energy which is the sum of the ionization energies to create them. This large amount of potential energy is released when interacting with solids and deposited into a small volume close to the surface. The resulting high excitation in the surface can thus induce various modifications [1]. Recently, it has been shown that hillock structures structures are formed on CaF_2 by HCI due to a localized phase transition [2].

In the case of the alkali halide crystal KBr we observed the formation nanostructures resulting from the desorption of the surface atoms from a single ion impact site [3]. For high enough charge states each ion produces a mono-atomic deep pit with a diameter of 10-30 nm (depending on the charge state) on the atomically flat surface.

Figure 1 shows a contact atomic force microscopy (AFM) image of a KBr (001) surface irradiated with 1×10^{10} cm^{-2} Xe^{34+} ions with a kinetic energy of 153 keV and the corresponding depth and size distribution of the created structures. The pit-like structures have a diameter of 13±4 nm and a depth of only 0.35 nm. They result from the simultaneous desorption of ~2700 atoms (K+Br) from the first atomic layer only. The desorption of such a high amount of material can not be induced by kinetic sputtering alone, which dominates in this kinetic energy regime, but is induced by the excitation due to the potential energy. For a kinetic energy of 40 keV a threshold in the potential energy of the HCI is found for the formation of these structures between Xe^{15+} and Xe^{20+} around 3 keV. Above this threshold the volume of the pits and therewith the potential sputtering yield exhibits a linear dependence on the potential energy. However, the kinetic energy also plays an important role. For higher kinetic energies the threshold shifts to lower values of the potential energy. In Fig. 2 a ”phase diagram” for the emergence of the pit structures as a function of the kinetic and potential energy is shown.

Comparing low fluence and high fluence irradiations at different charge states kinetic and potential effects on the formation of surface nanostructures can be distinguished. Evidence is

found in this way that the formation of complex defect centres, i.e. several self-trapped excitons in a small volume, induced by the combined excitation by the potential and kinetic energy of the HCIs are responsible for the formation of the pit structures on KBr surfaces.

This work has been supported by the European Project ITSLEIF (RII3#026015).

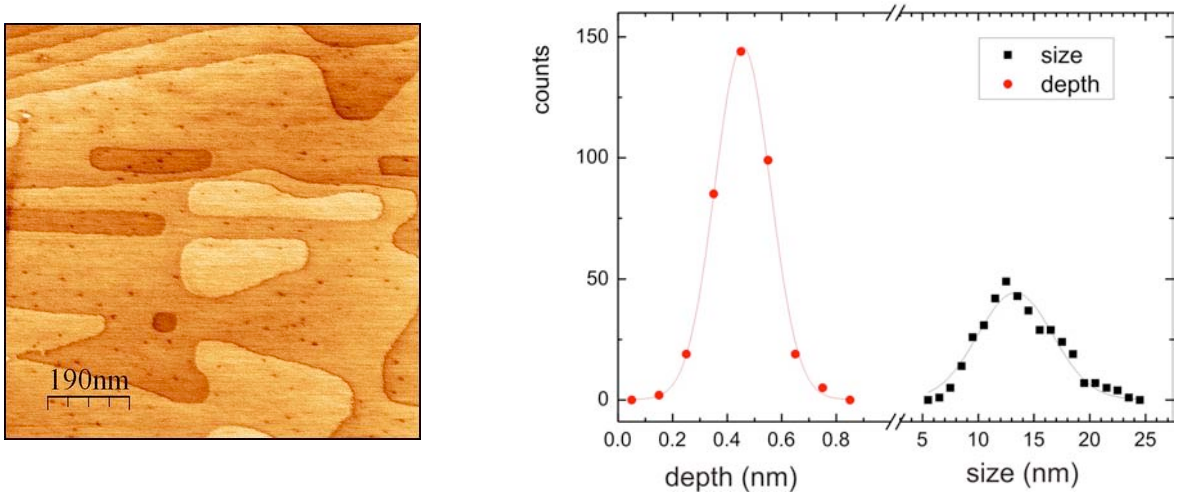

Fig. 1. left: c-AFM image of pit-like nanostructures (ø ≈ 20 nm) on (001) terraces of a cleaved KBr crystal induced by individual impacts of Xe^{34+} ions at 153 keV kinetic energy; right: depth and size distribution of pit structures.

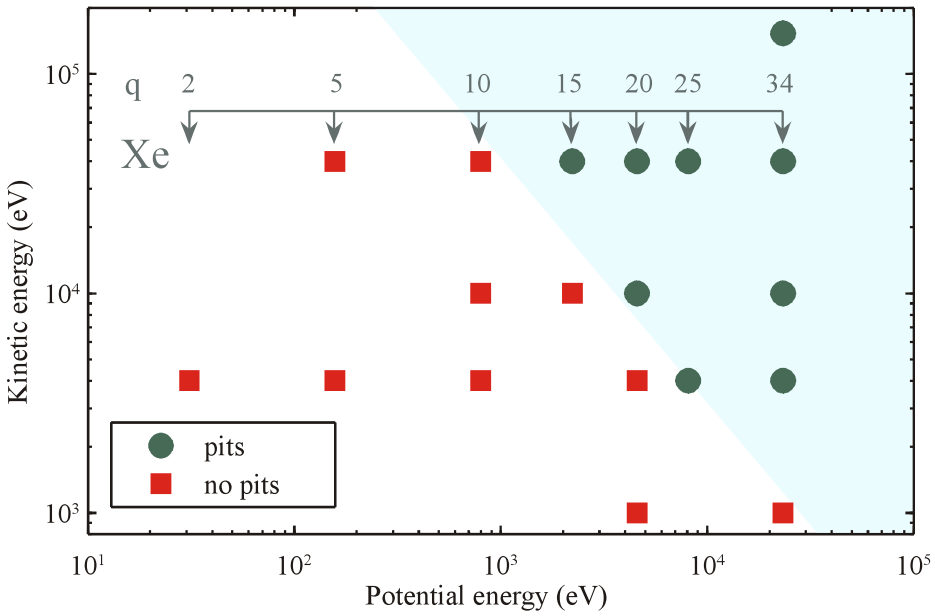

Fig. 2: Emergence of pits on KBr (001) surface as a function of kinetic and potential energy of Xe ions.

[1] S. Facsko, R. Heller, A. S. El-Said, W. Meissl and F. Aumayr, J. Phys.: Cond. Matter 21, 2240122 (2009) .

[2] A. S. El-Said, R. Heller, W. Meissl, R. Ritter, S. Facsko, C. Lemell, B. Solleder, I. C. Gebeshuber, G. Betz, M. Toulemonde, W. Moller, J. Burgdorfer and F. Aumayr, Phys. Rev. Lett. 100 237601 (2008).

[3] R. Heller, S. Facsko, R. Wilhelm, and W. Möller, Phys. Rev. Lett. 101, 096102 (2008).

Track formation in fast atom-insulator interactions

G. Wachter[1], K. Tökesi[3], G. Betz[2], C. Lemell[1], and J. Burgdörfer[1]

[1] *Institute for Theoretical Physics, Vienna University of Technology, A-1040 Wien, Austria*
(corresponding author: C. Lemell, e-mail: lemell@concord.itp.tuwien.ac.at)

[2] *Institute for Applied Physics, Vienna University of Technology, A-1040 Wien, Austria*

[2] *ATOMKI, Debrecen, Hungary*

Investigations of the interaction of fast heavy particles and slow highly charged ions (HCI) with insulator surfaces have shown common features. Above a threshold energy (potential energy for slow HCI, stopping power for fast heavy particles) restructuring of the target material was observed leading to hillock formation at the surface of the insulator or to track formation within its bulk. Recently, we have shown [1] that only parts of the threshold potential energy for slow HCI is effective for hillock formation due to the energy transfer processes involved in the neutralization and deexcitation of the projectile.

Following the same idea we now investigate the creation of tracks by swift heavy ions in an ionic crystal, CaF_2. Ionization of target atoms by swift projectiles along their trajectory is calculated in the CDW-EIS approximation. Electrons excited to the conduction band of the crystal are propagated in the material and may transfer parts of their energy to phonons thereby heating the target. Due to the smaller elastic and inelastic mean free paths low and medium energy electrons (E < 100 eV) contribute more efficiently to the heating (higher energy density) of the target. Therefore, only parts of the stopping power (threshold at S = 5 keV/nm) are transformed into heat.

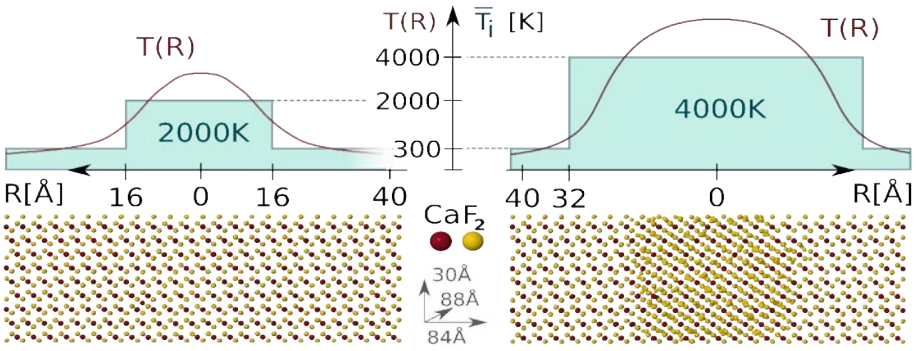

Fig. 1: *Above: Initial temperature distributions T(R) and average temperature distributions T_i, left: T_i = 2000K, R = 16 Angstrom; right: R = 32 Angstrom, T_i = 4000K.*
Below: MD simulation of track region after several picoseconds. In the high temperature case strong lattice disorder (track formation) is observed.

In a proof-of-principle molecular dynamics simulation, we then model the time evolution of ahot cylinder (radius R) of average temperature T_i in a CaF_2 crystal at room temperature. Depending on the initial conditions R and T_i, a remaining track of displaced F ions in the center of the formerly hot cylinder is observed as shown in Fig. 1. Similarly, the creation of nano-hillocks in CaF_2 due to the interaction of the crystal with slow HCI was modeled with the hot region (temperature T_i) being a half-sphere extending from the surface inwards up to a radius R. We observe the formation of hillocks depending on the parameters T_i and R.

[1] C. Lemell, A.S. El-Said, W. Meissl, I.C. Gebeshuber, C. Trautmann, M. Toulemonde, J. Burgdörfer, F. Aumayr, Solid-State Electronics **51**, 1398 (2007)

Guiding of Slow Ne^{7+}-Ions through Insulating Nano-Capillaries of Various Cross Section

P. Skog[1], HQ. Zhang[1], N. Akram[1], I. L. Soroka[2], C. Trautmann[3] and R. Schuch[1]

[1] *Department of Atomic Physics, Fysikum, Stockholm University, S-106 91 Stockholm, Sweden*
(corresponding author e-mail: schuch@physto.se)

[2] *Department of Materials Chemistry, Ångström Laboratory, S-751 21 Uppsala, Sweden*

[3] *GSI Helmholtzzentrum für Schwerionenforschung GmbH, D-64291 Darmstadt, Germany*

The transmission of slow Highly Charged Ions (HCI) through nano-capillaries in various insulating materials, such as PET, SiO2, Al2O3, and glass has been studied by several groups in recent years [1-4]. It has been shown that the ions are guided through by self-organized charge patches on the inner walls [1-3]. Typical results from these experiments are that the majority of transmitted ions retain their initial charge state and that they are guided through the nano-capillaries without any substantial loss in kinetic energy. Single tapered glass-capillaries have been used to produce micrometer sized ion beams [4].

The guiding of ions through insulating capillaries is a time dependent process; maximum transmission is achieved only after the charge patches inside the capillaries have reached a state of equilibrium between the incident ions and the draining through various discharge channels [1-3]. It has been reported for SiO2-capillaries that a small number of charge patches are sequentially formed on the capillary walls in the charging-up process [2].

All previous experiments on guiding of HCI through insulating nano-capillaries have utilized capillaries of circular cross-sections. We have now for the first time used membranes in which the capillaries have non-circular cross-sections.

Sheets of muscovite mica were irradiated with 11.4 MeV/nucleon Pb-ions at a fluence of 5·107 cm-2. When etching the damage tracks from the irradiation, the resulting capillary cross-section is rhombic and all the rhombi have the same orientation, as can be seen in Fig. 1. We performed a series of measurements on the transmission of Ne7+-ions through muscovite mica nano-capillary membranes using ion beams of kinetic energies ranging from 1-10 keV/q. The experiments with capillaries of rhombic cross-sections showed very interesting, and somewhat unexpected, results: we found a rectangular shape of the cross-sections of the transmission profiles (as shown in Fig. 2). The shape of the angular distributions of the transmission profiles seem to depend on the geometry of the capillary cross-section which, will be discussed in further detail at the conference.

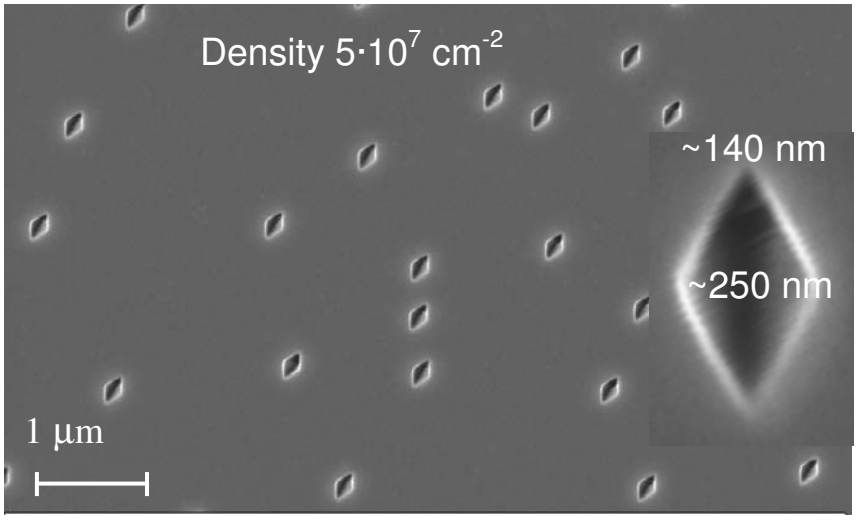

Fig. 1. SEM image of the muscovite mica membrane showing the rhombic capillaries, all with the same orientation. The inset in the lower right corner shows a 8x magnification of a rhombic capillary.

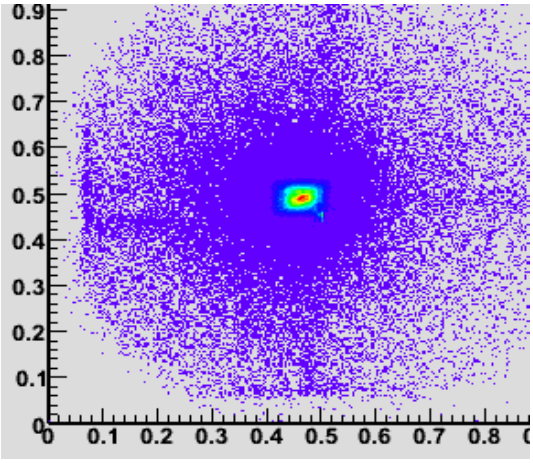

Fig. 2. Transmitted ion image for a capillay orientation as shown on the inset of Fig. 1.

Support by the Swedish Research Council (VR) and the European network ITSLEIF is gratefully acknowledged.

[1] N. Stolterfoht et al. Phys. Rev. Lett., 88 133201 (2002)
[2] P. Skog, HQ. Zhang, and R. Schuch, Phys. Rev. Lett., 101 223202 (2008)
[3] P. Skog et al. Nucl. Instr. Meth. Phys. B, 258 145 (2007)
[4] Y. Yamazaki, Nucl. Instr. Meth. Phys. B, 258 139 (2007)

Postersession

The oxidation and CO reduction of Pd nano particles: A high pressure x-ray photoelectron spectroscopy study

S. Blomberg[1], R. Westerström[1], J. Gustafson[1], J. N. Andersen[1], E. Lundgren[1], M. Messing[2], O. Balmes[3], M. E. Grass[4], Z. Liu[4], H. Bluhm[4]

1. Division of Synchrotron Radiation Research, Lund University, Lund, Sweden.
2. Solid State Physics, Lund University, Lund, Sweden
3. ESRF, Grenoble, France.
4. ALS, Lawrence Berkeley National Laboratory, Berkeley, CA, USA.

Sara.blomberg@gmail.com

The catalytic properties of the Pt-group metals have been studied intensely for many years. Because of the material complexity of a real industrial catalyst, model systems have been developed such as single crystal surfaces under Ultra High Vacuum (UHV) conditions. This effort has resulted in a fundamental understanding of surface reactions by different gases [1]. Therefore, UHV and *ex situ* techniques have been dominating the investigations and for real catalysis the results may not reflect realistic conditions. Recently, experimental techniques compatible with a higher gas pressure have been developed which allow *in situ* monitoring of the chemical and structural state of adsorbates and substrates under more realistic pressure conditions [2-5].

In this contribution we report on the *in situ* oxidation and CO reduction of aerosol deposited Pd particles using High Pressure X-ray Photoemission Spectroscopy (HPXPS). This technique can be used in pressures up to 1 Torr and due to its high surface sensitivity small changes of the surface state can be observed *in situ*. This is important for the determination of the active phase of the surface during for instance CO_2 production by oxidation of CO or CH_4.

The Pd particles were deposited by an aerosol method [6] onto a Si wafer with a native SiO_x surface layer. The particle size can be controlled to a high degree as confirmed by SEM studies as shown in Fig 1. We used Pd-particles of two different diameters, 15 and 35 nm, in order to study a possible size dependence of the oxidation/reduction reaction.

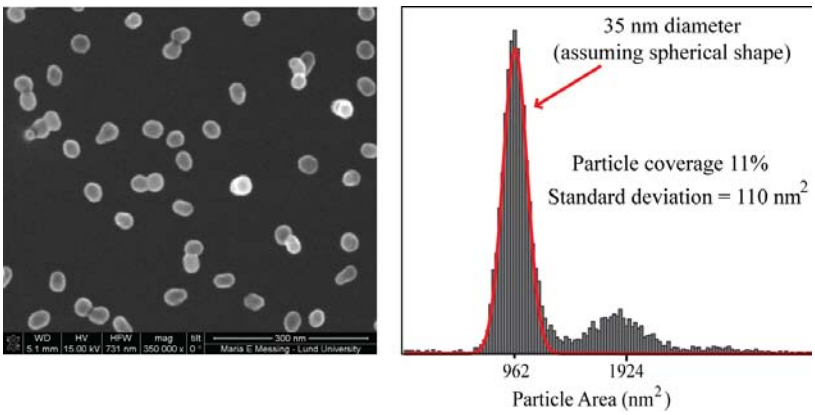

Figure 1. *At the left a SEM image of the pristine 35 nm Pd sample and at the right the size distribution of the particles where a spherical particle shape is assumed.*

The survey HPXPS spectra of the pristine samples show strong contamination by carbon. The carbon could be removed by heating the samples in 1 Torr of O_2 to 300 °C. This procedure resulted in heavily oxidized particles as seen by HPXPS where no Pd-metal bulk component could be observed. As a final cleaning step, the Pd-oxide particles were reduced by exposure

to 0.1 Torr of CO at 120°C which produced metallic Pd particles as evidenced by the Pd 3d spectra and the emergence of a strong Fermi edge. The oxidation of the 15 nm and 35 nm Pd-metallic particles thus formed was followed *in situ* with HPXPS in 1 Torr O_2 with increasing temperature as shown in Fig. 2a and b. The spectra show that a surface oxide is formed on both the 15 nm and 35 nm particles at 100°C. At a temperature of 200°C an intense bulk oxide component at 336.5 eV is present in the spectra. By comparing the spectra from the 15 and 35 nm Pd particles no large size dependence on the oxidation rate can be observed, although significant differences in the oxidation rate of bulk close packed single crystal surfaces can be detected [7-8]. Finally, the reduction of the PdO by CO is also discussed. SEM images after oxidation and reduction cycles show that particles are still present on the surface but have changed in shape and size depending on the gas exposures.

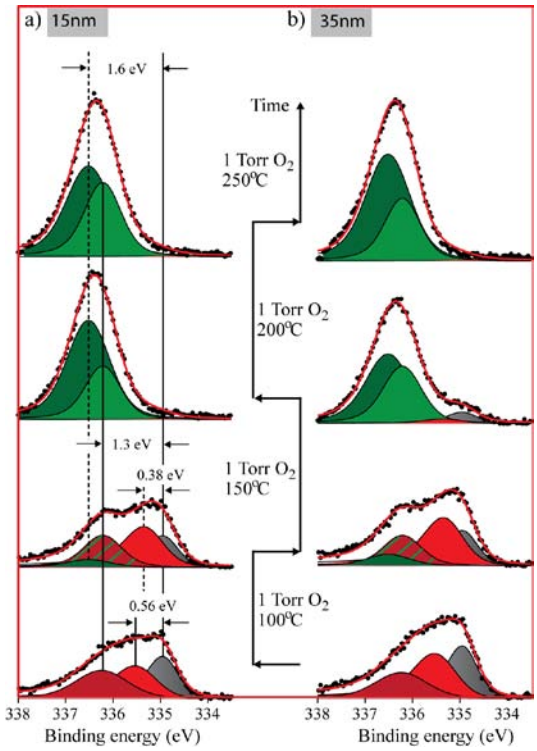

Figure 2. *HPXPS oxidation spectra of a) 15 nm and b) 35 nm Pd particles in a pressure of 1 Torr O_2. The temperature is increasing upwards in the plot and the arrows show the order the measurements were performed.*

Support by the Swedish Research Council, the Crafoord foundation, the Knut and Alice Wallenberg foundation, and the Anna and Edwin Berger foundation is gratefully acknowledged.

References

[1] G. Ertl, H. Knözinger, and J. Weitkamp, *Handbook of Heterogeneous Catalysis.* Wiley, New York, 1997
[2] A. Stierle and A. Moelenbroek, MRS Bull. **32**, 1000 (2007).
[3] E. Lundgren and H. Over, J. Phys. Condens. Matter **20**, 180302 (2008).
[4] Freund, Surf. Sci. **601**, 1438 (2007).
[5] D.F. Ogletree, H. Bluhm, E.B. Hebenstreit, M. Salmeron, Nucl. Instrum. Methods A **601** (2009).
[6] M. E. Messing, K. A. Dick, L. R. Wallenberg and K. Deppert, *Gold Bull.*, 20, **42**, (2009).
[7] E. Lundgren, J. Gustafson, A. Mikkelsen, J. N. Andersen, A. Stierle, H. Dosch, M. Todorova, J. Rogal, K. Reuter, M. Scheffler, Phys. Rev. Lett. 92, 046101 (2004).
[8] G. Ketteler, D. F. Ogletree, H. Bluhm, H. Liu, E.L.D. Hebenstreit, M. Salmeron, J. Am. Chem. Soc. **127**, 18269 (2005).

Substrate Cooperative Effects on Water Adsorption: Hydrogen Bond Strengthening

Pepa Cabrera-Sanfelix,[1] Andrés Arnau[1,2,3] and Daniel Sánchez-Portal [1,2]

[1] Donostia International Physics Center, Paseo Manuel de Lardizabal 4, San Sebastian 20018, Spain
[2] Centro de Física de Materiales CFM-MPC, Centro Mixto CSIC-UPV/EHU, Apdo. 1072, San Sebastián 20080, Spain
[3] Departamento de Física de Materiales UPV/EHU, Facultad de Química, Apdo. 1072, San Sebastián 20080, Spain

Density Functional Theory calculations have been performed to give a detailed insight into the intermolecular interaction of a water dimer adsorbed on a metallic substrate. We present a molecular-scale description of the reinforcement of the dimer hydrogen bond induced by the bond formation between the donor water molecule and different Ru substrates: a partially oxidized Ru surface or a small Ru cluster.

The compressed hydrogen bond of the adsorbed dimer, which is ~0.25Å shorter than for a relaxed dimer in vacuum, gives a clear indication of the strengthening of the intermolecular interaction induced by the substrate.[1] Figure1 shows the rearrangement of charge around due to bond formation for a water dimer adsorbed on a O(2x2)/Ru(0001) substrate, as compared with the relaxed water dimer in vacuum. We clearly observe the polarization effect of the substrate on the adsorbed water molecules: the Ru atom underneath the donor molecule strongly polarizes the Oxygen atom of the molecule, with a consequent weakening the covalent OH bonds. Thus, the fully charged Oxygen atom from the acceptor molecule pulls stronger the donor Hydrogen atom, as it is observed by the accumulation of charge close to the acceptor Oxygen. Therefore, the strengthen of the hydrogen bond and the weaken of the covalent OH bond of the donor molecule are directly interconnected. Weakening of inner OH bonds of the adsorbed

dimer on oxidized Ru substrates would support the experimental observation about low oxygen coverage θ_O on the surface promoting water dissociation over molecular adsorption.[2, 3] One could imagine that the disruption caused by the preadsorbed Oxygen to the water adlayer helps water molecules to form undirected bonds with the substrate; thus, some of the molecules remain attached through strong hydrogen bonds with the molecules well fixed to the substrate. Therefore, the major concentration of weaker covalent OH bonds from the donor molecules would facilitate dissociation versus intact molecular adsorption of water.[4]

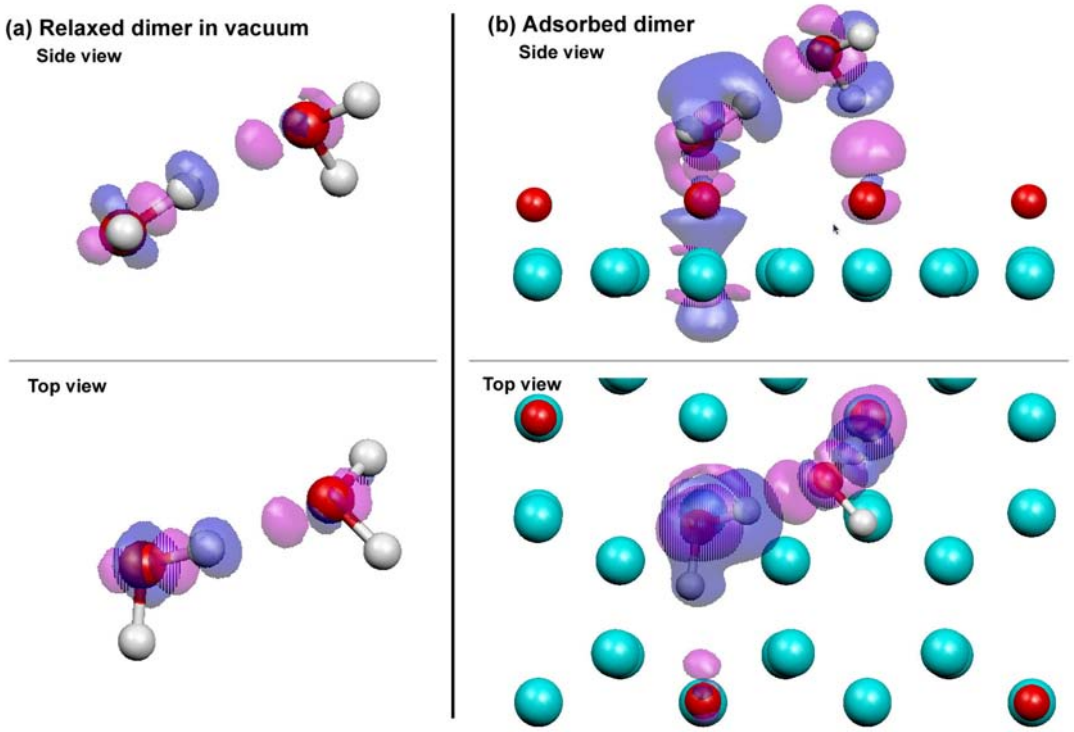

Figure 1. Calculated induced charge density Isovalue: ±0.003a.u. (a) for the relaxed water dimer in vacuum ($\rho_{ind} = \rho_{dimer} - \rho_{monomers}$) ; (b) for the adsorbed water dimer on the O(2x2)/Ru(0001) surface ($\rho_{ind} = \rho_{ads\_dimer} - \rho_{surface} - \rho_{monomers}$). Pink surface correspond to Isoval.= +0.003 a.u. (charge accumulation) and blue surface Isoval.= -0.003 a.u.(charge depletion).

1 P. Cabrera-Sanfelix, D. Sanchez-Portal, A. Mugarza, et al., Phys. Rev. B **76**, 205438 (2007).
2 C. Clay, S. Haq, and A. Hodgson, Chem. Phys. Lett. **388**, 89 (2004).
3 M. J. Gladys, A. A. El-Zein, A. Mikkelsen, et al., Physical Review B **78**, 035409 (2008).
4 P. Cabrera-Sanfelix, A. Arnau, and D. Sanchez-Portal, (In Preparation).

Kondo effect of substitutional Co atoms at Cu(100) and Cu(111) surfaces

P. Wahl[1], A.P. Seitsonen[2]. L. Diekhöner[3], M.A. Schneider[1], and K. Kern[1]

(corresponding author: L. Diekhöner, e-mail: ld@nano.aau.dk)

[1] *Max-Planck-Institut für Festkörperforschung, Stuttgart, Germany*

[2] *IMPMC, CNRS and Université Pierre et Marie Curie, Paris, France*

[3] *Institut for Fysik og Nanoteknologi, Aalborg Universitet, Denmark*

The Kondo effect has attracted new interest in the past decade since it has been found that it can be observed on single magnetic impurities by low temperature scanning tunneling spectroscopy (STS) [1]–[7]. It describes the screening of the spin of a magnetic impurity such as a magnetic adatom at temperatures well below the so-called Kondo temperature T_K due to an antiferromagnetic interaction between the impurity spin and the spins of the surrounding conduction band electrons. The formation of a many-body state leads to a sharp resonance in the local density of states (LDOS) near the Fermi energy which can be observed as a resonance with a Fano line shape on single magnetic impurities at surfaces by STS.

We will here present measurements on single cobalt atoms at substitutional sites in the first monolayer of the Cu(100) substrate. We find a surprisingly low Kondo temperature similar to that of adatoms on Cu(100), while the line shape is different—showing a strong peak in the tunneling spectrum rather than a dip as observed for adatoms on Cu(100). An explanation for the magnitude of the Kondo temperature is offered based on an evaluation of the hybridization between the cobalt d-orbital and the conduction band of the substrate from density functional theory (DFT) calculations [8]. Calculations have also been performed for Cu(111) and compared to experimental data by Quaas *et al* [9]

[1] V. Madhavan, W. Chen, T. Jamneala, M.F. Crommie, and N.S. Wingreen*, Science* **280** 567 (1998)
[2] J. Li, W.-D. Schneider, R. Berndt, and B. Delley, *Phys. Rev. Lett*. **80**, 2893 (1998).
[3] T. Jamneala, V. Madhavan,W. Chen and M.F. Crommie, *Phys. Rev.* B **61** 9990 (2000)
[4] H.C. Manoharan, C.P. Lutz and D.M. Eigler, *Nature* **403** 512 (2000)
[5] V. Madhavan, W. Chen,T. Jamneala, M.F. Crommie and NS Wingreen *Phys. Rev.* B **64** 165412 (2001)
[6] N. Knorr, M.A. Schneider, L. Diekhöner, P. Wahl and K. Kern*, Phys. Rev. Lett.* **88** 096804 (2002)
[7] P. Wahl, L. Diekhöner, M.A. Schneider, L. Vitali, G. Wittich and K. Kern, *Phys. Rev. Lett.* **93** 176603 (2005)
[8] P. Wahl, A.P. Seitsonen. L. Diekhöner, M.A. Schneider, and K. Kern, *New J. Phys*. **11** 113015 (2009)
[9] N. Quaas, M. Wenderoth, A. Weismann, R.G. Ulbrich, and K. Schönhammer, *Phys. Rev.* B **69** 201103 (2004)

Buckybowls at surfaces: tilting and tiling

T. Bauert[1], L. Merz[1], L. Zoppi[2], M. Parschau[1], K. K. Baldridge[2], J. S. Siegel[2], and K.-H. Ernst[1,2]

[1] *Empa, Swiss Federal Laboratories for Materials Testing and Research, CH-8600 Dübendorf, Switzerland*
(corresponding author: K.-H. Ernst, e-mail: karl-heinz.ernst@empa.ch)

[2] University Zürich, Organic Chemistry Institute, CH-8057 Zürich, Switzerland

The modification of surfaces with bowl-shaped molecules (Fig. 1) has been studied with scanning tunneling microscopy (STM). Investigation of fivefold-symmetric buckybowl self-assembly with bulky side groups reveals packing strategies for the molecules as previously predicted for hard pentagons.

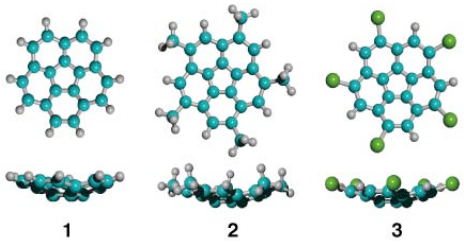

Fig. 1*: Molecular models of different derivatives of bucky-bowls: corannulene (1), pentamethyl-corannulene (2), and pentachlorocorannulene (3)*

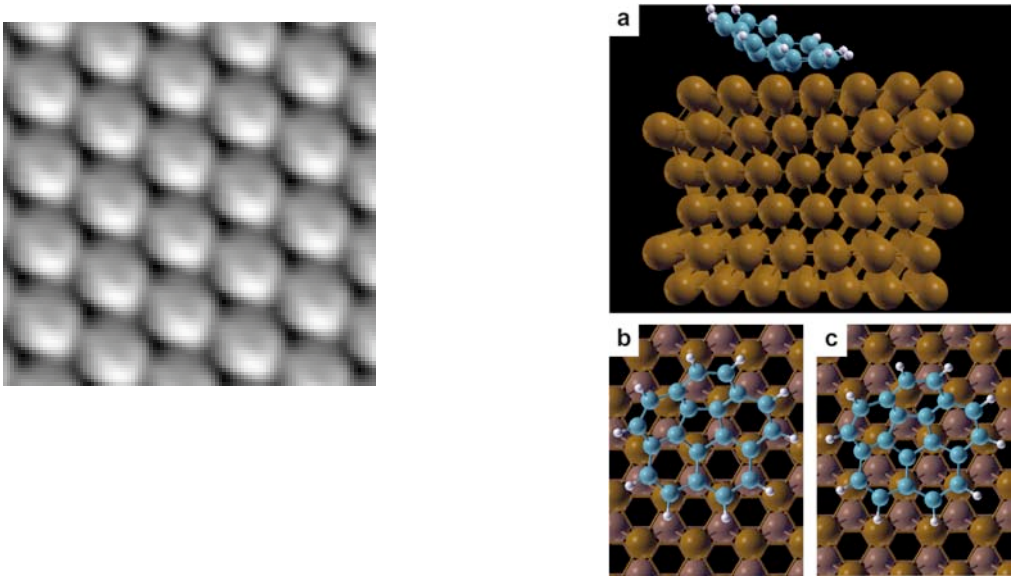

Fig. 2*: Left: Asymmetric appearance of corannulene molecules on Cu(111) in STM suggests a pronounced tilt. Right: Orientation of corannulene on Cu(111) as found by dispersion-corrected density functional theory (D-DFT) calculations.*

The local adsorbate geometry of corannulene on Cu(111) is such, that a hexagonal ring is oriented parallel to the surface plane and the C_5 axis of molecule is tilted with respect to the surface normal (Fig. 2) [1]. Therefore, the C_5 symmetry is not part of the structure and corannulene forms a quasi-hexagonal lattice at room temperature. The pentachloro and pentamethyl derivatives with their bulky substituents at the rim of the bowl should not allow such tilt. In STM the molecules are image as fivefold stars (Fig. 2), i.e. the five chloro or methyl substituents contribute to the STM appearance. The intramolecular STM contrast does not vary as observed for corannulene, indicating that there is indeed no pronounced tilt of the bowl. Weak depressions observed in the center of the molecules imply that the bowl opening points away from the surface. The structures of the derivatives reveal new close-packing strategies (Fig. 2). The pentachloro derivative forms a striped lattice with the pentagonal molecules arranged in antiparallel rows, but the order only extends for a short distance (Fig. 2b). The pentamethyl molecules form a more disordered 'rotator phase' in which the orientation of the molecules, their position with respect to the substrate and their chirality all vary, though their centroids still form a hexagonal lattice (Fig. 2c) [2,3]. Interestingly, these observed structures are compatible with results of mechanical modeling experiments and Monte-Carlo simulations of hard pentagons [4-6].

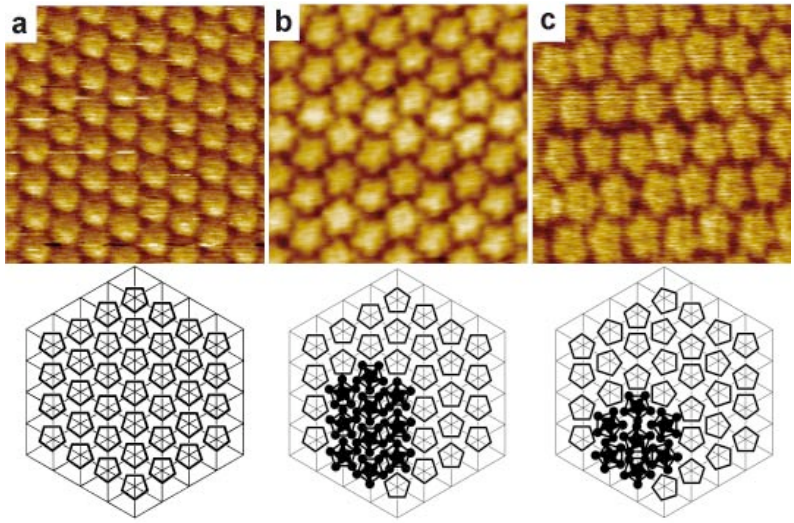

***Fig. 2**: Packing strategies for the fivefold-symmetric molecules corannulene (a), pentachloro-corannulene (b), and pentamethylcorannulene (c).*

Support by the Schweizerischer Nationalfonds is gratefully acknowledged.

[1] L. Merz, et al., Angew. Chem. Int. Ed. 48, 1966 (2009).
[2] T. Bauert, et. al., J. Am. Chem. Soc. 131, 3460 (2009).
[3] A. Pichon, Nature Chem. 1, 107 (2009).
[4] Schilling et al., Phys. Rev. E 71, 036138 (2005).
[5] S. Sachdev, D. R. Nelson, Phys. Rev. B 32, 1480 (1985).
[6] Limon Duparcmeur et al., J. Phys.: Condens. Matter 7, 3421 (1995).

Transport properties of touching molecules

Thomas Frederiksen,[1] Guillaume Schull,[2] Mads Brandbyge,[3] Richard Berndt[2]

[1] *DIPC – Donostia International Physics Center, E-20018 Donostia-San Sebastián, Spain (corresponding author: T. Frederiksen, e-mail: thomas_frederiksen@ehu.es)*

[2] *Institut für Experimentelle und Angewandte Physik, Christian-Albrechts-Universität zu Kiel, D-24098 Kiel, Germany*

[3] *DTU Nanotech, Technical University of Denmark, DK-2800 Kongens Lyngby, Denmark*

Intermolecular charge transport is central to numerous research fields. In biology electron hopping and tunneling processes between molecules play a vital role. Moreover, tunneling processes between molecular materials have opened new perspectives towards the realization of efficient molecular sensors and solar cells [1]. In a parallel direction the conductance properties of point contacts [2], single atoms [3], or single molecules [4] are intensely being investigated, and give a detailed view of charge transport through individual nanoscopic objects. Recently, experiments realized on 1D extended molecules [5], single conjugated polymers [6], and DNA wires [7] have been reported. A critical issue is now to understand and control the charge transfer mechanism from a single molecule to another one.

Here we report on the current flow through two C_{60} molecules suspended between the two electrodes of an STM junction [8]. Imaging and spectroscopy of single molecules on a substrate along with "reverse" imaging and spectroscopy of C_{60} on the STM tip enable characterization of the orientation and the electronic properties of both molecules before connecting them with atomic scale precision. While the contact conductance of a single molecule between two Cu electrodes can vary up to a factor of 3 depending on electrode geometry, the conductance of the C_{60}-C_{60} contact is consistently lower by 2 orders of magnitude. The experimental results are complemented by first-principles transport calculations based on the TranSIESTA code [9,10] which explain the experimental data and predict the conductance of longer chains. The theoretical analysis characterizes the current flow in terms of eigenchannel scattering states [11] to identify the limiting factors for electron conduction.

The picture emerging for chains of two C_{60} molecules is that the transport processes are mainly sensitive to the molecule-molecule interface with the intermolecular distance is limited by electrostatic repulsion. This is supported by an analysis of the real-space eigenchannel scattering states across the junction that shows that the electron waves are mainly reflected at the molecule-molecule interface. In this way the experiment is probing

how current passes through two touching molecules, the properties and the nature of both being controlled and tunable.

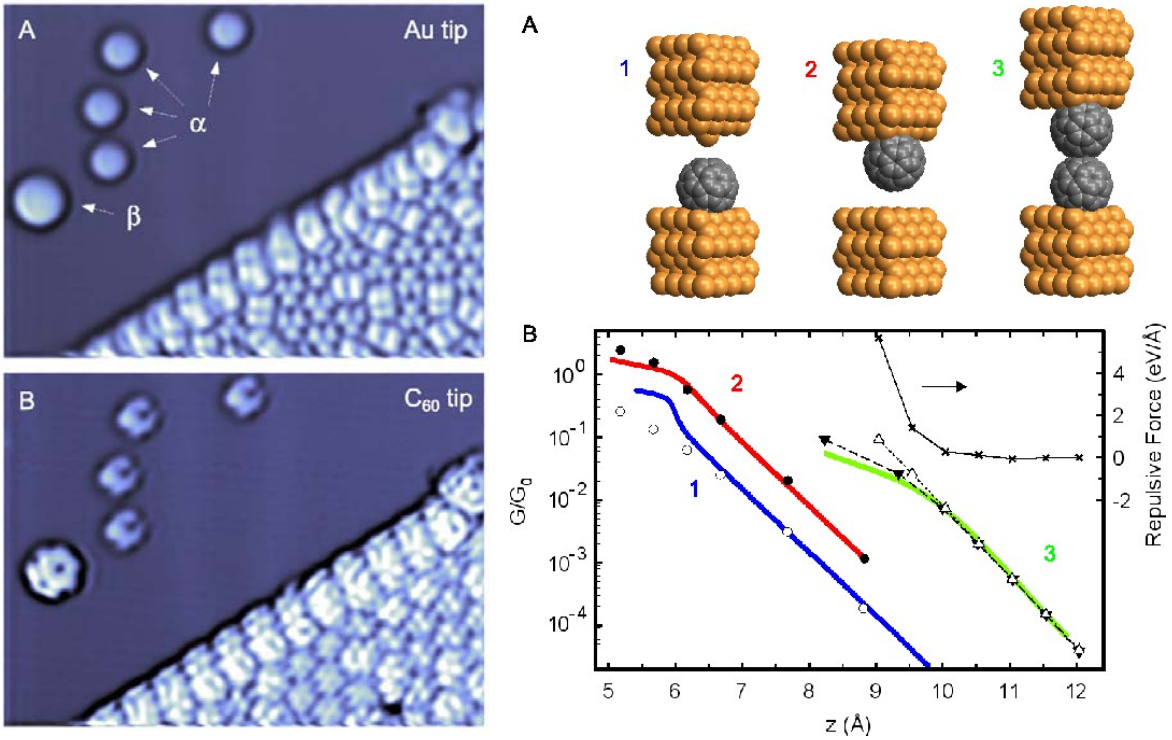

Figures: (left) STM images of Au(111) partially covered with C_{60} molecules (lower right) obtained with a (A) metal and (B) C_{60} tip over the same area. (right) Three distinct transport experiments as a function of the tip excursion z: (1) a single-C_{60} junction established with a metal tip, (2) a C_{60} tip approached to a clean Au(111), and (3) a C_{60}-C_{60} chain. A very good agreement is found between experimental (full lines) and theoretical (symbols) conductance traces (B). From Ref. [8].

Financial support via SFB 677, Innovationsfonds S-H, and FNU 272-07-0114 is gratefully acknowledged.

References:

[1] M. E. El-Khouly *et al.*, J. Photochem. Photobiol. C **5**, 79 (2004); R. H. Goldsmith *et al.*, Proc. Natl. Acad. Sci. U.S.A. **102**, 3540 (2005).

[2] A. G. M. Jansen *et al.*, J. Phys. C **13**, 6073 (1980).

[3] C. J. Muller *et al.*, Phys. Rev. Lett. **69**, 140 (1992).

[4] C. Joachim *et al.*, Phys. Rev. Lett. **74**, 2102 (1995); N. Neel *et al.*, Phys. Rev. Lett. **98**, 065502 (2007).

[5] S. Ho Choi *et al.*, Science **320**, 1482 (2008).

[6] L. Lafferentz *et al.*, Science **323**, 1193 (2009).

[7] H. Cohen *et al.*, Proc. Natl. Acad. Sci. U.S.A. **102**, 11589 (2005).

[8] G. Schull *et al.*, Phys. Rev. Lett. **103**, 206803 (2009)

[9] J. M. Soler *et al.*, J. Phys. Condens. Matter **14**, 2745 (2002).

[10] M. Brandbyge *et al.*, Phys. Rev. B **65**, 165401 (2002).

[11] M. Paulsson and M. Brandbyge, Phys. Rev. B **76**, 115117 (2007).

Nanostructured cobalt oxide films on Ir(100)

Lutz Hammer, Matthias Gubo, Christina Ebensperger, Wolfgang Meyer, and Klaus Heinz

Festkörperphysik, Univ. Erlangen-Nürnberg, Staudtstr. 7, D-91058 Erlangen, Germany
(corresponding author: Lutz Hammer, Email: Lutz.Hammer@physik.uni-erlangen.de)

The growth of ultrathin oxide films on metal substrates has been subject of many investigations so far in order to reveal the relation of their structural, electronic and catalytic properties. For transition-metal oxide films also the magnetic properties are subject of special interest in particular when coupling to a magnetic substrate occurs. For example, it has been shown that enclosing ferromagnetic cobalt metal particles by nanometer-thick antiferromagnetic cobalt oxide tremendously shifts the super-paramagnetic limit towards higher temperatures via exchange bias and might so be a key for the development of future recording devices [1].

In this study we have investigated the growth and structure of cobalt oxide monolayer films both on clean and Co-covered Ir(100) surfaces by means of STM and quantitative LEED.

Oxidizing a monolayer (ML) of cobalt pseudomorphically grown on the unreconstructed Ir(100) surface leads to a whole sequence of ordered structures as a function of oxygen exposure. For lowest oxygen coverage a (2×2) phase of chemisorbed oxygen is found, followed by two different sub-oxide structures with threefold periodicity, $(3\times3)_{I}$ and $(3\times3)_{II}$. For larger oxygen exposures and elevated temperatures also a c(10×2) and eventually a c(8×2) phase develops, which can be regarded as heavily distorted CoO(111) bi- and trilayers, respectively. For all phases except the last one their precise crystallographic structures have already been solved by means of full-dynamical LEED intensity analyses [2,3]. Of particular interest here is the $(3\times3)_{II}$ phase, the most stable one among all observed structures (decomposition temperature ~1100°C), which is strongly oxygen-deficient with a stoichiometry of Co_8O_5. Its basic structural element is a ring-like arrangement of four linked trigonal pyramids with oxygen at their top, whereby these "rings" are interconnected by additional oxygen species (Fig. 1).

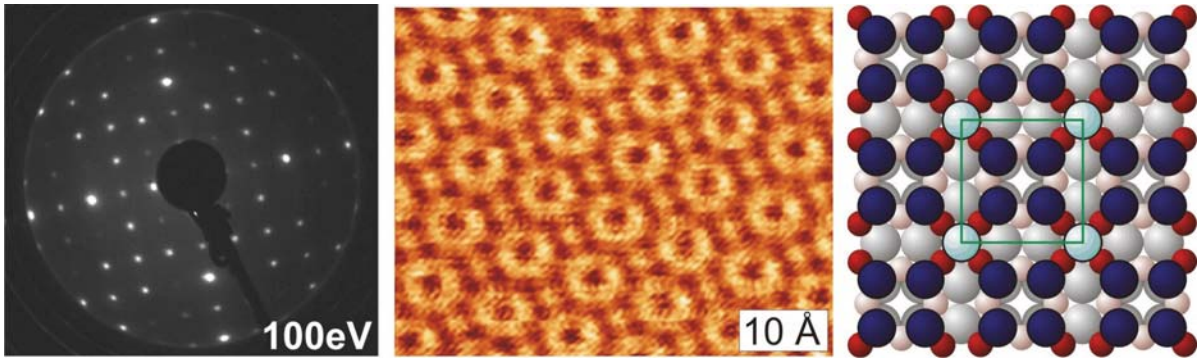

Fig. 1: LEED pattern, STM image (oxygen ions imaged) and structural model for the $(3\times3)_{II}$ cobalt oxide phase grown on Ir(100).

Starting with thicker cobalt films (e.g. 2-5 ML) pseudomorphically grown on Ir(100) the oxidation process leads to only one single monolayer oxide, namely to a c(4×2) phase. Virtually, it is an almost flat CoO(100) layer, however, with every fourth Co ion missing, giving rise to the observed periodicity (Fig. 2). Very similar structures have recently been identified for nickel oxide [4] and manganese oxide [5] both grown on a bare Pd(100) surface.

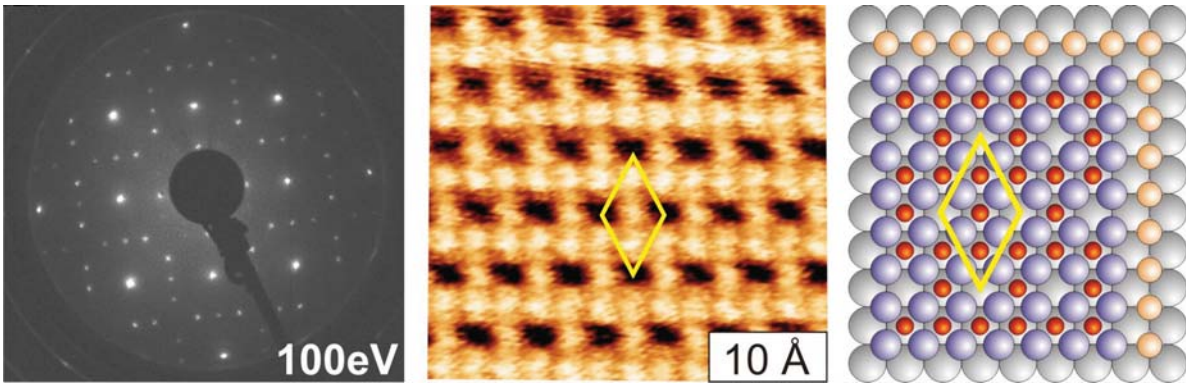

Fig. 2: LEED pattern, STM image (cobalt ions imaged) and structural model for the c(4×2) cobalt oxide phase grown on 1ML Co/Ir(100).

Obviously, even a single monolayer of unreacted cobalt below the oxide film leads to a completely different oxidation behaviour and oxide structure. Though, it appears tempting to study the oxide growth on an ordered, but mixed Co-Ir interface. Such an interface can be created by deposition of 0.8 ML of Co on the Ir(100)5×1-H surface [6], whereby an ordered Co_4Ir lateral superlattice is formed on top of the unreconstructed Ir(100) surface [7]. In fact, growing a monolayer cobalt oxide film on such an interface, the c(4×2) structure develops only on top of the narrow Co stripes. Above the mono-atomic Ir wires a completely different oxide is formed (structurally not yet solved), leading to an overall (4×5) film periodicity (Fig. 3). This proves that the local oxide-substrate interaction rules the crystallographic structure of the oxide and, as a consequence, this allows us to create ***an artificially nanostructured oxide film***.

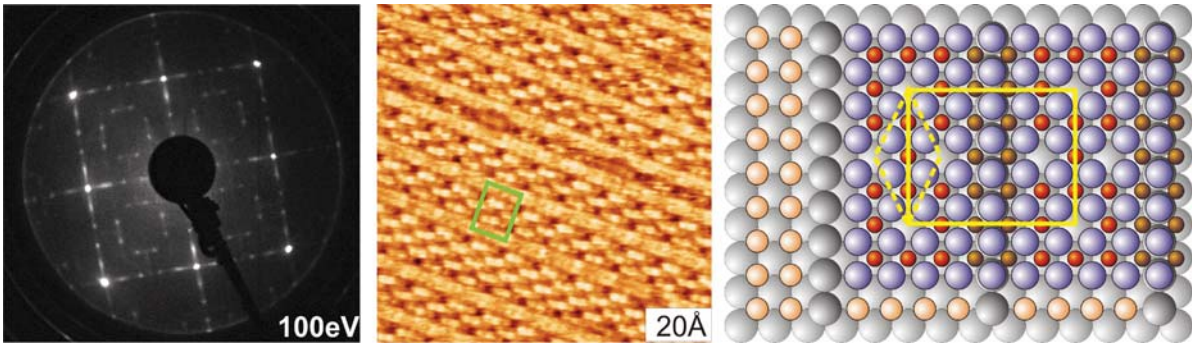

Fig. 3: LEED pattern, STM image (cobalt ions imaged) and structural model for the nanostructured (4×5) cobalt oxide phase grown on Co_4Ir /Ir(100).

Financial support of the Deutsche Forschungsgemeinschaft is gratefully acknowledged.

[1] *V. Skumryev et al.; Nature 423 (203) 850*
[2] *M. Gubo et al., J. Phys.: Cond. Matter, Vol. 21 (2009) 474211.*
[3] *C. Ebensperger et al., submitted to Phys. Rev. B.*
[4] *S. Agnoli et al., Surf. Sci. 576 (2005) 1.*
[5] *C. Franchini et al., J. Chem. Phys. 130 (2009) 124707.*
[6] *L. Hammer et al., Phys. Rev. Letters 91 (2003) 156101.*
[7] *C. Giovanardi et al., Phys. Rev. B 78 (2008) 205416.*

Cooperative molecular dynamics in surface reactions

K. R. Harikumar[1], L. Leung[1], I. R. McNab[1], J. C. Polanyi[1], H. Lin[2] and W. A. Hofer[2]

[1] *Department of Chemistry, University of Toronto, 80 St George Street, Ontario, M5S 3H6, Canada*

[2]*Department of Chemistry, University of Liverpool, Liverpool L69 3BX, United Kingdom*

The controlled imprinting of surfaces with specified patterns is important in the development of nanoscale devices. Previously, such patterns were created using self-assembled physisorbed adsorbate molecules that can be stabilized on the surface by subsequent chemical bonding. An important feature of such self-assembled molecules is their dipole moment and

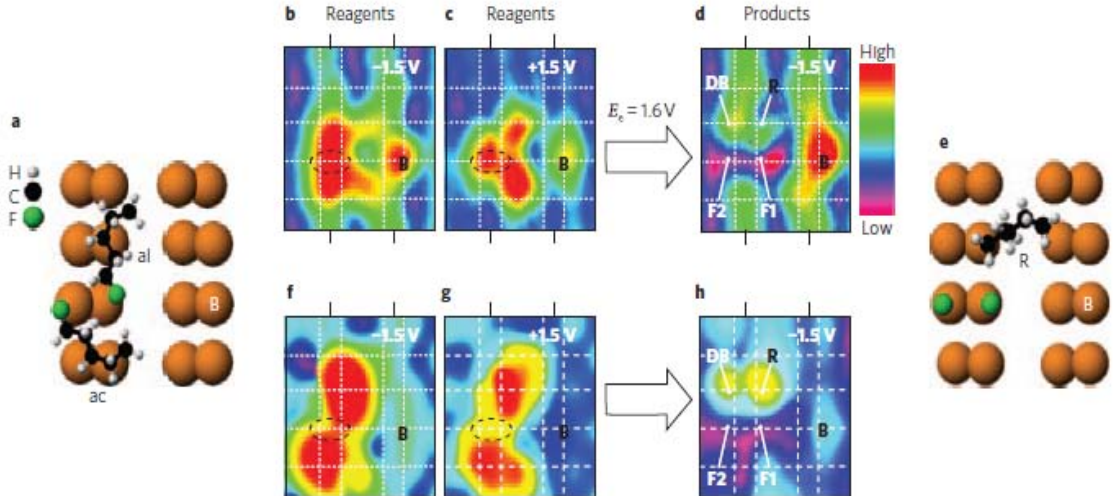

Fig. 1: Reaction of two fluoropentane molecules on Si(100). Injection of electrons at 1.6 eV leads to the attachment of the two fluorine atoms to the silicon surface. Top, experimental scans, bottom, simulations

the interplay between molecular dipole moments and induced dipoles at a surface due to charge transfer processes. We have shown in the past that this may lead to quite unexpected coupling e.g. between individual silicon dimer rows [1]. Here we show the analysis of a subsequent step towards use of the bonding within a surface to propagate reactions for patterning, namely the cooperative reaction of adjacent silicon atoms. We exploit the doublebonded silicon dimer pairs present on the surface of Si(100) and show that the halogenation of one silicon atom (induced by electrons or heat) results in cooperative halogenation of the neighbouring silicon atom with unit efficiency (see Fig. 1). The result is quite unexpected insofar as one single electron, which is most likely injected into an anti-bonding state of the Si-Si dimers of the reconstructed surface, is sufficient to break two fluorine carbon bonds, and to create two silicon fluorine bonds. The reactants used were two 1-halopentane molecules physisorbed over a pair of silicon atoms [2].

Subsequently we simulated the reaction process using one particular method to find the transition state, namely the nudged elastic band method [3]. The simulations showed that the

energy barrier to the reaction of about 1.4 eV, a value which agrees well with experimental findings, arises primarily from the bonding of the first molecule to the surface. Once this molecule is fragmented and the fluorine atom imprinted on the surface, the second reaction occurs practically instantanously and with a very low energy barrier of less than 0.1eV (see Fig. 2). This energy barrier indicates that the timelag between the first and the second reaction is in the range of femtoseconds.

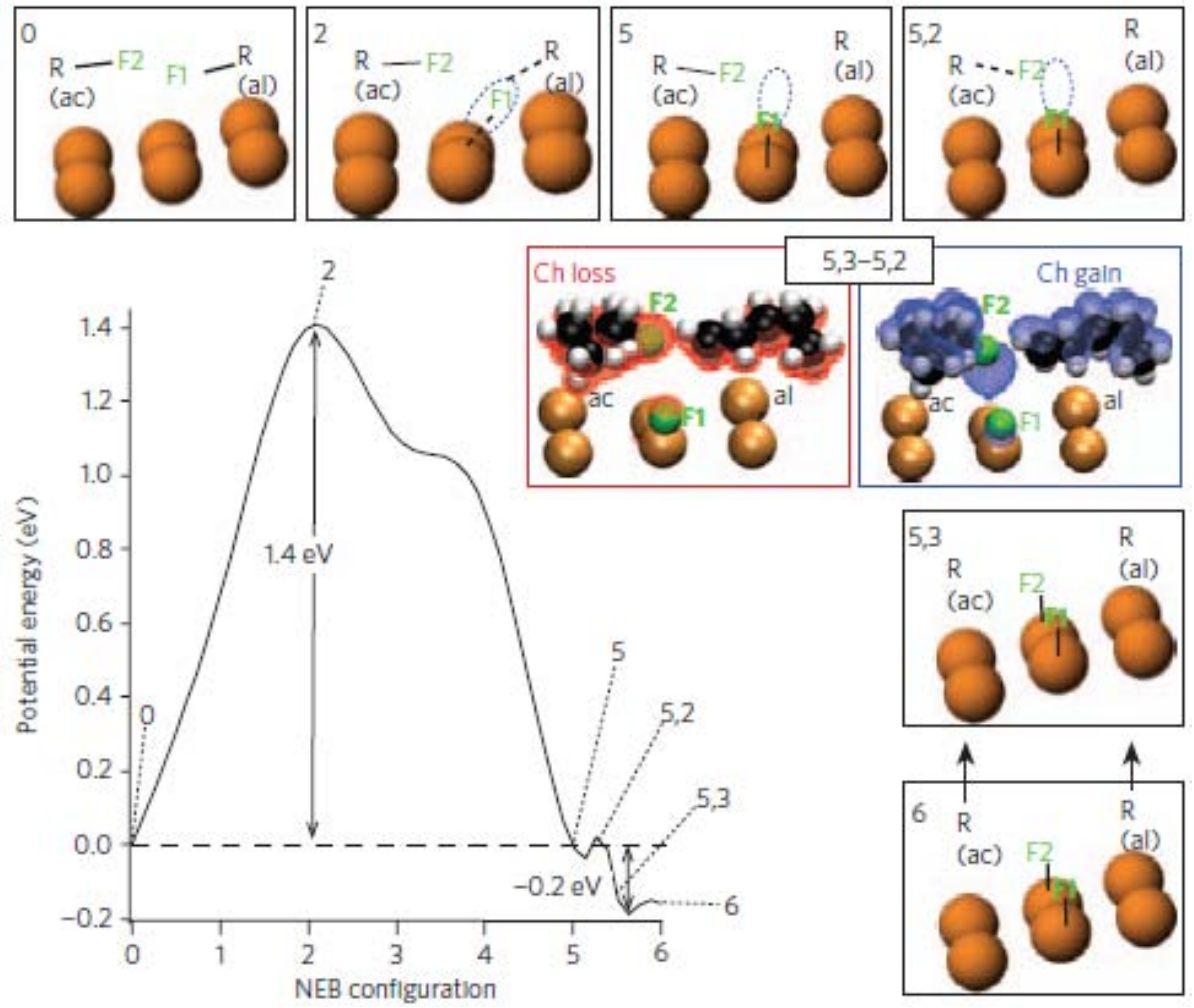

Fig. 2: Calculated minimum energy path for the bifluorination of silicon. The main activation barrier (frame 0 to frame 5) results from a single fluorination, while the second reaction occurs practically without an activation barrier (fram 5 to frame 6).

Acknowledgements: The project was supported by the Canadian Institute for Advanced Research under the Nanoelectronics Programme. WAH acknowledges support from the Royal Society London.

[1] K. R. Harikumar, T. Lim, I. R McNab, J. C. Polanyi, L. Zotti, S. Ayissi, and W. A. Hofer, *Nature Nanotechnology* **3**, 222 (2008).

[2] K. R. Harikumar, L. Leung, I. R. McNab, J. C. Polanyi, H. Lin, and W. A. Hofer, *Nature Chemistry* **1**, 716 (2009).

[3] G. Henkelman, B. P. Uberuaga, and H. Jonsson, *J. Chem. Phys.* **113**, 9901 (2000).

Surface plasmon polaritons in the vicinity of a metal corner

R. Kalousek, L. Břínek, L. Šustr, P. Dvořák, and T. Šikola

Institute of Physical Engineering, Brno University of Technology, Brno, Czech Republic
(corresponding author: R. Kalousek, e-mail: kalousek@fme.vutbr.cz)

Surface plasmon polaritons (often called plasmons) as evanescent waves propagating along the metal-dielectric interfaces were well described more than 60 years ago. During the last 15 years this kind of surface-bound electromagnetic field has found its direct applications in research on transfer of information, sensors, etc. [1]. Limiting metal-dielectric interfaces to the structures with dimensions of hundreds of nanometers (called antennas) localized surface plasmons (LSP) start to take place. Properties of the electromagnetic field in the vicinity of these structures are complex and, hence, they are usually studied numerically by finite element- or finite difference methods in time or frequency domain. However, also some simple analytical models usually based on standing-wave modes in a specific limited medium have been introduced [2]. These models are often capable to explain some basic features in reflection spectra, mostly in a semi-quantitative way.
In this presentation we suggest a more accurate analytical model for solving problems of electromagnetic waves in the proximity of metal-dielectric structures. We use the Helmholtz integral theorem in which by knowing the solution of the Helmholtz equation at a point *A* belonging to the boundary of some volume a solution at any point *B* inside this volume can be found (see Fig. 1). The Helmholtz integral theorem has the form

$$\psi(B) = \frac{1}{4\pi} \oint_{S(V)} [\psi(A)\vec{\nabla}_A G(r) - G(r)\vec{\nabla}_A \psi(A)] \cdot \vec{n} \mathrm{d}S$$

where $G(r)$ is the Green's function and $\vec{\nabla}_A$ is the gradient of a scalar function ψ at the point A with the respect to the normal vector $\vec{n}$.

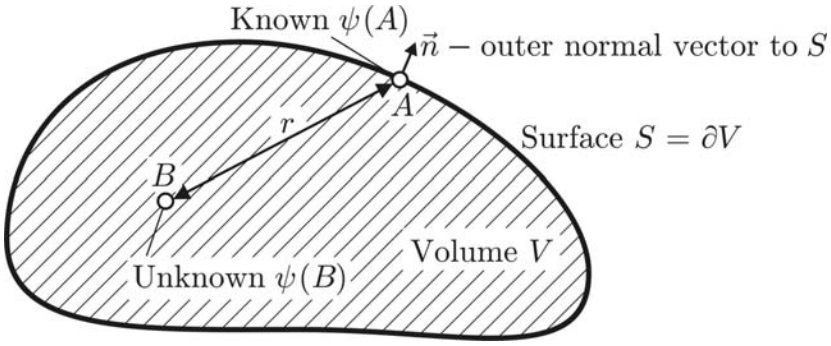

Fig. 1: Towards the explanation of the Helmholtz integral theorem.

We will show that the Helmholtz integral theorem can be used for the analytical calculation of electromagnetic field nearby an infinite (2D solution) metal-dielectric corner. In Fig. 2 the solution ψ of the Helmholtz equation and the related $|\psi|^2$ (connected to the energy density of the electromagnetic field) calculated numerically for the infinite corner are shown in Fig. 2. The capabilities, accuracy and possible applications of using the Helmholtz integral theorem will be discussed in detail.

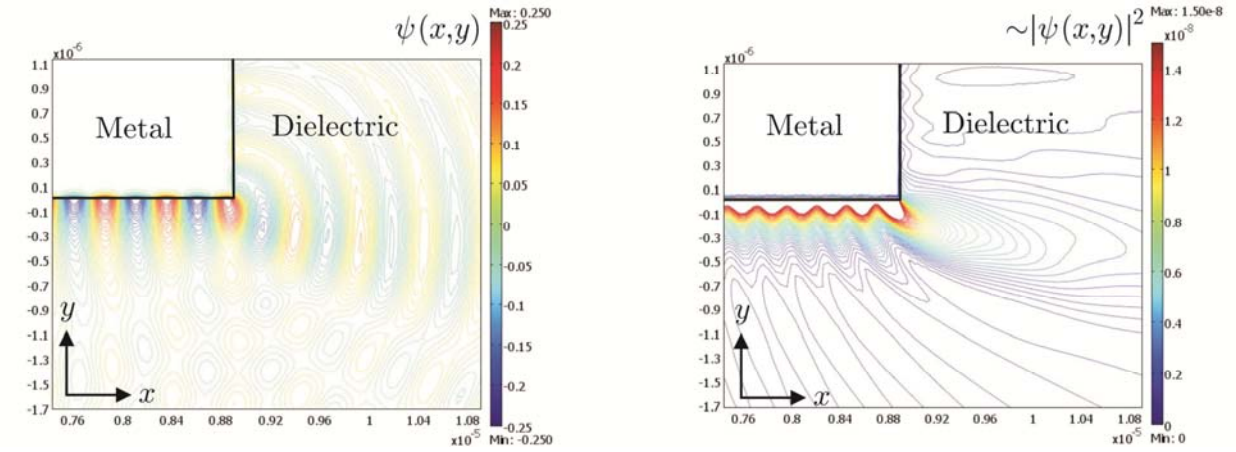

Fig. 2: The solution ψ of the Helmholtz equation (left) and the $|\psi|^2$ (right) describing the electromagnetic field in the vicinity of an infinite (a 2D problem) metal corner and being solved numerically in the COMSOL Multiphysics software package [3].

This work has been supported by the research programmes of the Ministry of Education of the Czech Republic (Projects No. MSM0021630508, 2E08017 and LC06040), the EUROCORES – GACR project (FON/06/E001), GACR (project no. 202/07/P486) and by the company Tescan.

[1] S. A. Maier: Plasmonics: Fundamentals and Applications. Springer, 2000.
[2] T. Šikola, R. D. Kekatpure, E. S. Barnard, et al.: Mid - IR Plasmonic Antennas on Silicon-Rich Oxinitride Absorbing Substrates: Nonlinear Scaling of Resonance Wavelengths with Antenna Length. App. Phys. Lett., in print.
[3] Current web page: www.comsol.com

Transmission of 4.5 keV Ar^{9+} ions through a single glass macrocapillary

G. Kowarik, R. J. Bereczky[1], C. Lemaignan, K. Tökési[1], and F. Aumayr

Institute of Applied Physics, TU Wien - Vienna University of technology, A-1040 Wien, Austria
(corresponding author: G. Kowarik, e-mail: kowarik@iap.tuwien.ac.at)

[1] *Institute of Nuclear Research of the Hungarian Academy of Sciences (ATOMKI), Debrecen H--4001, Hungary*

Recently, we were able to show the validity of the so-called guiding effect of highly charged ions, known from insulating nanocapillaries, up to a macroscopic length-scale of straight capillaries. The self-organized formation of charge-patches leads to a guiding electric field inside the glass capillary, causing stable transmission after a charge-up period. Our early investigations were mainly focused onto the quasi-static transmission behaviour. In this contribution we are going to present further systematic data on the quasi-stable transmission regime as well as the time-evolution of the transmission.

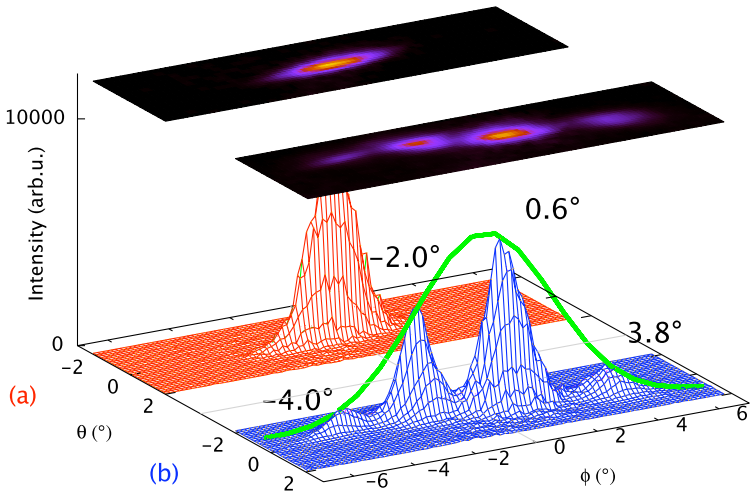

Figure 1: Angular distributions of the direct beam, collimated by a 0.5 mm aperture (a) in comparison with the guided distributions (b) for four different tilt angles as indicated. The z-axis shows the number of ion impacts per unit area. The solid curve is the result of a Gaussian fit of the maxima of the distributions. ϕ denotes the lateral deflection angle in the horizontal plane, the elevation angle is θ.

Since the discovery of the so-called guiding effect of slow highly-charged-ions (HCI) [1] many aspects of the underlying process have been subject of investigations in the case of nano-capillaries. The early experiments have used thin insulating foils with randomly distributed capillaries or alternatively ordered arrays of regular nano-capillaries. Macroscopic tapered capillaries are currently also subject of investigations concerning guiding of HCI, and have revealed distinct focusing properties (see e.g. [2]).

Recently, we were able to show the existence of the guiding effect, also in a straight, macroscopic glass capillary (length 11.6mm, 0.17mm diameter), which shows stable transmission for tilt angles of several degrees [3, 4] after some charge-up period, as illustrated in figure 1.

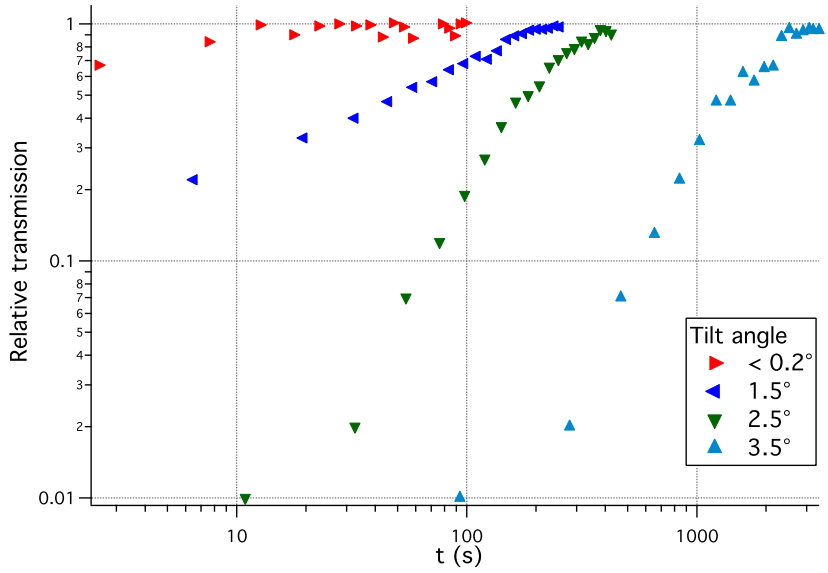

Figure 2: Time dependent relative transmission through the capillary for various tilt angles. The values are normalized to 1 for the equilibrium case.

Following these early measurements we are studying the stable transmission regime of the single glass capillary as well as its time dependent behaviour in the charge-up period. An example plot of the time dependent transmission for different tilt angles with respect to the ion beam axis is shown in figure 2. The measurements are carried out using 4.5 keV Ar^{9+} ions, produced by the 14.5 GHz Electron Cyclotron Resonance Ion Source in Vienna.

Support by the the Austrian Academy of Sciences (ÖAW), the EU network ITS-LEIF (RII3 – 026015), the Austrian FWF, by the "Stiftung Aktion Österreich-Ungarn", the Hungarian Academy of Sciences as well as the Hungarian National Office for Research and Technology and the Hungarian Scientific Re- search Found is gratefully acknowledged.

[1] N. Stolterfoht, J.-H. Bremer, V. Hoffmann, R. Hellhammer, D. Fink, A. Petrov, and B. Sulik, Phys. Rev. Lett. 88, 133201 (2002)

[2] T Ikeda, T. M. Kojima, Y. Iwai1, Y. Kanai, T. Kambara, T. Nebiki, T. Narusawa and Y. Yamazaki , J. Phys: Conf. Ser. 58, 68-73 (2007)

[3] R. J. Bereczky, G. Kowarik, K. Tőkési, F. Aumayr, Nucl. Instr. and Meth. Phys. B 267, 317 (2009)

[4] G. Kowarik, R. J. Berecky, F. Aumayr, K. Tőkési, Nucl. Instr. and Meth. Phys. B 267, 2277 (2009)

Influence of surface defects on hydrogen outgassing of stainless steel

M. Leisch and A. Juan[1]

Institut für Festkörperphysik, Technische Universität Graz, A-8010 Graz, Austria

(corresponding author : M. Leisch, e-mail: m.leisch@TUGraz.at)

[1] *Departamento de Fisica,Univ. National del Sur, 8000 Bahia Blanca, Argentina*

Stainless steel (SS) is one of the most commonly used constructional materials for vacuum chambers and components. Special applications like accelerator, storage ring facilities or advanced semiconductor device processing make need for extreme high vacuum (XHV). In the XHV regime a reduction of the outgassing rates of the materials used in the construction of the vacuum system is essential [1]. Beside surface treatment to reduce the surface roughness high temperature vacuum firing became an alternate method and widely accepted practice of reducing the amount of hydrogen dissolved in SS. For the description of the outgassing rate basically two models common as diffusion limited model (DLM) and recombination limited model (RLM) have been discussed [2-5]. Surface states which may influence the outgassing kinetics significantly are not considered in the DLM. The hydrogen atoms approaching the surface from the bulk are desorbing in a second-order process. It is well established that the rate of recombination depends strongly on the atomic structure of the surface and is e.g. generally higher on stepped surfaces than on flat close packed planes. In order to gain atomic level information on the real morphology of a surface after common bake-out and vacuum firing SS samples were imaged in the atomic force microscope (AFM) and the scanning tunnelling microscope (STM).

The main experimental work has been carried out on a combined STM – atom probe field ion microscope (AP-FIM) apparatus [6]. A unique feature of the particular combined instrument is that it allows a fully-predictive preparation of STM probe tips in situ by FIM which is important for a reliable imaging of complex surfaces.

After the thermal treatment surface inspection by Auger electron spectroscopy (AES) was performed. The spectra give reason for a composition change indicated by a reduction of the chromium signal in relation to the iron and nickel signal. Since the information depth of AES covers several atomic layers not only the top atomic layer of the sample is investigated. The atom probe allows measuring the chemical composition on the surface atomic layer by layer. For this reason the 3D atom probe additionally has been used to investigate the segregation behaviour on SS samples after bakeout and vacuum firing [7].

The surface after vacuum firing shows the formation of large flat terraces which can be assigned to (111) planes. These terraces are bounded by bunched steps and facets

corresponding in orientation almost to (110) planes and (100) planes. The deep grooved grain boundaries and facets formed by bunched atomic steps represent very active sites for adsorption and recombination. A close up view on the large (111) terraces by STM show that there are a lot of vacancies too [7,8].
Theoretical studies and simulations on the interaction of hydrogen with lattice imperfections [9] may provide a new insight in hydrogen outgassing. The energy calculations using the ASED method (Atom superposition and Electron Delocalization) plotted in Figure 1 result in lower energy levels in tetrahedral sites in Fe vacancies. It supports the picture that surface and subsurface defects form traps with different energetic levels. They may control the recombinative desorption process and give explanation for the observed outgassing behaviour of stainless steel. From this results a more complete description of the outgassing process may be given by a more or less dynamic equilibrium between diffusion, sojourn in different level traps and recombinative desorption.

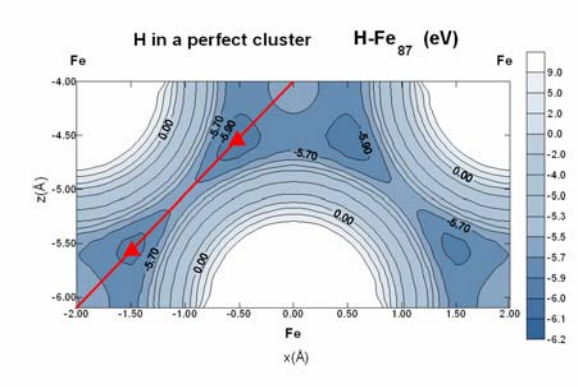

Figure 1a: Energy contour lines for the Fe87-H system.

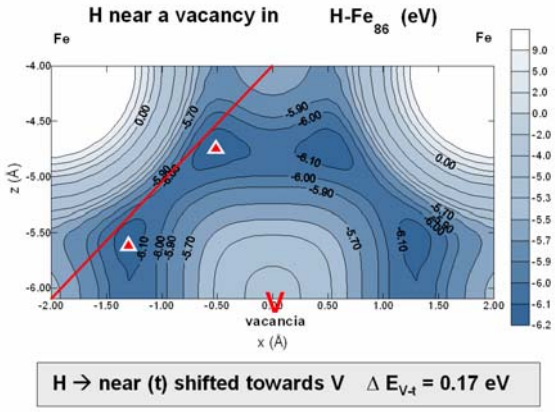

Figure 1b: Energy contour lines for the Fe86 + **V**acancy-H system. The energy minimum is shifted towards the vacancy and 0.17 eV lower.

This work was supported by the Austrian „Fonds zur Förderung der wissenschaftlichen Forschung“ P 12099 and the “Zukunftsfonds Steiermark”P 119.

[1] Redhead PA. Ultrahigh and Extreme High Vacuum *Foundations of Vacuum Science and Technology* ed Lafferty JM (New York: Wiley) 1998 p 625
[2] Moore BC *J. Vac. Sci. Technol.* A **13** (1995) 545
[3] Nemanič V Zajec B Šetina J *J. Vac. Sci. Technol.* A **19**(1) (2001) 215
[4] Ishikawa Y Nemanič V *Vacuum* **69** (2003) 501
[5] Bacher J-P Benvenuti C Chiggiato P Reinert M-P Sgobba S Brass A-M *J. Vac. Sci. Technol.* A **21**(1) (2003) 167
[6] Fian A, Leisch M. *Ultramicroscopy* **95** (2003) 189
[7] Stupnik A Leisch M *Vacuum* **81** (2007) 748
[8] Stupnik A Frank P Leisch M *Ultramicroscopy* **109** (2009) 563
[9] Rey Saravia D Juan A Brizuela G Simonetti S *I J Hydrogen Energy* **34** (2009) 8302

Step bunching to step meandering transition induced by electromigration on Si(111) vicinal surface.

Frédéric Leroy,[1] Daniela Karashanova,[1,2] Matthieu Dufay,[3,4] Jean-Marc Debierre,[4] Thomas Frisch,[4] Jean-Jacques Métois,[1] and Pierre Müller[1]

[1] *Centre Interdisciplinaire de Nanoscience de Marseille, CNRS - UPR 3118, Aix-Marseille Université Campus de Luminy Case 913, 13288 Marseille Cedex 09, France*
[2] *Central laboratory of Photoprocesses "Acad. J.Malinowski" Bulgarian Academy of Sciences Sofia 113, Bulgaria, Acad. G.Bonchev str., B1.109*
[3] *CNRS/The Rudolf Peierls Centre for Theoretical Physics, 1 Keble Road, Oxford OX1 3NP, United Kingdom*
[4] *Institut Matériaux Microélectronique Nanosciences de Provence, Aix-Marseille Université, Faculté des Sciences et Techniques de Saint-Jérôme, Case 151, 13397 Marseille Cedex 20, France*

The main goal of this contribution is to provide new insight into the well-known meandering/bunching transition of vicinal Si surfaces under a direct electric current [1, 2]. For this purpose, a temperature gradient has been maintained between the two ends of a Si(111) vicinal sample in order to observe on the same sample the evolution of the surface morphology versus temperature. The temperature gradient is simply obtained by clamping differently both ends of the sample. The sample surface is observed *ex situ* by optical microscopy. In Fig. 1 is shown a sequence of optical micrographs of the intermediate zone for which the morphology continuously changes from step bunching (high temperature zone) to step meandering (low temperature zone). For the lowest temperatures ($T < 1220$°C) ridges and valleys are observed perpendicular to the initial step direction and correspond to the formation of step-meandering. At higher temperature some small ridges parallel to the initial steps (and thus perpendicular to the ridges and valleys) appear. They progressively cover the whole surface and form a step-bunched morphology at $T > 1230$°C. This transition from meandering to step bunching takes place by local inhomogeneities that disturb the initial surface morphology.

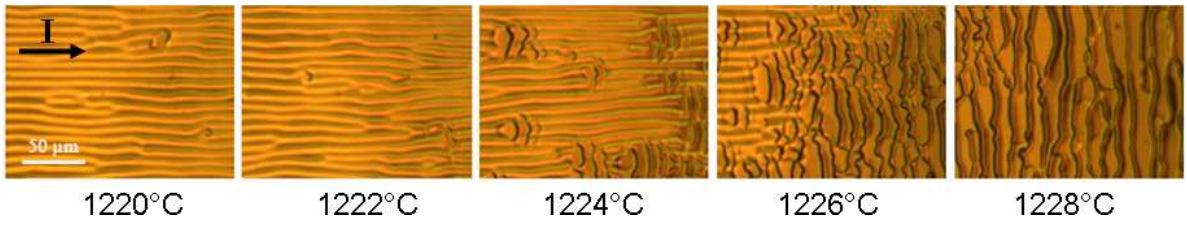

FIG. 1: Optical micrographs of the transition zone from step-meandering (left) to step-bunching (right).

The relative proportion of step meandering and bunching versus the local temperature is reported in Fig. 2a. The abruptness of the meandering/bunching transition ($\Delta T = 4$°C) arises from the competition between two unstable modes (bunching and meandering). This behavior can be easily explained in the framework of a simple linear analysis approach of a Burton-Cabrera-Franck type model [3] in which both instabilities can coexist at a given temperature but with different temperature dependence of the amplification factor (Fig. 2b). Thus at a critical temperature $T = 1225$°C step-bunching takes place to the detriment of step-meandering for step-down DC current (Fig. 2b). The experimental results can be recovered using a two-parameter model compatible with attachment/detachment limited kinetics [4].

[1] A.Latyshev, A.Aseev, A.Krasilnikov, S.Stenin, Surf. Sci. 213 (1989) 157.
[2] K. Yagi, H.Minoda, M.Degawa, Surf. Sci. Rep. 43 (2001) 45.

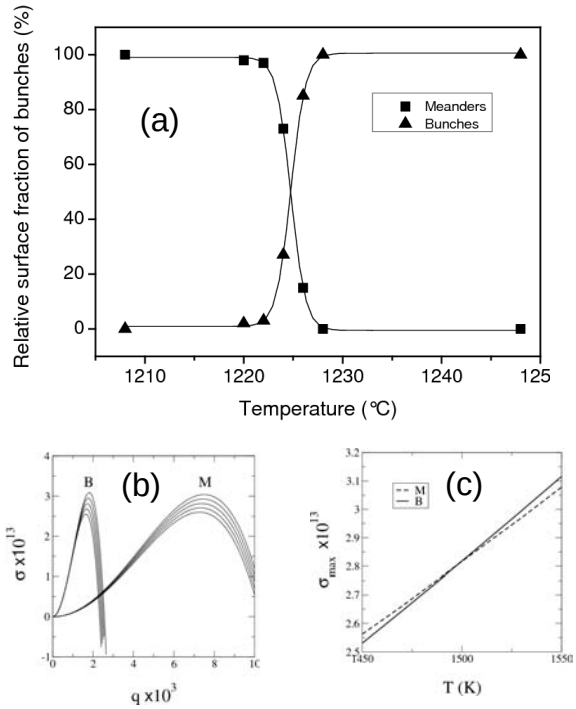

FIG. 2: (a) Experimental evolution of the meandering/bunching fraction of the surface as function of the temperature. (b) Calculation of the evolution of the amplification factors $\sigma_M(k)$ and $\sigma_B(k)$ with temperature (increasing from bottom to top by steps of 20 K). (c) Same as (b) for the maximum of the amplification factors M and B with temperature. The two curves cross at about 1225 °C.

[3] W. Burton, N. Cabrera, F. Frank, Phil. Trans. Roy. Soc. 243 (1951) 299.
[4] F. Leroy, D. karashanova, M. Dufay, J. M. Debierre, T. Frisch, J. J. Metois, P. Müller, Surf. Sci. 603 (2009) 507-512.

Fischer-Tropsch synthesis followed at high pressures with STM and XRD

V. Navarro, S.B. Roobol, R. van Rijn, O. Balmes, D. Wermeille, T. Dufrane, A. Resta, R. Felici and J.W.M. Frenken

The Fischer-Tropsch synthesis (FTS) is the reaction that leads to the production of hydrocarbons from a mixture of H_2 and CO in the presence of a catalyst under certain conditions of high temperature and pressure. As a method for producing a synthetic petroleum substitute FTS has stimulated significant interest in scientific research. Most of the studies about this reaction have been performed from the point of view of the industry whose main interest is to improve the efficiency of the reaction. However, there has not been much basic research towards understanding the atomic and molecular aspects of the reaction mechanisms under industrial conditions [1].

The techniques which are typically used in surface science can shed light on the fundamental mechanisms that govern the FTS. Most of these studies are performed under typical surface science conditions that differ significantly from the real conditions in commercial processes. The pressures typically used in surface science are several orders of magnitude lower than the pressures used in industrial FTS. Also the structure, composition and morphology can be very different. Those differences in the pressure regime and the material structure used in the reaction are known as pressure and material gaps respectively. The pressure and the material gaps can prevent the basic research on the FTS to understand the real catalytic processes that take place.

We are performing studies on the FTS with two innovative surface science techniques that approach the conditions at which the reaction takes place in industry. STM [2] and SXRD [3] have been used to study the catalytic surface under conditions of high pressure and high temperature. These techniques allowed us to study the structural changes on the surface of the catalyst at the same time as the reaction takes place. First results will be presented.

References:

1- Jon Wilson and Cor de Groot, *J. Phys. Chem.* ***99****,* 7860-7866 (1995).

2- Bas L.M. Hendriksen, Stefania C. Bobaru, and Joost W.M. Frenken, *Topics in Catalysis*, **36**, 1–4 (2005). J. Frenken and B. Hendriksen, *MRS Bull.* **32**, 1015–1021 (2007).

3- R. van Rijn, M.D. Ackermann, O. Balmes, T. Dufrane, H. Gonzalez, H. Isern, L. Petit, V.A. Sole, D. Wermeille, R. Felici, A. Geluk, E. de Kuyper, and J.W.M. Frenken. *To be published*, *Rev. Sci. Instrum.* (2010).

Single Adatom Diffusion on Pt and $Pt_{(x)}Co_{(1-x)}$(111) Surfaces

P. Scheiber, M. Schmid, and P. Varga

Institut für Angewandte Physik, Technische Universität Wien, A-1040 Wien, Austria
(corresponding author: P. Scheiber, e-mail: scheiber@iap.tuwien.ac.at)

For growing nanoscale materials it is necessary to gain knowledge about diffusion processes on surfaces and their parameters. By means of a Low Temperature - Scanning Tunneling Microscope (LT-STM) the Pt(111) surface and the diffusion behaviour of Pt and Co adatoms on this surface has been investigated. The first experiment was performed with Co adatoms diffusing on the Pt(111) surface at 50K. Many diffusion steps could be observed and even if they moved really close to each other, it seemed that there was an energy barrier for the formation of dimers. In contrast to this Pt adatoms diffused less and they formed stable dimers already at 80K (see Fig. 1). When the sample was heated to 84K all Pt adatoms formed dimers.

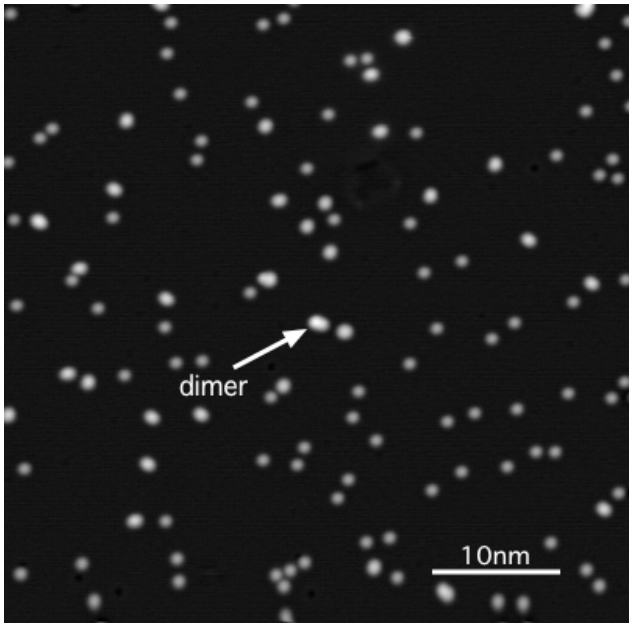

Figure 1: Single Pt adatoms and dimers on Pt(111) at 80K

Another result of these measurements was that Pt adatoms diffused even at temperatures, for which calculations predicted hardly any diffusion step. This unusual effect was analyzed in more detail and led to the conclusion that the electrical field between the LT-STM tip and the sample can influence the diffusion parameters quite strongly depending on its bias. For negative sample bias the influence of the electrical field of the tip was very strong and the. Single Pt adatoms were repelled by the field of the tip and due to this tip induced diffusion formed stable dimers. Using positive bias the diffusion of the Pt atoms could be observed as the calculation from the diffusion equation predicted and it was also possible to calculate the activation energy for performing a single diffusion step from consecutive STM images.

To study the influence of the surface composition a surface alloy was produced. The Pt(111) surface was sputtered at higher temperature which led to holes in the surface. Then Co was evaporated onto it and due to the high temperature diffused to the step edges. There it was incorporated into the surface by pushing a Pt surface atom away from the step and moving to the lower plane. Therefore no pure Co areas on the Pt surface were produced but a surface alloy [1]. This provided the possibility to investigate the diffusion behaviour of the Pt adatoms on the surface alloy compared to previous measurements. The potential energy of the surface was changed due to the incorporated Co and modified the diffusion barrier. Indeed, it was possible to find single Pt adatoms even at temperatures where on the pure Pt(111) surface only dimers are stable (see Figure 2).

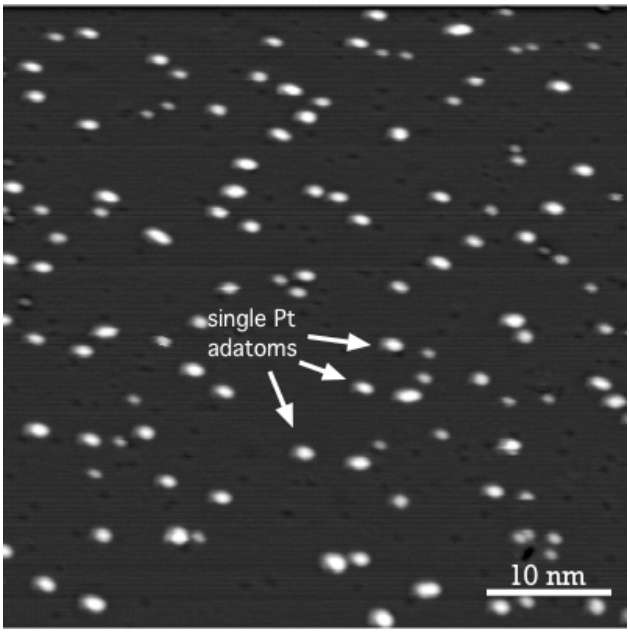

Figure 2: Single Pt adatoms and dimers on the $Pt_xCo_{(1-x)}$ surface alloy at 115K

[1] Lundgren, Stanka, Leonardelli, Schmid, Varga, Phys. Rev. Lett. 82, 5068 (1999)

Support by Fonds zur Förderung der Wissenschaftlichen Forschung.

Theoretical investigation of BN-nanomesh on Rh (111)

Yun Ding, Marcella Iannuzzi, Ari P Seitsonen, and Jürg Hutter

Physikalisch-Chemisches Institut der Universität Zürich

(corresponding author: Jürg Hutter,
e-mail: Hutter@pci.uzh.ch,
URL: http://www.pci.uzh.ch/)

The discovery of the two-dimensional BN films on Rh (111) [1] has lead to a wide interest in this structure as it exposes a regular network of pores of about 2 nm in size. The atomistic geometry was soon established and verified [2] to consist of a single, incommensurate layer of BN; the different relative positions of the boron and nitrogen atoms at different parts of the nanomesh relative to the outer-most substrate atoms lead to a modulated vertical height of the BN layer and electro-static potential above it. This structure provides potential to act as a template for controlled arrangements of adsorbates on the nanoscale.

Here we report density functional theory (DFT) calculations of the nanomesh on Rh(111). We study the atomic geometry and electronic properties of the structure, and show projected densities of states and electro-static potential of the nanomesh structure. As first studies on adsorption on the nanomesh we investigate the nano-ice assembled at the pores [3].

We also report results in the hydrogen intercalated structure [4], where the BN layer becomes essentially flat along the adsorption of the hydrogen atoms between the rhodium substrate and the layer.

URL: http://www.nanomesh.ch/

[1] *Boron Nitride Nanomesh*; Martina Corso, Willi Auwärter, Matthias Muntwiler, Anna Tamai, Thomas Greber & Jürg Osterwalder; Science **303** 217 (2004); DOI: 10.1126/science.1091979

[2] *Single layer model of the h-BN nanomesh on the Rh (111) surface*; R. Laskowski, P. Blaha, T. Gallauner, K. Schwarz; Phys. Rev. Lett. **98**, 106802 (2007)

[3] *Boron nitride nanomesh: A template for nano-ice*; Haifeng Ma, Thomas Brugger, Simer Berner, Yun Ding, Marcella Iannuzzi, Jürg Hutter, Jürg Osterwalder & Thomas Greber; arXiv:0908.0875

[4] *Reversible switching of surface texture by hydrogen intercalation*; Thomas Brugger, Haifeng Ma, Marcella Iannuzzi, Simon Berner, A. Winkler, Jürg Hutter, Jürg Osterwalder & Thomas Greber; arXiv:0911.1317

Quasi-free Standing Epitaxial Graphene on SiC by Hydrogen Intercalation

C. Riedl,[1] C. Coletti,[1] T. Iwasaki,[1] A. A. Zakharov,[2] and U. Starke[1,*]

[1]*Max-Planck-Institut für Festkörperforschung, D-70569 Stuttgart, Germany*

[2]*MAX-Lab, Lund University, Box 118, Lund, S-22100, Sweden*

The outstanding electronic properties of graphene - in combination with epitaxial growth on silicon carbide (SiC) make it a very promising material for future carbon based electronic devide applications. Epitaxial graphene on SiC combines most of the exciting properties of free standing graphene to a manufacturing friendly planar structure. A significant drawback up to now for a technologic application of this material is related to the strong interaction of the graphene layers with the SiC substrate. The SiC surface is covalently bound to the first carbon layer, which act as a buffer-layer and therefore fails in displaying graphene properties. The undesired effects originating from this strong coupling, such as intrinsic n-type doping and degraded transport properties, affect the overlying graphene layers.

An elegant solution to this problem of graphene-SiC coupling is provided by annealing the samples in molecular hydrogen [1]. Angular resolved photoemission spectroscopy (ARPES), high resolution core level photoemission spectroscopy (CLPES), low-energy electron diffraction (LEED) and low-energy electron microscopy (LEEM) demonstrate that hydrogen atoms migrate through the graphene layers, intercalate between the SiC substrate and the buffer-layer and bind to the Si atoms of the SiC(0001) surface. Thus the buffer-layer, decoupled from the SiC substrate, is turned into a quasi-free standing graphene monolayer, as shown in Fig. 1 by LEED data, ARPES measurements and a sketched model. It also shows that the decoupling is reverible by hydrogen desorption at elevated temperatures.

We will also show, that in an identical procedure, epitaxial monolayer graphene turns into a decoupled bilayer. Here, it is evident from the position of the Dirac energy that the intercalation and decoupling also lifts the intrinsic doping by eliminating the substrate-interface bonding. The intercalation process represents a highly promising route towards epitaxial graphene based nanoelectronics.

Support by the EC through the Access to Research Infrastructure Action is greatfully

*Electronic address: u.starke@fkf.mpg.de

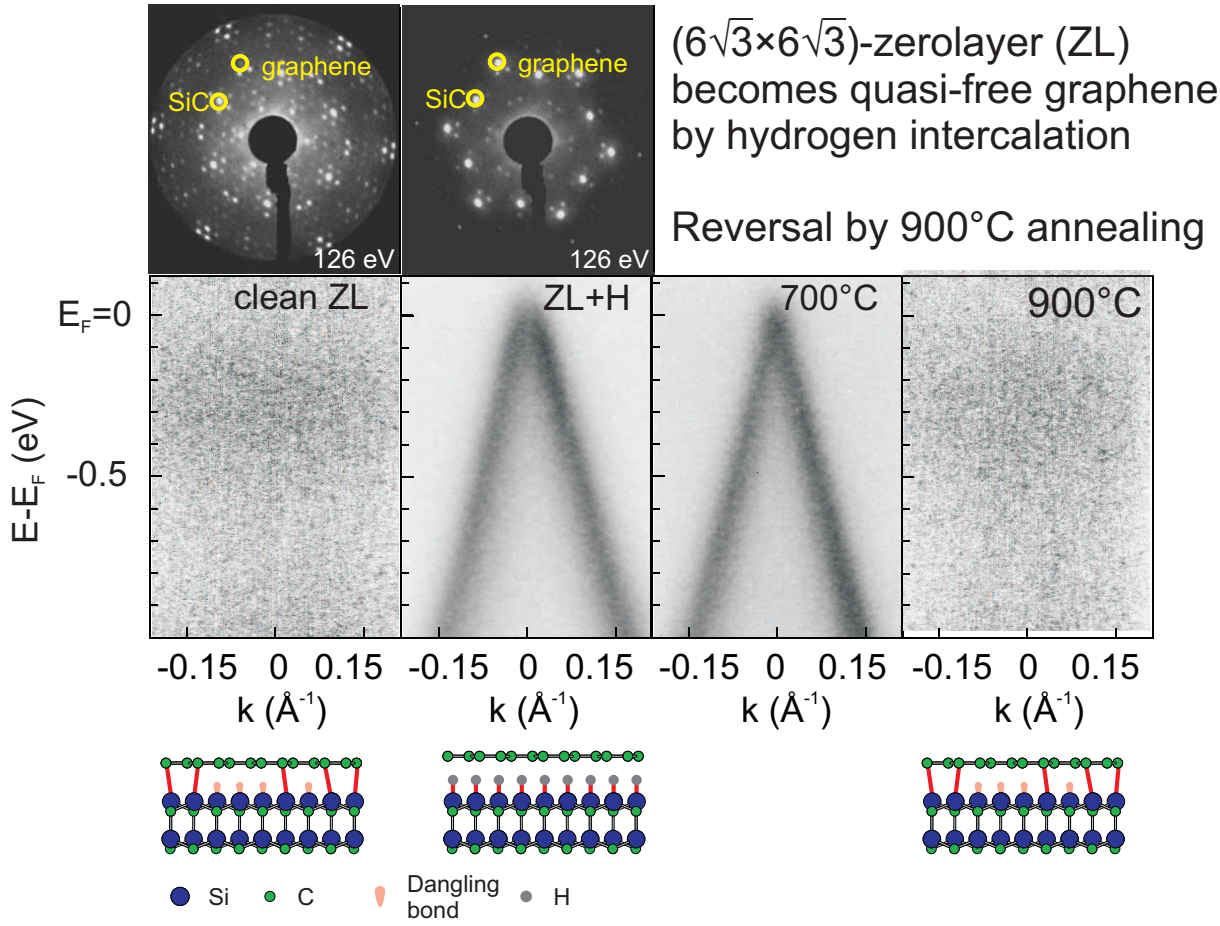

FIG. 1: top: LEED pattern for a $(6\sqrt{3}\times6\sqrt{3})$R30° zero-layer on SiC(0001) before (left) and after hydrogen intercalation (right). middle: Band structure measured via ARPES through the $\bar{\text{K}}$-point of the graphene Brillouin zone of a $(6\sqrt{3}\times6\sqrt{3})$R30° zero-layer on SiC(0001) before and after hydrogen intercalation, as well as after annealing to 700 °C and 900 °C (from left to right). Note, that the hydrogen intercalated graphene layer is undoped. bottom: model sketch for a $(6\sqrt{3}\times6\sqrt{3})$R30° zero-layer with interface bonds (left) and a quasi-free standing graphene layer after intercalation of hydrogen (middle). The zero-layer structure appears again after hydrogen desorption at 900 °C.

acknowledged. C.C. and T.I. acknowledge the Alexander von Humboldt research fellowship for financial support.

---

[1] C. Riedl, C. Coletti, T. Iwasaki, A. A. Zakharov, and U. Starke, Phys. Rev. Lett. **103**, 246804 (2009).

The development of an easy-to-use, versatile MEMS SPM scanner

F.C. Tabak, G.H. Wortel, P.C. van der Tuijn, J. W. Bakker, J.W.M. Frenken, W.M. van Spengen

LION, University of Leiden, Niels Bohrweg 2, 2333 CA Leiden
(corresponding author: F.C. Tabak, tabak@physics.leidenuniv.nl)

Scanning Probe Microscopy is a frequently used technique in surface science. It enables the study of surfaces down to the atomic level; it allows investigation of surface structures and surface processes, for example catalytic reactions. Unfortunately, scanning probe microscopes are relatively slow instruments. The combination of line-by-line scanning motion and ultra-high resolution (<0.1nm) makes the instrument very sensitive to vibrations. Therefore, the scan speed has to stay well below the resonance frequencies of both the instrument and the piezo element wich executes the scanning motion. In general, fast scanning probe microscopes are limited by the resonance frequency of the scanning piezo element. Depending on the specific geometry (piezo tube, piezo stack) a piezo element can have a fundamental resonance frequency ranging from a few kHz to ~200 kHz.
Micro-Electro Mechanical Systems (MEMS) can be designed to perform SPM z-motion while having a high resonance frequency (in the MHz range). Due to their small mass, MEMS motion will not excite resonance frequencies in the mechanical loop of the scanner. One of our MEMS SPM z-scanners is shown in figure 1. Other groups have worked on MEMS SPM scanners before, but none of them has focused on high-speed applications.
We present the latest developments of MEMS-based SPM design. We will focus on two aspects: tip growth on MEMS and the design of a scanner that allows incorporation of a fast MEMS z-scanner on a piezo x,y-scanner.

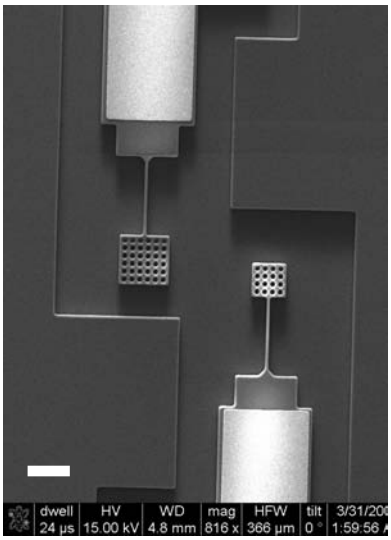

Figure 1: Two MEMS SPM z-scanners, a freestanding 'fly swatter' model that can be moved using electrostatic actuation.. The resonance frequency of the smaller scanner has been measured to be 980 kHz. Both scanners are z-scanners only (out-of-plane motion). The scale bar represents 25µm.

The size of MEMS scanners (10-100 µm) prevents the use of the common, macroscopic, etched tungsten tips: the MEMS are too small to carry the weight of these tips and mounting the tips manually is not possible. Therefore we apply a VLS (Vapour-Liquid-Solid) process first described by Wagner and Ellis [1]. In this process, silicon nanowire growth is enabled by a gold catalyst particle via the reaction:

$SiCl_4$ (g) + H_2 (g) → Si (s) + 4HCl (g)

The nanowire thickness can be controlled by three parameters. Firstly, the size of the catalyst particle: the diameter of the resulting nanowire will not exceed the diameter of the catalyst particle [2]. Secondly, wire thickness is controlled by the temperature. Thicker nanowires grow at higher temperatures than thin whiskers [3]. Thirdly, nanowire diameter is also controlled by the ratio of H_2 and $SiCl_4$ in the gas mixture [3].

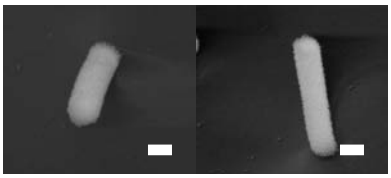

Figure 2: Tip growth on Si(111). These silicon nanowires are grown beneath gold catalyst particles. The nanowires can be sharpened by etching or Focused Ion Beam Milling to form SPM tips. Left:: no tilt (view perpendicular to the Si(111) surface), Right: tilt 45°. From the images we conclude that the wire is grown under an angle of 13°.The scale bar represents 1 μm.

We have built a setup to grow these nanowires on our MEMS devices. So far, we have already successfully grown nanowires on Si(111) wafers. One of the results is shown in figure 2. These nanowires can be sharpened, for instance by an etching process, to high-quality SPM tips. However, a lot of open questions remain regarding the composition of the tips and the possible growth directions on MEMS devices (which are, in our case, either polysilicon or Si(100)). Another viable route is the use of EBID deposited platinum tips, which we have also demonstrated [4].

We have designed and built an SPM scanner which is optimized for scanning with various MEMS devices. This scanner, shown in figure 3, is based on a Beetle/Besocke type scanner [5]. The approach mechanism is a stick-slip motor which consists of three piezo stacks walking up and down a ramp. A piezo stack is located in the middle of the scanner. This stack performs x,y-scanning and carries the MEMS z-scanner. This MEMS z-scanner can be easily exchanged, comparable to the exchange of AFM cantilevers. The scanning piezo element itself can also be exchanged and the scanner allows the incorporation of tube, stack and conical piezo elements, as well as the use of a counter piezo geometry. We use a small sample (1x1x1mm) which can be tilted to an accuracy of 0.6°. This allows accurate alignment of the MEMS scanner and sample. This is important when scanning with short tips (~10 μm), to ensure that contact is made between tip and sample instead of with the MEMS die edges/corners first. This sample holder was designed such that the required broadband I/V converter is located just below the sample, to minimize noise in the tunnel current.

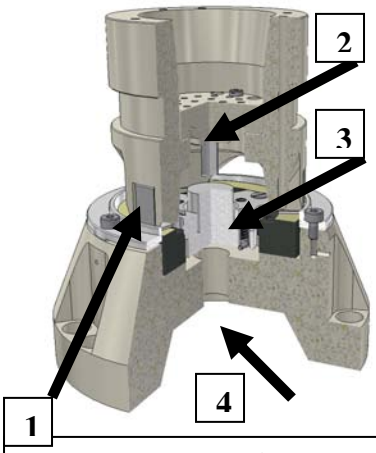

Figure 3: Scanner design for MEMS-SPM scanning. The approach motor(1) consists of three piezo stacks, walking up/down a ramp. In the center of the scanner, a piezo element (2) (which can be a tube, a stack or a conical element) is located which performs the xy-scanning motion and carries the MEMS z-scanner.The sample holder (3) carries the small sample and the I/V-converter will be located directly under the scanner (4).

With this setup, we will be able to test and characterize various MEMS SPM scanners. The optimized layout will enable high-speed scanning and we expect to present first measurement results at the conference.

This project is financially supported by a Netherlands SmartMix grant and the NIMIC partner organizations (www.nimic-project.com) through NIMIC, a public-private program.

[1] R. Wagner, W. Ellis, *Appl. Phys. Lett.* 4 89 (1964)
[2] E.I. Givargizov, A.N. Kiselev, L.N. Obolenskaya, A.N. Stepanova, *Appl. Surf. Sci*, 67, 73 (1993)
[3] Y. Zhang, Q. Zhang, N. Wang. Y. Yan, H. Zhou, J. Zhu, *Journ. Crys. Growth,* 226, 185 (2001)
[4] F.C. Tabak, E.C.M. Disseldorp, T.H. Oosterkamp, A.J. Katan, M.B.S. Hesselberth, J.W.M. Frenken, W.M. van Spengen, *Symposium on surface science, St. Moritz, Switserland 2009*
[5] K. Besocke, *Surf. Sci.* 181, 145 (1987)

He^+ Ion scattering from noble metal and alloy surfaces: Influence of Surface Structure and Composition on Neutralization

D. Primetzhofer, M. Spitz, S.N. Markin, P. Bauer

Institut für Experimentalphysik, Johannes Kepler Universität Linz, Austria

Edmund Taglauer

Max-Planck-Institut für Plasmaphysik, Garching bei München, Germany

Continuing our investigations of ion fractions, P^+, of He^+ ions scattered from various metal surfaces, we studied He^+ scattering from Ag, Au and CuAu surfaces in the low-energy ion scattering (LEIS) regime, i. e. with 0.6 to 9 keV primary energies. Ion yields were determined by an experimental set-up using the time-of-flight technique [1].

For the Ag(110) surface at lower energies Auger neutralization was observed with a characteristic velocity of 1.2×10^5 m/s, in good agreement with theoretical studies [2,3]. For the threshold energy above which collision induced processes are relevant a value of 1.25 keV was found. For scattering in two different azimuthal directions, (001) and (1-10), a small but distinct difference in P^+ was observed.

Ion fractions for Au were measured for polycrystalline Au, the reconstructed Au(110)1x2 surface and a CuAu(100) crystal surface. The ordered structure of the CuAu alloy surface [4] could be well confirmed. Our results show that P^+ for Au can depend strongly on the geometry and composition of the investigated surface. CuAu and polycrystalline Au exhibit similar neutralization behaviour, whereas for Au(110) a remarkably high fraction of surviving ions from the surface layer was deduced from the experimental results [5]. These studies also confirm that the TOF-LEIS technique is very useful for probing electronic and structural surface properties.

[1] M. Draxler, S.N. Markin, S.N. Ermolov, K. Schmid, C. Hesch, R. Gruber, A. Poschacher, M. Bergsmann, P. Bauer, Vacuum **73**, 39 (2004).

[2] D. Valdés, J.M. Blanco, V.A. Esaulov, R.C. Monreal, Phys. Rev. B **75**, 165404 (2007).

[3] M.A. Karolevski, Nucl. Instr. Meth. Phys. Res. B **230**, 402 (2005).

[4] E. Taglauer and R. Beikler, Vacuum **73**, 9 (2004).

[5] D. Primetzhofer, M. Spitz, S.N. Markin, E. Taglauer, and P. Bauer, Phys. Rev. B **80**, 125425 (2009).

Competition of Magnetism and Correlation in a Cobalt Dimer: from Kondo Screening to Local Moment Antiferromagnetism

J. Bork[1,2], P. Wahl[1], Y. Zhang[1], L. Diekhöner[2], P. Simon[3], L. Borda[4], J. Kroha[4], and K. Kern[1,5]

(corresponding author: P. Wahl, e-mail: wahl@fkf.mpg.de)

[1] Max-Planck-Institut für Festkörperforschung, Stuttgart, Germany
2 Institut for Fysik og Nanoteknologi, Aalborg Universitet, Denmark
3Laboratoire de Physique des Solides, Université Paris-Sud, F-91405 Paris-Orsay, France
4 Physikalisches Institut, Universität Bonn, Nussallee 12, D-53115 Bonn, Germany
5 Institut de Physique des Nanostructures, Ecole Polytechnique Fédérale de Lausanne (EPFL), CH-1015 Lausanne, Switzerland

Correlated electron materials owe their properties often to a subtle balance between Kondo screening and magnetic ordering of localized moments. The macroscopic properties of these materials change dramatically depending on which of the two dominates. Of particular interest are materials whose properties can be tuned between the two regimes as a function of a continuous external parameter such as magnetic field [1], pressure [2] or doping [3]. In these cases, the system can be a quantum phase transition, where the transition is at low temperatures governed by quantum fluctuations rather than by thermal fluctuations. However a theoretical description of these materials and their properties remains elusive. A simple model system, on which the competition between magnetic interaction and Kondo screening can be studied consists of the two-impurity Kondo problem.

Previous attempts to study this competition by STM for pairs of magnetic adatoms at surfaces suffered from being limited to discrete lattice sites for the positions of the atoms, thereby only yielding access to discrete values of the magnetic interactions [4,5]. Here we present measurements by low temperature scanning tunneling spectroscopy on a cobalt dimer, where one of the cobalt atoms is attached to the STM tip while the other sits on the surface. The interaction between the cobalt atoms can be continuously tuned by adjusting the tip-sample distance. From the spectral response of the cobalt dimer for different distances, information about the magnetic interactions and the ground state of the dimer can be deduced. An interpretation based on the competition between antiferromagnetic coupling and Kondo screening of the local moments is offered.

[1] S.A. Grigera *et al*., *Science* **294**, p. 329 (2001).
[2] N.D. Mathur *et al*., *Nature* **394**, p. 39 (1998).
[3] H.v. Löhneysen, *Jrnl. Phys.: Cond. Matt.* **8**, p. 9689 (1996).
[4] W. Chen, T. Jamneala, V. Madhavan, and M.F. Crommie, *Phys. Rev. B* **60**, p. R8529 (1999).
[5] P. Wahl, et al., *Phys. Rev. Lett.* **98**, 056601 (2007).

Atomic, electronic, and vibrational structure of epitaxial manganese oxide films: A combined STM, STS, and HREELS study

B. Bochmann, S. Sachert, S. Polzin, M. Huth, R. Shantyr, K. Gilmeister, K. Meinel, M. Schindler, Ch. Hagendorf, H. Neddermeyer, and W. Widdra

Institute of Physics, Martin-Luther Universität Halle, 06120 Halle, Germany
(Corresponding author: W. Widdra, e-mail: wolf.widdra@physik.uni-halle.de)

The growth as well as the atomic, electronic and phononic structures of ultra thin epitaxial manganese oxide films on Pt(111) and on Ag(100) have been studied using scanning tunneling microscopy (STM), high-resolution electron energy loss spectroscopy (HREELS), and low-energy electron diffraction (LEED and SPA-LEED). All films have been prepared by reactive metal deposition in an oxygen atmosphere. Depending on the preparation conditions ordered films with different Mn to O stoichiometry can be grown. For the Ag substrate, a strong diffusion of Ag atoms occurs during growth of the Mn oxide films even at room temperature, which yields an embedding of oxide islands and a roughening of the film/substrate interface.

For the monolayer, three different long-range ordered phases of Mn_xO_y with approximate stoichiometries of 1:1, 3:4 and 1:2 have been found on Pt(111) as well as on Ag(100). Despite the rather different reactivity and the different symmetry of the Pt(111) and the Ag(100) substrate, similar structures are formed. On Pt(111) at low oxygen pressure, a (19×1) uniaxially reconstructed MnO(100)-like structure is found by LEED and STM. Growth at higher oxygen pressures leads to long-range ordered intermediate Mn_3O_4-like monolayers which can be alternatively prepared by oxidation of the (19×1) monolayer at elevated temperatures. Under highly oxidizing conditions, a quasi-hexagonal monolayer with MnO_2 stoichiometry and 7 % misfit to the Pt(111) substrate is formed. STM indicates a wagon wheel like reconstruction of the O-MnO(111) trilayer of the MnO bulk structure. On Ag(100), analogous MnO(100), Mn_3O_4 and O-MnO(111) phases have been found. However, there in-plane misfit relaxation is different due to the different nature of the substrate.

For two and three layer thick films, again three different well-ordered manganese oxide structures can be grown as based on LEED and STM. HREELS allows separating these structures based on their different phonon spectra for oxide films grown with different ^{16}O and ^{18}O isotopes. For thicker manganese oxide layers, stable MnO(100), Mn_3O_4(001), and MnO(111) structures can be grown depending on the preparation conditions on both substrates. Additional investigations by X-ray absorption spectroscopy (NEXAFS) verify the MnO and Mn_3O_4 character of the thin films. Local spectroscopy based on STS for different

manganese oxide films indicates the different electronic structures for films with thicknesses in the range of one to four monolayers. Most prominently, the unoccupied Mn 3d state which is related to the narrow oxide conduction band has been identified. Additional states within the bulk band gap of the MnO appear for thicker films and are interpreted as 3d-derived surface states. On the Ag(001) substrate, the Mn_3O_4 films grow with a lattice vectors of the oxide structure aligned along the [110]-like directions of Ag(001). This specific film orientation implies an almost vanishing misfit with respect to the substrate. As a consequence, Mn_3O_4(001) films with high structural perfection are obtained. The development of the spinel-like Mn_3O_4(001) film structure can be understood as an alternating stacking of (2x1)-like Mn_2O_4 and (2x2)-like Mn spinel sublayers. According to theory [2], the Mn_2O_4 termination should be favored over a Mn termination since the former has the lower surface free energy. STM investigations provide evidence of the expected Mn_2O_4 termination. They indicate also a tendency for a structural transition of the termination layer from (2x1)- to c(2x2)-like ordering. The c(2x2) ordering is easily obtained from the (2x1) structure when one of two neighboring Mn ions are laterally shifted by one atomic step. The spreading of this more symmetric structure implies a reduction of (2x1) domain areas and domain boundary areas, respectively, which yield a reduction of domain boundary energy.

Support by the German joint research network Sonderforschungsbereich 762 “Functionality of oxidic interfaces” (projects A3, A7, and B8) of the Deutsche Forschungsgemeinschaft is gratefully acknowledged.

[1] Ch. Hagendorf, S. Sachert, B. Bochmann, K. Kostov, and W. Widdra: Phys. Rev. B 77 (2008) 75406.

[2] V. Bayer, R. Podloucky, C. Franchini, F. Allegretti, B. Xu, G. Parteder, M.G. Ramsey, S. Surnev, and F.P. Netzer, Phys. Rev. B 76 (2007) 165428.

Dynamics of electron solvation mediated by Na-D_2O complexes in amorphous ice

M. Meyer[1], J. Stähler[2], M. Bertin[1], U. Bovensiepen[3], and M. Wolf[1,2]

[1]*Freie Universität Berlin, Department of Physics, Arnimallee 14, 14195 Berlin, Germany*
e-mail: wolf@physik.fu-berlin.de

[2]*Fritz-Haber-Institut, Department of Physical Chemistry, Faradayweg 4-6, 14195 Berlin*

[3]*Universität Duisburg-Essen, Department of Physics, Lotharstr. 1, 47048 Duisburg, Germany*

Electron transfer across interfaces is of vital importance in various areas of physics, chemistry and biology. We have studied the ultrafast dynamics of electron transfer and solvation processes in amorphous and crystalline D_2O layers on metal surfaces using time-resolved two-photon-photoemission (2PPE) spectroscopy [1]. In these experiments, photoinjection of electrons from the metal into the adsorbate conduction band is followed by ultrafast localization and solvation of the excess electrons. The subsequent energetic stabilization of these solvated electrons due to nuclear rearrangements of the polar molecular environment is accompanied by an increasing degree of localization. The observed electron transfer rates strongly depend on the local structure of the ice. In crystalline D_2O layers we monitor the stabilization of trapped electrons at the ice vacuum interface continuously from femtoseconds up to minutes [2]. This behavior is fundamentally different from amorphous D_2O layers where the excess electrons have a much lower survival probability, which lifetimes of the order of 100 fs. Recently we have extended these studies to analyze the influence of coadsorbed Na ions coadsorbed at the ice surface

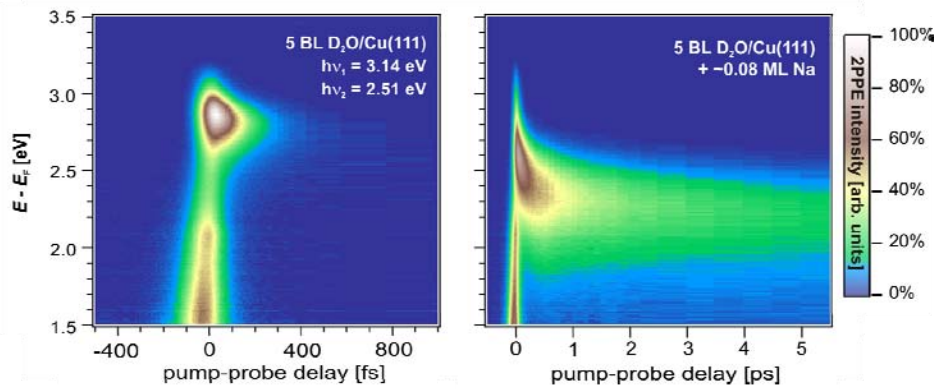

Fig. 1 Time resolved two-photon-photoelectron spectroscopy of electron transfer and solvation processes in amorphous ice layers on Cu(111). The population of photoinjected electrons above the Fermi level is displayed in a false color plot as a function of time delay between the UV pump pulse and the visible probe pulse. Left panel: Solvated electron in 5 BL D_2O/Cu(111) appear as a peak at $E-E_F = 2.9$ eV and decay within a few 100 fs. Right panel: Deposition of 0,08 ML of sodium on top of the ice film results in pronounced changes in the electron dynamics.

We have investigated the electron dynamics of photoinjected excess charges in amorphous ice layers in the presence of sodium ions bound near the ice –va cuum interface. Adsorption of sub-monolayer coverages of sodi um on top of m ultilayers of amorphous ice leads to the formation of Na^+ ions and to pronounced changes in the observed electron. As shown in Fig. 1 for 0,08 ML sodium on 5 BL D_2O/Cu(111) a new sp ecies of lon g-living electro ns can be observed which exhibits m uch lon ger lifetimes and a stronger energetic stabilization compared to solvated electrons in pure am orphous water ice. We attribute this species to an electron-sodium-ion-complex which is located at the ic e/vacuum-interface as il lustrated in Fig. 2. T his interpret ation is corroborated by coverag e dependent m easurements and by overlayer experiments.

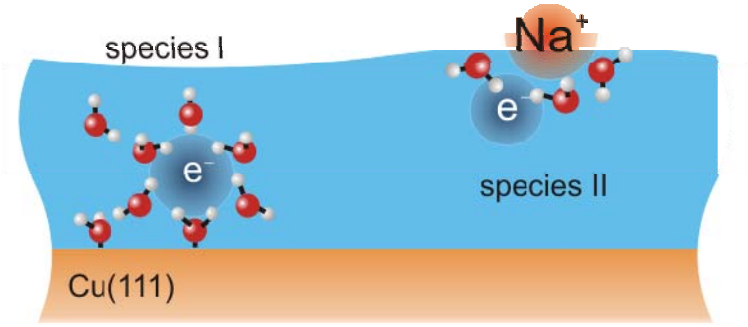

Fig. 2 Schematic illustration of different solvated electron species in the Na/D_2O/Cu(111). Solvated electrons are trapped in multilayers of amorphous ice within the first 2-3 layers from the metal interface which decay within a few 100 fs (species I). Coadsorption of sodium on top of the ice film leads to the formation of longlived species, which are attributed to Na^+-water complexes (species II).

Funding by the DFG through Sfb 450 and the Germn-Israelin-Foundation (GIF) is gratefully acknowledged.

[1] J. Stähler, U. Bovensiepen, M. Meyer, and M. Wolf, *A Surface Science Approach to Ultrafast Electron Transfer and Solvation Dynamics at Interfaces*, Chem. Soc. Reviews **37**, 2180 (2008)

[2] U. Bovensiepen, C. Gahl, J. Stähler, M. Bockstedte, M. Meyer, F. Baletto, S. Scandolo, X.-Y. Zhu, A. Rubio, M. Wolf, *A dynamic landscape from femtoseconds to minutes for excess electrons at ice-metal interfaces*, J. Phys. Chem. C **113**, 979 (2009)

Thursday

STM spin-excitation spectra on individual atoms against XMCD ensemble measurements

H. Brune

Institute of Condensed Matter Physics (IPMC), Ecole Polytechnique Fédérale de Lausanne (EPFL), Station 3, CH-1015 Lausanne

Spin excitation spectroscopy recorded with the STM above individual adsorbed magnetic atoms [1] complements since recent the established XMCD measurements recorded for well defined adatom ensembles [2]. We discuss the first systems for which a comparison between both techniques can be established.

The first is Fe and Co adsorbed on Cu_2N/Cu(100)-c(2 x 2). For Fe an easy axis and for Co an easy plane (hard axis) anisotropy have been deduced from the shifts of the inelastic steps in the differential tunneling conductance measured by means of STM at 0.4 K [3,4]. We present XMCD data for both systems together with spin-polarized density functional theory results for both systems [5]. A consistent picture can be drawn from all three techniques yielding information on spin, orbit, and induced moments and on the origin of the large magnetic anisotropy in these systems, which are distinctively different from metal substrates.

For Fe and Co/Pt(111) spin-excitation measurements [6] together with spin-polarized density functional theory calculations [6,7] complement earlier XMCD measurements for Co [8]. For Co the agreement between STM and XMCD is astonishingly good; however, for Fe STM finds no difference in anisotropy between the two threefold hollow sites whereas theory finds a dramatic difference. We show recent low-T STM results shedding light on this subject [9].

[1] A. J. Heinrich, J. A. Gupta, C. P. Lutz and D. M. Eigler, Science **306**, 466 (2004).

[2] H. Brune and P. Gambardella, Surf. Sci. **603**, 1812 (2009).

[3] C. F. Hirjibehedin, C. Y. Lin, A. F. Otte, M. Ternes, C. P. Lutz, B. A. Jones and A. J. Heinrich, Science **317**, 1199 (2007).

[4] A. F. Otte, M. Ternes, K. v. Bergmann, S. Loth, H. Brune, C. P. Lutz, C. F. Hirjibehedin and A. J. Heinrich, Nat. Phys. **4**, 847 (2008).

[5] M. Etzkorn, C. F. Hirjibehedin, A. Lehnert, S. Ouazi, S. Rusponi, S. Stepanow, P. Gambardella, C. Tieg, P. Thakur, A. I. Lichtenstein, A. Shick, C. P. Lutz, A. J. Heinrich and H. Brune, in preparation (2009).

[6] T. Balashov, T. Schuh, A. F. Takács, A. Ernst, S. Ostanin, J. Henk, I. Mertig, P. Bruno, T. Miyamachi, S. Suga and W. Wulfhekel, Phys. Rev. Lett. **102**, 257203 (2009).

[7] P. Blonski and J. Hafner, J. Phys.: Condens. Matter **21**, 426001 (2009).

[8] P. Gambardella, S. Rusponi, M. Veronese, S. S. Dhesi, C. Grazioli, A. Dallmeyer, I. Cabria, R. Zeller, P. H. Dederichs, K. Kern, C. Carbone and H. Brune, Science **300**, 1130 (2003).

[9] F. Calleja, M. Etzkorn, Q. Dubout, P. Gambardella, L. Claude and H. Brune, in preparation (2009).

Comments on Two Catalytic Processes: Oxidative Coupling for Methane Conversion to Ethylene and Oxidation of Ethylene to Ethylene Oxide

Matthias Scheffler[1], Patrick Rinke[1], Sergey Levchenko[1], Catherine Stampfl[2], and Simone Piccinin[2,3]

[1] *Fritz-Haber-Institut der Max-Planck-Gesellschaft, Faradayweg 4-6, D-14195 Berlin, Germany*

[2] *School of Physics, The University of Sydney, Sydney, New South Wales 2006, Australia*

[3] *CNR-INFM DEMOCRITOS National Simulation Center, Trieste, Italy*

Natural gas consists predominantly of methane (CH_4). It is an abundant energy source but for efficient utilization transformation into higher hydrocarbons is necessary. The conversion into ethylene (C_2H_4) is one important step, and Li doped MgO has been suggested to be a good catalyst. Already in the early 1980's [1] it had been reported that Li-doped MgO efficiently catalyses the oxidative coupling of methane (OCM): $2CH_4 + O_2 \rightarrow C_2H_4 + 2H_2O$. The catalyst was demonstrated to be stable [2] and highly selective towards production of C_2 hydrocarbons. The combination of the high selectivity, stability, and low cost made the Li/MgO catalyst a prototype system in attempt to understand the OCM process at the molecular level. The activity of this catalyst was attributed to the presence of Li substituting Mg in the MgO lattice, but, the concentration and geometry of these centers at the surface under reaction conditions is still unknown, and the catalytic mechanism is still unclear.

We have used density-functional theory (DFT) to evaluate the electronic structure and formation energies of the substitutional Li defects in the (001) surface, at the subsurface, and in the bulk of MgO. The results exhibit some hitherto unknown properties of the material and raise worries that Li is playing a direct role in the catalytic process. On the other hand, we find that the concentration of oxygen vacancies may be very high for Li/MgO under catalytic conditions, and these defects are found to be largely affected by effects beyond a standard DFT-LDA/GGA description. Calculations for the bulk vacancies, using many-body perturbation theory (i.e. going "beyond DFT"), demonstrate this interesting point. Corresponding studies for vacancies at the surface are under way.

A second example of this talk [3] is concerned with the catalytic epoxidation of ethylene (C_2H_4). There are actually two possible reaction products which have the same stoichiometry but different conformations: i) The desired ethylene oxide (C_2H_4O) and ii) the thermodynamically more stable, but unwanted, acetaldehyde (CH_3CHO). The common catalyst for ethylene epoxidation is Ag on an alpha-Al_2O3 support. While pure Ag exhibits a selectivity of just 25-50% towards the formation of ethylene oxide, [4] recent experiments

and first-principles calculations by Linic and Barteau suggest that alloying Ag with small concentrations of Cu noticeably improves the selectivity. [5] The rationalization of this improvement assumed the presence of a two-dimensional Ag-Cu surface alloy. [5] Though these arguments may sound plausible and are widely accepted, our density-functional theory (DFT) calculations reveal that this material is not stable in an environment containing O_2 and C_2H_4 at temperatures and pressures relevant for industrial applications. In fact, our results show that copper segregates to the surface forming thin surface oxides. Thus, there is no alloy at the surface but a thin oxide layer. We also find that there are several possible surface structures with similar energies, suggesting that they dynamically coexist under catalytic conditions.

1. T. Ito and J. H. Lunsford, Nature 314, 721 (1985).

2. V. R. Choudhary and B. S. Uphade, Catal. Surv. from Asia 8, 15 (2004).

3. S. Piccinin et al., Phys. Rev. Lett., January/February (2010).

4. K. Weissermel and H. J. Arpe, *Industrial Organic Chemistry* (VCH, Weinheim, 1993).

5. S. Linic et al., J. Catal. 224, 489 (2004), J. T. Jankowiak et al., J. Catal. 236, 366 (2005), S. Linic et al., J. Am. Chem. Soc. 125, 4034 (2003). A. Kokalj et al., J. Catal. 254, 304 (2008).

Formation, thermal stability and activity of PdZn near-surface alloys: a combined PM-IRAS, XPS and TPD study

Christian Weilach , Astrid Kitla, Karin Föttinger, Günther Rupprechter

Institute of Materials Chemistry, Vienna University of Technology, Austria
(corresponding author: grupp@imc.tuwien.ac.at)

Hydrogen technology still has to cope with the difficulties of H_2 storage/transport but methanol could be used as alternative energy carrier. Hydrogen generation from CH_3OH can be carried out by catalytic methanol steam reforming (MSR): $CH_3OH + H_2O \rightarrow CO_2 + 3H_2$. In addition to industrially used copper-based catalysts, reduced states of Pd/ZnO have been identified as efficient MSR catalysts [1]. However, rather than Pd alone, the active phase is a PdZn alloy, formed during reductive catalyst activation. For methanol steam reforming, the CO_2 selectivity is most important, because the undesired by-product CO poisons the fuel cell´s anode. Considering that Pd dehydrogenates CH_3OH to CO and H_2 [2], it is apparent that controlling the formation of the active alloy and its characterization are key issues.

To obtain further insight into structure-selectivity correlations, we have utilized a model catalyst approach, preparing PdZn near-surface alloys in ultrahigh-vacuum (UHV), combined with analysis under UHV and ambient pressure [2,3] by Polarization Modulation IR Reflection Absorption Spectroscopy (PM-IRAS), X-ray Photoelectron Spectroscopy (XPS), Temperature Programmed Desorption (TPD), and Low Energy Electron Diffraction (LEED). Based on previous [4-9] and the present results, 1:1 PdZn(111) surface alloys of varying thickness were prepared by depositing Zn on Pd(111) at 300 K, followed by annealing in the range 473-873 K. Alloy formation was monitored by XPS, detecting alloy related features at a binding energy of 335.6 eV (Pd $3d_{5/2}$) and 1020.9 eV (Zn $2p_{3/2}$). Nevertheless, when using MgKα (1253.6 eV) the Pd bulk below the alloy still contributes to the XPS spectra.

To exclusively examine the PdZn surface layer, we have thus utilized PM-IRAS spectroscopy of adsorbed CO to monitor the formation, thermal evolution/stability and adsorption sites of the PdZn alloy. Fig. 1 shows selected PM-IRAS spectra, acquired at a CO pressure of 10^{-6} mbar at 150 K, after annealing a PdZn multilayer alloy to the indicated temperatures. After annealing to 500-573 K a single sharp peak at 2071 cm^{-1} was observed. Taking into account results derived from LEED (2x1 structure), XPS and DFT [4-8], the vibrational resonance is characteristic of CO adsorbed on-top of individual Pd atoms in the Pd rows of the PdZn surface alloy. In light of the desorption temperature of CO from PdZn (~210 K), as observed by TPD, the surface is saturated with CO (θ_{sat}=0.5 ML), with each Pd atom occupied by a CO molecule [8]. This demonstrates the structural homogeneity of the entire alloy surface, because in case of remaining Pd patches bridge-bonded CO (at ≈1955 cm^{-1}) and on-top CO (at ≈2085 cm^{-1}) would additionally occur at these p/T conditions [3].

Annealing to 623 K induced a small shift of on-top CO to 2073 cm^{-1}, paralleled by the evolution of a weak broad peak around 1890 cm^{-1}. Considering corresponding XPS/LEIS/AES measurements [9,10] this indicates the formation of a Zn-lean monolayer alloy. Annealing to 773 K led to an IR spectrum basically identical to that of Pd(111).
Taking advantage of the elevated pressure capability of PM-IRAS, spectra were also taken at 200 K, close to the desorption temperature of CO from PdZn. The 1 mbar spectrum on PdZn is again characteristic for the CO saturated surface (increasing the pressure to 100 mbar had no effect). Consequently, even at elevated CO pressure the PdZn 1:1 surface remained well-defined with no adsorption sites other than on-top on individual Pd atoms being populated.

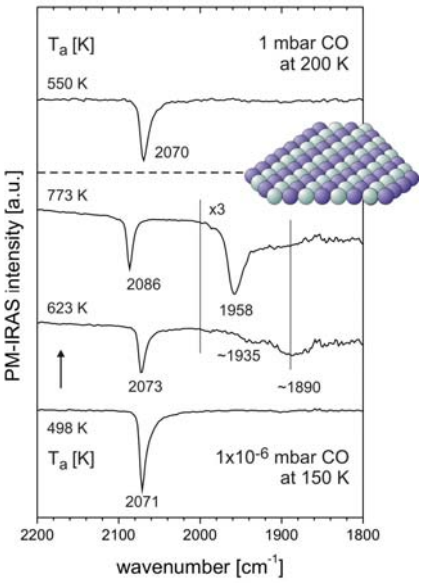

Figure 1: PM-IRAS spectroscopy on PdZn/Pd(111). Spectra were acquired at 150 K in 10^{-6} mbar CO, after successive annealing to the indicated temperatures. An elevated pressure (1-100 mbar) spectrum of CO adsorption on PdZn, annealed to 550 K, is included.

The interaction of PdZn surface alloys with methanol was examined by XPS and PM-IRAS. Compared to Pd(111), the PdZn surface shows higher resistance against coking (carbon deposition by CH_3OH decomposition) and produces hardly any CO. The higher stability of formaldehyde CH_2O on PdZn [4], enabling reaction with water to produce CO_2, is most likely responsible for the high CO_2 selectivity of PdZn surfaces. The results obtained on PdZn will be contrasted to corresponding experiments on Pd(111) and will be complemented by LEIS, HP-XPS and microreactor studies of PdZn near-surface alloys of varying thickness [10].

[1] Iwasa N., Takezawa N., Topics Catal., 2003, 22, 215.
[2] Bäumer M., Libuda J., Neyman K.M., Rösch N., Rupprechter G., Freund H.-J., PCCP, 2007, 9, 3541.
[3] G. Rupprechter, Advances in Catalysis 2007, 51, 133.
[4] K. Neyman, K.H. Lim, Z.-X. Chen, L.V. Moskaleva, A. Bayer, A. Reindl, D. Borgmann, R. Denecke, H.-P. Steinrück, N. Rösch, PCCP 2007, 9(27), 3470.
[5] H. Gabasch, S. Penner, B. Jenewein, B. Klötzer, A. Knop-Gericke, R. Schlögl, K. Hayek, J. Phys. Chem. B 2006, 110(23), 11391.
[6] E. Jeroro, J.M. Vohs, J. Am. Chem. Soc. 2008, 130, 10199.
[7] G. Weirum, M. Kratzer, H.-P. Koch, A. Tamtögl, J. Killmann, I. Bako, A. Winkler, S. Surnev, F.P. Netzer, R. Schennach, J. Phys. Chem. C 2009, 113(22), 9788.
[8] A. Tamtögl, M. Kratzer, J. Killman, A. Winkler, J. Chem. Phys. 2008, 129, 224706
[9] W. Stadlmayr, S. Penner, B. Klötzer, N. Memmel, Surf. Sci. 2009, 603(1), 251.
[10] Ch. Rameshan, W. Stadlmayr, Ch. Weilach, S. Penner, H. Lorenz, M. Hävecker, R. Blume, T. Rocha, D. Teschner, A. Knop-Gericke, R. Schlögl, N. Memmel, D. Zemlyanov, G. Rupprechter, B. Klötzer, submitted

Mapping electron resonances on nanosized alkali metal dots grown on Cu(100)

S. Stepanow[1], A. Mugarza[1], G. Ceballos[1], and P. Gambardella[1,2]

[1]*Centre d'Investigacions en Nanociència i Nanotecnologia (CIN2-ICN), E-08193 Bellaterra, Barcelona, Spain*

[2]*Institució Catalana de Recerca i Estudis Avancats (ICREA), E-08193 Barcelona, Spain*

I. Aldazabal,[3,4] A. Borisov[4,5] and A. Arnau[3,4,5]

[4] *Centro de Física de Materiales CFM, Centro Mixto CSIC-UPVE/EHU, San Sebastián, Spain*

[5] *Donostia International Physics Centre (DIPC), Manuel de Lardizabal 4, San Sebastián, Spain*

[6] *LCAM, UMR CNRS-Université Paris-Sud 8625, Bât. 351, 91405 Orsay CEDEX, France*

[7] *Departamento de Física de Materiales UPV/EHU, Facultad de Química, San Sebastián, Spain*

Scanning Tunneling Spectroscopy (STS) can be used to explore unoccupied states well above the Fermi level. However, in the field emission regime, the applied bias is larger than the surface work function and these unoccupied states are distorted by the electric field. For example, image potential states are stark-shifted and actually become field emission resonances (FERs) as observed on different metal[1] and semiconductor surfaces[2]. Since the energetics of FERs is to a large extent determined by the electric field at the junction, the interpretation of the data is relatively simple. It can be done using one dimensional models[3,4], as long as both the tip radius of curvature and lateral extension of the surface area under interest are large compared to the tip-surface distances (a few nanometers when operating the STM at high bias voltages). Thus, one can use the FERs to chemically identify different surface terminations from a study of the local changes in the surface work function [5-7]. However, when the size of the nanostructures on a metal surface is not too large, the lateral confinement gives rise to a series of nanostructure-localised resonances [8]. *A priori*, these are also modified by the electric field. In this case, the interpretation of dI/dV maps and point spectra requires the use of three dimensional models that explicitly include the applied field. In this work, we present high resolution low temperature Scanning Tunneling Spectroscopy data of alkali (Li) nanoislands grown on Cu(100), as well as model calculations explaining the observed trends in both point spectra and dI/dV maps.

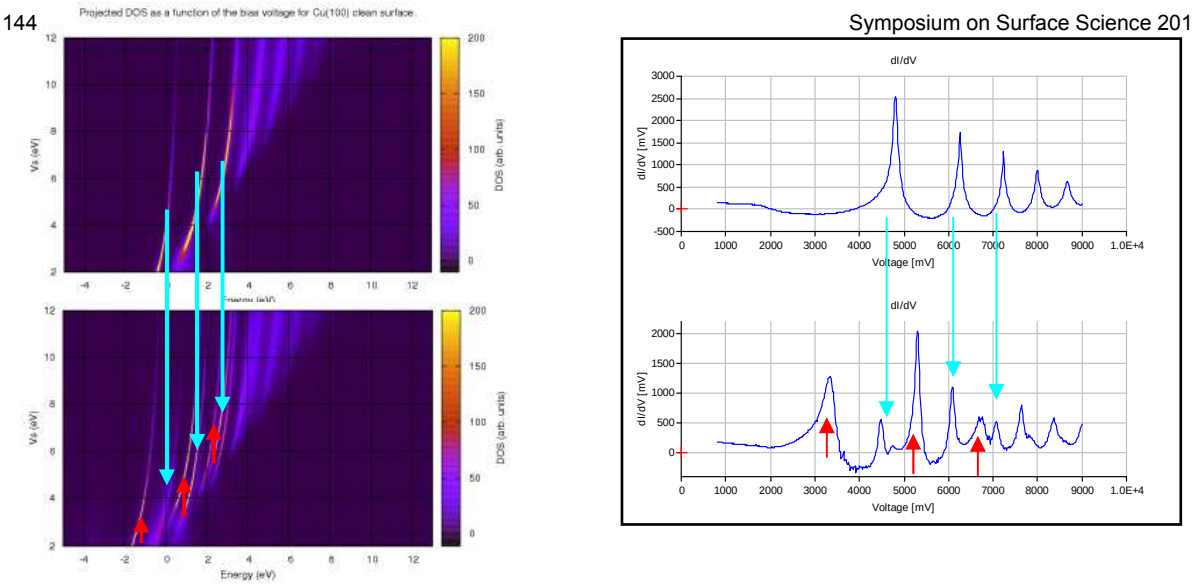

Figure: (Left) Calculated (m=0) density of states DOS(E,Vs) as a function of electron energy (E) and applied bias voltage (Vs) along a linear Z(Vs) characteristic. E=0 corresponds to the vacuum level. Upper panel: clean Cu(100) surface. Lower panel: a model nanosized alkali island. (Right) Constant current conductance spectra (dI/dV) taken on the clean Cu(100) surface (upper panel) and on top of the island (lower panel). The blue and red arrows indicate the metal- and island- like resonances, respectively.

We find that, apart from the well-known field emission resonances spatially extended all over the metal surface, the nanoisland induces new type of resonances with different symmetry (m quantum number) [9]. They originate from the island-localised image potential-like states pinned (for low quantum numbers) to the local vacuum level above the island. Depending on their spatial distribution and energy position with respect to the image states of the pristine metal surface, the island-localized FERs can mix with conventional FERs of the metal giving rise to the multiple structures observed in dI/dV maps and spectra.

We acknowledge financial support from GV-UPV/EHU (grant IT-366-07) and MCI (grants FIS2007-66711-C02-01 and MAT2007-62341).

[1] G. Binnig, K. H. Frank, H. Fuchs, N. Garcia, B. Reihl, H. Rohrer, F. Salvan, and A. R. Williams, Phys. Rev. Lett. **55**, 991 (1985); R. S. Becker, J. A. Golovchenko, and B. S. Swartzentruber, Phys. Rev. Lett. 55, 987 (1985).
[2] J. A. Kubby, Y. R. Wang, and W. J. Greene, Phys. Rev. Lett. **65**, 2165 (1990).
[3] J. M. Pitarke, F. Flores, and P. M. Echenique, Surf. Sci. **234**, 1 (1990).
[4] J. I. Pascual, C. Corriol, G. Ceballos, I. Aldazabal, H.-P. Rust, K. Horn, J. M. Pitarke, P. M. Echenique, and A. Arnau,, Phys. Rev. B75 165326 (2007).
[5] T. Jung, Y.W. Mo, and F.J. Himpsel, , *Phys. Rev. Lett.* **74**, 1641-1644 (1995).
[6] M. Pivetta, F. Patthey, M. Stengel, A. Baldereschi, and W.-D. Schneider, *Phys. Rev. B* **72**, 115404-1-6 (2005).
[7] P. Ruffieux, K. Aït-Mansour, A. Bendounan, R. Fasel, L. Patthey, P. Gröning, and O. Gröning, Phys. Rev. Lett. **102**, 086807 (2009).
[8] S. Crampin, H. Jensen, J. Kröger, L. Limot, R. Berndt, Phys. Rev. B **72**, 035443 (2005).
[9] A. G. Borisov, J. P. Gauyacq, A. K. Kazansky, E. V. Chulkov, V. M. Silkin, and P. M. Echenique, Phys. Rev. Lett. 86, 488 (2007).

DFT Periodic study of Cu segregation within Al surfaces

A. Benali[1,2], C. Lacaze-Dufaure[1], J. Morillo[2]

[1] *Centre Interuniversitaire de Recherche et d'Ingénierie des Matériaux, ENSIACET, UMR CNRS 5085, 4 allée Emile Monso, 31432 Toulouse cedex 4, France*
(corresponding author: A. Benali, e-mail:anouar.benali@ensiacet.fr)

[2]*Centre d'Elaboration de Matériaux et d'Etudes Structurales, UPR CNRS 8011, 29 rue Jeanne Marvig, BP 94347, 31055 Toulouse Cedex 4, France*

Al-Cu alloys are the most used alloys in the aeronautic field, due to their remarkable mechanical properties associated to there lightness. Aluminum is also very interesting due to its capacity to form a very stable oxide (Al_2O_3). Thus, it leads to high temperature resistant coatings with good resistance to oxidation and corrosion in aggressive environments. However, the first stage of the oxidation depends strongly on the surface structure of the alloy. We thus start to investigate the Cu interactions with Al surfaces at low Cu concentrations.

The Al (111) and (100) surfaces are expected to be the more represented ones in any bulk piece of Al due to their lowest surface energies. We have thus theoretically studied the structural and electronic properties of Cu segregation at these surfaces. The calculations have been made with the Vienna *ab initio* simulation package (VASP) [1–3] in the framework of the density functional theory (DFT), within the projector-augmented plane-wave method (PAW) [4,5] and its both generalized gradient approximation (GGA) [6] and local density approximation (LDA) [7]. Prior to the segregation study, an extensive study of bulk and surface properties of Cu and Al has been performed to check the accuracy of the LDA (GGA) and pseudopotential approximations. The slab geometry (number of layers and vacuum size) has been fully optimized.

We have studied first the layer Cu-segregation parallel to the (111) surface at various concentrations (X_{Cu}=1/9, 1/3, 2/3 and 1) and at different positions, from the surface itself to 5 layers beneath it. It results that there is only a slight tendency to Cu surface segregation in sub surface layers, reflecting the Cu preference for a high degree of coordination. The surface position is always energetically unfavourable with a positive formation energy. The substitution of a full monolayer of copper (X_{Cu}=1) within the aluminium (111) slab leads to the most stable system with sub-subsurface Cu-segregation. Clearly, Cu atoms prefer highly coordinated sites with homoatomic bonding.

It is experimentally well established [8-12] that increasing Cu concentration in the (Al) α phase of the Al-Cu phase diagram, results in Cu (100) clustering leading to the formation of the so-called Guinier-Preston (GP) zones [13,14] which are the precursors of the θ' and θ

phases that stabilize at higher Cu concentration. Subsequent GP zones stages are distinguished as GP1 and GP2 zones as they change their structure during annealing. The study of the interaction between the GP zones and the Al (111) surface requires the use of too large simulation cells for a DFT study, due to the nanometric size of the clusters and their (100) orientation. Only very small (100) Cu clusters, representing the first stages of formation of the GP zones could be studied. It appears that, like in the (111) in-plane study, the Cu-clusters prefer to be buried beneath the surface.

Concerning the (100) surface segregation, since the GP zones are (100) plane clusters, we start our investigation with a full (100) Cu monolayer in an Al (100) slab. Here also, Cu atoms prefer to be buried into the Al matrix, this tendency being higher at this surface than at the (111) surface. The Cu (100) full monolayer prefers to be deep in the bulk: there is no surface segregation.

Surface segregation is usually roughly described as being governed by three driving forces (differences in surface energy, size effect and chemical mixing energy). In the present case they are all unfavourable to Cu surface segregation in Al, in agreement with our results. However, since Cu atoms nevertheless tend to segregate just beneath the surface in the most stable Al surface, one cannot exclude a different oxidation behaviour of Cu-Al rich alloys compared to pure Al.

Support by the National Research Agency ASURE (ANR support number BLAN08-2 342506) and by the French ministry of research. This work was granted access to the HCP resources of CINES under allocation 2009 095076 made by GENCI (Grand Equipement National de Calcul intensif), and to the HCP resources of CalMiP (Calcul Midi-Pyrenees) under project number P0840, is gratefully acknowledged,

[1] G. Kresse and J. Hafner, Phys. Rev. B. 47, R558 (1993)
[2] G. Kresse and J. Furthmüller, Phys. Rev. B. 54, 11169 (1996)
[3] G. Kresse and J. Furthmüller, Comput. Mater. Sci. 6, 15 (1996).
[4] P. Blöchl, Phys. Rev. B. 50, 17953 (1994)
[5] G. Kresse and D. Joubert, Phys. Rev. B. 59, 1758 (1999)
[6] J. Perdew, J. A. Chevary, S. H. Vosko, K. A. Jackson, M. R. Pederson, D. J. Singh, and C. Fiolhais, Phys. Rev. B. 46, 6671 (1992)
[7] D. M. Ceperley and B. J. Alder, Phys. Rev. Lett. 45, 566 (1980)
[8] V. Gerold Z. Metall., 1954. 54: p. 599
[9] A. Guinier, Solid State Phys. 1959, 9, p: 293
[10] V. Gerold Scripta Metalla., 1988. 22: p. 927
[11] J. B. Cohen, Solid State Phys. 1986, 39, p: 131
[12] T. J. Konno et al. Scripta Mater. 2001, 44, p: 2303
[13] A. Guinier, Nature 142, 569 (1938)
[14] G. D. Preston, Nature 142, 570 (1938)

Confinement of the interface state between NaCl and Ag(111)

A. Sabellek, S. Heidorn, K. Morgenstern

Institut für Festkörperphysik, Abteilung für atomare und molekulare Strukturen (ATMOS)
Gottfried Wilhelm Leibniz Universität, Appelstr.2, D-30167 Hannover, Germany
(corresponding author: K. Morgenstern, e-mail: morgenstern@fkp.uni-hannover.de)

It has long been realized that the surface states of fcc(111) surfaces show quantisation characteristics, if confined laterally [1]. This confinement has been imaged in real space by means of scanning tunnelling microscopy [2,3]. On the other hand, adsorption of weakly interacting species might turn this surface state into an interface state with an onset usually at higher energy, e.g. Xe [3] or NaCl [4].

In our study we use low temperature scanning tunnelling microscopy and spectroscopy to investigate the interface state between NaCl and Ag(111) with respect to its onset and intensity for NaCl bilayer islands on Ag(111) of sizes in the range of a few ten nanometers.

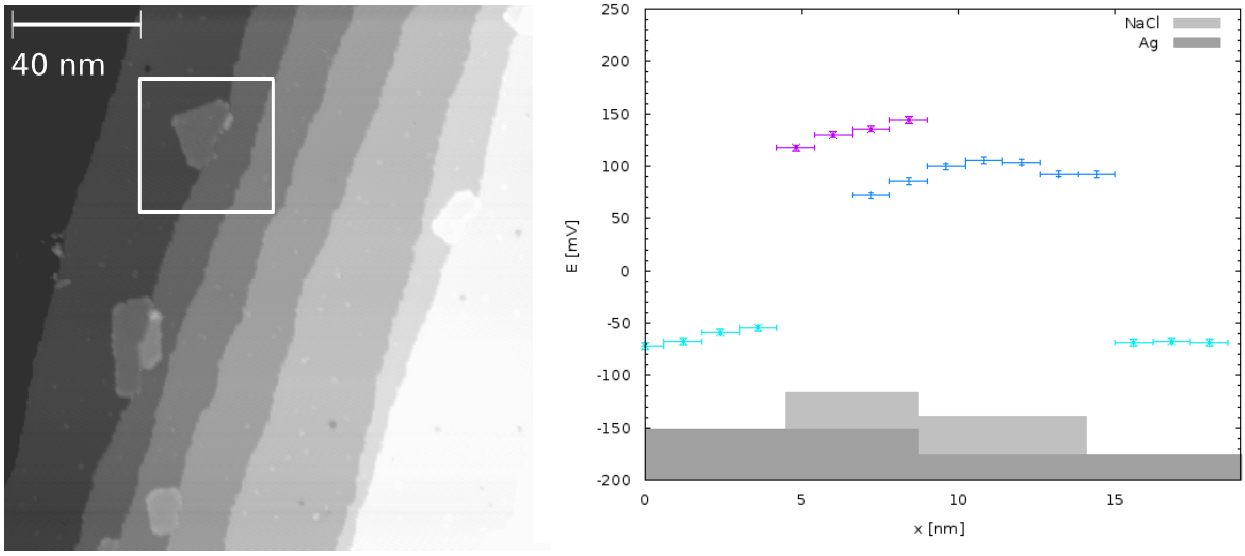

Figure 1: left: Overview image of NaCl grown on Ag(111) at room temperature and imaged at 5 K; right: position of surface state and interface state onset on Ag terrace and NaCl island, respectively, in dependence of position on the island that is shown schematically at the bottom.

As shown in Figure 1, left-hand side, islands of the appropriate size can be grown on stepped regions of the Ag(111) at room temperature. On such islands the onset of the interface state

depends on the size of the island and the varies across the island. These variations are evidence for the quantisation of the interface state.

[1] O. Sánchez, J. M. García, P. Segovia, J. Alvarez, A. L. Vázquez de Parga, J. E. Ortega, M. Prietsch, R. Miranda, Phys. Rev. B 52 (1995) 7894.

[2] M.F. Crommie, C.P. Lutz, D.M. Eigler, Nature 363 (1993) 524.

[3] L. Bürgi et al. Phys. Rev. Lett. 81 (1998) 5370.

[4] H. Hövel, B. Grimm, B. Reihl, Surf. Sci. 477 (2001) 43

[5] J. Repp, G. Meyer, K.-H. Rieder, Phys. Rev. Lett. 92, 036803 (2004)

Modelling adsorbate-induced surface segregation in metal alloys

T. Kerscher, W. Landgraf, and S. Müller

Universität Erlangen-Nürnberg,
Lehrstuhl für Theoretische Physik 2 and Lehrstuhl für Festkörperphysik,
Staudtstr. 7, D-91058 Erlangen
∗ *e-mail: stefan.mueller@physik.uni-erlangen.de*

For many decades, the existence of adsorbate-induced reconstruction is well known and studied via a large number of experimental and theoretical methods for many surface systems. However, if the template consists of more than one chemical species, a second effect comes into play, namely the influence of the adsorbate on the chemical substitution of the surface layers. The quantitative knowledge of such an *adorbate-induced surface segregation* is the prerequisite for the discussion of e.g. alloy surfaces and adsorbates as candidates for catalytic reactions or corrosion protection. A quantum-mechanical based modelling of this effect is not an easy task, because it demands the control over huge configuration spaces. Although it has been shown that the combination of density functional theory (DFT) and cluster expansion (CE) provides a powerful tool for studying configurational problems, the number of necessary DFT calculations for the stabilization of the CE-Hamiltonian heavily increases with the number of the different chemical species. Even for the adsorption of one species on a binary alloy surface, one has to deal with four different chemical species, namely the two types of atoms forming the alloy surface, the occupied and the unoccupied adsorption sites. Our new code UNCLE [1] allows for an efficient handling of such a system by breaking it into a "bi-binary" expansion, as sketched in Figure 1:

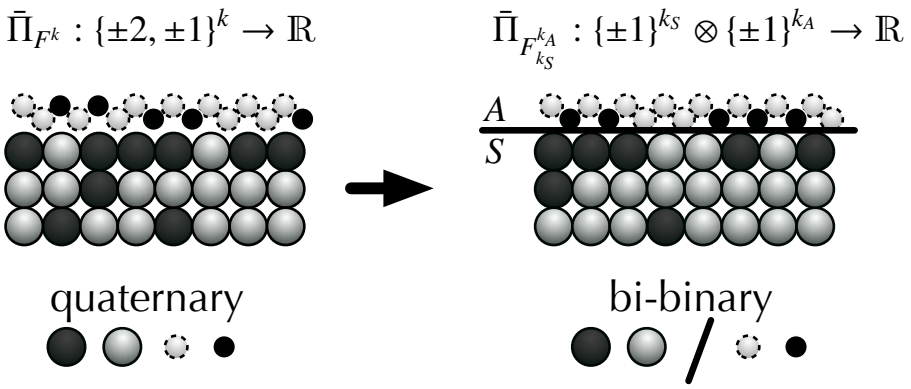

Figure 1: The basis function of the quaternary system (left) characterized by four individual spins ±1, ±2, is separated into the adsorption and the surface system (right) which makes the construction of the corresponding many-particle Hamiltonian much easier.

Instead of using basis functions $\bar{\Pi}_{F^k}$ of a figure class F with k vertices (sites per figure) and four individual spins, the system is decribed by a tensor product of the adsorbate system (occupied or

unoccupied adsorption site) and the alloy surface (A or B atom). This ansatz works as long as the adsorbate does not occupy subsurface sites.

As an example, we have investigated the influence of the carbon adsorption on the segregation profile of the $Pt_{25}Rh_{75}(100)$ surface. Our model includes correlations between segregation, substitutional ordering of adsorbates and substrate atoms, as well as local atomic relaxations. It is known from STM, LEIS, and LEED studies performed in the group of Peter Varga, TU Vienna [2, 3], that this surface shows a strong Pt enrichment in the top atomic layer and a depletion underneath. Yet, even a small amount of carbon impurity (8% of a monolayer) leads to a considerable decrease in the Pt top layer concentration.

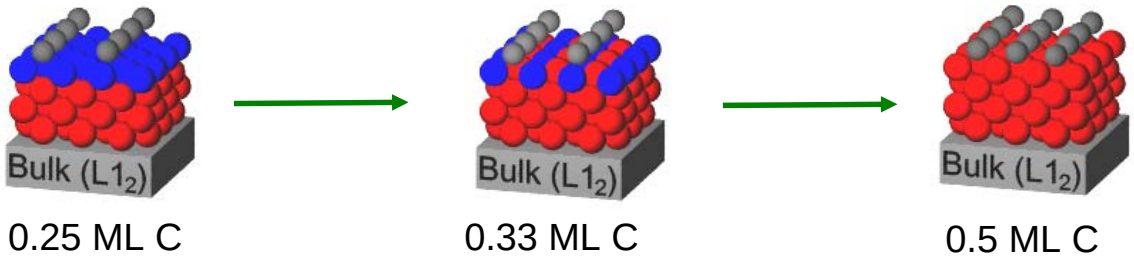

Figure 2: Calculated segregation profile of the $Pt_{25}Rh_{75}(100)$ as function of carbon coverage. For $\Theta \approx 0.5$ ML, no Pt is left in the near surface layers.

We have systematically studied the properties of this adsorption system as function of carbon coverage (Figure 2): The properties of the system are found to be controlled by two competing effects: the different segregation energies of Pt and Rh, and their individual binding energies to C. While the former clearly favours the enrichment of the top layer with Pt atoms, the opposite is true for the latter. Indeed, for C coverages around 50 percent, there is not Pt left in the top layers.

Supported by Deutsche Forschungsgemeinschaft

References

[1] D. Lerch, O. Wieckhorst, G.L.W. Hart, R. Forcade, and S. Müller, Modelling Simul. Mater. Sci. Eng. **17**, 05503 (2009).

[2] E. L. D. Hebenstreit, W. Hebenstreit, M. Schmid, P. Varga, Surf. Sci. **441** (1999) 441.

[3] E. Platzgummer, M. Sporn, R. Koller, S. Forsthuber, M. Schmidt, W. Hofer, and P. Varga, Surf. Sci. **419**, 236 (1999).

ReactorAFM™; from vision to reality

M.E. Cañas-Ventura, A. Ofitserov[1], W. Onderwaater, C.T. Herbschleb, Q. Liu, V. Navarro, J. Bakker, D. Stoltz, I. Taminiau, P.C. van der Tuijn, G. Verdoes, A.C. Geluk, E. de Kuyper, G.J.C. van Baarle[1], R.C.T. Koehler, C.F. Overgauw and J.W.M. Frenken

Kamerlingh Onnes Laboratory, Leiden University, P.O. Box 9504, 2300 RA Leiden, The Netherlands (corresponding author: M. E. Cañas-Ventura, e-mail: canasventura@physics.leidenuniv.nl)

[1] *Leiden Probe Microscopy BV, Leiden, The Netherlands, www.LeidenProbeMicroscopy.com*

The atomic-scale investigation of supported catalysts is on the move towards experiments with state-of-the-art techniques, close to industrial conditions: high pressures and high temperatures. This line of investigation is a primary target in the framework of our project Nano-IMaging under Industrial Conditions (NIMIC; www.realnano.nl). The close collaboration with the chemical industry, gives us the privileged situation to focus on their current matters of interest. Since 80% of the processes in the chemical industry are based on catalysis, improving the efficiency of one of these steps has immediate effects on the use of energy and resources, and the efficiency and cost effectiveness.

Previous work in our group with the first version of the ReactorSTM™ [1], a miniature flow reactor integrated with a scanning tunneling microscope (STM), has provided direct insight into the relation on catalytic metal surfaces between the structure, morphology and reactivity [2]. This work has indicated several potential improvements in the microscope. In addition, it has provided us with a further urge to widen range of model catalysts that can be studied under reaction conditions with atomic or near-atomic resolution, to the typical geometry of oxide-supported metal nanoparticles. In this way we would bridge not only the so-called "pressure gap" but also the "materials gap".

For this purpose, we have now developed the ReactorAFM™. With special attention paid to vibration isolation, low-expansion materials and fast electronics, the instrument operates at temperatures up to 570 K and pressures up to 5 bar, at relatively high speed (up to 1 image per second) and with atomic resolution. Furthermore, a newly designed gas cabinet allows us to set fluxes from 0 to 10 ml_n/min at 1 bar, mixtures of up to four different gases with ratios ranging from 1:1 to 1:100. It has a minimal volume and no dead volume, allowing us to rapidly refresh the capillaries and the reactor and to introduce well-defined, sharp pulses of gas. A quadrupole mass spectrometer enables the analysis of all mass fractions from 1 to 100 amu in less than 2 seconds.

The atomic force microscope (AFM) is housed in a vacuum system with several additional preparation and surface analysis techniques. Finally, the AFM head also measures the

tunneling current, allowing us to operate the instrument in a variety of modes with a wide range of signals acquired simultaneously.

We will show first images obtained with the ReactorAFM™ on several test samples, such as Au particles on a mica substrate and on highly ordered pyrolytic graphite (HOPG). A combination of scans and frequency shift versus distance (Δf vs. Z) curves demonstrates the good behavior of the setup in air, i.e. at a gas pressure of 1 bar.

The remarkable variety of information that the ReactorAFM™ offers will be used to investigate many relevant catalytic reaction systems under relevant reaction conditions.

The authors gratefully acknowledge M. E. Messing, K. Deppert, and E. Lundgren for the preparation of the some samples, and R. Smit for stimulating discussion. This work is part of the SmartMix project Nano-IMaging under Industrial Conditions (NIMIC or REAL NANO), which support is gratefully acknowledged.

[1] P. B. Rasmussen, B. L. M. Hendriksen, H. Zeijlemaker, H. G. Ficke and J. W. M. Frenken, Rev. Sci. Instrum. 68, 3879 (1998); B.L.M. Hendriksen, S.C. Bobaru, J.W.M. Frenken Topics in Catalysis 36, 43 (2005).

[2] B. L. M. Hendriksen and J.W. M. Frenken, Phys. Rev. Lett. 89, 046101 (2002); B.L.M. Hendriksen, S.C. Bobaru, J.W.M. Frenken, Surf. Sci. 552, 229 (2004); B.L.M. Hendriksen, S.C. Bobaru, J.W.M. Frenken, Catalysis Today 105, 234 (2005).

Structure of zinc oxide nanolayers on a Pd(111) surface: STM and DFT study

G. Weirum[1,2], G. Barcaro[3], A. Fortunelli[3], R. Schennach[2], S. Surnev[1], and F.P. Netzer[1]

[1]*Institute of Physics, Karl-Franzens University Graz, A-8010 GRAZ, Austria*
(corresponding author: S. Surnev, e-mail: svetlozar.surnev@uni-graz.at)
[2]*Institute of Solid State Physics, Graz University of Technology, A-8010 GRAZ, Austria*
[3] *Molecular Modelling Laboratory, IPCF-CNR, Pisa, I56124, Italy*

Zinc oxide has attracted significant scientific and technological interest, since it is widely used in catalysis, gas sensing, and in the fabrication of optoelectronic devices. If the wurtzite ZnO crystal is cleaved parallel to the basal plane (0001), two structurally and chemically different surfaces are created on each side of the crystal, which are Zn- and O-terminated. The structure stabilisation mechanism of these two polar surfaces has been extensively investigated [1,2], but consensus models have not evolved yet. For nano-size oxide objects, such as ultrathin films with a thickness of only few atomic layers, new depolarisation mechanisms may become effective, which originate from the stabilising role of the support and/or from the ability of finite systems to sustain a non-zero polarisation along the polar axis [3]. In the case of ZnO, it has been theoretically predicted that unsupported thin films adopt a non-polar graphite-like or hexagonal boron nitride (h-BN) structure [4,5]. This result has been recently experimentally confirmed for ZnO films grown on a Ag(111) surface [6], which study has demonstrated that the h-BN sheet structure is maintained for the first two atomic layers and then transforms gradually into the bulk wurtzite structure upon increasing the film thickness.

Here we have investigated the surface structure of zinc oxide monolayers grown on a Pd(111) surface by scanning tunneling microscopy (STM), low energy electron diffraction (LEED) and density functional theory (DFT) calculations. The choice of the Pd substrate has been motivated by the catalytic relevance of the Pd/ZnO system, in particular for the steam reforming of methanol [7]. The zinc oxide layers have been prepared either by reactive evaporation of Zn in oxygen atmosphere ($5x10^{-8}$–$5x10^{-6}$ mbar) onto the Pd substrate or by post-oxidation of Zn metal deposits. In the sub- to monolayer coverage range two 2D hexagonal ZnOx phases coexist on the Pd(111) surface: one with an open honeycomb (4x4) structure (Fig. 1a), and the other one with a close-packed structure with a lattice constant of 3.3 Å, which is close to the bulk value of ZnO(0001) surfaces (3.25 Å). The latter phase displays a (6x6) Moiré structure (6 Pd lattice spacing = 5 ZnO unit cells) (Fig. 1c). The (4x4) structure dominates at Zn coverages up to 0.5 ML and is stable in a broad oxygen pressure range of $5x10^{-8}$ - $1x10^{-6}$ mbar. The DFT calculations suggest a model for the (4x4) phase (top of Fig. 1b), which contains a honeycomb arrangement of Zn atoms, located in threefold hollow Pd sites, and O atoms, occupying the Zn corner- and bridge-sites. This polar oxide

structure is stabilised by terminating the O atoms with H atoms, yielding a formal $Zn_6(OH)_5$ stoichiometry. The simulated STM image (bottom of Fig. 1b) reproduces well the experimental contrast. The (6x6) Moiré phase becomes dominant at monolayer Zn coverages, forming a wetting layer at $p(O_2) < 1x10^{-6}$ mbar. According to the DFT calculations, this layer consists of a non-polar graphite-like structure with a ZnO stoichiometry (Fig. 1d), i.e. identical to that reported for Zn-oxide layers on Ag(111) [6]. At higher oxygen pressure the single (6x6) layer dewets into bilayer islands, with the second layer exhibiting the same structure as the first one. The driving force for this transition is explained in the DFT framework as due to a competition of the monolayer phase with a mixture of the ZnO bilayer and the Pd(111) surface covered with chemisorbed oxygen.

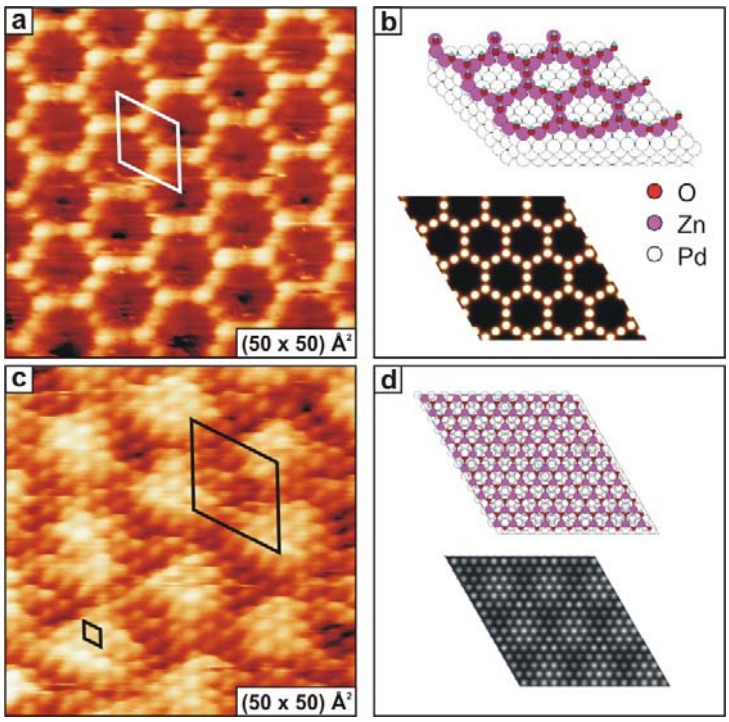

Fig. 1: (a) High-resolution STM-image of the (4x4)-phase, (50Åx50Å; +10 mV, 3 nA); (b) DFT model (top) and STM simulation (bottom) of the (4x4) structure; (c) High resolution STM-image of the (6x6)-phase, (50Åx50Å; +100 mV, 2 nA); (d) DFT model (top) and STM simulation (bottom) of the (6x6) structure.

Supported by the Austrian Science Funds (FWF) via the FWF Project P19198-N02 and the National Research Network "Nanoscience on Surfaces". FPN and AF acknowledge the European Research Council (ERC Advanced Grant SEPON) for the financial support.

References:

[1] O. Dulub, L.A. Boatner, and U. Diebold, Surf. Sci. 519, 201 (2002)
[2] O. Dulub, U. Diebold, and G. Kresse, Phys. Rev. Lett. 90, 016102 (2003)
[3] J. Goniakowski, F. Finocchi, and C. Noguera Rep. Prog. Phys. 71 (2008) 016501
[4] F. Claeyssens, C.L. Freeman, N.L. Allan, Y. Sun, M.N.R. Ashfold, and J.H. Harding, J. Mater. Chem. 15 (2005) 139
[5] F. Claeyssens, C.L. Freeman, N.L. Allan, and J.H. Harding, Phys. Rev. Lett. 96 (2006) 066102
[6] C. Tusche, H.L. Meyerheim, and J. Kirschner, Phys. Rev. Lett. 99, 026102 (2007)
[7] N. Iwasa, S. Kudo, H. Takahashi, S. Masuda, and N. Takezawa, Catal. Lett. 19 (1993) 211

Surface carbides in palladium catalysts ?

N. Seriani, F. Mittendorfer

Faculty of Physics, Universität Wien, and Center for Computational Materials Science, A-1090 Wien, Austria
(corresponding author: F. Mittendorfer, e-mail: Florian.Mittendorfer@univie.ac.at)

Partial hydrogenation reactions play a fundamental role in the chemical industry. Common catalysts for the partial hydrogenation of ethyne to ethylene are based on palladium nanoparticles, as these catalysts show a high selectivity towards ethylene formation. It has recently been suggested that this high selectivity is directly related to the formation of a 1.4 nm thick carbon-rich phase at the surface of the metal [1]. Although it has been proposed that this phase might be related to dissolved carbon, its actual structure is unknown. In addition, the question why the formation of PdC phases instead of graphite is observed remains open.

We have therefore investigated the stability of PdC bulk- and surface phases with the help of density functional theory (DFT) calculations [2]. A comparison of the formation energies of various hypothetical PdC structures, including a wide range of know transition metal carbide structures such as Mn_XC, Fe_XC, Ni_3C and Mo_2C, showed that the most stable bulk carbid phase has a stochiometry of Pd_6C (Fig.1, left), corresponding to a carbon content of 14 at%. In this structure, the carbon atoms are arranged in the octahedral sites of the Pd fcc lattice, resulting in a lattice expansion of 3%. Even in this energetically most stable configuration, the formation energy is slightly endothermic (+0.23 eV/C) with respect to a phase separation into graphite and metallic palladium.

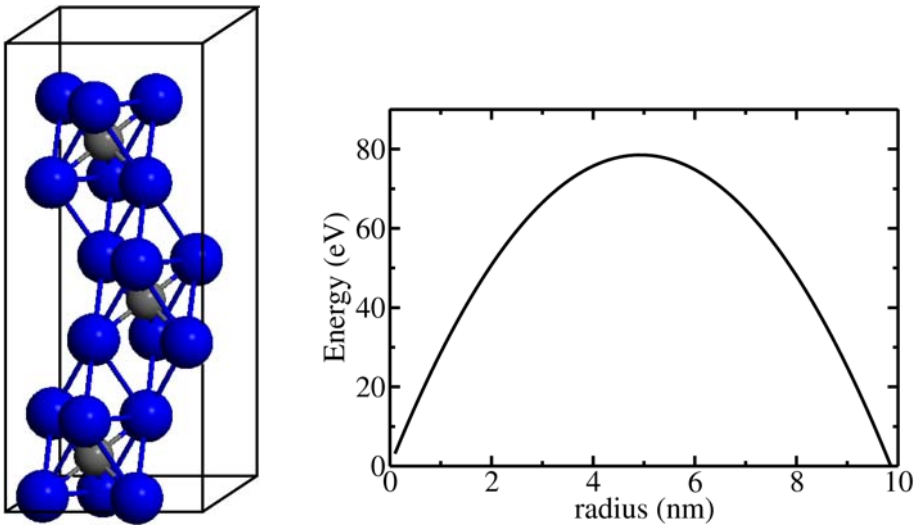

Fig. *1: (left) Structual Model of the Pd_6C bulk carbide(Pd atoms in blue, C atoms in grey) and (right) formation energy vs. island radius of a graphene patch supported on Pd(100).*

This observation also holds for carbon adsorbates at Pd surfaces. At the close-packed Pd(111) surface, we observe a strong thermodynamic driving force for the carbon atoms to penetrate the surface and to adsorbe in a subsurface site instead of a surface site ($\Delta E = 0.75$ eV). This is in contrast to the more open Pd(100) surface, where the adsorption of the carbon atoms starts at the surface. Increasing the coverage, we find an arrangement of the carbon atoms which is rather similar to the Pd_6C bulk phase.

As both the formation of the Pd_6C bulk phase and the surface phases are endothermic with respect to the formation of graphene, the latter process must be hindered. It order to address this point we have evaluated the competition between the energy gain from the formation of a graphene patch and the energetic cost resulting from the edges of the patch in classical nucleation theory for the growth of a graphene patch on Pd(100). We find that the edge energy of the supported graphene patch is significantly lower than the edge energy of unsupported graphene, but in a simplified model the crucial size of the patch is still about 5nm (Fig.1, right). Therefore, the formation of bulk graphite is delayed by the large critical radius necessary for the graphite nucleation.

Support by the Austrian Fonds zur Förderung der Wissenschaftlichen Forschung (project “Nanoscience on Surfaces”) is gratefully acknowledged.

[1] D. Teschner, J. Borsodi, W. Wootsch, Z. Revay, M. Hävecker, A. Knop-Gericke, S. D. Jackson and R. Schlögl, Science 320, 86 (2008);
D. Teschner, Z. Revay, J. Borsodi, M. Hävecker, A. Knop-Gericke, R. Schlögl, D. Milroy, S. D. Jackson, D. Torres, and P. Sautet, Ange. Chem. Int. Ed. 47, 9274 (2008)

[2] N. Seriani, F. Mittendorfer and G. Kresse, J. Chem. Phys., *accepted for publication*

Live Catalysts under Industrial Conditions imaged with Atomic Resolution

C.T. Herbschleb[1,*], P.C. van der Tuijn[1], Q. Liu[1], A. Ofitserov[2], G.J.C. van Baarle[1,2], G. Verdoes[1], M.E. Cañas-Ventura[1], L. Crama[1], J.W. Bakker[1], V. Navarro-Paredes[1], I. Taminiau[1] and J.W.M. Frenken[1]

[1]Kamerlingh Onnes Laboratory, Leiden University, P.O. box 9504, 2300 RA Leiden, The Netherlands
[2]Leiden Probe Microscopy, Kamerlingh Onnes Laboratory, P.O. box 9504, 2300 RA Leiden, The Netherlands
[*]Herbschleb@physics.leidenuniv.nl

In order to further understand the underlying fundamental physics of catalytic systems such as for instance the reactions in the three-way car catalyst and synthesis reactions in the petrochemical industry [1], we developed a second generation high-pressure, high-temperature scanning tunneling microscope, the ReactorSTM™ [2]. This dedicated instrument has improved resolution, imaging speed, vibration insensitivity and operates under a wider range of pressures and temperatures with respect to the original prototype [3].

The ReactorSTM™ consists of a 0.5 ml flow reactor, housed in a dedicated ultrahigh vacuum (UHV) system. The reactor can be operated up to a total pressure of 5 bar (reactants plus products) and up to a sample temperature of 600 K. The UHV system enables us to combine the high-pressure experiments with traditional, high-quality sample preparation and analysis, for example with, ion sputtering, metal deposition, LEED, AES, and XPS.

We demonstrate the imaging performance of the new instrument with results for catalytic CO oxidation on Pt(110). Figure 1 shows an STM image of the freshly prepared surface, with the characteristic (1x2) missing-row reconstruction, imaged at room temperature in a modest vacuum; the distance between the rows is 0.75 ±0.03 nm. Figure 2 shows the unreconstructed (1x1) surface, with a row distance of 0.37 ± 0.02 nm, that results after exposing Pt(110) to a flow of CO at 1 bar and 450 K (note that the scale is different from that of Fig. 1). Figure 3 shows that we still observe atom rows in O_2-rich O_2/CO mixtures. The doubled row distance of 0.72 ± 0.06 nm is fully consistent with the oxidic structure proposed by Ackermann et al. [4], which is shown in Figure 4. By changing the precise gas composition, we have been able to make the surface switch back and forth between the structures of Figures 2 and 3.

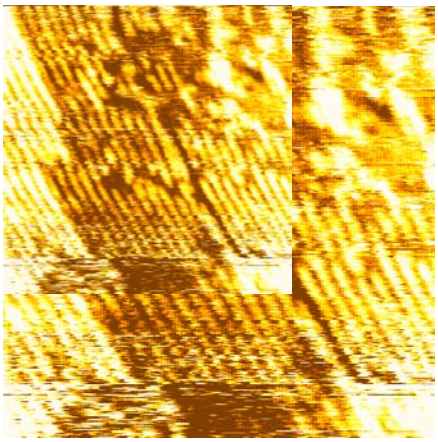

Fig. 1 – 25 x 25 nm^2 STM image of the (1x2) missing row reconstruction on Pt(110), I = 0.2 nA, V = 0.1 V. T = 450 K; P_{tot} = 1 bar

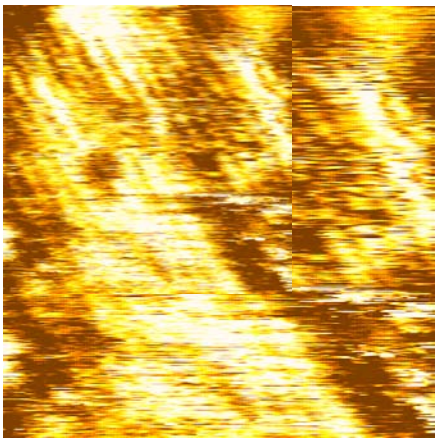

Fig.2 – 5x5 nm^2 STM image of Pt(110) in a CO-rich flow at room temperature and in modest vacuum, I = 0.2 nA, V = 0.3 V.

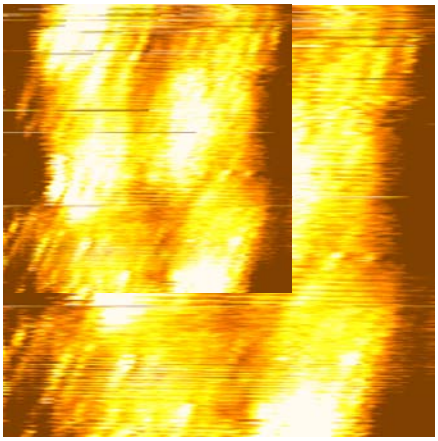

Fig. 3 – 12.5 x 12.5 nm^2 STM image in O_2-rich flow, I = 0.2 nA, V = 0.4 V. T = 450 K; P_{tot} = 1 bar

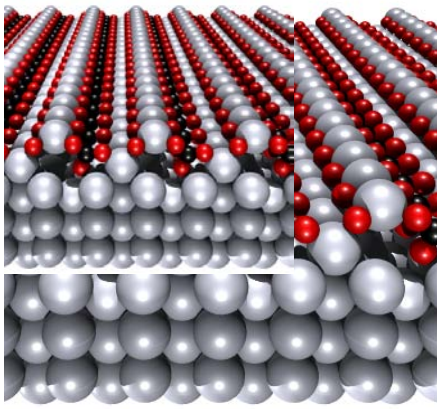

Fig. 4 – Model of the surface oxide proposed by Ackermann et al.

[1] The basis and applications of heterogeneous catalysis; M. Bowker; Oxford Chemistry Primers (1998)
[2] C.T. Herbschleb et al.; to be published
[3] The "Reactor STM": A scanning tunneling microscope for investigation of catalytic surfaces at semi-industrial reaction conditions; P.B. Rasmussen et al.; Rev. Sci. Instr. **69**, 3879 (1998)
[4] Structure and reactivity of surface oxides on Pt(110) during catalytic CO oxidation; M.D. Ackermann et al.; Phys. Rev. Lett. **95**, 255505 (2005)

3S10 – Symposium on Surface Science 2010, 7-13 March 2010, St. Christof am Arlberg, Austria

Strain effects in oxide nanostructures

[1]F. Li, [1]F. Allegretti, [2]C. Franchini, [1]G. Parteder, [1]L. Grangnaniello, [3]R. Podloucky, [1]S. Surnev, [1]F.P. Netzer

[1] *Institute of Physics, Surface and Interface Physics, Karl-Franzens University Graz*
falko.netzer@uni-graz.at
[2] *Faculty of Physics, University of Vienna*
[3] *Institute of Physical Chemistry, University of Vienna*

Elastic strain in heteroepitaxial growth resulting from the lattice mismatch between a substrate and an overlayer plays an important role in determining the structure and the physico-chemical properties of the interface and thus of the growing film. In ultra thin films or nanostructures the interfacial strain may become a decisive quantity and new strain-stabilised structures, unknown in the corresponding bulk materials, may become the stable ground state of the systems. Here we discuss the 2-D oxide nanolayer phases of the antiferromagnetic rocksalt-structure monoxides MO (M = Ni, Co, Mn) grown on a Pd(100) substrate surface. The (100) planes of all three monoxides exhibit a considerable lattice misfit to the Pd(100) surface (NiO → 7%; CoO → 9%; MnO → 14%). Nevertheless, commensurate (100)-type overlayer structures are observed, in which, however, the interfacial strain becomes released by the formation of cation vacancies, thereby forming c(4x2) superstructures with formal M_3O_4 stoichiometries [1-3]. The c(4x2) phases of NiO, CoO, and MnO have been investigated experimentally with atomically resolved STM and theoretically by DFT calculations. Various ground state structure models have been examined in terms of their electronic structure and magnetic properties.

While NiO and CoO yield well-ordered c(4x2) wetting layers, the case of MnO is more complex. MnO(100) exhibits the largest lattice misfit to Pd(100) and the creation of cation vacancies appears to be insufficient to release the strain. The result is a poorly ordered c(4x2) Mn_3O_4 overlayer, with small ordered domains separated by disordered boundary regions. The c(4x2) Mn_3O_4 overlayer can be significantly stabilised in the vicinity of steps. We have therefore investigated the strain relief in the Mn_3O_4 monolayer in detail on a stepped Pd(1 1 19) surface, where a perfectly ordered overlayer can be obtained. The latter allows us to measure with great accuracy the lattice parameters of the Mn_3O_4 structure from the upper to

the lower step edges across the terraces. We find a new strain relaxation phenomenon in terms of a gradual stress release in the overlayer across the terraces, which is possibly accompanied by a concomitant expansion of the topmost substrate layers.

Work supported by the Austrian Science Funds, the ERC Advanced Grant SEPON and the Karl-Franzens University Graz.

References:

[1] S. Agnoli, M. Sambi,G. Granozzi, J. Schoiswohl, S. Surnev, F.P. Netzer, M. Ferrero, A.M. Ferrari, C. Pisani, J. Phys. Chem. B109 (2005) 17197

[2] C. Franchini, R. Podloucky, F. Allegretti, F. Li, G. Parteder, S. Surnev, F.P. Netzer, Phys. Rev. B79 (2009) 035420

[3] F. Allegretti, G. Parteder, L. Gragnaniello, S. Surnev, F.P. Netzer, A. Barolo, S. Agnoli, G. Granozzi, C. Franchini, R. Podloucky, Surface Sci. 2010, in press

Friday

Catalytic reaction between O_2, CO and NO over Rh(111)

J. Gustafson, R. Westerström, O. Balmes[1], A. Resta[1], R. van Rijn[1,2], and E. Lundgren

Div of Synchrotron Radiation Research, Lund university, Box 118, SE-221 00 Lund, Sweden
[1] ESRF, 6, rue Jules Horowitz, F-38043 Grenoble cedex, France
[2] Kamerlingh Onnes Laboratory, Leiden University, P.O. Box 9504, 2300 RA Leiden, The Netherlands
E-mail: johan.gustafson@sljus.lu.se

Recently, there has been a strong debate concerning the most active phase of late transition metal based CO oxidation catalysts, in which some groups (including us) have presented results indicating that the catalytic surface is oxidized when the catalyst is highly active [1-9], while others claim that the surface is metallic [10-14]. Below we show clear evidence of the Rh surface oxide growing in conjunction with the model catalyst switching from low to high activity. It is, however, difficult to state whether the oxide growth is the cause of the high activity or rather a result thereof. In this contribution we will discuss the catalytic activity of Rh model catalysts, as well as the role of oxide phases, in different mixtures of O_2, CO, and NO under varying temperatures.

Figure 1 shows results of an *in situ* surface x-ray diffraction (SXRD) study of the catalytic activity of a Rh(111) surface. 7 mbar CO and 5 mbar O_2 was flowing through the reactor chamber while the sample temperature was increased and lowered between 130 and 300°C (see panel c). Panel a shows the partial pressures of CO, O_2 and CO_2 during the experiment, and the CO_2 signal, which directly monitors the catalytic activity, is shown in more detail in panel b (black solid curve). Panel d (black solid curve) shows the SXRD signal corresponding to the surface oxide, monitoring whether the Rh surface is in a metallic or surface oxidized phase.

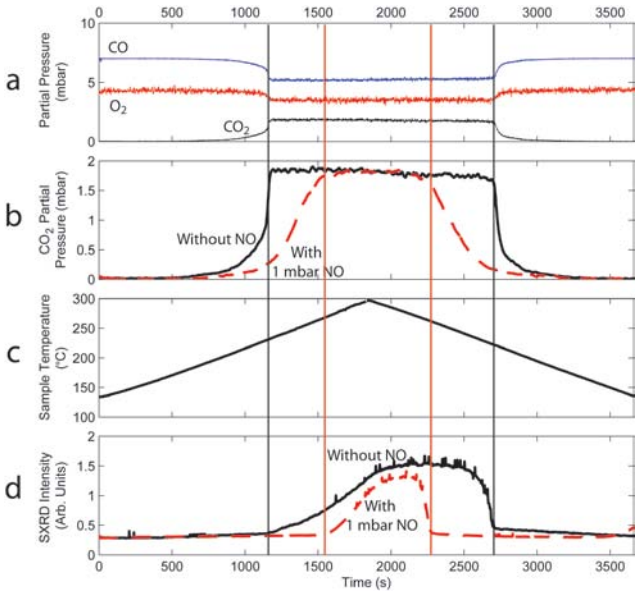

Figure 1: CO oxidation over Rh(111) in a flow of 5 mbar O_2 and 7 mbar CO, while varying the temperature. a) Partial pressures of O_2, CO and CO_2. b) Zoom-in of the CO_2 partial pressure directly monitoring the catalytic activity. c) Sample Temperature. d) SXRD signal in the surface oxide reflection. The red dashed curves in panel b and d shows the effect of adding 1 mbar NO to the flow.

Starting at low temperature, the surface is found in a metallic, CO covered phase with very low activity. After about 1200 s, at a temperature of about 230°C, the CO_2 production rate suddenly rises to a temperature independent level. This is the so-called mass transfer limit (MTL), indicating that the activity is no longer limited by the reactivity of the catalyst, but

rather by the amount of reactants that reach the catalytic surface. In this case, where we are over stoichiometric in O_2, this means that all CO that reaches the surface is transformed into CO_2. In conjunction with the jump into the MTL, the surface oxide signal starts to grow in the SXRD data.

The above measurements clearly show that as soon as the surface oxide is present, the reactivity is high enough to hit the MTL. Inversely, the surface oxide is there as soon as we hit the MTL. It is very difficult to establish whether the surface oxide is the cause of the high activity, or if it is only the result. What we can safely say is that the reactivity just after the appearance of the surface oxide is higher than for the CO covered surface.

The reaction will obviously deplete the partial pressure of the reactants near the surface. If the activity is high enough, the depletion approaches the mass transfer limit, where the partial pressure at the surface, of one of the reactants, is zero. In the example above, the gas mixture is over stoichiometric in O_2, implying that, in the MTL regime, the CO partial pressure approaches zero, and the surface effectively is exposed to an mixture of O_2 and inert CO_2. Assuming that the depletion is similar for CO and O_2, the O_2 partial pressure at the surface will be $(5 \times 2 - 7)/2 = 1.5$ mbar, which we know from previous measurements leads to oxidation. I.e., if the MTL is reached, the surface will get oxidized.

The red dashed curves in panel b and d of figure 1 show the effect of adding 1 mbar of NO to the gas flow. The NO lowers the CO oxidation rate significantly and, although NO is increasing the oxidative effect of the gas, the surface oxide now appears later. The appearance does, however, again coincide with reaching the MTL, but this time the transition into the MTL is smooth and there is no sign of an increased reactivity due to the oxide formation. In the presentation we will try to shed some light on this behaviour.

This work was financially supported by the Swedish Research Council, the Crafoord Foundation, the Anna and Edwin Berger foundation, and the Knut and Alice Wallenberg Foundation. Support by the ESRF staff is gratefully acknowledged.

[1] H. Over, *et al.*, Science 2000, 287, 1474.
[2] H. Over, and M. Mühler, Prog. Surf. Sci. 2003, 72, 3.
[3] H. Over, O. Balmes, and E. Lundgren, Catalysis Today 2009, 145, 236.
[4] B. L. M.Hendriksen, and J. W. M. Frenken, Phys. Rev. Lett. 2002, 89, 046101.
[5] B. L. M. Hendriksen, S. C. Bobaru, and J. W. M. Frenken, Surf. Sci. 2004, 552, 229.
[6] M. D. Ackermann, *et al.*, Phys. Rev. Lett. 2005, 95, 255505.
[7] R. Westerström, *et al.*, Phys.: Condens. Matter 2008, 20, 184019.
[8] J. Gustafson, *et al.*, E. Phys. Rev. B 2008, 78, 045423.
[9] J. Gustafson, *et al.*, Catalysis Today 2009, 145, 227.
[10] M. S. Chen, *et al.*, Surf. Sci. 2007, 601, 5326.
[11] F. Gao, *et al.*, Surf. Sci. 2009, 603, 65.
[12] S. M. McClure, and D. W. Goodman, Chem. Phys. Lett. 2009, 469, 1.
[13] F. Gao, *et al.*, J. Phys. Chem. C 2009, 113, 174.
[14] F. Gao, *et al.*, J. Phys. Chem. C 2009, 113, 182.

Activation of Small Molecules over Ceria Based Model Catalysts: Why do Nanostructured Materials Behave Differently?

J. Libuda, Y. Lykhach, T. Staudt, M. P. A. Lorenz, R. Streber, C. Papp, H.-P. Steinrück, L. Hammer[1], A. Schneider[1], F. Viñes[2], A. Görling[2], N. Tsud[3], T. Skala[4], V. Matolin[3], K. C. Prince[4]

Lehrstuhl für Physikalische Chemie II, Friedrich-Alexander-Universität Erlangen-Nürnberg, D-91058 Erlangen, Deutschland

(corresponding author: J. Libuda, e-mail: libuda@chemie.uni-erlangen.de)

[1]*Lehrstuhl für Festkörperphysik, Friedrich-Alexander-Universität Erlangen-Nürnberg, D-91058 Erlangen, Deutschland*

[2]*Lehrstuhl für Theoretische Chemie, Friedrich-Alexander-Universität Erlangen-Nürnberg, D-91058 Erlangen, Deutschland*

[3]*Charles University, Department of Plasma and Surface Science, 18000 Prague 8, Czech Republic*

[4]*Sincrotrone Trieste, 34012 Basovizza-Trieste, Italy*

The activation of small hydrocarbons and carbon dioxide are key steps in future energy technology. Dry reforming of methane, for example, opens a promising route to the production of synthesis gas from CH_4/CO_2 mixtures, but undesired side reactions leading to carbon formation hamper the application of this technology. Reducible oxides such as CeO_2 may help to remove carbonaceous species before aggregation to graphitic carbon occurs and, thus, may improve the performance of the catalyst by adding self-cleaning properties.

In order to obtain microscopic-level insights into the elementary processes on complex ceria-based catalysts, we follow a model catalyst approach. Ordered CeO_2 thin films are grown on Cu(111) and modified by deposition of Pt and MgO nanoparticles. Their reactivity with respect to CO_2, CH_4 and C_2H_4 is explored using scanning tunneling microscopy (STM), X-ray photoelectron spectroscopy (XPS), high resolution photoelectron spectroscopy (HR-PES), resonant photoelectron spectroscopy (RPES) using synchrotron radiation (ELETTRA, Trieste and BESSY, Berlin) and molecular beam (MB) techniques in combination with density functional theory (DFT) calculations.

In a first step, the growth of (1.5x1.5)CeO_2/Cu(111) is studied by STM and low energy electron diffraction (LEED) and optimized. Using kinetically limited growth of ceria at low temperature and subsequent homoepitaxial growth, closed and atomically flat CeO_2 films with single-crystal-like defect structures are obtained.

Pt nanoparticles are grown on (1.5x1.5)CeO_2/Cu(111) by physical vapor deposition and characterized by STM. XPS shows that upon Pt deposition a small amount of Ce^{3+} centers are formed, suggesting an intermediate reaction at the metal oxide interface. The density of Ce^{3+} increases upon annealing to 500 K, which is attributed to thermally activated reverse spillover of oxygen. We have investigated the activation of methane using a supersonic MB of high kinetic energy CH_4. In strong contrast to Pt(111), it is found that dehydrogenation is more facile on the Pt nanoparticles, leading to formation of CH and C, even at 100 – 130 K. This finding is in excellent agreement with DFT calculations on Pt nanoparticles, predicting that the corresponding activation barriers are strongly reduced at particle edge sites. This holds not only for the dehydrogenation of CH_x, but also for the initial step of the CH_4 activation. HR-PES experiments for C_2H_4 show a very similar behavior, with dehydrogenation via ethylidene to ethylidyne occurring at substantially lower temperature than on Pt(111). These findings suggest a general trend for dehydrogenation reactions on Pt nanoparticles. HR-PES and RPES allow us to monitor spillover / reverse spillover of H, formation / desorption of OH, stepwise reduction of CeO_2, reverse spillover of O and, finally, self cleaning from atomic C, thus providing detailed insights into reaction mechanism and kinetics.

CO_2 activation was studied on reduced (1.5x1.5)CeO_{2-x}/Cu(111) and on MgO/(1.5x1.5)CeO_{2-x}/Cu(111), with the idea of tuning the reactivity towards CO_2 by MgO deposition. Briefly, we detect the formation of two CO_2-derived species, namely carbonate (CO_3^{2-}) and carboxylate (CO_2^-) groups. Slow partial reoxidation of reduced CeO_{2-x}/Cu(111) occurs at large doses of CO_2. For the MgO-containing samples the propensity for carbonate formation strongly increases. In contrast, the tendency for reoxidation of Ce^{3+} to Ce^{4+} by CO_2 decreases with increasing degree of intermixing between MgO and CeO_{2-x}.

The authors acknowledge financial support by the Deutsche Forschungsgemeinschaft (DFG) within the ERACHEM program (“NanoFunC” project) and additional support from the DFG within the Excellence Cluster “Engineering of Advanced Materials” in the framework of the excellence initiative. Furthermore, we acknowledge support by the Fonds der Chemischen Industrie, the DAAD (PPP, Acciones Integradas Hispano-Alemanas) and the European Union (COST D-41).

[1] Thorsten Staudt, Yaroslava Lykhach, Lutz Hammer, M. Alexander Schneider, Vladimir Matolín, Jörg Libuda, Surf. Sci. 603, 3382 (2009).

[2] Y. Lykhach, T. Staudt, M. P. A. Lorenz, R. Streber, A. Bayer, H.-P. Steinrück, and J. Libuda, ChemPhysChem, in press.

[3] Y. Lykhach, T. Staudt, R. Streber, M. P. A. Lorenz, A. Bayer, H.-P. Steinrück, and J. Libuda, submitted.

[4] F. Viñes, Y. Lykhach, T. Staudt, M. P. A. Lorenz, R.. Streber, Ch. Papp, H.-P. Steinrück, J. Libuda, K. M. Neyman, A. Görling, in preparation.

Vibration Spectroscopy of Water on Stepped Gold Surfaces

Harald Ibach

Institute for Bio- und Nano-Systems (IBN3), Jülich Forschungszentrum
D 52425 Jülich

This work was motivated by recent surprising results on the capacitance of Au(11*n*) electrodes in $HClO_4$-electrolytes [1]. It was found that the concentration-independent part of the total capacitance, the so-called Helmholtz-capacitance or inner-layer capacitance is dramatically reduced on stepped surfaces. On the Au(11*5*) surface e.g., the Helmholtz-capacitance amounts to only 54% of the Helmholtz-capacitance on Au(100). Since the electronic polarizability of metal surfaces tends to increase with the step density because of the higher flexibility of electrons at steps [2] the reduction of the Helmholtz-capacitance must be attributed to the structure of water and possibly to a reduced polarizability of water which may result from the structure of water adjacent to the surface.

In the absence of theory and as experiments on the structure of liquid water at stepped surfaces may prove even more difficult than on flat surfaces, studies on the solid form of water (ice) at stepped surfaces may be useful as an intermediate step to elucidate the strange behavior of the Helmholtz-capacitance. The ice-like form of water is readily obtained in ultra-high vacuum by adsorbing water at low temperatures and has therefore been studied extensively in the past (for a review on the early work see [3]). Concerning the structure, it is universally agreed that water molecules, if adsorbed as molecules in the temperatures range of 80K to 150K, aggregate to form hexagonal bilayers. In a single complete bilayer, 75% of the hydrogen atoms are engaged in hydrogen bonds between the oxygen atoms. The remaining 25% may provide bonding to a second bilayer or, in case of a single bilayer, remain in a non-H-bonded (NHB) state. Variants of the original model for a single bilayer proposed in 1980 [4] differ in the placement of these NHB-hydrogen atoms. Theoretical studies on Au(111), Ag(111), Pt(111) and Pd(111) find nearly equal binding energies for these atoms to point upwards ("H-up" bilayer) or downwards ("H-down bilayer) with a slightly higher binding energy for the latter [5, 6]. Partial dissociation such as to bond the surplus hydrogen atoms directly to the surface has been considered for Ru(0001) surfaces [7, 8].

The present work is a study of the vibration spectrum of water adsorbed at ~140K on Au(100), Au(11*11*) and Au(11*5*) surfaces using electron energy loss spectroscopy (EELS) [9]. For all three surfaces, the spectra display the well-known vibration signature of water bi- and multilayers, respectively. Fig. 1 displays an example that corresponds to the coverage of the surface with about one bilayer.

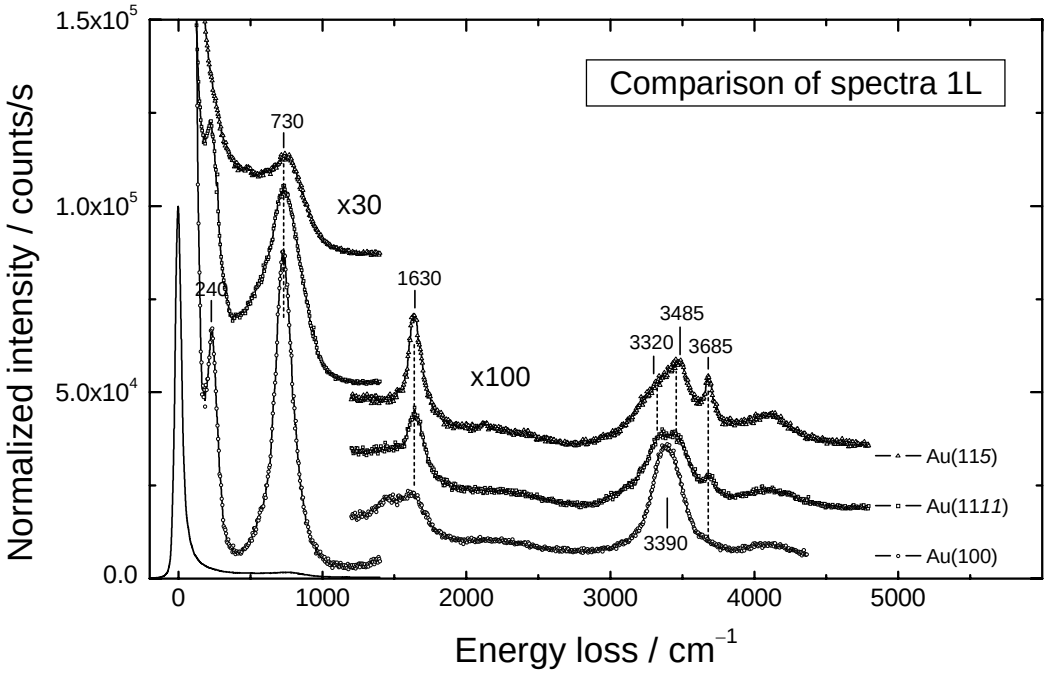

Fig. 1: Energy loss spectra of Au(100), Au(11*1*1) and Au(11*5*) surfaces after dosing with 1 L of water at 140 K. The elastic peak is that of the Au(11*5*) surface, normalized in intensity to 1×10^5 counts/s. The magnifications ×30 and ×100 refer to the elastic line of that surface. The wave numbers indicated in the stretching regime were obtained by fitting to a set of Lorentzians.

The sharp OH-stretching mode at around 3700 cm^{-1}, which is characteristic for NHB-hydrogen, is completely absent for Au(100) at any coverage which is indicative of a realization of the H-down configuration. The mode is present, however, on the stepped surfaces. The intensity of the NHB-mode scales with the step density. Most remarkably, roughly the same relative intensity of the NHB-mode is observed from a single bilayer up to ten bilayers. Furthermore, the NHB-mode survives prolonged annealing of the water layers up to the desorption temperature. This indicates that on stepped surfaces it is steric impossible to simultaneously establish bonds to the surface and engage all hydrogen atoms in H-bonds as on flat surfaces. This result may be relevant also for the metal/liquid-water interface. Spectral features of water bonded to step sites were obtained after dosing the surface with small amounts of water, in particular after moderate annealing of the surface. The spectra are discussed in terms of models for the structure of water on flat and stepped surfaces.

[1] G. Beltramo, M. Giesen, H. Ibach, Electrochim. Acta 54 (2009) 4305.
[2] H. Ibach, W. Schmickler, Phys. Rev. Lett. 91 (2003) 016106.
[3] P. A. Thiel, T. E. Madey, Surf. Sci. Rep. 7 (1987) 211.
[4] H. Ibach, S. Lehwald, Surf. Sci. 91 (1980) 187.
[5] S. Meng, E. G. Wang, S. Gao, Phys. Rev. B 69 (2004) 195404.
[6] S. Schnur, A. Groß, New J. Phys. 11 (2009) 125003.
[7] P. Feibelman, Science 295 (2002) 99.
[8] J. Weissenrieder, A. Mikkelsen, J. N. Andersen, P. J. Feibelman, G. Held, Phys. Rev. Lett. 93 (2004) 196102.
[9] H. Ibach, Surf. Sci. http://dx.doi.org/10.1016/j.susc.2009.11.034 (2010).

Spin-split electronic structures of non-magnetic surfaces observed by high-efficiency spin- and angle-resolved photoelectron spectroscopy

Y. Takeichi, A. Nishide, M. Ogawa, Ke He, T. Okuda, A. Harasawa, I. Matsuda, and A. Kakizaki

Institute for Solid State Physics, The University of Tokyo,
5-1-5 Kashiwanoha, Chiba 277-8581, Japan

We have developed a high-efficiency electron-spin polarimeter based on Very Low Energy Electron Diffraction (VLEED) with the efficiency of 1.9 x 10^{-2}, which is approximately 100 times higher than a conventional Mott detector [1]. Combined with high-resolution hemispherical energy analyzer (PHOIBOS 150), we have observed spin- and angle-resolved photoelectron spectroscopy (SARPES) spectra of so-called Rashba system and quantum spin-Hall system with high energy- and angular-resolution (ΔE = 50 meV and $\Delta\theta$ = +- 0.7°).

Using new spin-polarimeter, we have investigated the electronic structure of ($\sqrt{3}$x$\sqrt{3}$) BiAg surface metal alloy grown on Ag(111). The surface states (SS) are spin-split by the Rashba effect and hybridized with quantum well states in Ag film [2, 3]. The energy dispersion of the spin-split SS is significantly modified by the hybridization. In SARPES spectra, we have found that the quantum well states (QWS) show free electron like energy dispersion when the spins of QWS and SS are anti-parallel, while QWS form energy gaps when the spins of QWS and SS are parallel. The results are well described by the band hybridization model including spin-polarization of QWS.

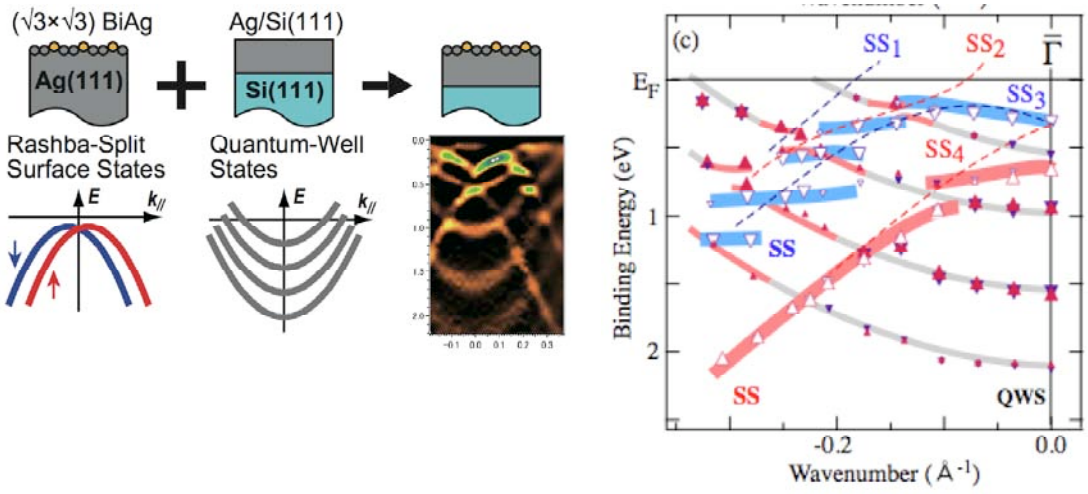

We also investigated spin-dependence of the surface electronic structures of $Bi_{1-x}Sb_x(111)$ (x=0.12-0.13) single crystal, which is known to be a three-dimensional topological insulator, where the surface states, i.e. the edge states of three-dimensional materials are metallic and carrying spin current at the surface, while the bulk states are insulating. In the SARPES spectra, we have observed that the surface states crossing the Fermi level and determined the spin-polarizations of all these states. The result reveals the evidence for the quantum spin-Hall effect in this material and agrees with the theoretical prediction based on the first principle calculations [4, 5].

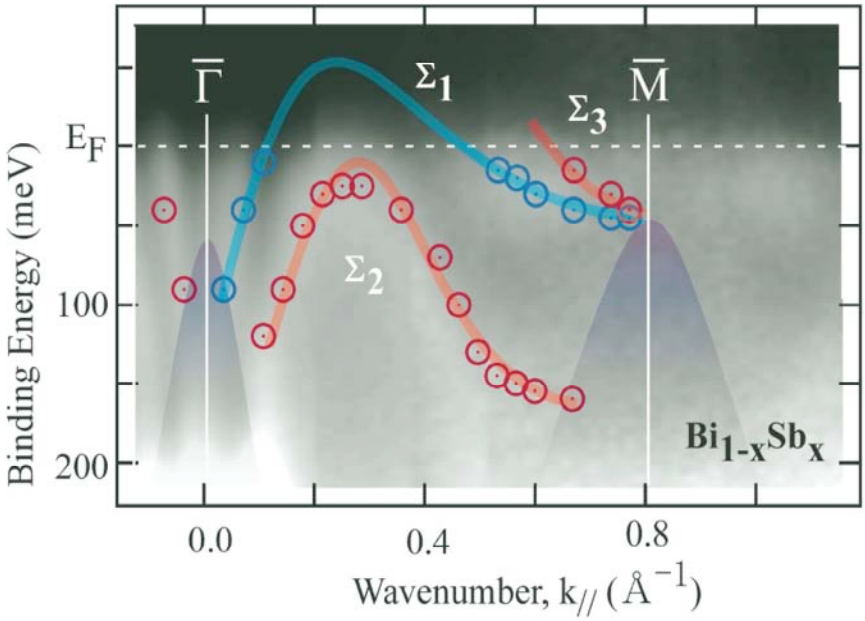

[1] T. Okuda et al., Rev Sci. Instrum. **79**, 123117 (2008).
[2] K. He et al., Phys. Rev. Lett. **101**, 107604 (2008).
[3] K. He et al., submitted to Phys. Rev. Lett.
[4] L. Fu and C. L. Kane, Phys. Rev. B **76**, 045302 (2007).
[5] A. Nishide et al., submitted to Phys. Rev.

Localized surface plasmons and their application in plasmonics

T. Šikola, E. S. Barnard[1], P. Van Dorpe[2], L. Břínek, O. Tomanec, D. Y, Lei[3], R. Kalousek, L. Šustr, L. Dittrichová, S. A. Maier[3] and M. L. Brongersma[1]

Institute of Physical Engineering, Brno University of Technology, Brno, Czech Republic
(corresponding author: T. Sikola, e-mail: Sikola@fme.vutbr.cz)

1 The Geballe Laboratory for Advanced Materials, Stanford University, USA
2 IMEC, Leuven, Belgium
3 Experimental Solid State Group, Physics Department, Imperial College London, London SW7 2AZ, United Kingdom

Localized surface plasmons (LSP) are non-propagating excitations of conduction electrons of metalic nano- and micro-structures coupled to electromagnetic field. Upon resonances they cause a field enhancement in the near-field zone of the structure reaching up to several orders of magnitudes. This ocures both in visible and IR spectral regions and finds its application for instance in enhanced local scattering and absorption techniques like Surface Enhanced Raman Scattering (SERS), Tip Enhanced Raman Scaterring (TERS), localized PL sources and sensors [1,2].
To tune LSP resonances to specific frequencies and maximize effectiveness of the field enhancement, dipole nano- and micro-antennas have become a subject of intensive research [3-5]. Until now plasmonic resonant antennas have mostly been analyzed on transparent, non-absorbing substrates. Both in visible and infrared, a linear dependences of resonant wavelength on the antenna length has been observed.[6,7]

In this presentation we report on the resonant properties of platinum IR dipole antennas fabricated on a silicon-rich-oxinitride (SRON) thin film with substantial materials absorption in the mid IR (near $\lambda^{-1} \approx 1100$ cm^{-1}) [8]. This work was motivated by an effort to exploit electromagnetic energy concentration at antenna resonances for the thermal transformation of SRON beneath antenna gaps into a nanocrystalline Si material [9]. To increase temperature in the SRON film via resonant enhancement of the field in the close vicinity of antennas an absorption of electromagnetic energy in this material is essential.

Platinum antennas consisting of a pair of identical rectangular arms separated by a feed gap were fabricated at the Stanford Nanofabrication Facility. To this end, we used electron beam lithography (EBL) by a RAITH 150 EBL tool, metallization (evaporation of 5 nm-Cr- buffer layer and 60 nm-Pt film), and a lift-off technique. As substrates, Si (111) single crystals covered with a 300 nm-thick-SRON film deposited by plasma enhanced chemical vapor deposition (PECVD) were used.

In this work we observed a non-linear scaling between the resonant wavelength and the length of antennas in the mid-IR close to the SRON absorption maximum. The observed saturation behavior (Fig. 1) can be attributed to the coupling of a geometrical antenna resonance and an absorption resonance of the substrate material. This has been confirmed both by an analytical model and simulations carried out via FDTD and FDFIT numerical codes [10].

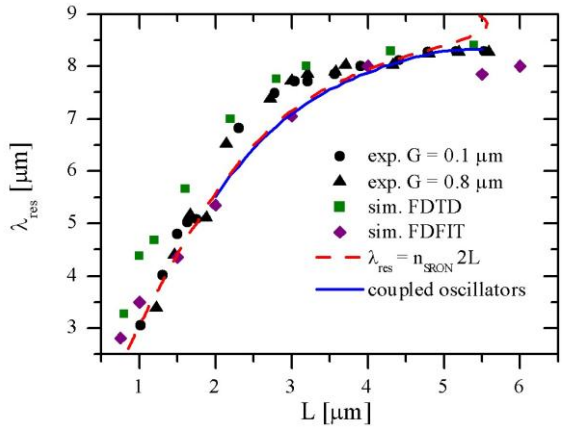

Fig. 1 Resonant wavelength vs. antenna length: experiment (G = 0.1 and 0.8 μm), analytical formula ($\lambda_{res} = n_{SRON}\ 2L$), 3D FDTD (G=0.1μm, near-field) and FDFIT (G = 0.4 μm, reflection) simulations, and a model of two coupled oscillators (coupling turned on for the antenna resonance frequencies from 8.1 μm up).

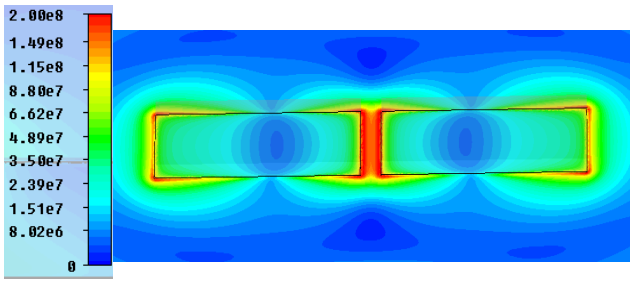

Fig. 2 Map of electric field distribution in a plane at the bottom of a Pt antenna obtained by 3D FDFIT (Frequency Domain Finite Integration Technique, CST Microwave Studio) simulation for λ= 6,67 μm (on resonance).

This work was supported by the Fulbright commission. The work was supported by the National Science Foundation, and the Ministry of Education of the Czech Republic (Projects No. MSM0021630508, 2E08017 and LC06040) and GAAV (Project No. KAN400100701). P.V.D. acknowledges financial support from the F.W.O. (Flanders). D. Y. Lei, and S. A. Maier acknowledge support by the UK Engineering and Physical Sciences Research Council (EPSRC).

[1] S. A. Maier, Plasmonics: Fundamentals and Applications, Springer, 2000.
[2] Bohren, Huffman. Absorbtion and Scattering of Light by small Particles, Wiley, 1998
[3] J. N. Farahani, D. W. Pohl, H.-J. Eisler, and B. Hecht, Phys. Rev. Lett. **95,** 017402 (2005).
[4] P. Mühlschlegel, H.-J. Eisler, O. J. F. Martin, B. Hecht, D. W. Pohl, Science **308**, 1607 (2005).
[5] E. S. Barnard, J. S. White, A. Chandran, and M. L. Brongersma, Optics Express **16** (21), 16529 (2008).
[6] L. Novotny, Phys. Rev. Lett. **98**, 266802 (2007).
[7] K. B. Crozier, A. Sundaramurthy. G. S. Kino, and C. F. Quate, J. Appl. Phys. **94** (7), 4632 (2003).
[8] R. González-Luna, M.T. Rodrigo, C. Jiménez, J.M. Martínez-Duart, Thin Solid Films 317, 347 (1998).
[9] A. Tewary, R.D. Kekatpure. and M.L.Brongersma, Applied Physics Letters 88, 093114 (2006)
[10] T. Šikola, R. D. Kekatpure, E. S. Barnard, et al., " Mid - IR plasmonic antennas on silicon-rich oxinitride absorbing substrates: nonlinear scaling of resonance wavelengths with antenna length", APL, in print.

Vanishing friction: Super-slipperiness or thermolubricity?

S.Yu. Krylov [1,2] and J.W.M. Frenken [1]

[1] *Kamerlingh Onnes Laboratory, Leiden University, 2300 RA Leiden, The Netherlands*

[2] *Institute of Physical Chemistry and Electrochemistry, Russian Academy of Sciences, 119991 Moscow, Russia*

(corresponding author: S.Yu. Krylov, e-mail: krylov@physics.leidenuniv.nl)

The possibility of vanishing friction — a dream of humankind since the invention of the wheel — celebrated the fifth anniversary of its direct observation in atomic scale (AFM) experiments [1,2]. As had long been expected, friction should nearly vanish under conditions for which the atomic scale "roughness" of the surfaces — more precisely, the corrugation of the contact interaction potential — falls below a certain level. This so-called "superlubricity" signals the disappearance of mechanical stick-slip instabilities. Two key experiments [1,2], published simultaneously in 2004, were thought to establish solid proof of this prediction. However, since then we have found that atomic scale friction is strongly complicated by the dynamics of the nanocontact, which is extremely rapid since the contact has an ultra-low effective mass [3,4]. This introduces a zoo of new sliding and friction regimes [5]. We now show that in the two observations of super-slipperiness friction has been vanishingly low due to "thermolubricity": sliding is assisted by strong, temperature-driven motion [6]. This demonstrates dramatically that temperature plays a much stronger role in friction than has ever been expected.

The reconsideration of the nanotribology experiments is based on the first fully quantitative and self-consistent description reached within an advanced two-mass-two-spring model, which explicitly takes into account the high flexibility of the tip (asperity) apex and the corresponding, ultra-low effective mass of the contact. An important element is the analysis of the relation between two basic observables, the mean friction force and maximal lateral force, which enables us to verify the consistency between theory and experiment avoiding any *a priori* assumptions about the unknown potential corrugation and the effective mass of the contact. An example of the excellent fit to the measurements is shown in Fig. 1. Importantly, the positions of the experimental points with respect to the dashed line (corresponding to the mechanistic Prandtl-Tomlinson model) unambiguously indicate that nearly vanishing friction was observed well above the threshold for the familiar, mechanistic superlubricity. This provides us with a direct proof of the thermolubricity-induced ultra-low friction force in ref. [2]. Our fit to the data of ref. [1] is of similar quality and again indicates that thermolubricity has dominated the dramatic reduction in friction. We can further verify the assignment of the dissipation regimes that we have identified before [5] by a detailed inspection of individual traces of the lateral force as a function of the tip position (time), as shown in the insets of Fig. 1. A nontrivial message from the experiment is hidden in the very regular variations of the

lateral force in the low friction regime (bottom-right inset) which were thought [2] to be a direct manifestation of true mechanistic superlubricity. Actually, the inherent dynamics of the system in the regime of thermolubricity also turns out to be very regular [5]. This counterintuitive result reflects the nearly complete averaging of the effective tip-surface interaction, as experienced by the measuring system, over the rapid thermally activated jumps of the tip's apex.

A remarkable bonus of the phenomenon of thermolubricity is the fact that friction can nearly vanish at much higher potential corrugations than expected from mechanistic reasons: a factor of three or so (depending on the contact geometry) is really dramatic. This holds promise for potential applications.

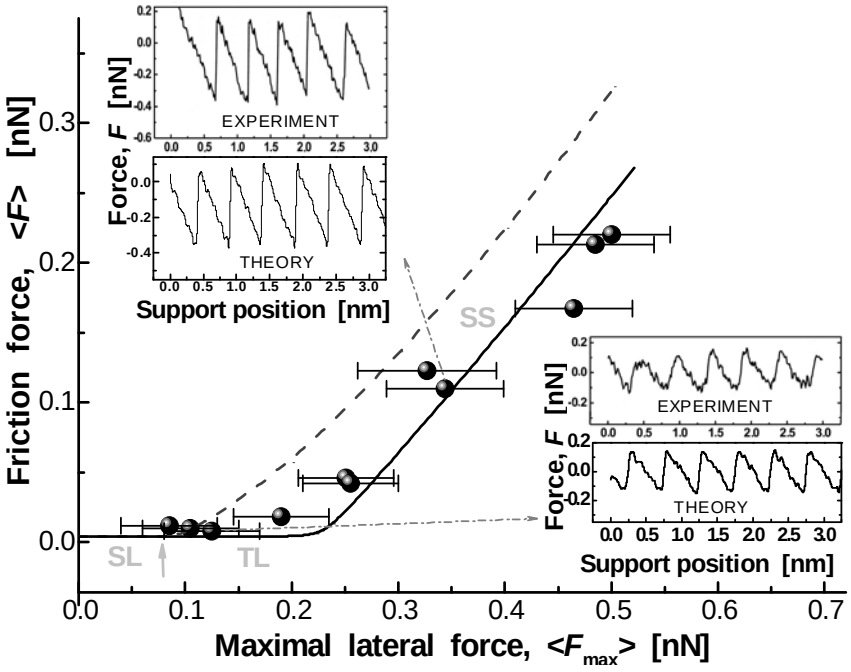

Fig. 1. Theory vs experiment: vanishing friction in friction force microscopy measurements. Experimental data and system parameters were taken from Ref. [2]. The solid curve was calculated by varying the potential corrugation. The dashed curve corresponds to the mechanistic Prandtl-Tomlinson model. Different regimes of friction are indicated: ordinary stick-slip (SS), true thermolubricity (TL) and superlubricity (SL). Insets compare experimental and theoretical force-vs-position scans in the SS-regime (top-left) and at low force levels (bottom-right).

[1] M. Dienwiebel, G.S. Verhoeven, N. Pradeep, J.W.M. Frenken, J.A. Heimberg, and H.W. Zandbergen, Phys. Rev. Lett. 92, 126101 (2004)

[2] A. Socoliuc, R. Bennewitz, E. Gnecco, and E. Meyer, Phys. Rev. Lett. 92, 134301 (2004)

[3] S.Yu. Krylov, J.A. Dijksman, W.A. van Loo, and J.W.M. Frenken, Phys. Rev. Lett. 97, 166103 (2006)

[4] D.G. Abel, S.Yu. Krylov, and J.W.M. Frenken, Phys. Rev. Lett. 99, 166102 (2007)

[5] S.Yu. Krylov and J.W.M. Frenken, New J. Phys 9, 398 (2007); J. Phys.: Condens. Matter 20, 354003 (2008)

[6] S.Yu. Krylov and J.W.M. Frenken, Phys. Rev. B, in press

Dynamics of excited electrons in thin films of lead

E.V. Chulkov[1,2,3], A. Zugarramurdi[2,4], X. Zubizarreta[1,2], I.Yu. Sklyadneva[1], P.S. Kirchmann[5], L. Rettig[5], I-Po Hong[6], Ch. Brun[6], V. M. Silkin[1,7], N. Zabala[1,4], A.G. Borisov[8], R. Heid[9], P. M. Echenique[1,2,3], K. P. Bohnen[9], U. Bovensiepen[5,10], W.-D. Schneider[6]

[1] *Donostia International Physics Center (DIPC), P. de Manuel Lardizabal 4, 20080 San Sebastian/Donostia, Spain*
(corresponding author: E.V. Chulkov, e-mail: waptctce@ehu.es)

[2] *Departamento de Fisica de Materiales, Facultad de Ciencias Quimicas, UPV/EHU, Apdo. 1072, 20080 San Sebasian, Basque Country, Spain*

[3] *Centro de Fisica de Materiales CFM – Materials Physics Center MPC, Centro Mixto CSIC-UPV/EHU, Edificio Korta, Avenida de Tolosa 72, 20018 San Sebastian, Spain*

[4] *Elektrizitatea eta Elektronika Saila, Zientzia eta Teknologia Fakultatea, Euskal Herriko Unibertsitatea UPV/EHU, 644 P.K., 48080 Bilbao/Bilbo, Spain*

[5] *Fachbereich Physik, Freie Universität Berlin, Arnimallee14, D-14195 Berlin-Dahlem, Germany*

[6] *Ecole Polytechnique Federale de Lausanne (EPFL), Institut de Physique de la Matiere Condensee, CH-1015 Lausanne, Switzerland*

[7] *IKERBASQUE, Basque Foundation for Science, 48011 Bilbao, Spain*

[8] *Laboratoire des Collisions Atomiques et Moleculaires (CNRS UMR8625), Bâtiment 351, Universite Paris-Sud, 91405 Orsay Cedex,France*

[9] *Forschungszentrum Karlsruhe, Institut für Festkörperphysik, P.O. Box 3640, D-76021, Karlsruhe, Germany*

[10] *Fakultät für Physik, Universität Duisburg-Essen Lotharstr. 1, D-47048 Duisburg, Germany*

Confinement of valence electrons in metallic films, as thin as a few electron Fermi wavelengths, results in discrete quantum well states (QWSs), which are the origin of quantum size effects. The latter effects are manifested in oscillations of many properties of thin films such as superconducting transition temperature [1], stability of thin films [2], work function [3], and electronic growth [4] as well. These kinds of oscillations have been related to crossing the Fermi level by QWSs at distinct film thicknesses. Another type of oscillations is variation of electron-phonon (e-ph) coupling in QWSs and in surface states on thin films

[5,6,7] which is not related to the Fermi level crossing and is predetermined by the QWS position itself.

Here we report on first-principles calculation results for electron-electron (e-e) and e-ph contributions to the lifetimes of excited electron and holes in QWSs in thin films of Pb(111).

We show that the e-e contribution to the lifetime broadening follows quadratic dependence on energy [8]. This is explained in terms of strong screening of e-e interaction in lead. We demonstrate the important role of e-ph interaction in the excited electron dynamics: strong e-ph coupling and e-ph contribution to the lifetime broadening well comparable to the e-e one.

We demonstrate strong oscillations of e-ph coupling strength parameter λ, e-e and e-ph contribution with the film thickness.

Finally the calculation results are compared with recent scanning tunnelling and time-resolved two-photon photoemission spectroscopy data for thin lead films grown on silicon surfaces [9,10,11].

[1] Ch. Brun et al., Phys. Rev. Lett. **102**, 207002 (2009)
[2] D.A. Luh et al., Science **292**, 1131 (2001)
[3] J.J. Paggel et al., Phys. Rev. B **66**, 233403 (2002)
[4] R. Otero et al., Surf. Sci. **447**, 143 (2000)
[5] T. Valla et al., J. Phys. Cond. Matter **12**, L477 (2000)
[6] S. Mathias et al., Phys. Rev. Lett. **97**, 236809 (2006)
[7] S. Mathias et al., Phys. Rev. Lett. **103**, 026802 (2009)
[8] A. Zugarramurdi et al., Phys. Rev. B **80**, 115425 (2009)
[9] I. P. Hong et al., Phys. Rev. B Rapid Commun. **80**, 081409 (2009)
[10] P .S. Kirchmann and U. Bovensiepen, Phys. Rev. B **78**, 035437 (2008)
[11] P .S. Kirchmann et al., submitted (2009)

Surface chemistry of fusion first wall materials – from fundamental data to modeling

Ch. Linsmeier, M. Reinelt, K. Schmid

Max-Planck-Institut für Plasmaphysik, EURATOM Association,
Boltzmannstr. 2, 85748 Garching b. München, Germany
(corresponding author: Ch. Linsmeier, e-mail: linsmeier@ipp.mpg.de

Based on many years of research in the field of plasma-wall interactions, the combination of beryllium, tungsten, and carbon has been chosen for the start-up first wall materials for the next-step fusion device, the International Thermonuclear Experimental Reactor (ITER) [1, 2]. This decision implies that material mixing processes due to erosion, transport and re-deposition quickly lead to surface compositions which deviate from the installed bulk materials. Many processes which determine the plasma-wall interaction (PWI), like sputtering, chemical erosion, hydrogen re-emission are, however, influenced or even dominated by the chemical composition of the first wall surfaces. For the prediction of PWI processes and the evolution of the first wall during operation of a fusion device, the detailed knowledge of the fundamental surface physical and chemical processes are essential.

During the last years, efforts were undertaken to study the influence of parameters like temperature, diffusion and reaction on the layer properties at the surface of first wall candidate elements. In dedicated laboratory experiments, reactions in binary and ternary systems were studied, both subject to thermal and energetic particle impact. As a result, many of these fundamental reactions are now well described by activation energies and reaction kinetics. This knowledge forms the basis for a predictive modeling of first wall processes.

The binary Be—W system is of specific interest, since most of the ITER first wall (~94%) is cladded with these elements. The literature data on this system was limited to bulk properties. Thin Be layers on W substrates show the formation of a thin Be_2W alloy layer [3], excess Be evaporates. Alloying (and the modification of the physical properties of the wall material) is therefore limited to the first nanometers. The inverse system, W layers on Be, forms a $Be_{12}W$ alloy layer in which the entire available W is incorporated [4]. Depth profile analysis allows the determination of a diffusion coefficient. Although the alloy formation is a diffusive process, the $Be_{12}W$ surface alloy is stable and no W dissolution into the bulk occurs. A detailed analysis of a concentration-dependent diffusion coefficient shows that a strong variation of the diffusion coefficient with Be concentration causes this behavior. Extending the binary Be—W system to the ternary Be—W—C system allows a prediction of the reaction scenarios for a ITER first wall. The comparison with results from the W—C and

Be—C binary systems enables to describe the respective diffusive and reactive processes which govern the surface and surface-near bulk reactions.

Due to the varying conditions at different locations along the first wall of ITER (variable surface temperatures, surface compositions, particle fluxes, e.g. due to the different functionalities of the respective wall sections), it is the aim to use the fundamental surface reaction data to predict locally the phase formation at the ITER first wall. Using the fundamental parameters describing the surface chemistry of mixed materials, the compound formation can be modeled as a function of temperature and available species. This approach treats the material evolution at the first wall in a simplified way, allowing finally integrating these surface processes in an overall model which aims to describe the composition of the first wall and the erosion fluxes in steady state, and therefore predicting the plasma impurity concentrations determined by the first wall. This approach is benchmarked for a binary system: Be—C. In laboratory experiments, the necessary activation energy for Be_2C formation is determined. Together with available reaction data from the literature, a set of differential equation is able to reproduce the evolution of thin Be layers deposited on graphite with increasing temperature. The presentation focuses on the description of the surface processes and demonstrates the modeling concept which includes the dynamic mixed material reactions.

[1] G. Federici, C.H. Skinner, J.N. Brooks, J.P. Coad, C. Grisolia, A.A. Haasz, A. Hassanein, V. Philipps, C.S. Pitcher, J. Roth, W.R. Wampler, and D.G. Whyte, Nucl. Fusion 41 (2001) 1967.

[2] K. Ikeda et al., *Progress in the ITER Physics Basis*, Nucl. Fusion 47 (2007).

[3] A.Wiltner and Ch. Linsmeier, New J. Physics 8 (2006) 181.

[4] Ch. Linsmeier, K. Ertl, J. Roth, A. Wiltner, K. Schmid, F. Kost, S.R. Bhattacharyya, M. Baldwin, and R.P. Doerner, J. Nucl. Mater. 363-365 (2007) 1129.

Wave and particle in molecular quantum interference lithography

Thomas Juffmann[1], Stefan Truppe[1], Philipp Geyer[1], András G. Major[1], Sarayut Deachapunya[1,2], Hendrik Ulbricht[1,3] and Markus Arndt,[1*]

[1]Faculty of Physics, University of Vienna, Boltzmanngasse 5, 1090 Vienna, Austria,
[2]Department of Physics, Faculty of Science, Burapha University, Chonburi 20131, Thailand
[3]School of Physics and Astronomy, University of Southampton, SO17 1BJ, UK

The quantum wave nature of massive particles is both a corner stone of modern physics and a widely utilized feature in the characterization and generation of materials. Here we report on the first quantum interference lithography experiment which allows to visualize the wave-particle duality of large molecules in a single image. This is achieved by combining the surface-deposition of an interference-modulated molecular beam with surface probe microscopy.

An effusive source is used to create a molecular beam, which, after being velocity selected, passes a Talbot-Lau matter-wave interferometer. Diffraction and interference generates a molecular density pattern, which is accumulated on a thermally reconstructed Si (111) 7×7 surface. Fullerenes as well as many other nanoparticles are chemisorbed and exceptionally well immobilized on this surface, even at T=300 K (*1*).

The surface and the deposited interference fringes are then imaged with an STM. The reported method is an intuitive scheme for visualizing quantum interference of clusters and molecules, showing both the localized particle character and the delocalized wave properties in one and the same image. It also presents the non-intuitive discrepancy between the intrinsic quantum randomness in the location of each individual molecule and the well-determined posi-

tion distribution of the molecular ensemble. Further, this new approach allows the non-contact, positive and parallel writing of periodic molecular nanostructures over millimeter-sized areas. Future experiments exploiting the fractional Talbot effect shall enable us to deposit patterns of functional nanoparticles in periods smaller than those of the diffracting masks (*2*).

References and Notes

1. D. Chen, D. Sarid, *Surf. Sci.* **74**, 318 (1994).

2. B. Brezger, M. Arndt, A. Zeilinger, *J. Opt. B.* **5**, S82 (2003).

3. This work has been supported by the FWF Wittgenstein project Z149-N16. AM acknowledges support by the FWF Lise-Meitner fellowship M887-N02 and SD is grateful for funding through a Thai royal scholarship.

Charge density waves without Peierls transitions

M. Czubanowski, D. Lükermann, C. Tegenkamp, H. Pfnür,

Institut für Festkörperphysik, Leibniz Universität Hannover. D-30167 Hannover, Germany
(corresponding author: H. Pfnür, e-mail: pfnuer@fkp.uni-hannover.de)

One-dimensional (1D) electronic systems have attracted great interest recently because of their exotic electronic properties such as quantization of conductance, charge-density waves (CDW), spin-density waves (SDW) triplet superconductivity, and Luttinger-liquid behaviour [1]. As a consequence, low dimensional systems, and in particular 1D chains, exhibit a variety of instabilities with a wealth of associated phase transitions. Especially 1D metallic chains should undergo a Peierls instability accompanied by a significant change of the conductivity due to a metal-insulator transition. In the classical picture, electron-phonon interaction drives CDW formation (Peierls instability) and the opening of a band gap at the Fermi surface [2].

Metallic wires exceeding the length of a few atoms cannot be suspended freely, i.e. they have to be embedded into a two- or three-dimensional environment causing inevitably 2D or 3D interactions of the 1D system with its surroundings. These interactions modify the properties of a 1D system, and need to be controlled precisely, therefore. On the other hand, control of these interactions may allow tuning of certain physical properties, e.g. suppression of the metal-insulator transition. Here we concentrate on Pb nanowires on Si(557) close to the physical monolayer, which represent a completely different physical scenario than all of those known previously. Because of the high concentration of Pb, coupling between the wires cannot be neglected and leads to an interesting interplay of one- and two-dimensional properties between electronic transport, spectroscopy, and geometric structure.

As shown previously, Pb on vicinal Si(557) refacets the surface into a (223) facet orientation at a Pb coverage of 1.31ML. This facet formation is electronically stabilized by Fermi nesting and leads to one-dimensional conductance. Up to this Pb coverage, steps remain uncovered due to energetically less favorable positions for Pb at the step edges, which, however, are filled at higher Pb concentrations. The (223) facet orientation turns out to remain stable at all coverages higher than 1.31 ML.

Contrary to general expectations, the excess Pb atoms decorate steps not randomly, but atomic chains are formed at the step edges with periodic separations up to six (223)-terrace widths (28 lattice constants, 93 Å), as found by a quantitative SPALEED investigation [3]. These new periodicities depend inversely on excess Pb concentration and end at a concentration of 1.52 ML when all steps are decorated with a line density equal to the Si density at steps. Two concentrations (1.52 and 1.41 ML, respectively) are shown schematically in Fig.1.

Electronic correlation, similar to the case at 1.31 ML of Pb, seems to be responsible also for the periodic arrangement of atomic Pb chains at concentrations exceeding 1.31 ML. Indeed,

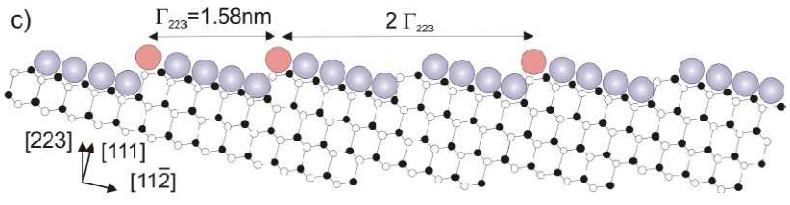

Fig. 1: Side view of the (223) facet structure showing (locally) step decoration (red atoms),when 0.2 ML (left, Γ_{223}) or 0.1 ML (right, $2\Gamma_{223}$) of excess Pb is adsorbed.

these one-dimensional periodicities can be explained assuming that new split-off bands are formed within the band gap at 1.31 ML. As shown in Fig. 2, these new bands are exactly filled by two electrons per Pb atom at the respective excess Pb concentrations at the periodicities indicated. Similar to the case at 1.31 ML, they result again in gap opening and reduction of the electronic energy, but now within a purely 1d model, and with reduced effective band gaps. This is exactly what we measured with our macrosocopic 4-point conductivity technique at these coverages. In the direction normal to the steps, the metal/insulator phase transition at 78 K found at 1.31 ML quickly disappears as a function of excess Pb concentration, but the system remains insulating. As expected from the model described above, the effective activation barrier as a function of Pb concentration gets smaller and disappears at 1.52 ML of Pb.

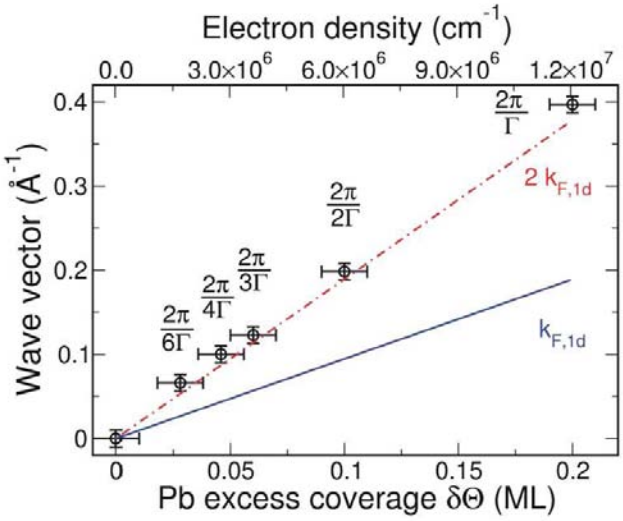

Fig. 2: Plot of reciprocal lattice vectors of the periodicities caused by the Pb excess coverage (relative to 1.31 ML). The solid (blue) curves represent the Fermi wave vector $k_{F,1d}$ of a 1d electron gas induced by the Pb excess coverage assuming a valence state of two. The coincidence of $2k_F$ (dashed-dotted (red) line) with the lattice vectors of the superlattice results in nesting.

This behavior is reminiscent of formation of charge density waves with tunable wavelengths as a function of excess Pb concentration, and indicates persistent strong electron correlation in this strongly anisotropic 2d system. However, contrary to the situation at 1.31 ML Pb, no structural phase transitions are seen any more. They disappear, since for atomic chains at step edges there is no lattice distortion necessary that counteracts the electronic reduction of energy by formation of multiple periods. Thus only the electronic part remains.

[1] G. Grüner, Review of Modern Physics 60, 1129 (1988).
[2] G.Grüner, *Density Waves in Solids*, (Addison-Wesley, 1994)
[3] M. Czubanowski, H. Pfnür, C. Tegenkamp, Surf. Sci. 603 (2009) L121.

Author Index

Nanotechnology is our Profession!

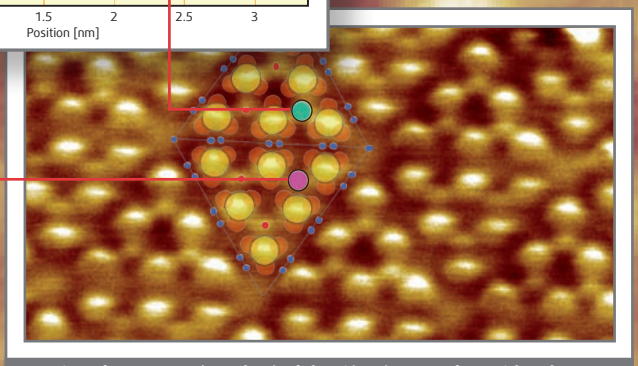

Imaging of rest atoms (raw data) of the Si(111) 7x7 surface with QPlus AFM at 50 K. Line profile showing the height difference of the rest atoms. Measurement: A. Bettac, Omicron

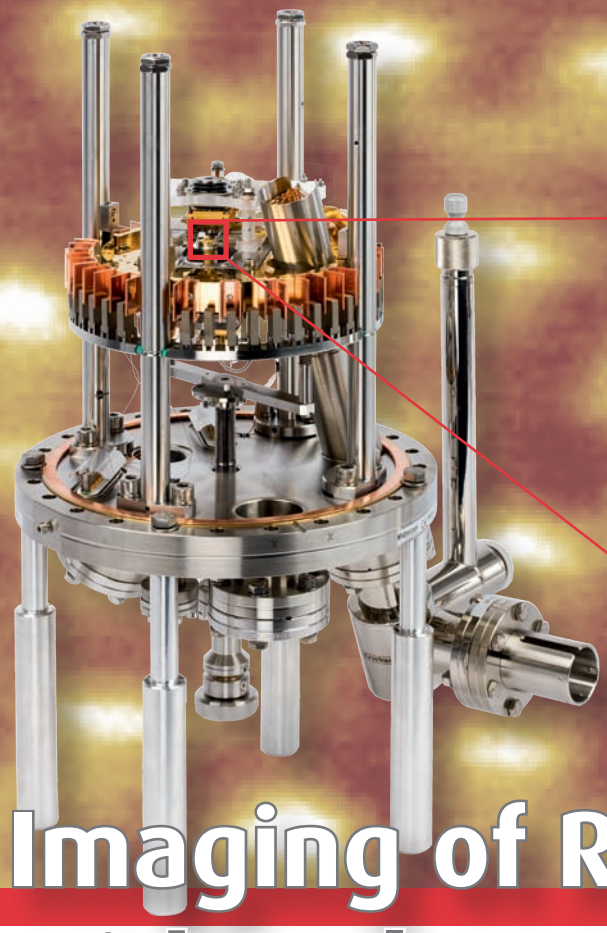

QPlus sensor mounted on an exchangeable tip carrier.

Imaging of Rest Atoms with QPlus AFM at 50 K

Variable Temperature SPM with QPlus AFM:

- 25 K - 1500 K
- True pA STM
- Improved dI/dV Spectroscopy
- Beam Deflection AFM
- QPlus AFM
- In-situ Evaporation

Omicron NanoTechnology

Omicron NanoTechonology GmbH
Limburger Strasse 75
65232 Taunusstein, Germany
Tel.: +49(0) 6128/987-0
e-mail: info@omicron.de
Web: www.omicron.de

AD VT QPlus_3510 / 10-Feb

3S'10

SYMPOSIUM ON SURFACE SCIENCE 2010
St. Christoph am Arlberg, Austria
March 7 - March 13, 2010

Friedrich Aumayr and Peter Varga, organizers
Institute of Applied Physics, Vienna University of Technology (TU Wien)

Sunday, 7 March 2010

16:00 - 18:30 **REGISTRATION**

18:30 - 19:30 **DINNER**

20:00 - 20:20 **OPENING**

chair: ***VARGA***

20:25 - 20:45	**GIESSIBL**
20:45 - 21:05	**SCHNEIDER**
21:05 - 21:25	**GARCIA-LEKUE**

Monday, 8 March 2010

07:15 - 08:00	**BREAKFAST**

chair: ***SEITSONEN***

08:00 - 08:20	**WÖLL**
08:20 - 08:40	**THORNTON**
09:15 - 12:00	**DISCUSSION FORUM**
12:00 - 13:00	**LUNCH**
13:30 - 15:30	**FREE DISCUSSIONS**

chair: ***HOFER***

16:30 - 16:50	**REUTER**
16:50 - 17:10	**PIRUG**
17:10 - 17:30	**LIN**
17:30 - 17:50	**BUCK**
17:50 - 18:10	**GREBER**
18:10 - 18:30	**MENZEL**
18:30 - 19:30	**DINNER**

chair: ***ERNST***

19:30 - 19:50	**BARTH**
19:50 - 20:10	**MARBACH**
20:10 - 20:30	**BJÖRK**
20:30 - 20:50	**VITALI**

Tuesday, 9 March 2010

07:15 - 08:00	**BREAKFAST**

chair: ***WOLF***

08:00 - 08:20	**GÖLZHÄUSER**
08:20 - 08:40	**FASEL**
09:15 - 12:00	**DISCUSSION FORUM**
12:00 - 13:00	**LUNCH**
13:30 - 15:30	**FREE DISCUSSIONS**

chair: ***HEINZMANN***

16:30 - 16:50	**AMBROSCH - DRAXL**
16:50 - 17:10	**RUFFIEUX**
17:10 - 17:30	**DONG**
17:30 - 17:50	**VÁZQUEZ DE PARGA**
17:50 - 18:10	**DIL**
18:10 - 18:30	**MEIER**
18:30 - 19:30	**DINNER**

chair: ***MÜLLER P.***

19:30 - 19:50	**KOSHIKAWA**
19:50 - 20:10	**LEROY**
20:10 - 20:30	**SUCHORSKI**
20:30 - 20:50	**SÁNCHEZ - PORTAL**

Wednesday, 10 March 2010

07:15 - 08:00	**BREAKFAST**

chair: ***EBERHARDT***

08:00 - 08:20	**ALTMAN**
08:20 - 08:40	**LUNDGREN**
09:15 - 12:00	**DISCUSSION FORUM**
12:00 - 13:00	**LUNCH**
13:30 - 15:30	**FREE DISCUSSIONS**

chair: ***AUMAYR***

16:30 - 16:50	**FACSKO**
16:50 - 17:10	**LEMELL**
17:10 - 17:30	**SCHUCH**

chair: ***MÜLLER S.***

17:30 - 18:30	**POSTERINTRODUCTION**
18:30 - 19:30	**DINNER**
19:30 - 21:30	**POSTERSESSION**

Thursday, 11 March 2010

07:15 - 08:00	**BREAKFAST**

chair: ***ECHENIQUE***

08:00 - 08:20	**BRUNE**
08:20 - 08:40	**SCHEFFLER**
09:15 - 12:00	**DISCUSSION FORUM**
12:00 - 13:00	**LUNCH**
13:30 - 15:30	**FREE DISCUSSIONS**

chair: ***WIDDRA***

16:30 - 16:50	**RUPPRECHTER**
16:50 - 17:10	**ARNAU**
17:10 - 17:30	**BENALI**
17:30 - 17:50	**MORGENSTERN**
17:50 - 18:10	**MÜLLER S.**
18:10 - 18:30	**CAÑAS-VENTURA**
18:30 - 19:30	**DINNER**

chair: ***HAMMER***

19:30 - 19:50	**SURNEV**
19:50 - 20:10	**MITTENDORFER**
20:10 - 20:30	**HERSCHLEB**
20:30 - 20:50	**NETZER**

Friday, 12 March 2010

07:15 - 08:00	**BREAKFAST**

chair: ***STARKE***

08:00 - 08:20	**GUSTAFSON**
08:20 - 08:40	**LIBUDA**
09:15 - 12:00	**GIANT SLALOM RACE**
12:00 - 13:00	**LUNCH**
13:30 - 15:30	**FREE DISCUSSIONS**

chair: ***LEISCH***

16:30 - 16:50	**IBACH**
16:50 - 17:10	**KAKIZAKI**
17:10 - 17:30	**ŠIKOLA**
17:30 - 17:50	**KRYLOV**
17:50 - 18:10	**CHULKOV**

chair: ***TAGLAUER***

18:30 - 18:50	**LINSMEIER**
18:50 - 19:10	**JUFFMANN**
19:10 - 19:30	**PFNÜR**
19:30 - 19:45	**GIANT SLALOM RACE AWARD CEREMONY**
20:00	**CONFERENCE DINNER**